

**Applications Related
PHENOMENA
in TITANIUM
ALLOYS**



STP 432

American
Society for
Testing and
Materials



APPLICATIONS RELATED PHENOMENA IN TITANIUM ALLOYS

A symposium
presented at a meeting of
Committee B-10 on
Reactive & Refractory Metals and Alloys
AMERICAN SOCIETY FOR
TESTING AND MATERIALS
Los Angeles, Calif., 18-19 April, 1967

ASTM SPECIAL TECHNICAL PUBLICATION NO. 432

List price \$20.00; 30 per cent discount to members



published by the
AMERICAN SOCIETY FOR TESTING AND MATERIALS
1916 Race Street, Philadelphia, Pa. 19103

© BY AMERICAN SOCIETY FOR TESTING AND MATERIALS 1968
Library of Congress Catalog Card Number: 68-18768

NOTE

The Society is not responsible, as a body,
for the statements and opinions
advanced in this publication.

Printed in Baltimore, Md.
March, 1968

Foreword

The Symposium on Applications Related Phenomena in Titanium Alloys was presented 18–19 April 1967 in Los Angeles, Calif. ASTM Committee B-10 on Reactive and Refractory Metals and Alloys sponsored the symposium. Hans Conrad, University of Kentucky, was the symposium chairman. It was divided into four sessions, and presiding as chairmen of these sessions were Dr. Conrad; R. I. Jaffee, Battelle Memorial Institute; H. P. Kessler, Reactive Metals, Inc.; and W. W. Minkler, Titanium Metals Corporation of America.

Related ASTM Publications

**New Structural Materials for Aerospace Vehicles, STP
379 (1965), \$6.00**

**Stress-Corrosion Cracking of Titanium, STP 397 (1966),
\$14.00**

Structural Fatigue in Aircraft, STP 404 (1966), \$18.50

**Plain Strain Crack Toughness Testing of High Strength
Metallic Materials, STP 410 (1967), \$5.50**

Contents

Introduction	1
Fracture Toughness and Notch Strength	
Source of Fracture Toughness: The Relation Between K_{Ic} and the Ordinary Tensile Properties of Metals—G. T. HAHN AND A. R. ROSENFELD	5
A Review of Factors Influencing the Crack Tolerance of Titanium Alloys—J. L. SHANNON, JR., AND W. F. BROWN, JR.	33
Structural Ductility of High Strength Titanium Alloys—RALPH PAPIRNO	64
Toughness of Two-Phase 6Al-4V Titanium Microstructures—W. W. GERBERICH AND G. S. BAKER	80
Relation of Strength and Toughness to Fine Structures in a Beta Titanium Alloy—B. R. BANERJEE, J. J. HAUSER, AND J. M. CAPENOS	100
Plane Strain Fracture Toughness and Mechanical Properties of 5Al-2.5Sn ELI and Commercial Titanium Alloys at Room and Cryogenic Temperatures—C. M. CARMAN AND J. M. KATLIN	124
Fracture Toughness in Aqueous Saline Environments	
Metallurgical and Mechanical Aspects of the Sea-Water Stress Corrosion of Titanium—I. R. LANE AND J. L. CAVALLARO	147
The Influence of Composition and Heat Treatment on the Aqueous-Stress Corrosion of Titanium—S. R. SEAGLE, R. R. SEELEY, AND G. S. HALL	170
Effects of Heat Treating Environmental Conditions on the Stress-Corrosion Cracking Resistance of Several Titanium Alloys—D. G. HOWE AND R. J. GOODE	189
Environmental Related Phenomena	
The Initiation of Hot-Salt Stress Corrosion Cracking of Titanium Alloys—S. P. RIDEOUT	205
Crevice Corrosion of Titanium—J. D. JACKSON AND W. K. BOYD	218
Biaxial Properties of Titanium Alloys at Cryogenic Temperatures—S. F. FREDERICK AND D. L. CORN	227
Texture Strengthening and Fracture Toughness of Titanium Alloy Sheet at Room and Cryogenic Temperatures—T. L. SULLIVAN	236
Low Cycle Fatigue and Wear	
Effects of a 3.5 Per Cent Sodium Chloride Aqueous Saline Environment on the Fatigue Crack Propagation Characteristics of Titanium Alloys—T. W. CROOKER AND E. A. LANGE	251
Lubricants and Wear Coatings for Titanium—S. J. KOSTMAN	268
Surface Treatment of Ti-6Al-4V for Impact-Fatigue and Wear Resistance—R. D. WELTZIN AND G. KOVES	283

Introduction

The use of titanium alloys in aerospace and other systems has experienced a rapid increase in the past several years. This increased application has revealed that titanium alloys exhibit certain behavior characteristics which can lead to serious consequences if not given proper consideration. Some of the more important phenomena related to these characteristics are fracture toughness, stress-corrosion (aqueous and hot salt), crevice corrosion, hydrogen effects, low-cycle fatigue, and wear. These are the topics covered in this volume.

Recognizing the importance of keeping the engineer informed on research under way on such problems, the joint ASTM-ASME Committee on Effect of Temperature on the Properties of Metals sponsored a symposium on "Stress Corrosion Cracking in Titanium Alloys" at the Fall Meeting of the ASTM in Seattle, Washington, on 1 and 2, Nov., 1965. The success of this meeting prompted the sponsoring committee to recommend a follow-up symposium to be held within one to two years on related subjects in titanium alloys. ASTM Committee B-10, at its regular meeting on 3, Nov., 1965, acted on this recommendation and offered to sponsor such a symposium, since titanium alloys are within its scope. It was subsequently decided to cover a broad range of applications related phenomena rather than limit the symposium to stress-corrosion. This broader subject matter, therefore, was taken as the theme for the present symposium.

Most of the papers presented at the symposium are found in this volume. They represent both survey papers by invited speakers and submitted papers of recent work, the combination giving the latest results and thinking on the topics covered. One can conclude from these papers that, although the mechanisms associated with the discussed applications related phenomena are still not well understood, there is sufficient information to indicate that they do not offer severe limitations to the continued and increased use of titanium alloys.

Although the papers in this volume are directed principally to the practicing metallurgist and design engineer, they provide a good back-

ground for the more basic oriented materials scientist who wishes to investigate the detailed atomic mechanisms associated with applications related phenomena in titanium alloys.

Hans Conrad

Chairman, Department of Metallurgical
Engineering, University of Kentucky,
Lexington, Ky.; symposium chairman.

Fracture Toughness and Notch Strength

Sources of Fracture Toughness: The Relation Between K_{Ic} and the Ordinary Tensile Properties of Metals

REFERENCE: Hahn, G. T. and Rosenfield, A. R., "Sources of Fracture Toughness: The Relation between K_{Ic} and the Ordinary Tensile Properties of Metals," *Applications Related Phenomena in Titanium Alloys*, ASTM STP 432, American Society for Testing and Materials, 1968, pp. 5-32.

ABSTRACT: This paper examines crack extension from a metallurgical standpoint. Stress and strain intensification at the crack tip and the basic flow and fracture properties of the material are considered. Insights derived from etch-pitting experiments are reviewed. These reveal the two characteristic types of local yielding: (1) plane strain or "hinge-type" relaxation and (2) plane stress or through-the-thickness relaxation. Two simplified elastic-plastic treatments that model plane strain and plane stress are identified. They offer approximate equations connecting K (the stress intensity parameter) with the plastic zone size and the crack-tip displacement, which are in good accord with experiment. They also help to define limiting conditions for plane strain and plane stress. A method of relating the crack-tip displacement to the peak strain is described, and this is combined with a critical strain criterion for ductile fracture. In this way, the plane strain fracture toughness parameter K_{Ic} is formulated in terms of ordinary tensile properties: $K_{Ic} \approx \sqrt{\frac{2}{3} E Y n^2 \epsilon^*}$ (E is the modulus, Y the yield stress, n the strain hardening exponent, and ϵ^* the true strain at fracture of a smooth tensile bar). This expression is shown to be in good accord with available data on a variety of titanium, aluminum, and steel alloys. Since the influence of composition and heat treatment on tensile properties is already established in many cases, the tensile properties can now serve as a link between fracture toughness and the backlog of metallurgical experience. This possibility is demonstrated for Type 4340 steel heat treated to different strength levels.

KEY WORDS: crack extension, fracture toughness, plastic flow, tensile properties, testing, metals, ductility, crack-tip displacement, stress gradient, strain hardening

Irwin's concept of fracture toughness has been the subject of many papers and seminars. Ways of measuring K_{Ic} and K_c and the factors that correct for end effects and special shapes are finding their way into the literature [1].² However, virtually nothing has been said about the origins

¹ Metal Science Group, Battelle Memorial Institute, Columbus Laboratories, Columbus, Ohio.

² The italic numbers in brackets refer to the list of references appended to this paper.

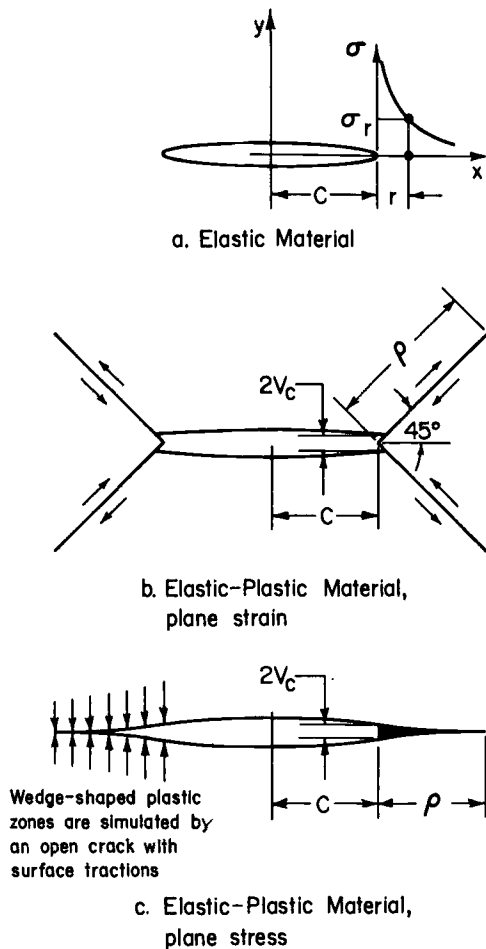


FIG. 1—Models of a stressed crack: (a) Inglis [3] model for an elastic material, (b) Bilby-Swinden [4,5] model for plane strain relaxation in an elastic-plastic material, and (c) Dugdale-Muskhelishvili [6] model for plane stress relaxation in an elastic-plastic material.

of crack extension resistance. What basic metallurgical factors contribute to the toughness of an alloy? How can composition, processing, and heat treatment be manipulated to enhance the value of K_{Ic} ? Answers to these questions would not only benefit alloy development but would simplify quality control and the task of preparing specifications.

The metallurgy of crack extension resides in the small region ahead of a crack that yields, flows, and ultimately ruptures. This region has been inaccessible in the past. It could not be measured, and it could not be dealt with analytically. Now, more and more studies are penetrating the plastic zone. Recent advances already contain insights useful to the metallurgist.

This paper consolidates findings about the yielded region that point to the metallurgical origins of fracture toughness. The paper draws on theory and experiments to construct simplified pictures of plane strain and plane stress plastic relaxation. Measurements and analytical results are combined, and these define quantitative relations between K_{Ic} and K_c and the ordinary tensile properties of metals: the elastic modulus, yield stress, strain hardening index, and the true strain at fracture. Since the influence of composition and heat treatment on tensile properties is already established in many cases, the tensile properties become a link between fracture toughness and the backlog of metallurgical experience. This paper confines itself to ductile fracture modes. A possible treatment of cleavage has been proposed elsewhere [2]. Cyclic loading

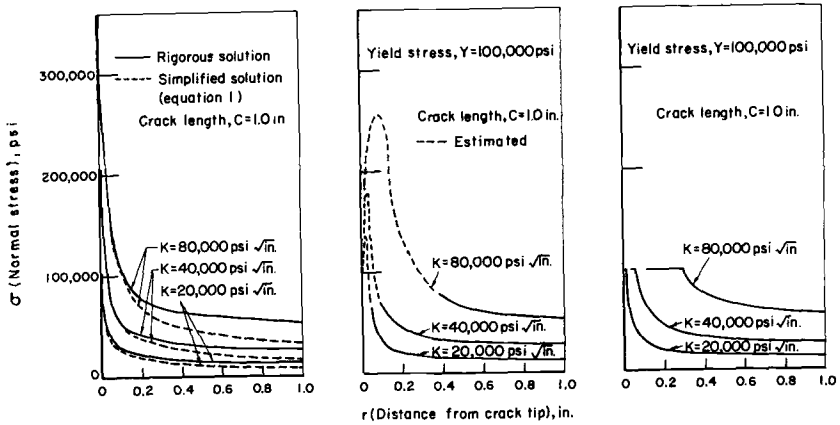


FIG. 2—Stress gradients ahead of a sharp crack: (a) elastic material, (b) nonwork hardening elastic-plastic material under plane strain [9] and (c) nonwork hardening elastic-plastic material under plane stress [11].

and environmental effects are also very important but are beyond the scope of the present treatment.

Significance of K , K_{Ic} , and K_c

Irwin's [1] concept of stress intensity and fracture toughness—the parameters K , K_{Ic} , and K_c —stem from the following expression for the stress ahead of a sharp crack in a linear elastic material (Fig. 1):³

$$\sigma = T\sqrt{\pi C} (2\pi r)^{-1/2} \dots \dots \dots (1)$$

³ The term σ is the normal stress a distance r in front of the crack (see Fig. 1a), T is the nominal applied stress, and $2C$ is the crack length. Equation 1, a simplified version of the Inglis solution for a crack in an infinite plate, is only valid close to the crack tip (when $r \lesssim 0.5 C$) provided there is no plastic relaxation. The rigorous form of the Inglis [3] solution for a sharp crack is: $\sigma/T = \text{Coth } \alpha$, $\text{Cosh } \alpha = x/C$, and this is compared with the simplified version in Fig. 2a.

TABLE 1—Approximate relations valid near the crack tip.

Elastic Material ^a	Elastic-Plastic Material ^b
$r_{(\sigma)} \propto K^2$	$\rho \propto (K/Y)^2$
$\sigma_{(r)} \propto K$	$\sigma_{r>\rho} \propto K$
	$\sigma_c = Y$
	$\sigma_{max} = f[Y, (K/Y)^2 1/t]$
$\epsilon_{(r)} \propto K/E$	$\epsilon_{max} = f[K/Y, (K/Y)^2 1/t, E, n]$
	$v_c \propto (Y/E)(K/Y)^2$
$We \propto K^2C/E$	$W_p \propto (Y^2/E)(K/Y)^4$
$dWe/dC \sim G \propto K^2/E$	

^a Derived from Eq 1.

^b Based on the Bilby-Swinden [4] and Dugdale-Mushkelishvili [6, 11] treatments, and valid at low stress levels (that is, when $T/Y < 0.7$)

- $K \equiv T\sqrt{\pi C}$,
- T = nominal applied stress,
- $2C$ = crack length,
- Y = yield stress,
- E = Young's modulus,
- $r_{(\sigma)}$ = distance corresponding to σ ,
- ρ = plastic zone size,
- n = strain hardening index,
- t = plate thickness,
- $r = (x - c)$,
- $\sigma_{(r)}, \epsilon_{(r)}$ = stress and strain front of the crack at, $x = r + c, y = 0$,
- σ_c = crack-tip normal stress,
- σ_{max} = the peak normal stress,
- ϵ_{max} = the peak crack tip tensile strain,
- v_c = crack tip displacement,
- W_e = stored elastic energy,
- W_p = stored plastic energy, and
- G = elastic energy release rate.

The term $T\sqrt{\pi C}$ has special properties—it is proportional to σ and reflects an equivalence between the effects of T and \sqrt{C} —and is given special names:

$$K \equiv \text{stress intensity parameter}^4 \quad \equiv T\sqrt{\pi C} \dots \dots \dots (2)$$

⁴The matter of terminology is confused because McClintock and Irwin [7] define K_{Ic} as the Mode I fracture toughness parameter but do not make it clear how to distinguish between (1) plane strain, (2) plane stress, (3) the onset of slow growth, and (4) the onset of unstable propagation. We use the following definitions in this paper for Mode I because they are close to general practice and still make the necessary distinctions:

K_{Ic} = stress intensity (value of K) at the onset of slow (stable) crack growth under *plane strain*. T^* is the corresponding value of applied gross section stress.

K_c = stress intensity at the onset of slow (stable) crack growth when the state of stress throughout the loading has been predominantly *plane stress*.

The reader should also note that the relation $K_{Ic}, K_c \equiv T^* \sqrt{\pi C}$ is valid for a small centrally located through-crack in a large plate, that is, $2C$ is smaller than $\frac{1}{10}$ the width dimension. For larger cracks, edge cracks or different geometries the proper relation is $K_{Ic}, K_c = \varphi T^* \sqrt{\pi C}$ where φ is a correction factor for the particular configuration [8].

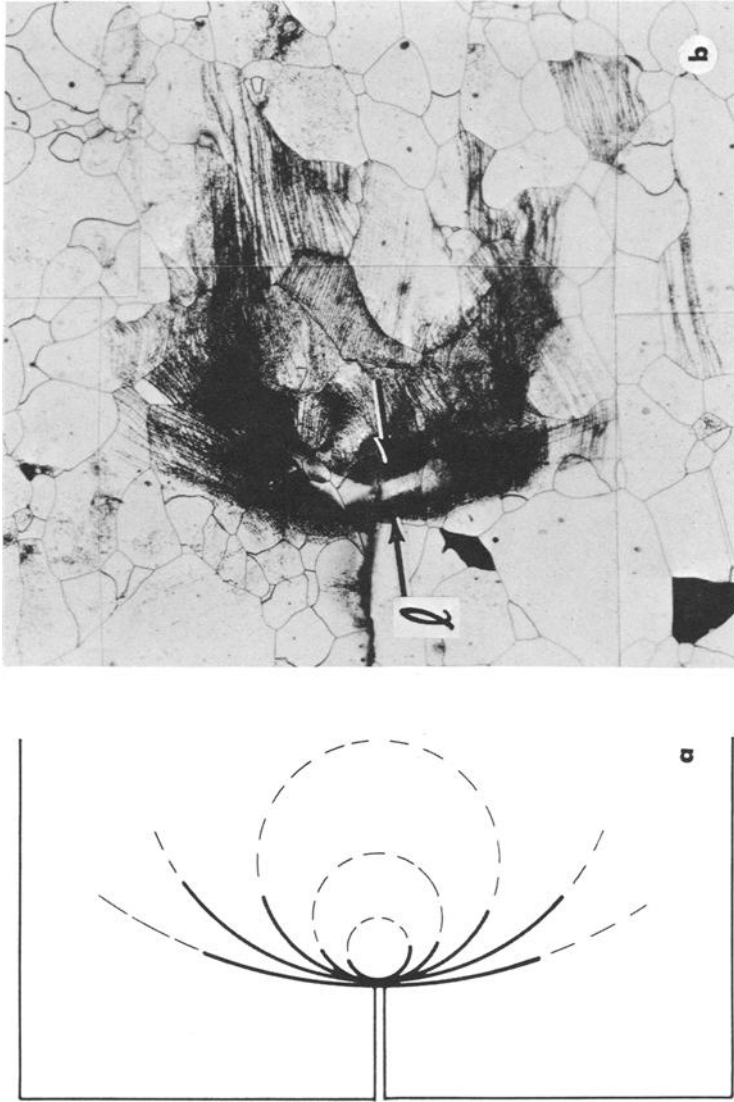


FIG. 3—Plane strain relaxation: (a) schematic and (b) an actual zone revealed by etching an 0.060-in.-thick, precracked silicon steel plate after loading to $K/Y = 0.25 \sqrt{\text{in.}}$, $(K/Y)^2/t = 0.95$, $l_0 \approx 0.002 \text{ in.} = 0.5 \text{ mm}$ ($\times 200$).

$$K_{Ic} \equiv \text{plane strain fracture toughness} \equiv T^* \sqrt{\pi C} \dots \dots \dots (3)$$

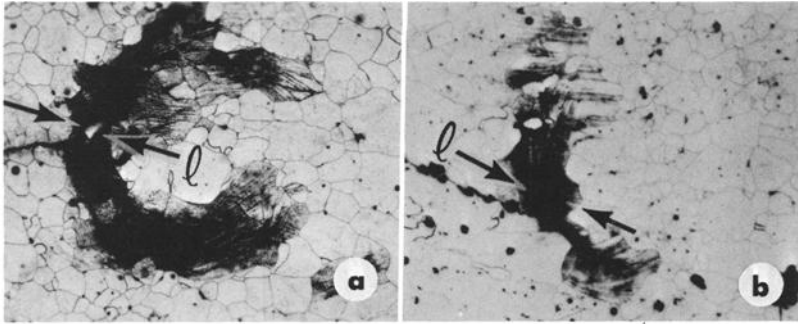
parameter (see footnote⁴)

$$K_c \equiv \text{plane stress fracture toughness} \equiv T^* \sqrt{\pi C} \dots \dots \dots (4)$$

parameter (see footnote⁴)

The fracture toughness concept for an elastic material then follows from one additional step. A criterion for fracture is introduced: rupture occurs at the crack tip when a critical normal stress, $\sigma = \sigma^*$ is attained at a fixed distance r^* . The terms σ^* and r^* are regarded as basic properties of the material. This is combined with Eq 1, 3, or 4 and leads to the important conclusion:

$$T^* \sqrt{\pi C} \equiv K_{Ic}, K_c = \sigma^* (2\pi r^*)^{1/2} = \text{constant} \dots \dots \dots (5)$$



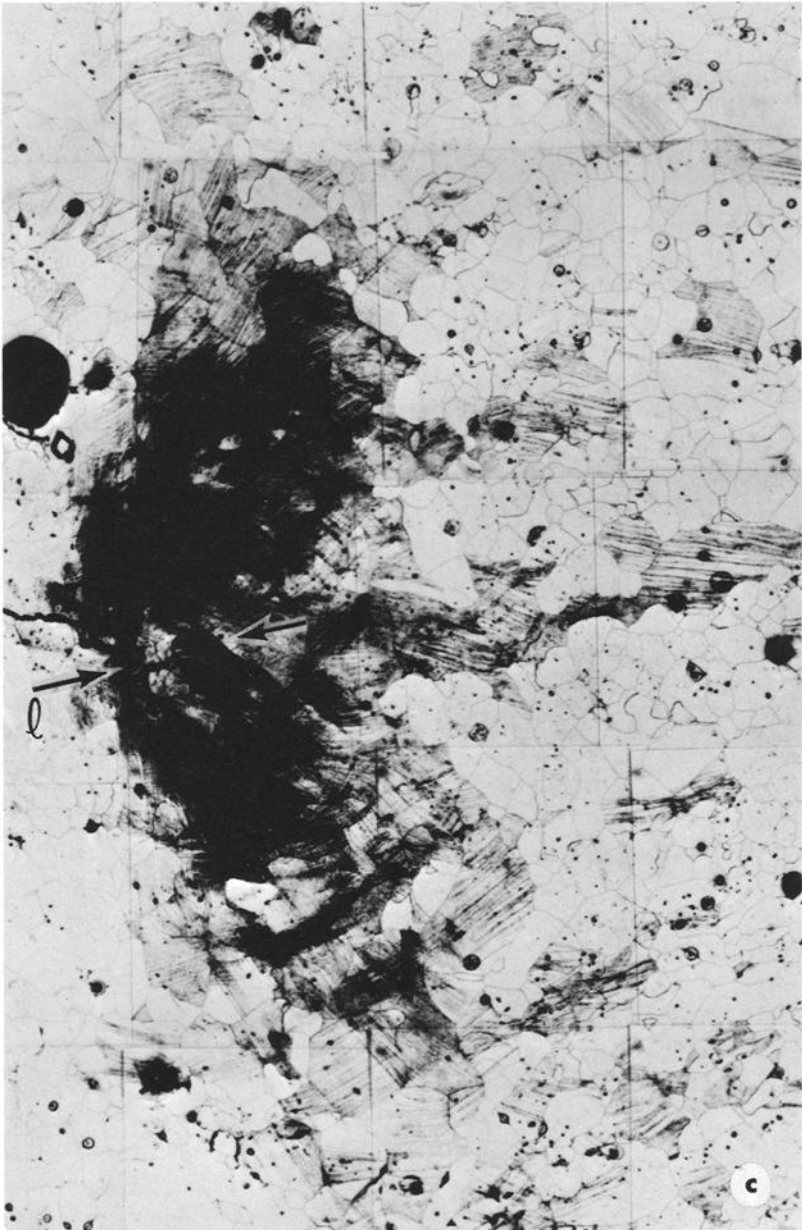
(a) Plate surface and (b) plate midsection, $K/Y = 0.3 \sqrt{\text{in.}} = 1.51 \sqrt{\text{mm}}$, $(K/Y)^2 l/t = 0.36$, $l_{(a)} = 0.002 \text{ in.} = 0.5 \text{ mm}$.

FIG. 4—Examples of plane strain relaxation in precracked 0.250-in.-thick Fe-3Si steel plates revealed by etching after loading.

In other words, K_{Ic} and K_c have several unique properties:

1. They are material constants independent of crack length.
2. They identify the conditions for crack extension—the critical stress level-crack length combinations.
3. They can be related to basic material parameters, for example, σ^* and r^* .
4. In principle, the value of K_{Ic} and K_c can be determined from a single experiment, which involves breaking a precracked specimen in the laboratory and measuring the applied stress at fracture.

Commercial alloys also display constant K_{Ic} and K_c values in spite of the fact that these alloys yield and relax plastically at the crack tip. It is surprising: (a) because Eq 1 does not describe the stresses in an elastic-plastic material (compare Fig. 2a with b and c), and (b) because the maximum stress criterion is inappropriate for the common ductile



(c) Plate midsection, $K/Y = 0.45 \sqrt{\text{in.}} = 2.3 \sqrt{\text{mm}}$, $(K/Y)^2 l/t = 0.8$, $l_{(c)} \approx 0.005$ in. = 1.27 mm. ($\times 100$).

FIG. 4 (c)

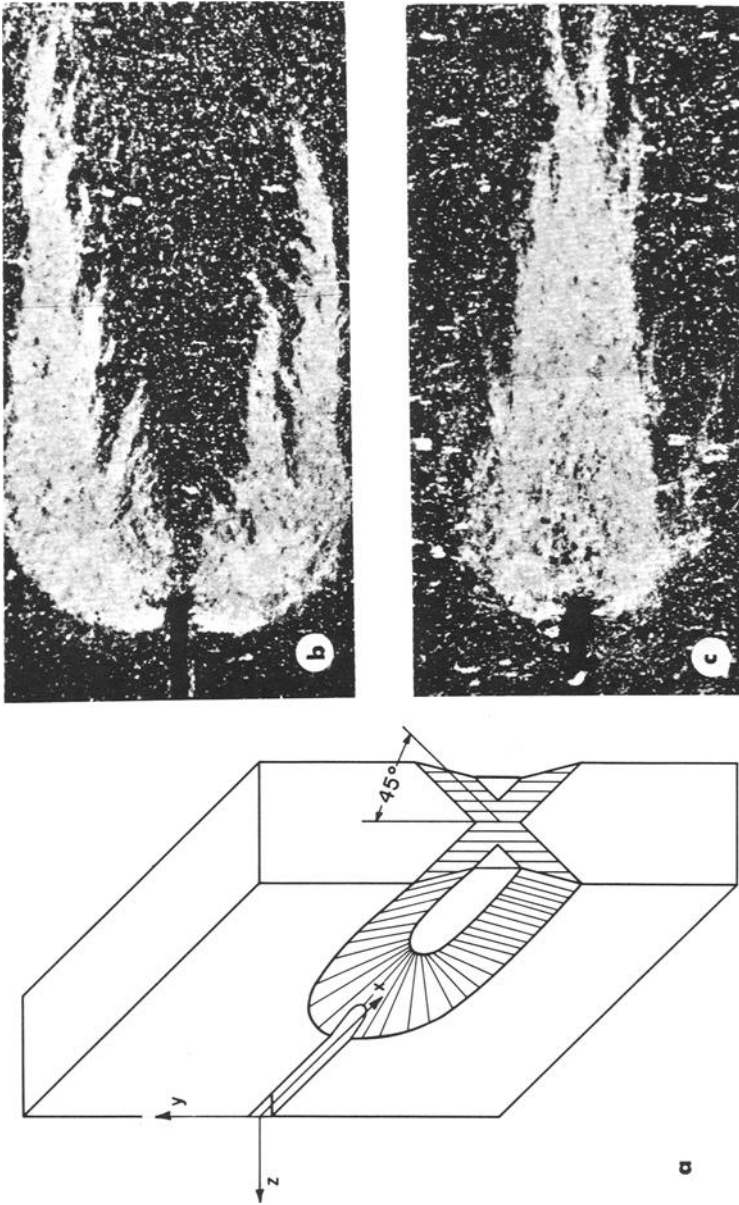


FIG. 5—Plane stress relaxation: (a) schematic, (b) plate surface, and (c) plate midsection are an actual zone revealed by etching a 0.128-in.-thick edge-notched silicon steel plate after loading to $K/Y = 0.76 \sqrt{\text{in.}} = 3.9 \sqrt{\text{mm}}$, $(K/Y)^2/t = 4.5$. Oblique lighting ($\times 13.5$).

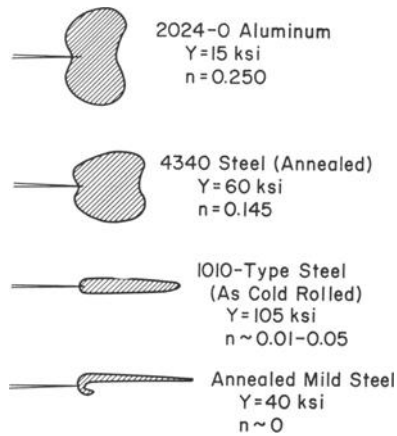


FIG. 6—Plane stress plastic zone shapes observed by Gerberich [12] and the present authors. The zones are not drawn to the same scale.

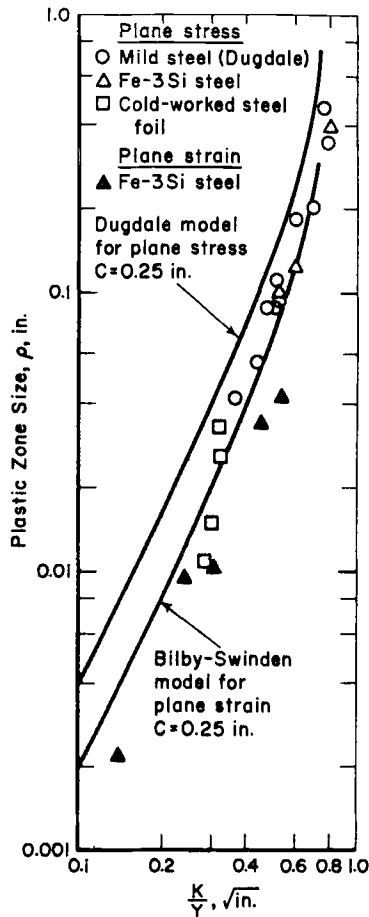


FIG. 7—Comparison of plastic zone size values derived from the simple models [4-6,11] with experiments. Details are given in Table 2.

modes of fracture [10]. At one time this ambivalence puzzled many workers, but it can now be understood in the light of several "pseudo" elastic-plastic crack tip analyses [4-6,11]. Two useful models are illustrated in Figs. 1b and c. These analyses are approximate because they

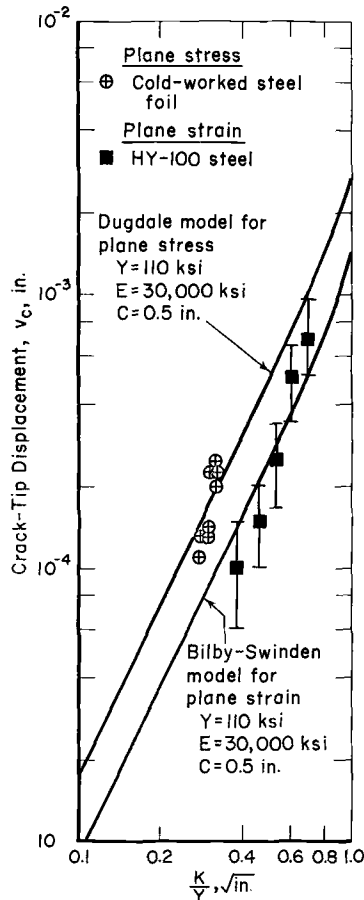


FIG. 8—Comparison of crack tip displacement values derived from the sample models [4-6,11] with experiments. Details are given in Table 2.

treat idealized plastic zones and neglect strain hardening, but they have the virtue of offering the relatively simple expressions listed in Table 1.

Table 1 illustrates that the general features of Irwin's elastic mechanics are also displayed by elastic-plastic solutions:

1. The term K continues to express the equivalence between applied stress and crack length (though only at low stress levels, that is, when $(T/Y) < 0.7$).

2. Such features as ρ , the plastic zone size, v_c the crack tip displacement, and ϵ_c the crack tip strain are monotonic—though not linear—

functions of K . This means that a fracture criterion based on a constant limiting value of either v_c or ϵ_c must lead to a constant value of K_{Ic} or K_{Ic} .

The simple elastic-plastic treatments also recognize an additional materials parameter: Y , the yield stress, but do not describe σ_{max} or ϵ_{max} , the peak tensile stress and strain at the crack tip, explicitly. These quantities depend on the exact geometry and on the strain hardening index, factors that are dealt with in the next two sections.

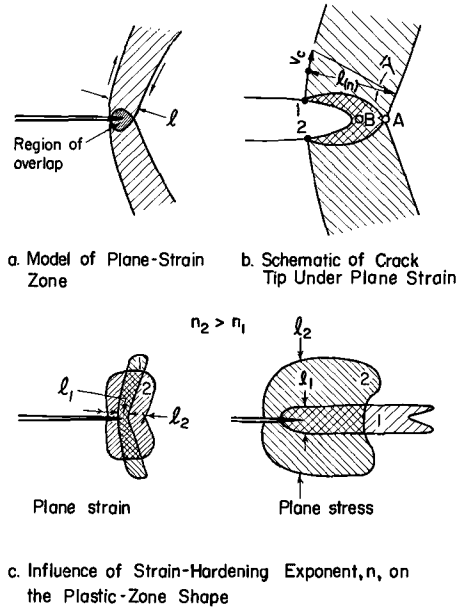


FIG. 9—Schematic drawings of plane strain and plane stress plastic zones showing the influence of strain hardening.

Plane Strain and Plane Stress Relaxation

Plastic relaxation at the crack tip takes two characteristic forms [11]:
Plane Strain—Figure 3 illustrates that the plastic zone has some of the features of a hinge when the zone is small relative to the plate thickness. Essentially no strains are observed in the thickness direction. The zone also has the same appearance on interior sections parallel to the plate surface (see Fig. 4). This implies that the plastic displacements are the same on the surface and on interior sections and that the displacement vectors are parallel to the plate surface, or, in other words, that the plastic relaxation is plane strain.

The two regions of shear on either side of the crack resemble the simple model (Fig. 1b). In both cases the extent of the zone—the distance ρ —becomes larger as K is increased. Note that the idealized zone (Fig. 1b) confines the shear to a single slip plane inclined at 45 deg,

TABLE 2—Description of zone size and displacement measurements.

Material	$Y, ^\circ \text{ksi}$	n	$t, \text{in.}^c$	Zone Type	$(K/Y)^{2/3} 1/t$	Quantity Measured	Technique	Reference
Fe-3Si steel.....	68	0.0 to 0.2 ^b	0.060 to 0.400	plane strain	0.01 to 0.9	ρ	etching internal surface	^a
HY-100 steel.....	109	~ 0.1	0.348	plane strain	0.5 to 1.4	v_c	moiré pattern on surface	^a
Fe-3Si steel.....	64	0.0 to 0.2 ^b	0.017	plane stress	15 to 37	ρ	etching	[12]
Mild steel (annealed).....	26	~ 0.0	0.050	plane stress	2.6 to 13	ρ	Lüders bands observed on surface	[6]
Mild steel (cold worked).....	105	0.01 to 0.05	0.002	plane stress	~ 50	ρ, v_c	interferometry	^a

^a Unpublished work by the authors.

^b The stress-strain curve for this material displays a Lüders extension ($n \approx 0$) followed by work hardening ($n \approx 0.2$).

^c These data may be expressed in metric form by multiplying stress in ksi by 0.7031 to obtain kgf/mm² and inches by 25.4 to obtain mm.

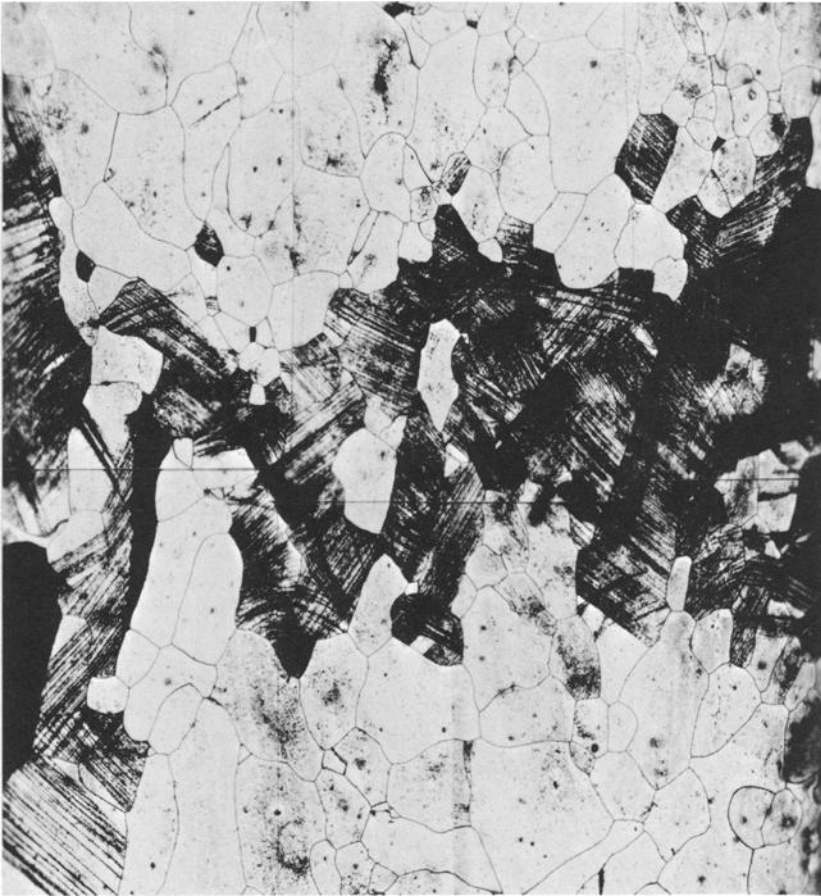


FIG. 10—The central portion of the etched cross section of the plastic zone reproduced in Fig. 3b. Etching reveals some through-the-thickness deformation even though the relaxation is predominantly plane strain, for example, $(K/Y)^2 l/t = 0.95$ ($\times 200$).

while the real zones poses a finite width and an inclination closer to 75 deg. Real zones are, in fact, quite narrow close to the crack tip. This is important because the zones accommodate relatively large displacements, and this means that they also harbor intense plastic strains.

Another feature of the plane strain zone is the constraint imposed on it by the surrounding elastic matrix. This produces a triaxial stress state in the interior of the plate which can support normal stresses as high as $2.7 Y$.⁵

⁵ Plasticity theory suggests that maximum constraint $\sigma_{\max}/Y = 2.7$ is attained ahead of a sharp crack as soon as the plastic zone appears. On the other hand, a special interpretation of experimental data has suggested to the authors that the constraint develops gradually [9]: $(\sigma_{\max}/Y) \approx 1 + 2(K/Y)$. This relation, consistent with crack length expressed in inches, was used to construct Fig. 2b, but it is open to question.

Plane Stress—When the extent of the hinge zone is comparable to the plate thickness, shear on planes inclined at 45 deg can penetrate the plate. Through-the-thickness deformation then supplants the hinges, and this is illustrated in Fig. 5. This form of relaxation cannot support stresses normal to the plate surface. For this reason, the triaxial stress state decays to a biaxial or plane stress state. In contrast to the plane strain zone, peak stress values here cannot be greater than the yield or flow stress, and this is shown in Fig. 2*b*.

Another important difference is that the width of the plane stress zone is relatively free to spread out normal to the tensile axis. The same crack-tip displacement, therefore, will produce a smaller strain concentration under plane stress than under plane strain. However, the zone can be quite narrow even under plane stress when the material does not strain harden, for example, when it displays a Lüders' extension. Such narrow wedge-shaped zones are illustrated in Fig. 6*d* and closely resemble the Dugdale model.

Plane strain and plane stress represent two extremes that describe some, but bracket most, of the situations encountered in practice. They are useful concepts because they are associated with the lower and the upper limit of toughness and because they are easier to deal with analytically. Figures 7 and 8 compare, with experiments, the following theoretical expressions for ρ and v_c , the zone size and crack-tip displacement derived from the simple elastic-plastic models [4,5,11] (Fig. 9):⁶

⁶ The curves drawn in Figs. 7 and 8 are actually derived from the more complete forms of these expressions:

$$\rho_{(\text{plane strain})} = \frac{C}{2} \left[\sec \left(\frac{\pi T}{2Y} \right) - 1 \right] \dots \dots \dots (6a)$$

$$\rho_{(\text{plane stress})} = C \left[\sec \left(\frac{\pi T}{2Y} \right) - 1 \right] \dots \dots \dots (7a)$$

$$v_{c(\text{plane strain})} = \frac{2YC}{\pi E} \ln \sec \left(\frac{\pi T}{2Y} \right) \dots \dots \dots (8a)$$

$$v_{c(\text{plane stress})} = \frac{4YC}{\pi E} \ln \sec \left(\frac{\pi T}{2Y} \right) \dots \dots \dots (9a)$$

which reduce to Eqs 6 to 9 at low stress levels, that is, when $T/Y < 0.7$. At the high stress levels, the equivalence between T and \sqrt{C} expressed by K is not obeyed. Also note that while the quantities ρ and v_c are clearly defined for the simple models, their meaning becomes fuzzy when the zone is spread out. The experimental values quoted here are defined in Figs. 1 and 9. The value of v_c under plane strain is the plastic part of the displacement at the edge of the zone (between the Points 1 and 2 in Fig. 9*b*). Under plane stress it is the plastic part of the displacement across the entire enclave at the crack tip (marked I_1 and I_2 in Fig. 9*d*). Since the materials described here work harden little (HY-100 steel is the exception), the zones are narrow and the two sets of definitions are nearly the same.

$$\rho_{(\text{plane strain})} \approx \frac{\pi}{16} \left(\frac{K}{Y}\right)^2 \dots\dots\dots (6)$$

$$\rho_{(\text{plane stress})} \approx \frac{\pi}{8} \left(\frac{K}{Y}\right)^2 \dots\dots\dots (7)$$

$$v_{c(\text{plane strain})} \approx \frac{Y}{4E} \left(\frac{K}{Y}\right)^2 \dots\dots\dots (8)$$

$$v_{c(\text{plane stress})} \approx \frac{Y}{2E} \left(\frac{K}{Y}\right)^2 \dots\dots\dots (9)$$

Relatively few systematic measurements of these quantities have been reported so far, especially values reflecting predominantly plane strain

TABLE 3—Estimates of limiting conditions for plane strain and plane stress relaxation and fracture.

Type	ρ	$(K/Y)^2 1/t$
<i>Plane Strain:</i> ^a		
Relaxation and fracture.....	$< t/4, < t/10^d$	$< 1.3, < 0.4^d$
<i>Plane Stress:</i>		
Relaxation ^b	$> 2t^e$	> 5.2
Fracture ^c	$> 4t^e$	> 10.4

^a Deformation is and fracture is preceded by predominantly plane strain relaxation, and there is no significant loss of constraint as a result of through-the-thickness relaxation.

^b Transition to plane stress state is substantially complete, although distribution of strain within plastic zone is still influenced by prior plane strain relaxation.

^c Deformation and stress history preceding fracture is predominantly plane stress.

^d More conservative limits proposed by Brown and Srawley [16] to assure a plane strain fracture with no loss of constraint.

^e Plane stress zone size.

or plane stress relaxation that are not complicated by slow crack growth. The measurements quoted here are described more fully in Table 2. They show that Eqs 6 to 9 are not only sound qualitative guidelines but can also offer reasonably good quantitative descriptions. Additional evidence along these lines has been reported by Wells [13], who first drew attention to the connection between v_c and K , and also by Tetelman [14]. These conclusions are based on materials that display little or no strain hardening. The equations may have to be modified for materials that strain harden extensively.

Etching reveals that the transition from plane strain to plane stress is a gradual process. For example, Fig. 10, a section normal to the zone reproduced in Fig. 3*b*, shows evidence of through-the-thickness deformation at a stage where $\rho_{(\text{plane strain})} = t/6$ (t is the plate thickness). Even Fig. 4 shows evidence of some through-the-thickness deformation, and here $\rho_{(\text{plane strain})} = t/25$. Through-the-thickness deformation does

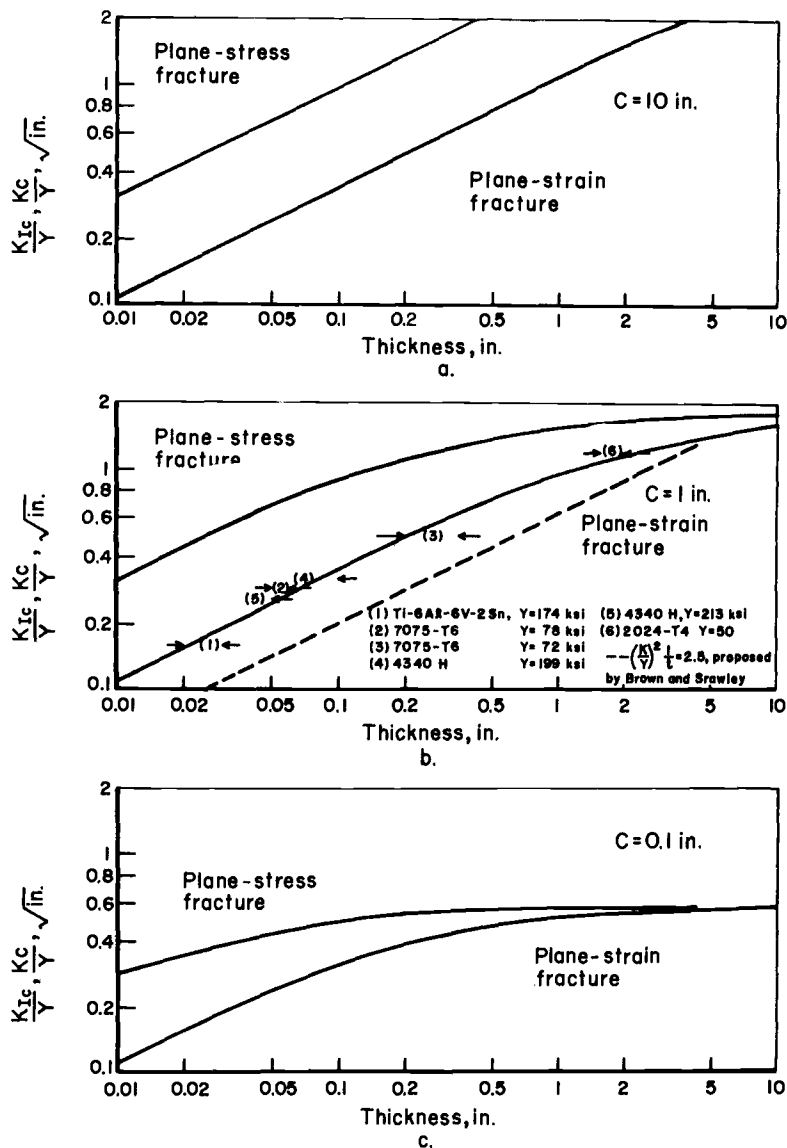
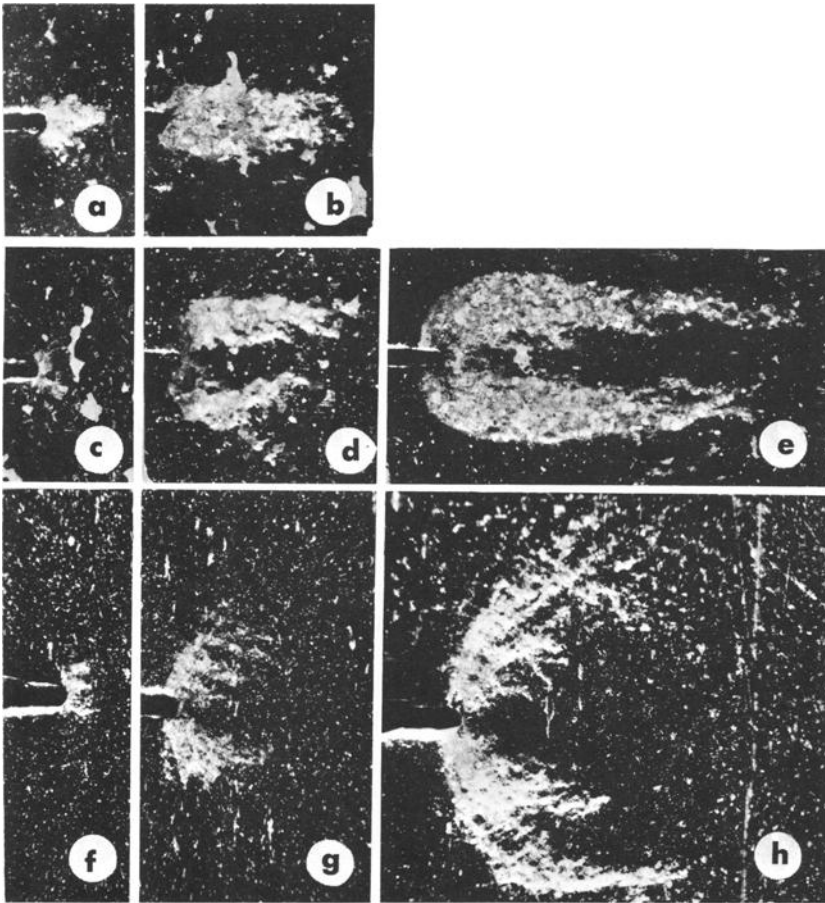


FIG. 11—Limits for plane strain and plane stress fracture calculated for (a) $C = 10$ in. 25.4 mm, (b) $C = 1.0$ in. 2.54 mm, and (c) $C = 0.1$ in. 0.254 mm. Arrows identify the thickness range within which fracture toughness values measured by Irwin [15] and Brown and co-workers [17] begin to increase with decrease in plate thickness.

become noticeable when $\rho_{(\text{plane strain})} = t/2$, and this means that it begins to detract sooner from plane strain relaxation and the attending triaxiality. On this basis $\rho_{(\text{plane strain})} = t/4$ is a reasonable first estimate of the beginning of a significant shift away from plane strain. This condition, equivalent to $(K/Y)^2 1/t = 1.3$ at low stress levels, is shown



- (a) [6.4] $t = 0.017$ in. (0.43 mm)
 (b) [14] $t = 0.017$ in. (0.43 mm)
 (c) [1.1] $t = 0.058$ in. (1.5 mm)
 (d) [4.2] $t = 0.058$ in. (1.5 mm)
 (e) [8.2] $t = 0.058$ in. (1.5 mm)
 (f) [0.54] $t = 0.200$ in. (5.1 mm)
 (g) [1.2] $t = 0.200$ in. (5.1 mm)
 (h) [2.1] $t = 0.200$ in. (5.1 mm)
 (i) [2.7] $t = 0.200$ in. (5.1 mm)

FIG. 12—Influence of stress level and thickness on the appearance of plastic zones revealed by etching edge-notched Fe-3Si steel plates. Photographs show zones etched on plate surface. Oblique lighting ($\times 9.5$). The numbers in the brackets are the values of $(K/Y)^2 1/t$.

graphically for three different crack lengths in Fig. 11. As shown in Fig. 11b, it is in good accord with upper limits for plane strain deduced from K_{Ic} measurements. The limiting condition proposed by Brown and Srawley (see Fig. 11b and Table 3) is similar but more conservative [16].

The plastic zone is a mixture of plane strain and plane stress relaxation when $\rho_{(\text{plane strain})} = t/2$ or $(K/Y)^2 1/t = 2.6$, and this can be seen in Fig. 12*h* and *i*. The zones revealed by etching show that the deformation occurring when $\rho_{(\text{plane stress})} = 2t$ is mainly of the through-the-thickness variety (see Fig. 10*d*), and this is a tentative and approximate lower limit for plane stress. However, at this stage much of the accumulated deformation is still of the plane strain variety. Consequently, ρ at fracture must be even larger, that is, $>4t$, for the fracture to have a



FIG. 12—(Continued.)

strong history of plane stress, consistent with the definition of K_c used here.⁴ These limits are summarized in Table 3 and graphed in Fig. 11.

Strain and Strain Hardening

The expressions for crack-tip displacement, Eqs 8 and 9, are the simplified elastic-plastic counterparts of Eq 1. However, the displacement values only become meaningful to the metallurgist when they are converted to local plastic strain. This can be done approximately with the help of additional experimental inputs. For example, the etching results (Figs. 3 and 4) suggest that the plane strain zone can be modeled by two regions of shear. Near the crack tip these regions overlap and have a finite width l , as shown in Fig. 9. In a similar way, plane stress zones

can also be characterized by a finite width l (see Fig. 9). The value of l is *not* a constant for each type of zone but depends on stress level and strain hardening rate. For example, plane strain zones reproduced in Fig. 4 show $l \sim 0.002$ in. (0.5 mm) for $K/Y = 0.3 t$ and $l \sim 0.005$ in. (1.3 mm) for $K/Y = 0.45$. The influence of strain hardening may be even more important. Figure 6 illustrates systematic changes in the shape of the plane stress zone that accompany changes in n , the strain hardening exponent. Such an increase in l and the accompanying decrease in the strain concentration at the crack tip was first noted by Gerberich [12], and other examples can be found in his paper. Although evidence of this kind for plane strain zones is lacking, a similar effect is to be expected, and this is shown schematically in Fig. 9c.

Etched zones also show that the strain is not uniform across the sheared region. In the calculations that follow a linear shear strain gradient is assumed, but this is merely a crude, first approximation. The situation is made even more complicated under plane stress by the necking instability that usually precedes crack extension. This tends to confine strain in the final stages of loading to a region comparable to the sheet thickness. To emphasize the fact that l is related to strain hardening and thickness the symbols $l_{(n)}$ and $l_{(n,t)}$ are used to denote the zone width under plane strain and plane stress, respectively.

As shown in Fig. 9b, $\bar{\gamma}_c$, the average shear strain at the crack tip in one of the sheared regions is [9]:

$$\bar{\gamma}_c \approx \frac{v_c}{l_{(n)}}; \dots\dots\dots (10)$$

The average tensile strain $\bar{\epsilon}_c$ in the region where the zones overlap is:

$$\bar{\epsilon}_c \approx \frac{v_c}{l_{(n)}} \dots\dots\dots (11)$$

Assuming that the distribution of strain is linear, ϵ_c the peak crack tip strain is:

$$\epsilon_c \approx 2\bar{\epsilon}_c, \dots\dots\dots (12)$$

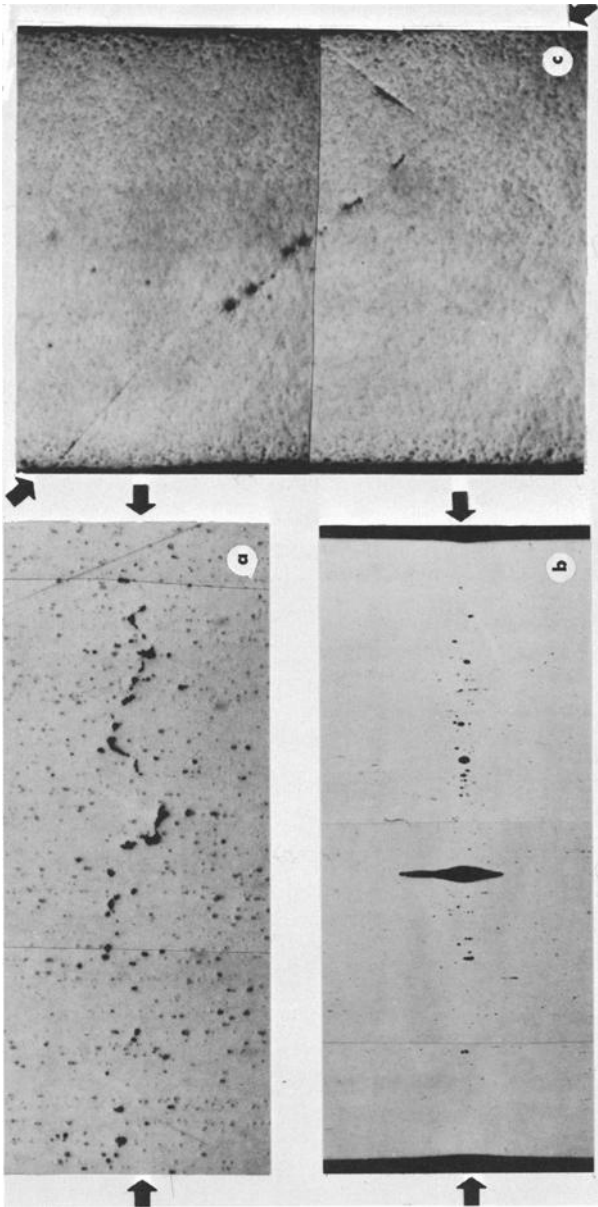
combining Eqs 8, 11, and 12 gives the sought-for result:

$$\text{plane strain } \epsilon_c \approx \frac{Y}{2l_{(n)}E} \left(\frac{K}{Y}\right)^2 \dots\dots\dots (13)$$

For plane stress, we have shown [11] that $\bar{\epsilon}_c \approx 2v_c/l_{(n)}$ and by a similar argument to that used in deriving Eq 13:

$$\text{plane stress } \epsilon_c \approx \frac{2Y}{l_{(n,t)}E} \left(\frac{K}{Y}\right)^2 \dots\dots\dots (14)$$

Evidence that Eq 13 can offer reasonable estimates of the local strain



(a) 7075-T6 aluminum, $Y = 73$ ksi (51 kg/mm^2), reduction of area = 35 per cent, $K = 42 \text{ ksi } \sqrt{\text{in.}}$ ($150 \text{ kgf/mm}^{3/2}$), $(K/Y)^{21}/t = 3.5$. Section taken 0.006 in. (1.5 mm) from the crack tip ($\times 100$). (b) Mild steel, $Y = 41$ ksi (29 kgf/mm^2), reduction of area = 56 per cent, $K = 37 \text{ ksi } \sqrt{\text{in.}}$ ($132 \text{ kgf/mm}^{3/2}$), $(K/Y)^{21}/t = 1.6$. Section taken 0.002 in. (0.5 mm) from the crack tip ($\times 10$). (c) Ti-6Al-4V, $Y = 139$ ksi (98 kgf/mm^2), reduction of area = 46 per cent, $K = 155 \text{ ksi } \sqrt{\text{in.}}$ ($550 \text{ kgf/mm}^{3/2}$), $(K/Y)^{21}/t = 30$. Section taken near the tip of a slowly growing crack 0.041 in. (1 mm) from the notch ($\times 100$).

FIG. 13—Metallographic evidence of incipient cracking displayed by stressed but unbroken plates in the heavily deformed region ahead of a sharp notch. Sections are normal to the plate surface and the crack plane (the latter is indicated by arrows).

at low stress levels, that is, $T/Y < 0.7$ is contained in Appendix B, Ref 9. Equation 14 is less accurate, and both expressions should be regarded only as first approximations.

Ductile Fracture Criteria

Ductile fracture frequently involves the nucleation of voids and the linking up of these voids to form a crack. Several examples of incipient ductile cracking in the heavily strained region just ahead of a crack are reproduced in Fig. 13. McClintock [18,19] has recently calculated the critical true strain, $\bar{\epsilon}^*$ that will expand a system of cylindrical void

TABLE 4—Stress states and corresponding ductility values.

Type	$(\sigma_{max} + \sigma_T)/\bar{\sigma}$	$\bar{\epsilon}^*/\bar{\epsilon}^*(\text{tension test})$	
		Calculated, ^a	Measured, ^f
Round tensile bar (with necking) . . .	1 to 1.7 ^a	1.0	...
Pure plane stress ^b	1.5	1.0	...
Plane stress zone ^c (with necking in the thickness direction)	~2.1	~0.65	0.52, ^g 0.52, ^h 0.39 ⁱ
Plane strain zone ^d (maximum constraint)	~4.7	~0.10	...

$\bar{\epsilon}^*$ True fracture strain.
^a Calculated from Ref 10 for $\bar{\epsilon}^* = 0$ to 1.0.
^b $\sigma_1 = \bar{\sigma}, \sigma_2 = \frac{1}{2}\bar{\sigma}, \sigma_3 = 0, \epsilon_1, \epsilon_2 = 0, \epsilon_3 = -\epsilon_1$.
^c $\sigma_1 = 1.3\bar{\sigma}, \sigma_2 = 0.8\bar{\sigma}, \sigma_3 = 0.3\bar{\sigma}, \epsilon_1, \epsilon_2 = 0, \epsilon_3 = -\epsilon_1$.
^d $\sigma_1 = 2.6\bar{\sigma}, \sigma_2 = 2.1\bar{\sigma}, \sigma_3 = 1.6\bar{\sigma}, \epsilon_1, \epsilon_2 = 0, \epsilon_3 = -\epsilon_1$.
^e Calculated for Refs 18, 19.
^f Measured at the midsection of a deep, blunt-notched sheet coupon, notch root radius = $2t$.
^g 2219-T86 Al: $Y = 59$ ksi, $\bar{\epsilon}^*(\text{tension test}) = 0.45, n = 0.085$.
^h 7075-T6 Al: $Y = 73$ ksi, $\bar{\epsilon}^*(\text{tension test}) = 0.45, n = 0.061$.
ⁱ Type 4340 steel: $Y = 189$ ksi, $\bar{\epsilon}^*(\text{tension test}) = 0.60, n = 0.064$.

nuclei to the stage where the voids link-up. These calculations indicate that $\bar{\epsilon}^*$ is markedly reduced by a triaxial stress state, that is, large values of $(\sigma_{max} + \sigma_T)/\bar{\sigma}$ where σ_{max} is the normal stress, σ_T the transverse stress (normal to the cylinder axis) and $\bar{\sigma}$ the flow stress. Table 4 compares the stress state in uniaxial tension with that existing in the plane stress and plane strain plastic zone ahead of a crack, and the corresponding critical strain values derived from the McClintock treatment. Experimental results for deep blunt-notched sheet coupons (which approximate the plane stress zone) are also quoted, and these tend to support the calculations. However, the large reduction in the ductility of material within a plane strain zone is difficult to check and open to question. For one thing, there is some evidence that full triaxiality is not attained immediately [9]. Even if it is, the triaxiality will be generated near the elastic-plastic boundary where the plastic strain is small (near A in Fig. 9b), while the peak strains will occur near the root of the crack

(near B in Fig. 9b) where a plane stress state prevails. Consequently, the ductility under plane strain may be quite similar to plane stress. There are further complications because of the directionality of properties. It is well known that flat rolled products are weakest in the thickness direction. Whereas a transverse stress is developed in this direction under plane strain, no such stress is developed under plane stress. On this basis the following are not unreasonable as first approximations:

$$\bar{\epsilon}^*_{(\text{ahead of a crack})} \propto \bar{\epsilon}^*_{(\text{tension test})} \dots \dots \dots (15a)$$

and

$$\bar{\epsilon}^*_{(\text{plane strain zone})} \sim (1/3)\bar{\epsilon}^*_{(\text{tension test})} \dots \dots \dots (15b)$$

TABLE 5—Summary of K_{Ic} , tensile properties and the $l_{(n)}$ values calculated for a number of aluminum, titanium, and steel alloys.

Alloy, References	E, ksi	Y, ksi	$\frac{K_{Ic}^b}{\text{ksi-in.}^{1/2}}$	ϵ^*	n	$l_{(n)}^*$ (in.) Calculated
2219-T87 [20,22].....	1.0×10^4	59	33	0.39	0.085	7.1×10^{-3}
7075-T6 [20,21,24,26].....	1.0	73	37	0.34	0.061	6.5×10^{-3}
2014-T6 [24].....	1.0	68	35	0.37	0.08	7.5×10^{-3}
2024-T4 [15,26].....	1.0	50	59	0.32	0.16	3.2×10^{-2}
Ti-8Al-1Mo-1V [25].....	1.7	145	76	0.34	0.11	1.00×10^{-2}
Ti-6Al-4V [24,25].....	1.7	138	49	0.56	0.05	2.7×10^{-3}
Ti-5Al-2.5Sn ELI ^a [27].....	1.7	170	60	0.36	0.06	4.6×10^{-3}
4330M [20,23].....	3.0	189	90	0.60	0.064	3.5×10^{-3}
18Ni Maraging [28,29].....	3.0	275	70	0.76	0.013	7.8×10^{-4}
4340(400) [28,30].....	3.0	210	65	0.60	0.056	1.7×10^{-3}
4340(600) [28,30].....	3.0	200	65	0.80	0.028	1.3×10^{-3}

^a - 196 C.

^b K_{Ic} may be expressed in metric form by multiplying the values in this Table by 3.57 to obtain the value in kgf/mm^{3/2}.

and

$$\bar{\epsilon}^*_{(\text{plane stress zone})} \sim (1/2)\bar{\epsilon}^*_{(\text{tension test})} \dots \dots \dots (15c)$$

Although only Eq 15a is essential to the argument presented here, it is probably the crudest of the assumptions made and the largest source of error.

Calculating Fracture Toughness

The parameters K_{Ic} and K_c can now be formulated by combining Eqs 13 and 14, the expressions for the peak strain, with Eqs 15b and 15c which describes the critical strain for ductile rupture, and by noting that, by definition, K_{Ic} , $K_c = K_{(\epsilon_c = \epsilon^*)}$:

$$K_{Ic} \approx \sqrt{(2/3)EYl_{(n)}^* \bar{\epsilon}^*} \dots \dots \dots (16)$$

$$K_c \approx \sqrt{(1/4)EYl_{(n,t)}^* \bar{\epsilon}^*} \dots \dots \dots (17)$$

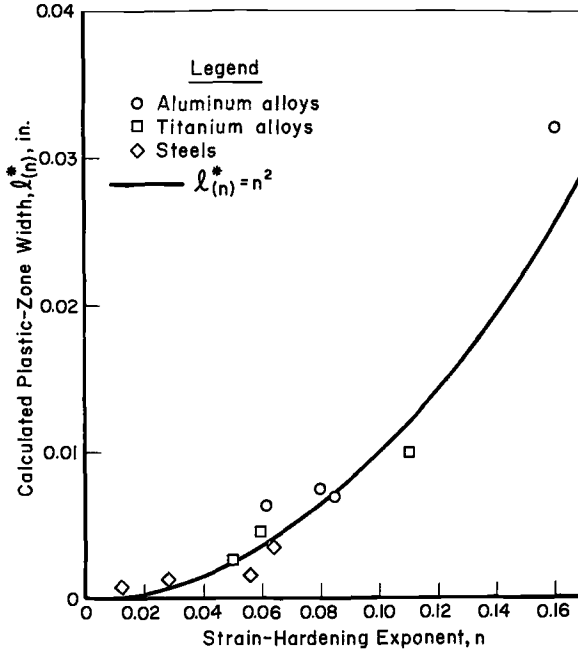


FIG. 14—Relation between calculated values of the plastic zone width $l^*(n)$, and the strain hardening index for the alloys in Table 5.

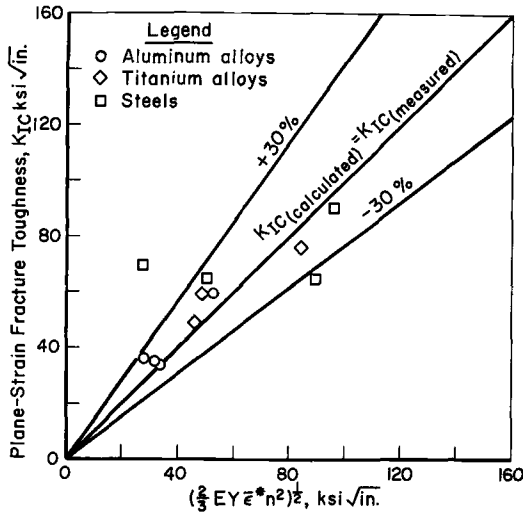


FIG. 15—Comparison of measured K_{Ic} values with values calculated from ordinary tensile properties with Eq 19.

where $l^*_{(n)}$ and $l^*_{(n,t)}$ are the values of l at the onset of cracking. One way of testing these expressions is to calculate the value of l^* when K_{Ic} (or K_c) E , Y and $\bar{\epsilon}^*$ are known and compare this value with measurements. This is done in Table 5 for a number of alloys for which K_{Ic} ,

E , Y , $\bar{\epsilon}^*$ and n are known. Most of the values range from $l_{(n)}^* = 0.001$ to 0.007 in. (0.25 to 1.8 mm), and this agrees with the value of l displayed by plane strain zones in Fe-3Si steel at comparable K/Y levels. This supports the idea that the value of $l_{(n)}^*$ is not artificial but has a physical basis.

The value of $l_{(n)}^*$ should also depend on strain hardening, and this is also borne out. When the $l_{(n)}^*$ values calculated for eleven different alloys are plotted in Fig. 14 against n , the strain hardening exponent, a correlation is obtained:

$$l_{(n)}^* \text{ (inches)} \approx n^2 \dots \dots \dots (18)$$

This correlation not only contains the effect of n on $l_{(n)}^*$ but makes adjustments for: (a) the effects of n on the flow stress, on v_c and on the ductility criterion, and (b) any errors in the assumptions for $\bar{\gamma}$ and ϵ_c .

The term $l_{(n)}^*$ can now be replaced by n^2 in Eq 16:

$$K_{Ic} \approx \sqrt{(\frac{2}{3})EY\bar{\epsilon}^*n^2} \dots \dots \dots (19)$$

Figure 15 shows that all but one of the measured K_{Ic} values in Table 5 can be predicted from tensile properties to within \pm about 30 per cent with this expression. The one exception is the 18 per cent nickel maraging steel which has an unusually low strain hardening exponent ($n = 0.013$). The value quoted may be in error. Alternatively, a more complicated form of Eq 18, that is, $l_{(n)}^* \approx (0.0005 + n^2)$ inches, is more appropriate when $n < 0.02$, and if this were used all the values would fall within the ± 30 per cent limits. In view of the relatively small volume of data drawn on by the correlation, this refinement is probably not yet warranted. The precision with which the calculations match the experiments must be regarded as very good considering: (a) that measured K_{Ic} values frequently vary from specimen to specimen and laboratory to laboratory by more than ± 10 per cent, (b) that the n values used may not be exact, and (c) that strain hardening effects have been neglected until the very end. Finally, it should be noted that the same approach can be used to formulate the value of $l_{(n,t)}^*$, when more K_c values (as defined here) become available.

Discussion

The conclusion that strain hardening has an important influence on crack extension resistance is not new; Krafft [31] and Krafft and Irwin [32] have also proposed that $K_{Ic} \propto n$, but arrive at this conclusion by a different route.⁷ Other data supporting a linear relation between K_{Ic} and n have been reported by Lauter and Steigerwald [28].

⁷ Krafft [31] assumes that $\epsilon^* = n$ and that the elastic strain gradient is valid near the crack tip. This gives the result: $K_{Ic} = \sqrt{2\pi E^2 n^2 d}$, where $r_{(t=n)} = d$, and d is regarded as a ligament spacing. The difficulty with this approach is that the assumptions are open to question.

The role of strain hardening helps to explain the general effect of heat treating on K_{Ic} . Higher yield stress values are usually obtained in this way at the expense of strain hardening (and sometimes at the cost of ductility). The differential form of Eq 19:

$$\frac{\Delta K_{Ic}}{K_{Ic}} = \frac{1}{2} \frac{\Delta Y}{Y} + \frac{1}{2} \frac{\Delta \bar{\epsilon}^*}{\bar{\epsilon}^*} + \frac{\Delta n}{n} \dots \dots \dots (20)$$

shows that the value of K_{Ic} tends to fall unless the fractional increase in yield stress is twice the accompanying decrease in n . The data reproduced in Fig. 16a and b illustrate this effect. Figure 16a reproduces the tensile properties of 4340 steel tempered at different temperatures from 375 to

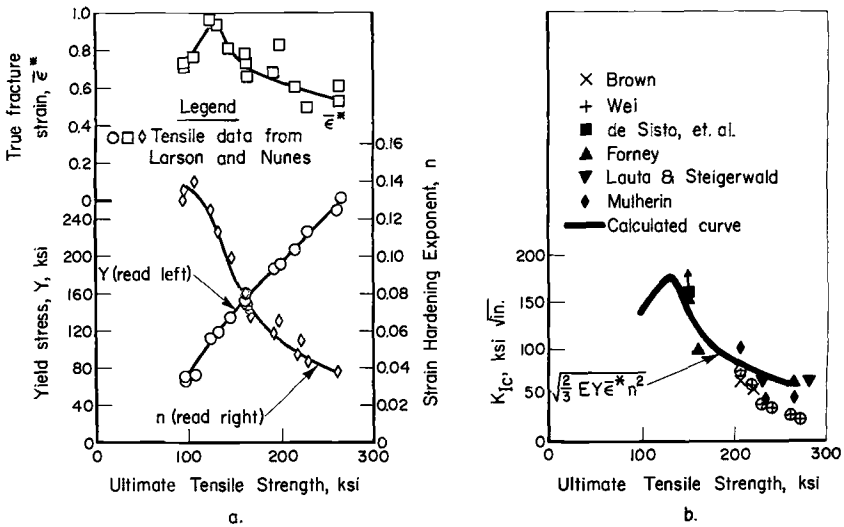


FIG. 16—Properties of Type 4340 steel heat treated to different strength levels: (a) tensile properties reported by Larson and Nunes [30] and (b) K_{Ic} values calculated from (a) and measured by different investigators [16,24,28,30,33–35].

1200 F (190 to 650 C). Over this range the yield stress shows a 4-fold increase, n a $3\frac{1}{2}$ -fold decrease, and $\bar{\epsilon}^*$ shows increases and decreases. These properties were used to calculate K_{Ic} , and the results are compared with actual measurements taken from the literature. The agreement is reasonably good considering that the comparison involves different heats of Type 4340. They show the expected trend to lower K_{Ic} values at the higher strength levels, and this is associated mainly with the reduced strain hardening. Discrepancies at the highest stress levels may be caused by the onset of a “cleavage-type” fracture mechanism [36] that does not obey a strain criterion. Figure 16 illustrates another advantage of Eq 19. By relating K_{Ic} with the ordinary tensile properties, it offers a way of bringing existing metallurgical experience to bear on fracture toughness problems. The K_{Ic} values of new alloys can be anticipated. The prospect

of a higher strength level can be weighed against a projected reduction in K_{Ic} . Effects of composition, microstructure, and even texture may be interpreted more easily. In some cases, it may be possible to insure a minimum K_{Ic} level by specifying permissible variations in the tensile properties. Finally, the analysis draws attention to the important role of ductility and especially strain hardening rate (or the yield to ultimate ratio which is closely related to n) and the need for improving these along with yield stress to produce even tougher alloys.

Conclusions

1. This paper identifies four basic factors that contribute to the fracture toughness of metals: (a) the character of plastic relaxation at the crack tip—whether it is plane strain or plane stress, (b) the amount of plastic flow near the crack tip, (c) the peak strain generated, and (d) the critical strain for ductile rupture. These factors can be described numerically with the aid of two simplified elastic-plastic treatments.

2. The character of relaxation depends on the size of the plastic zone relative to the plate thickness. The absolute size of the zone $\rho \propto (K/Y)^2$.

3. The amount of flow is described in terms of a crack-tip displacement $v_c \propto Y/E(K/Y)^2$.

4. The peak strain is determined by the way the deformation is distributed. This is characterized by the dimension $l_{(n)}$, the width of the plastic zone close to the crack tip under plane strain, which depends on the strain hardening exponent, $l_{(n)} \propto n^2$. The peak strain $\epsilon_c \propto V_c/l_{(n)}$.

5. The critical true strain for coalescing voids $\bar{\epsilon}^*$ depends on the microstructure and state of stress and is related to the true strain at fracture displayed by ordinary tension specimens: $\bar{\epsilon}^*$ (ahead of a crack) $\propto \bar{\epsilon}^*$ (tension test).

6. The plane strain fracture toughness parameter K_{Ic} can be expressed in terms of ordinary tensile properties by combining the various descriptions and correlating the result with existing measurements: $K_{Ic} \approx \sqrt{2/3} EY\bar{\epsilon}^*n^2$. The expression is accurate to within about ± 30 per cent for eleven different aluminum, titanium, and steel alloys and offers useful insights to the metallurgical origins of K_{Ic} .

Acknowledgments

The authors wish to thank the Strength and Dynamics Branch of the Air Force Materials Laboratory, especially W. J. Trapp and A. W. Brisbane, for supporting the preparation of this report. They have drawn on research sponsored at Battelle Memorial Institute by this agency, The Ship Structure Committee, and The Army Research Office, and work for the American Gas Association which has previously been reported. The authors are grateful for the support of these groups. They also wish to thank R. I. Jaffee for his encouragement; A. K. Mukherjee,

P. N. Mincer, R. L. Stephenson, R. C. Barnes, T. L. Buckner, J. S. Duerr, and J. L. McCall, who made important contributions to the unpublished experimental work that is reported; and Carolyn Pepper for her help in preparing the manuscript.

References

- [1] *Fracture Toughness Testing and Its Applications, ASTM STP 381*, American Society for Testing and Materials, 1965.
- [2] Hahn, G. T. and Rosenfield, A. R., "Mechanics and Metallurgy of Brittle Crack Extension," *Proceedings of the American Society of Civil Engineers, Engineering Mechanics Division Specialty Conference*, Washington, D. C., Oct. 1966.
- [3] Inglis, C. E., "Stresses in a Plate Due to the Presence of Cracks and Sharp Corners," *Transactions of the Institute of Naval Architects*, Vol. 55, 1913, p. 219.
- [4] Bilby, B. A. and Swinden, K. H., "Representation of Plasticity at Notches by Linear Dislocation Arrays," *Proceeding*, Royal Society of London, Vol. 285, 1965, p. 22.
- [5] Rice, J. R., "The Mechanics of Crack Tip Deformation and Extension by Fatigue," Brown University Report on NSF Research Grant GK 286, May 1966.
- [6] Dugdale, D. S., "Yielding of Steel Sheets Containing Slits," *Journal of the Mechanics and Physics of Solids*, Vol. 8, 1960, p. 100.
- [7] McClintock, F. A. and Irwin, G. R., "Plasticity Aspects of the Fracture Mechanics," *Fracture Toughness Testing and Its Applications, ASTM STP 381*, American Society for Testing and Materials, 1965, p. 84.
- [8] Davis, P. C. and Sih, G. C., "Stress Analysis of Cracks," *Fracture Toughness Testing and Its Applications, ASTM STP 381*, American Society for Testing and Materials, 1965, p. 30.
- [9] Hahn, G. T. and Rosenfield, A. R., "Experimental Determination of Plastic Constraint Ahead of a Sharp Crack Under Plane-Strain Conditions," *Transactions*, American Society for Metals, Vol. 59, 1966, p. 909.
- [10] Bridgman, P. W., *Studies in Large Plastic Flow and Fracture*, Harvard Press, Cambridge, Mass., 1964.
- [11] Rosenfield, A. R., Dai, P. K., and Hahn, G. T., "Crack Extension and Propagation Under Plane Stress," *Proceedings of the First International Conference on Fracture*, Vol. 1, 1965, p. 223.
- [12] Gerberich, W. W. "Plastic Strains and Energy Density in Cracked Plates, Part I, Experimental Techniques and Results," *Experimental Mechanics*, Vol. 4, 1964, p. 335.
- [13] Wells, A. A., "Notched Bar Tests, Fracture Mechanics and Strength of Welded Structures," *British Welding Journal*, Vol. 12, No. 1, Jan. 1965.
- [14] Tetelman, A. S., "The Effect of Plastic Strain and Temperature on Microcrack Propagation in Iron—3% Silicon," *Acta Metallurgica*, Vol. 12, 1964, p. 993.
- [15] Irwin, G. R., "Fracture Mode Transition for a Crack Traversing a Plate," *Transactions*, American Society of Mechanical Engineers, Series D, Vol. 82, 1960, p. 417.
- [16] Brown, W. F. Jr., and Srawley, J. E., "Current Status of Plane Crack Toughness Testing," Technical Memorandum NASA TMX-52209, June 29, 1966.
- [17] Jones, M. H., Fisher, D. M., and Brown, W. F., Jr., "Progress Report on NASA-NRL Cooperative Fracture Testing Program," Oct. 12, 1966, also Jan. 23, 1967.
- [18] McClintock, F. A., "A Criterion for Ductile Rupture," (to be published).
- [19] Rosenfield, A. R. and Hahn, G. T., "Numerical Descriptions of the Ambient Low-Temperature, and High-Strain Rate Flow and Fracture Behavior of

- Plain Carbon Steel," *Transactions*, American Society for Metals, Vol. 59, 1966, p. 962.
- [20] Mukherjee, A. K. et al, "Notch Behavior in Metals," AFML-TR-66-266, Air Force Materials Laboratory Report, 1966.
- [21] Boyle, R. W., Sullivan, A. M., and Krafft, J. M., "Determination of Plain Strain Fracture Toughness with Sharply Notched Sheets," *Welding Journal*, Vol. 41, 1962, pp. 428s-432s.
- [22] Tiffany, C. F., Lorenz, P. M., and Hall, L. R., "Investigation of Plane-Strain Flow Growth in Thick Walled Tanks," NASA CR-54837, NASA Report, Feb. 1966.
- [23] Irwin, G. R. and Srawley, J. E., "Progress in The Development of Crack Toughness Fracture Tests," Presented to the Deutsches Verband für Material prüfung, Würzburg Meeting, March 1961.
- [24] Forney, J. W., "Fracture Toughness Evaluation of Titanium," Aluminum and Steel, Memorandum Report M66-20-1 (AD632926), Frankford Arsenal, 1966.
- [25] De Sisto, T. S., "The True Stress True Strain Properties of Titanium and Titanium Alloys as a Function of Temperature and Strain Rate," Report No. WAL-TR-405.2/4, Watertown Arsenal, 1959.
- [26] Kaufman, J. G., "True Stress-Strain Properties of Aluminum Alloys," Report No. 9-61-32, Alcoa Research Laboratory, Oct. 1961.
- [27] Carman, C. M., Forney, J. W., and Katlin, J. M., "Plane Strain Fracture Toughness and Mechanical Properties of 5A1-2.5Sn ELI Titanium at Room and Cryogenic Temperatures," FA Report R-1796, Frankford Arsenal, April 1966.
- [28] Lauta, F. J. and Steigerwald, E. A., "Influence of Work Hardening Coefficient on Crack Propagation in High-Strength Steels," AFML-TR-65-31, Air Force Materials Laboratory, May 1965.
- [29] Kula, E. B. and Hicky, C. F., "Evolution of Maraging Steels at The Army Materials Research Agency," Third Maraging Steel Project Review, RTD-TDR-63-4048, Air Force Materials Laboratory, Nov. 1963, p. 439.
- [30] Larson, F. R. and Nunes, J., "Low Temperatures Flow and Fracture Tension Properties of Heat Treated SAE 4340 Steel," *Transactions*, American Society for Metals, Vol. 53, 1961, p. 663.
- [31] Krafft, J. M., "Correlation of Plane Strain Crack Toughness with Strain Hardening Characteristics of a Low, a Medium, and a High-Strength Steel," *Applied Materials Research*, Vol. 3, 1963, p. 88.
- [32] Krafft, J. M. and Irwin, G. R., "Crack Velocity Considerations," *Fracture Toughness Testing and Its Applications*, ASTM STP 381, American Society for Testing and Materials, 1965, p. 84.
- [33] Wei, R. P., "Fracture Toughness Testing in Alloy Development," *Fracture Toughness Testing and Its Applications*, ASTM STP 381, American Society for Testing and Materials, 1965, p. 279.
- [34] De Sisto, T. S., Carr, F. L., and Larson, F. R., "The Influence of Section Size on the Mechanical Properties and Fracture Toughness of 7075-T6 Aluminum, 6Al-6V-2Si Titanium and AISI 4340 Steel," AMRATR64-05 Army Mats. Res. Agency, 1964.
- [35] Mulherin, J. H., "Stress-Corrosion Susceptibility of High-Strength Steel, in Relation to Fracture Toughness," *Transactions*, American Society of Mechanical Engineers, 1967 (Paper 66-Met-5).
- [36] Shih, C. H., Averbach, B. L., and Cohen, M., "Some Effects of Silicon on the Mechanical Properties of High-Strength Steels," *Transactions*, American Society for Metals, Vol. 48, 1956, p. 86.

A Review of Factors Influencing the Crack Tolerance of Titanium Alloys

REFERENCE: Shannon, J. L., Jr., and Brown, W. F., Jr., "A Review of Factors Influencing the Crack Tolerance of Titanium Alloys," *Applications Related Phenomena in Titanium Alloys, ASTM STP 432*, American Society for Testing and Materials, 1968, pp. 33-63.

ABSTRACT: The paper reviews a number of factors which influence the crack tolerance of titanium alloys, particularly those which are generally encountered in the application of titanium alloys to aerospace hardware. Among these factors are cryogenic temperatures, heat treatment, interstitial element content, elevated temperature exposure, cold working, and aggressive environments. In addition a discussion of plane strain fracture toughness data for titanium alloys is given.

KEY WORDS: fracture toughness, fracture mechanics, crack propagation, fracturing, titanium alloys

This paper is a review of information relating to a number of factors which influence the strength potential of titanium alloys in the presence of cracks or crack-like flaws. Ideally it would be desirable to discuss these strength limiting factors within the framework of linear elastic fracture mechanics and to report fracture toughness information in terms of the critical values of the stress intensity factors K_c or K_{Ic} . However, while both K_c and K_{Ic} information appear in the literature, serious problems of interpretation arise. This is because a major portion of the information was obtained before clearly defined fracture toughness testing procedures were established. Consequently the results are often not truly representative of the material to which they pertain. In this connection, we wish to emphasize that evaluation of sheet fracture properties by K_c (plane stress) testing has turned out to be much more complicated than first supposed and that at present there is no unambiguous definition for K_c [1,2].² For this reason, when discussing the fracture properties of sheet alloys, we prefer to report the notch strength

¹ Strength of Materials Branch, NASA Lewis Research Center, Cleveland, Ohio. Mr. Brown is a personal member ASTM.

² The italic numbers in brackets refer to the list of references appended to this paper.

(or the ratio of notch strength to the yield or tensile strengths) obtained from tests on sharply notched or fatigue-cracked specimens symmetrically loaded in tension. The notch strength of a fixed size of this type of specimen is a clearly defined quantity which can serve as a useful qualitative index of the tolerance to through-the-thickness cracks. One should remember, however, that the index so obtained applies only to the material thickness investigated and that tests on other thicknesses might alter conclusions derived from tests on the single thickness. On the other hand, the plane strain fracture toughness, K_{Ic} , is a thickness independent parameter which controls fracture behavior in sufficiently heavy sections, and when properly determined is a quantitative index of crack tolerance under plane strain conditions. A separate section of this report is devoted to a summary of results which we believe represent either true K_{Ic} values or useful estimates of these values. In this connection, we wish to point out that published K_{Ic} data derived from the fracture loads of surface cracked sheet specimens are often not valid. The difficulty arises primarily from the fact that the specimens are sometimes of insufficient thickness to insure that plane strain conditions exist at the maximum load [3]. However, the notch strength of such specimens is, of course, a useful indicator of the tolerance to this type of commonly encountered flaw.

A substantial amount of data appears in the literature relating to the strength of mildly notched specimens of various titanium alloys. While these data may be useful for special purposes, we do not know how to relate them to crack tolerances, and therefore have not included them in this survey. Information derived from drop weight tear tests and explosion tear tests such as employed by Pellini and his co-workers at the Naval Research Laboratory (NRL) is certainly valuable for assessing the performance of annealed titanium alloys in special classes of service such as deep diving submarines. However, as yet this type of information cannot be directly translated into plane strain fracture toughness values. For this reason data from these special Naval Research Laboratory tests are not reviewed here. The reader is referred to the reports issued on The Advanced High Strength Structural Metals Program at NRL (for example, [4]) for information concerning the behavior of titanium alloys using a variety of test methods.

There are, of course, a very large number of factors which influence the crack tolerance of metallic alloys; however, in this review we have included only those factors that are generally encountered in the application of titanium alloys to aerospace hardware. Among these are cryogenic temperatures, heat treatment, interstitial element content, elevated temperature exposure, cold working, and aggressive environments. A final section presents data on plane strain fracture toughness. We have not considered the influence of repeated loading nor have we attempted

to evaluate the fracture properties of weldments. Both of these factors are of great practical importance but require the use of special testing techniques tailored to a particular hardware design problem. Information relating to the general effects of repeated loading on crack propagation and to problems in weldment evaluation may be found in *ASTM STP 381* [5,6].

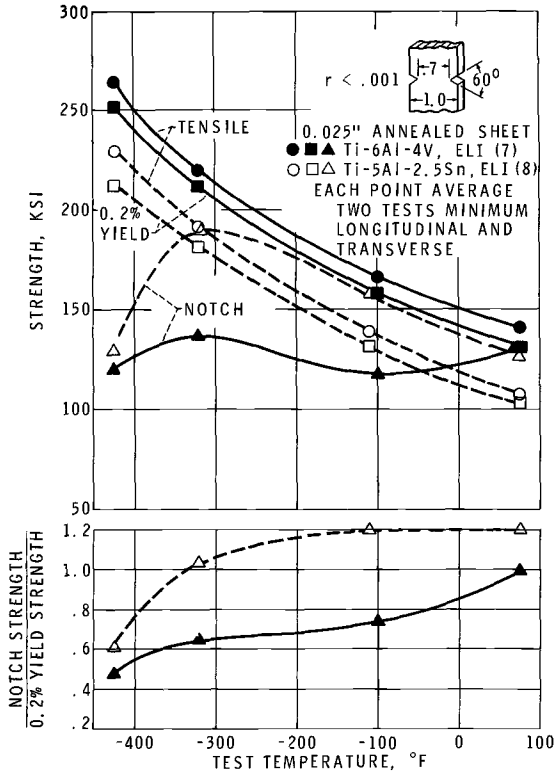


FIG. 1—Influence of test temperature on smooth and sharp notch tensile characteristics of 0.025-in.-thick Ti-6Al-4V and Ti-5Al-2.5Sn ELI grade annealed sheet.

Cryogenic Temperatures

Titanium alloys exhibit very substantial increase in both yield and tensile strength as the test temperature is reduced from room temperature to -423 F. This increase can amount to a factor of nearly 2.5 for β alloys and is in the order of two for most α and $\alpha + \beta$ alloys. As might be expected, the crack tolerance exhibits a corresponding decrease and when titanium alloys are used at cryogenic temperatures particular attention must be given to design against brittle fracture.

The embrittling effect of cryogenic temperatures may be illustrated

by the results of sharp-edge-notch tension tests on annealed Ti-6Al-4V [7] and Ti-5Al-2.5Sn [8] ELI grade sheet alloys shown in Fig. 1. Presently, these are the preferred compositions for use in pressure vessels containing cryogenic fluids. In these tests sharp notch-to-yield strength ratios of unity or above represent tough metal conditions, and this behavior characterizes both alloys at room temperature. As the test temperature is reduced, both alloys lose toughness. This loss, however, is more pronounced and occurs at higher temperatures for the Ti-6Al-4V alloy than for the Ti-5Al-2.5Sn alloy. An important point to note is that the embrittlement of the Ti-5Al-2.5Sn alloy exhibits a substantial increase between -320 and -423 F. Similar behavior in this temperature range also characterizes other titanium alloys in the annealed and heat treated conditions [9].

On the basis of the data shown in Fig. 1, it would appear that the Ti-5Al-2.5Sn alloy has slightly greater crack tolerance at -423 F. This, in general, has been our experience in tests on sheet of these two compositions. However, as will be seen later, the cryogenic fracture behavior of titanium alloys is strongly influenced by metal composition and processing factors. For this reason firm generalizations regarding the relative superiority of these two alloys can only be made on the basis of more extensive data than is available to us. The slight minimum in notch strength of Ti-6Al-4V at -100 F is unexpected at normal testing speeds. At slower testing speeds, however, minima are often observed in $\alpha + \beta$ alloys at temperatures between 0 and -150 F, and are attributed to slow strain rate hydrogen embrittlement.

Heat Treatment

The complex influences of conventional heat treatments on the fracture characteristics of titanium alloys are as yet poorly understood. One complicating factor is the development of a Ti_3Al phase over a rather wide range of temperatures and compositions in the titanium-aluminum (Ti-Al) system. In describing the formation of this phase, some authors (for example, Blackburn [10] and Clark et al [11]) refer to a classical ordering reaction. In contrast, Crossley [12] has shown that a simple precipitation reaction produces the Ti_3Al phase. Since no conclusive evidence exists to indicate that ordering *per se* takes place in the Ti-Al system, we must side with Crossley in referring to the development of the Ti_3Al phase as a conventional precipitation (aging) reaction. There is some disagreement between Clark and Crossley regarding the number of phases that appear and also on the solubility of aluminum in these phases. In this regard we feel that Crossley had clearly shown that only one second phase (Ti_3Al) exists at aluminum contents less than that corresponding to Ti-Al and that it has virtually no solid solubility range.

Although there is disagreement on the reaction mechanism and products, all three investigators seem to agree that the lower critical temperature for the appearance of a second phase is between 1000 and 1100 F, and in this temperature range equilibrium is obtained only after several hundred hours at temperature. The most recent investigation by Crossley indicates considerably wider compositional limits than previously reported by the other investigators. The equilibrium diagram obtained by Crossley is shown in Fig. 2, and it will be noted that the compositional limits at the lowest temperature investigated extend from about 4 to 24 weight per cent (about 7 to 36 atomic per cent)

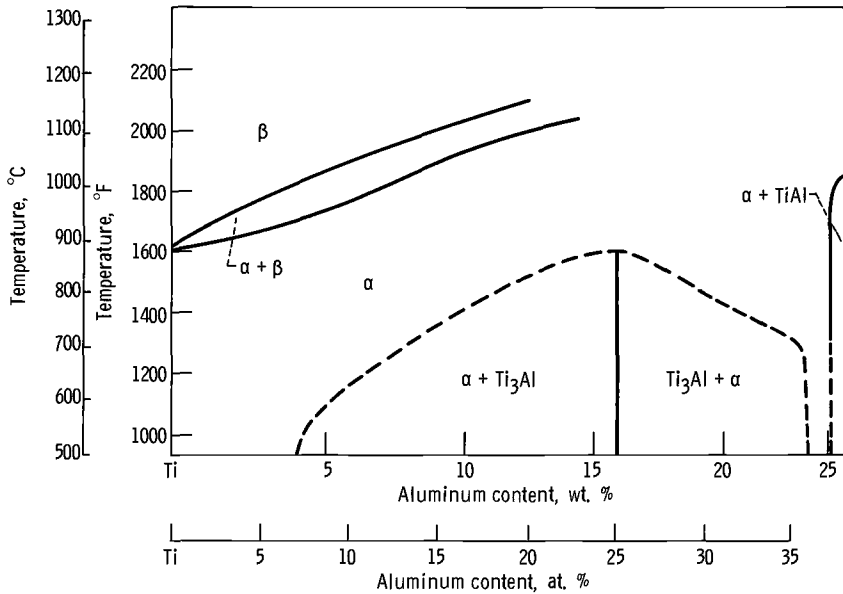


FIG. 2.—Titanium-rich end of the titanium-aluminum system [12].

aluminum. As will be evident from the following discussion, the development of the Ti_3Al phase in Ti-Al alloys appears to cause a loss in toughness.

Annealing

The crack tolerance of both the Ti-8Al-1Mo-1V and the Ti-5Al-2.5Sn alloys appears to be influenced by the rate of cooling from the annealing temperature with slow (furnace) cooling resulting in reduced toughness. The most direct evidence for this effect in Ti-8Al-1Mo-1V is given by data obtained by Piper [13] and shown in Fig. 3. It will be noted that the -110 F strength of 9-in.-wide, center-cracked panel decreases with an increase in the cooling time from 1450 to 900 F. A substantial portion of this embrittlement occurs with essentially no

change in yield strength. Additional information showing the deleterious effect of slow cooling from the annealing temperature is also available from data reported by Roy et al [14,15] and by Espey et al [16]. These data, shown in Fig. 4, clearly indicate the superior toughness of duplex-annealed sheet as compared with mill-annealed sheet of approximately the same thickness. The mill-annealed material was furnace cooled in packs, while the duplex annealed material was given a two-step heat treatment (1850 F, 5 min, air cooled + 1375 F, 15 min, air cooled)³, following mill annealing, both steps involving rapid cooling.

Data obtained by the authors several years ago [8] indicate the

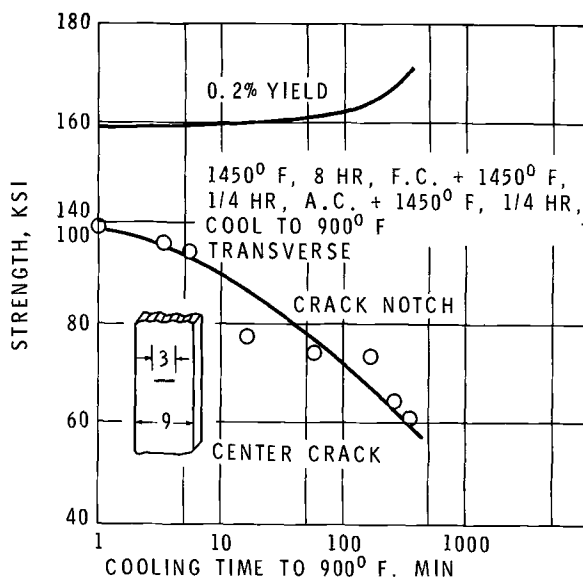


FIG. 3—Effect of cooling rate from reannealing temperature on the -110 F crack notch properties of 0.040-in. thick duplex annealed Ti-8Al-1Mo-1V sheet [13].

toughness of Ti-5Al-2.5Sn alloy also to be sensitive to cooling rate from the annealing temperature. Sheets of various thicknesses in both air-cooled and furnace-cooled conditions were tested at -423 F. As indicated in Fig. 5, the smooth tensile and yield strengths are unaffected by the difference in cooling rates at all thicknesses investigated. In contrast, at thicknesses greater than about 0.050 in. the air-cooled sheet has substantially higher sharp notch strength.

The observed embrittlement associated with slow cooling rates in

³ Similar room and low temperature properties can be obtained by air cooling from a single anneal at 1450 F.

both these alloys may be related to the development of the Ti_3Al phase discussed previously. In the case of the Ti-8Al-1Mo-1V alloy, this reaction seems quite probable. Recent equilibrium diagram data obtained by Crossley (see Fig. 2) suggest the possibility that the same reaction can also occur in alloys of lower aluminum content. Further work in this area would certainly be indicated. In particular, information is needed concerning the influence of other common alloying elements on the development of the embrittling phase.

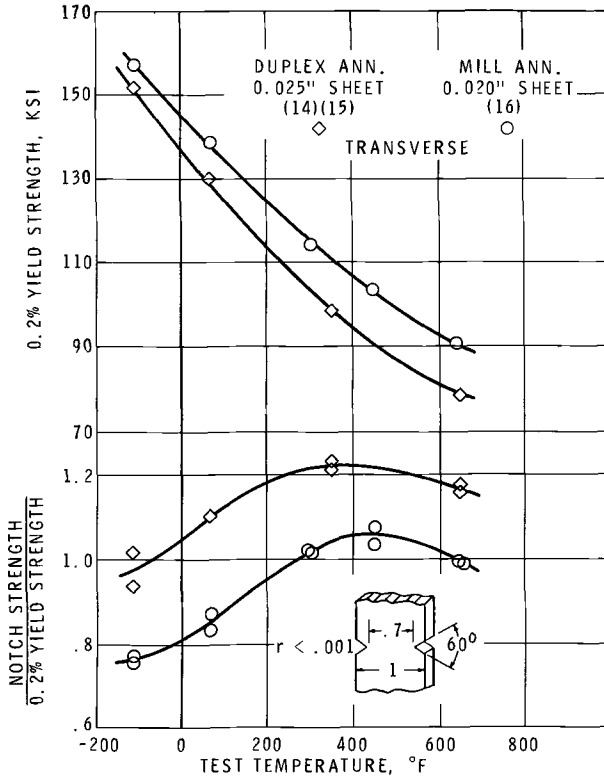


FIG. 4—Effect of annealing treatment on smooth and sharp notch tensile characteristics of Ti-8Al-1Mo-1V sheet.

From a practical standpoint it can be important to take advantage of the beneficial effects of fast cooling from the annealing temperature. However, as will be discussed later, the fast cooled structure is somewhat unstable and long-time exposure at elevated temperature will reduce the toughness of this material. On the other hand, for material to be used at cryogenic temperature, where instability effects would not be operative, air cooling would be a relatively inexpensive way to improve the product.

Aging

For some titanium alloys, large increases in tensile and yield strengths are available by aging. Unfortunately, however, these gains are often purchased at a considerable sacrifice in crack tolerance. An extensive program was conducted at NASA-Lewis in 1960 [9] to establish the influence of aging temperature on the sharp notch strength of a number

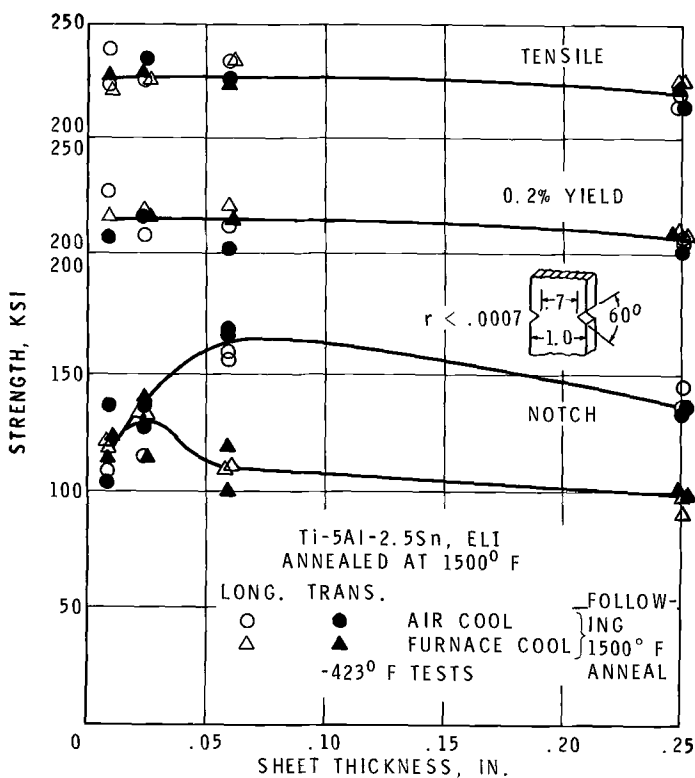


FIG. 5—Influence of cooling rate from the annealing temperature on the -423 F smooth and sharp notch tensile characteristics of Ti-5Al-2.5Sn ELI sheet of various thicknesses [8].

of titanium alloys of interest to the DOD Sheet Rolling Program. Typical results are illustrated in Fig. 6 which show a pronounced response to the aging treatment for the Ti-4Al-3Mo-1V alloy tested at room temperature. As expected, both the smooth tensile and yield strengths exhibit a maximum at an intermediate aging temperature, and a corresponding minimum is observed in the sharp notch strength. At the time of the DOD Sheet Rolling Program, the recommended aging treatments were generally those producing the highest strength. Unfortunately, these treatments also produced a structure having a relatively

low crack tolerance. As noted for the Ti-4Al-3Mo-1V alloy, underaging or overaging can result in a considerable increase in toughness with relatively small sacrifices in yield and tensile strengths. Underaged conditions, of course, may lack the necessary stability for use at elevated temperatures.

The tendency to use titanium alloys in their strongest conditions and to judge the worth of new alloys primarily on the basis of their tensile

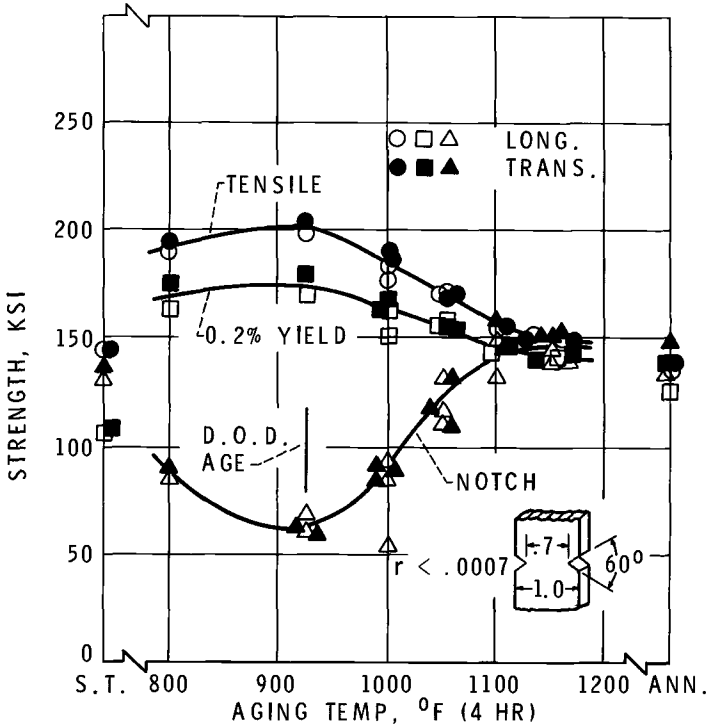


FIG. 6—Room temperature smooth and sharp notch tensile characteristics of 0.063-in.-thick aged Ti-4Al-3Mo-1V sheet [9].

and yield strengths is unfortunately still too prevalent. No titanium alloy development program should be started without adequate provisions for determining the crack tolerance of the alloys.

Interstitial Element Content

It has been known for some time that excessive amounts of the interstitial elements hydrogen, carbon, oxygen, and nitrogen can embrittle titanium alloys [17,18]. More recently it has been established that variations in the amount of interstitials within the normal compositional limits can strongly influence the toughness of titanium alloys [8,9,19].

These effects are particularly pronounced at low temperatures where the toughness is already limited. The embrittling effects of interstitials are illustrated in Fig. 7 by results obtained in an investigation of the Ti-5Al-2.5Sn alloy using sharply notched specimens. Three interstitial levels were investigated for several different sheet thicknesses. The Low I composition is from a laboratory heat extra low in its interstitial and iron contents. The Low II composition is typical of the commercial ELI grade, and Normal I and Normal II compositions are representa-

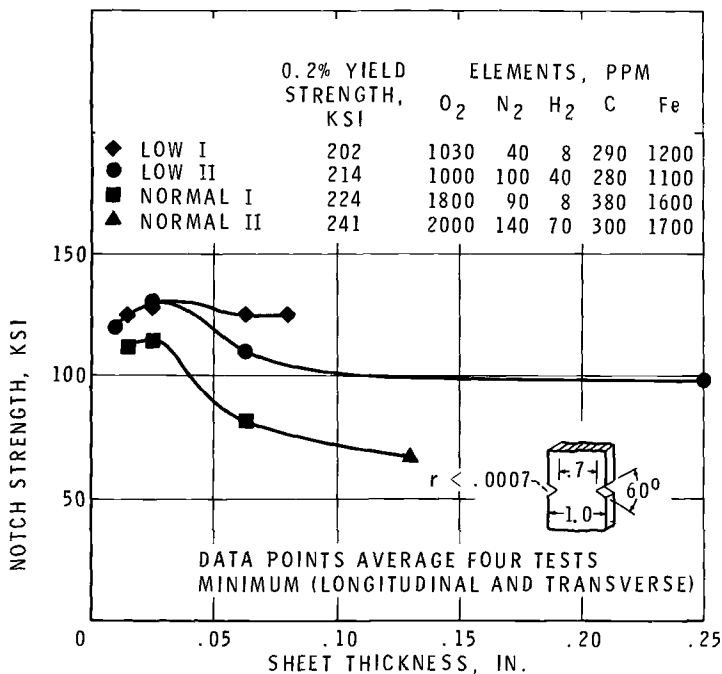


FIG. 7—Influence of interstitial element content on -423 F sharp notch strength of annealed (1500 F, furnace cooled) Ti-5Al-2.5Sn sheet of various thicknesses [8].

tive of the normal mill product. All sheet was annealed in an argon atmosphere at 1500 F and furnace cooled. As expected, the yield strength increases with increasing interstitial content and the notch strength decreases.

As a consequence of these data and similar information obtained by Titanium Metal Corporation of America [20] and by General Dynamics/Convair, Inc. [19], specifications for ELI grades were formulated by the alloy producers. These specifications generally also call for reduced contents of iron and other beta stabilizing elements in the Ti-5Al-2.5Sn alloy. While iron is not an interstitial element, it does embrittle the Ti-5Al-2.5Sn alloy at cryogenic temperatures [20]. From the data shown

in Fig. 7, it appears that reductions of the interstitials to still lower levels than those corresponding to the ELI grades would give further improvements in the crack tolerance.

Elevated Temperature Exposure

The problems to be discussed are concerned with the effects of moderately elevated temperatures in the absence of stress. Problems of

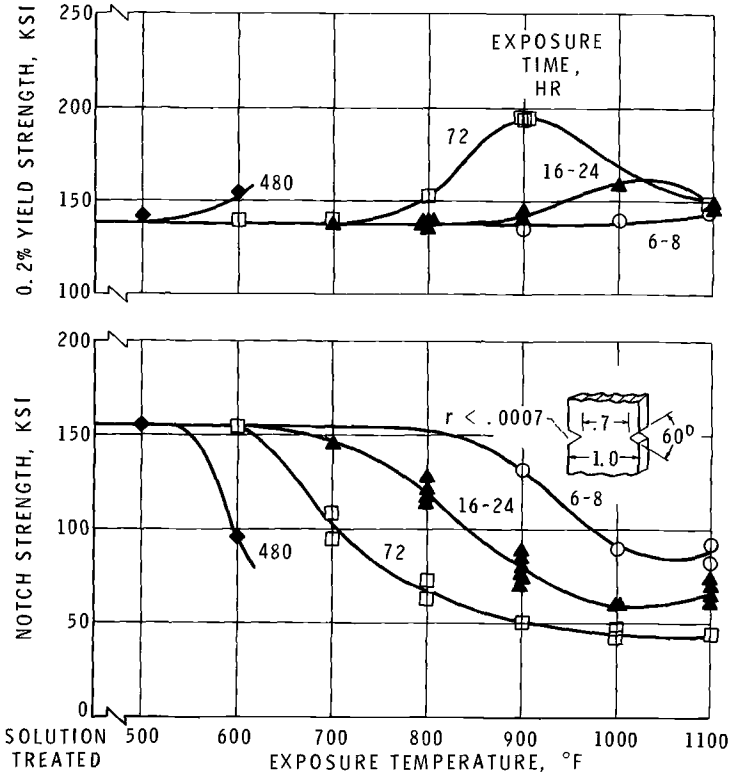


FIG. 8—Influence of exposure temperature and time on the longitudinal room temperature smooth and sharp notch tensile characteristics of 0.050-in.-thick solution treated beta (Ti-13V-11Cr-3Al) sheet.

this nature are encountered when solution treated material is subjected to long-time exposure at temperatures well below those normally used in aging, and also when the precipitation of the Ti_3Al phase is involved. In either case considerable loss in crack tolerance can precede any indication of strengthening.

Instability of Solution Treated Structures

The beta alloy Ti-13V-11Cr-3Al is exceptionally tough in the solution treated condition; however, previously unpublished results obtained

by the authors show that this toughness can be reduced by long-time exposure to temperatures well below those employed in aging. Both smooth and sharp notch tests were made at room temperature following exposure in air to temperatures between 500 and 1100 F. Exposure times varied from 6 to 480 hr. Figure 8 shows the expected trends for the yield strength with maxima appearing at lower temperatures for longer exposure times. The notch strength follows an inverse trend to

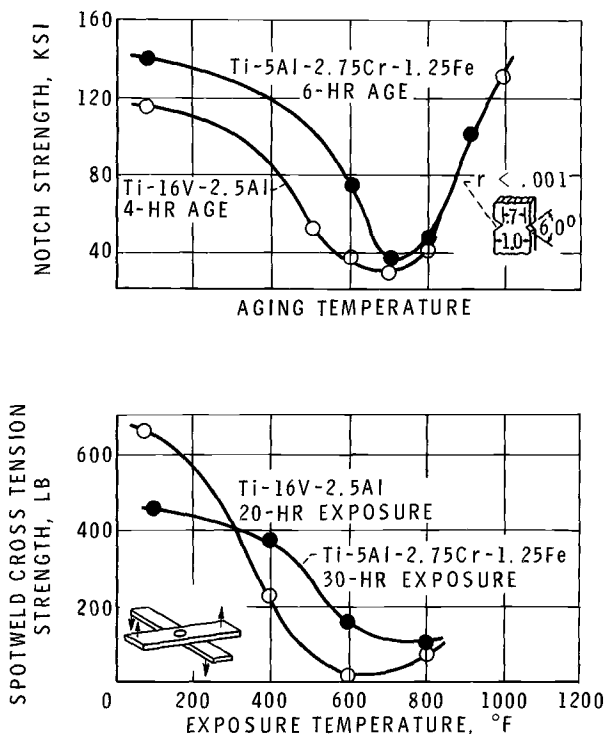


FIG. 9—(a) Effect of aging temperature on the room temperature sharp notch strength of two titanium alloys [21].

(b) Effect of exposure temperature on the spot weld strength at room temperature for two titanium alloys aged at 1000 F before welding [21].

the yield strength. Note, however, that reductions in notch strength precede yield strength increases. For example, at 700 F the yield strength is unchanged following a 72-hr exposure, but a 30 per cent loss in notch strength is observed. Presumably very long times at temperatures below 500 F could produce appreciable embrittlement.

A related and interesting observation concerns the possible effect of exposure to elevated temperatures on the strength of spot welds. The spot-welded area is heated to a high temperature and rapidly quenched. The spot-weld nugget is therefore essentially solution treated and may age

to a brittle condition during long-time service. This effect is most severe if low temperature aging produces relatively poor crack tolerance. Data reported by Sachs and Sessler [21] demonstrate this embrittlement in Ti-16V-2.5Al and Ti-5Al-2.75Cr-1.25Fe sheet. It will be noted from Fig. 9a that a very low sharp notch strength is produced by aging these alloys between 600 and 800 F. If sheet aged at 1000 F is spot welded, exposed for 20 or 30 hr at various temperatures and then tested at room temperature, the spot weld strength, Fig. 9b, also shows a pronounced minimum between 600 and 800 F. This behavior of

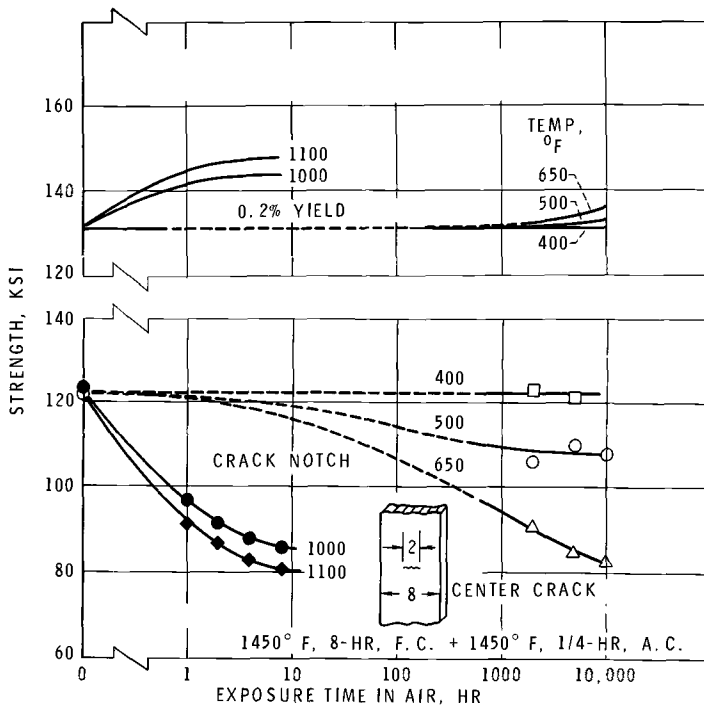


FIG. 10—Effect of elevated temperature exposure on smooth and crack notch strengths of 0.050-in.-thick duplex annealed Ti-8Al-1Mo-1V sheet [13].

spot welds may characterize other alloys where the mechanism of hardening involves aging from a solution-treated condition.

Instability of Annealed Structures

As mentioned previously, the crack tolerance of both Ti-8Al-1Mo-1V and Ti-5Al-2.5Sn alloys is reduced when furnace cooled rather than air cooled from the mill annealing temperature. This deleterious effect of slow cooling was attributed to the formation of the Ti_3Al phase during slow cooling. According to data obtained by Piper [13] long-time exposure of air cooled (duplex annealed) Ti-8Al-1Mo-1V sheet at

moderately elevated temperatures results in an embrittlement. This effect is illustrated in Fig. 10 which shows the yield and center-cracked-specimen strengths as a function of exposure time in air for several exposure temperatures. The loss of crack tolerance is larger the higher the exposure temperature, and as might be expected occurs rapidly at 1000 and 1100 F. It will be noted that the damaging effect of exposure to 650 F for 10,000 hr is about equivalent to that produced in 10 hr at 1100 F. This instability is probably associated with the appearance of the same Ti_3Al structure which is present in the furnace cooled material. Presumably other annealed titanium-aluminum alloys could undergo similar changes after long-time exposure to moderately elevated temperatures.

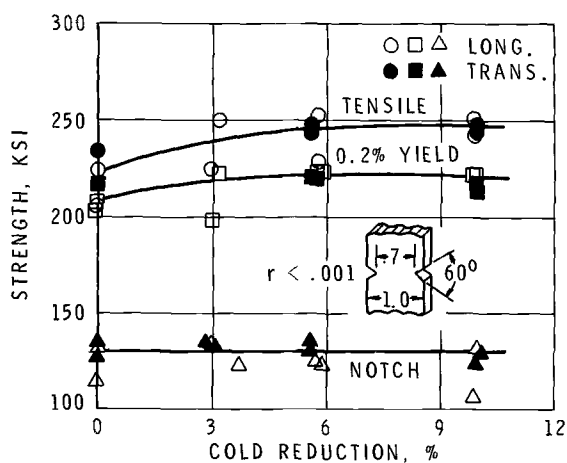


FIG. 11—Influence of cold rolling small amounts on the -423 F smooth and sharp notch tensile characteristics of 0.025-in.-thick Ti-5Al-2.5Sn, ELI sheet [8].

Cold Working

The effects of cold working are of interest because frequently small amounts of cold rolling are used to flatten sheet after final annealing and because certain fabrication operations involve stretching. In addition, it is possible to appreciably strengthen the β titanium alloy Ti-13V-11Cr-3Al by cold rolling or a combination of cold rolling and aging.

Cold Working of α Titanium

Some engineering specifications permit as much as 10 per cent thickness reduction in flattening 0.010-in. annealed sheet. In an investigation at NASA-Lewis [8] the influence of cold reductions up to about 10 per cent on the -423 F smooth and sharp notch strength of Ti-5Al-2.5Sn annealed sheet having an initial thickness of 0.025 in. was studied. The results are given in Fig. 11 and show that the tensile and yield

strengths increase with cold reduction and reach a constant value between 6 and 10 per cent reduction. The elevation in tensile strength is approximately 10 per cent, while the yield strength increases approximately 7 per cent. The notch strength is unaffected over the range of rolling reductions investigated. Similar experiments were made [8] to determine the effects of stretching on the -423 F smooth and sharp notch strengths of Ti-5Al-2.5Sn annealed sheet having initial thicknesses of 0.010, 0.025, and 0.060 in. Specimens were tested only in the stretching direction. The results were similar to those obtained by cold rolling in that moderate increases in tensile strength were observed with no loss in the sharp notch strength for stretching strains up to about 16 per cent.

These results on the effects of cold working indicate no loss in crack tolerance for the sheet thicknesses investigated, but should not be extrapolated to larger amounts of plastic deformation nor to other alloy compositions. A particularly damaging effect of cold rolling can be the production of very small surface cracks. These may be due to excessive amounts of cold work between annealing cycles, insufficient annealing, or to interstitial contamination during annealing. These cracks are difficult to detect and can greatly increase the sensitivity to aggressive environments.

Cold Working β Titanium

The effects of various combinations of cold rolling and aging on the room temperature smooth and sharp notch strength of the Ti-13V-11Cr-3Al alloy were investigated by Repko and Brown [22] and by Bomberger [23]. In the former investigation, solution treated sheet with an initial thickness of 0.125 in. was given cold reductions up to 46 per cent. The cold rolled material was then machined to 0.063-in. thickness and tested either in the unaged condition or following aging at several aging temperatures between 650 and 900 F. The results of cold reduction without aging are illustrated in Fig. 12. Both the tensile and yield strengths increase at a nearly constant rate over the range of reductions investigated, and exhibit negligible directionality. The sharp notch-to-tensile strength ratio decreases gradually with cold reduction up to a value of about 30 per cent. At 46 per cent cold reduction a substantial embrittlement is observed. As might be expected, the notch strength is lower in the transverse than in the longitudinal direction.

The fracture behavior of this alloy in the cold rolled condition is compared with that of the cold rolled plus aged conditions in Fig. 13 which shows the sharp notch-to-tensile strength ratio as a function of the yield strength. A range of yield strength levels was achieved in the latter case by cold rolling various amounts followed by aging at various temperatures for various times. The longitudinal notch strengths of the

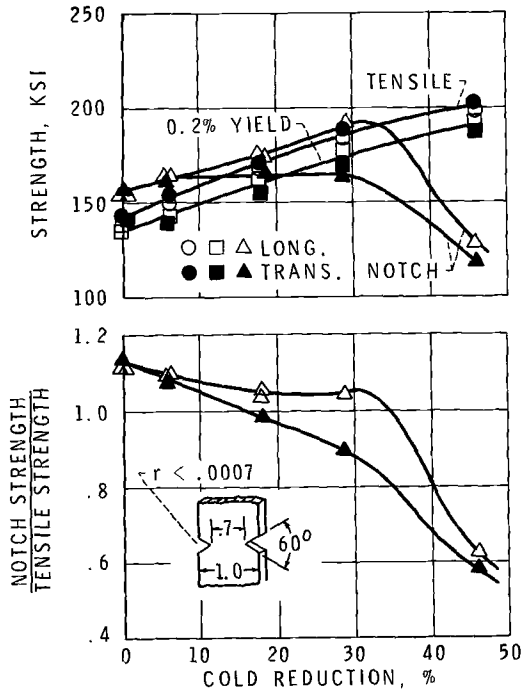


FIG. 12—Influence of cold rolling on the room temperature smooth and sharp notch tensile characteristics of 0.063-in.-thick solution-treated beta (Ti-13V-11Cr-3Al) sheet [22].

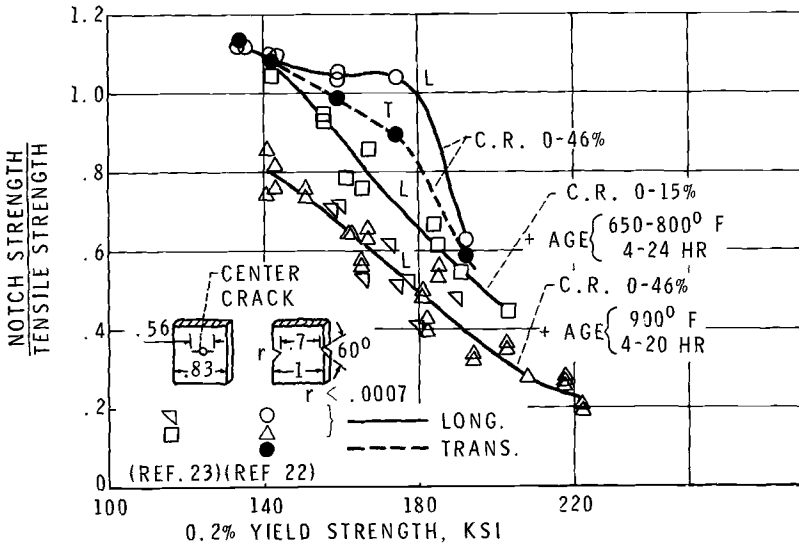


FIG. 13—Influence of various combinations of cold reduction and aging on room temperature notch characteristics of 0.063-in.-thick beta (Ti-13V-11Cr-3Al) sheet.

cold rolled plus aged conditions are used for purposes of this comparison. The transverse notch strengths would be somewhat lower at a given yield strength level. There are insufficient data to clearly establish the embrittling effects of specific combinations of cold reduction and aging temperature at a given yield strength level. However, the data define two general types of behavior. Thus, sheet cold rolled and aged at 900 F exhibits lower notch strength ratios at an equivalent yield strength level than sheet cold rolled and aged at temperatures between 650 and 800 F. Furthermore, the sheet cold rolled but not aged possesses superior crack tolerance to any of the aged conditions at yield strength levels up to about 180 ksi.

Aggressive Environments

Commonly used titanium alloys such as Ti-6Al-4V are subjected to an extremely wide range of service temperatures and environments. As might be expected, various problems directly associated with the environment have turned up as new applications are developed. This section deals with the problem generally classified as a form of stress corrosion where the resistance to crack propagation is decreased by the action of an aggressive agent in the environment. Generally titanium alloys are considered to be exceptionally resistant to attack by aqueous environments including most inorganic salt solutions. However, if a crack is present, delayed failure under sustained load can occur in aqueous solutions of certain halides and in some cases in distilled water. The following section will consider the influence of salt water as well as several unusual liquid environments on the delayed failure behavior of titanium alloys.⁴

Many different kinds of tests have been used to study the influences of aggressive environments, but few of these lend themselves to a clear interpretation in terms of the service performance of the alloy. In our opinion the most informative of the tests are those which employ specimens containing cracks and which are designed so that the results are interpretable in terms of linear elastic fracture mechanics.

A useful and relatively simple test of this type is that proposed by B. F. Brown [26] using an edge-fatigue-cracked bar loaded in cantilever bending by means of dead weights. A polyurethane reservoir

⁴ Solid sodium chloride (and other solid chlorides) cause stress cracking in smooth titanium test samples at moderately elevated temperatures, and for future high performance jet engine applications this phenomenon may limit the service life of compressor blades. However, this subject will not be discussed here because of the uncertainty which still surrounds the choice of suitable laboratory tests and the absence of a way to determine the influence of hot salt on the propagation of existing cracks in titanium. For detailed information on the subject of solid salt corrosion the reader is referred to the information and references given in the Ti-8Al-1Mo-1V chapter of the "Aerospace Structural Metals Handbook" [24] and to *ASTM STP 397* [25].

surrounds the crack and contains the aggressive liquid environment. Crack extension is monitored by measuring changes in beam deflection. In these tests a specimen is first loaded continuously to rupture in a presumably neutral environment and the stress intensity factor at maximum load (based on the initial crack length) is used to calculate a value K_{I_x} which serves as a basis for determining a delayed failure curve. Subsequent specimens are subjected to successively lower values of the stress intensity factor (K_{I_i}) and the times to rupture recorded.⁵ The results are expressed in terms of a plot relating K_{I_i} or K_{I_i}/K_{I_x} to the failure time. Another test procedure, used by Tiffany and his co-workers [5], subjects surface cracked specimens to static tensile loads in order to develop a delayed failure curve. The results of these tests are expressed in terms of a plot of K_{I_i} or K_{I_i}/K_{I_e} as a function of failure time. The value of K_{I_e} is calculated from the initial crack dimensions and the failure load for a specimen continuously loaded to rupture in a presumably neutral environment. It should be noted that in most cases the specimen dimensions were inadequate to permit obtaining the true plane strain fracture toughness of the alloy [3]. For this reason we have followed the practice used by Brown and his co-workers [26,27] and identified the stress intensity factor at fracture during continuous loading as K_{I_x} .

Sustained Load Tests in Salt Water

Typical results for salt water sustained load tests on three titanium alloys are shown in Fig. 14. These data were obtained by Curtis et al [28] using fatigue-cracked notch bend specimens and show significant reductions in load carrying capacity for all three alloys in the presence of 3.5 per cent sodium chloride solution. There appears to be a threshold value of K_{I_i} designated as $K_{I_{sec}}$ above which failure occurs rapidly. It will be noted that this threshold is considerably lower for the Ti-8Al-1Mo-1V alloy than for the Ti-6Al-4V or Ti-4Al-3Mo-1V alloys.

Most delayed failure results cover a time period of only a few hours, and there is no conclusive evidence that failure would not be observed below the reported $K_{I_{sec}}$ values if the times under load were sufficiently long. However, it is certainly clear that stress intensity levels exceeding this value are dangerous. In this connection, Curtis et al [28] show that alternating loads in the presence of 3.5 per cent sodium chloride solution can cause extension at K_{max} levels below the $K_{I_{sec}}$ measured in static tests.

In delayed failure tests of the type described, the quantity $K_{I_{sec}}$ presumably represents the stress intensity threshold under plain strain

⁵ Some investigators raise the load (K_{I_i}) if a specimen does not begin crack propagation in a short time and time is then counted from the application of the highest load.

conditions. This would imply that the value of $K_{I_{sec}}$ is thickness independent providing metallurgical effects associated with variations in the thickness were absent. The proper way to investigate the thickness effect is to test specimens of various thicknesses machined from a single plate. To the best of our knowledge such tests to determine $K_{I_{sec}}$ have not been made. In the absence of this information the size requirements for a valid K_{I_c} determination [3] can be applied to the $K_{I_{sec}}$ threshold values to judge whether they correspond to plane strain fracture conditions. Thus, both the crack length and the specimen thickness should be equal to or greater than $2.5(K_{I_{sec}}/\sigma_{YS})^2$. The $K_{I_{sec}}$ data for the Ti-8Al-

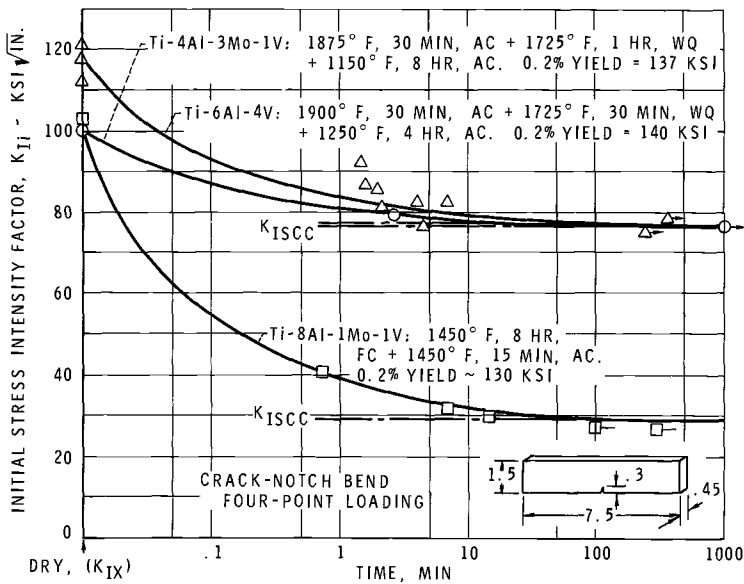


FIG. 14—Delayed failure stress corrosion cracking results at room temperature for three titanium alloys tested in 3.5 per cent sodium chloride solution [28].

1Mo-1V alloy shown in Fig. 14 meet these requirements, while the Ti-6Al-4V and Ti-4Al-3Mo-1V specimens were only about one half the required thickness.

The thickness effect that would be expected in stress corrosion tests if the specimen thickness was less than about $2.5(K_{I_{sec}}/\sigma_{YS})^2$ is illustrated in Fig. 15 for tests by Hatch et al [29] on Ti-8Al-1Mo-1V tested in two thicknesses, both of which are less than $2.5(K_{I_{sec}}/\sigma_{YS})^2$. In this case a portion (but not all) of the observed thickness effect may be associated with the fact that the sheets were rolled to the thickness tested rather than machined from a single thickness. Until the thickness effect in $K_{I_{sec}}$ testing is better understood it would be advisable to always study thicknesses as close as possible to those used in service.

Effects of Composition and Heat Treatment on Sensitivity to Salt Water

The following observations are based on data obtained using fatigue cracked specimens subjected to sustained loading in 3.5 per cent sodium chloride solution. Interpretation of these data, however, is complicated by the fact that the sensitivity of a particular alloy can be changed substantially by variations in heat treatment and processing history. Furthermore, in many cases the specimen thicknesses employed were not sufficient to ensure plane strain conditions during crack propagation. Under these circumstances, as discussed earlier, the sensitivity could vary with the thickness. For these reasons it cannot be stated unequivocally that a particular composition or heat treated condition is completely immune to delayed failure in aqueous salt solutions.

Regarding the effects of composition, it appears from the work of

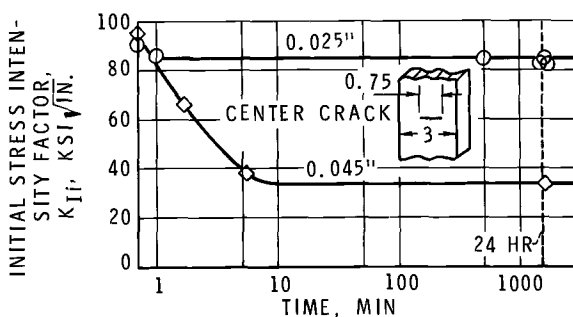


FIG. 15—Delayed failure stress corrosion cracking results at room temperature for two thicknesses of Ti-8Al-1Mo-1V sheet tested in 3.5 per cent sodium chloride solution [29].

Lane et al [30], Hatch et al [29], and various investigators at the Naval Research Laboratory [4,27] that sensitivity to delayed failure is reduced by lowering the aluminum content and by addition of molybdenum, and columbium. For example, such alloys as Ti-6Al-2Mo, Ti-6Al-2Cb-1Ta-0.8Mo, and Ti-6Al-4V appear to be superior to Ti-8Al-1Mo-1V or Ti-7Al-1Mo-1V. The same investigators associate superior resistance to delayed failure with a microstructure containing substantial amounts of transformed β phase, so that the α phase exists in isolated islands. It is generally agreed that low interstitial content is beneficial since this increases the basic toughness of the alloy and therefore the critical crack size. According to Lane slow cooling from the solution annealing temperature or holding at temperatures around 1100 F tends to increase the sensitivity of Ti-7Al-2Cb-1Ta alloy. Similar behavior might be expected for Ti-8Al-1Mo-1V and other high aluminum-titanium alloys. As suggested by Lane, this increased sensitivity may be associated with the previously discussed Ti_3Al phase in the Ti-Al system.

A considerable amount of information concerning the development of optimum heat treatments for plate is available from the investigations of Curtis et al [28] carried out at the Boeing Co. in connection with an alloy selection program for the supersonic transport. Both Ti-6Al-4V and Ti-4Al-3Mo-1V alloys were tested in the form of 1/2 in.-thick plate at room temperature using fatigue cracked bend specimens 0.45 in. thick by 1.5 in. deep. The K_{Ii} value necessary to cause failure

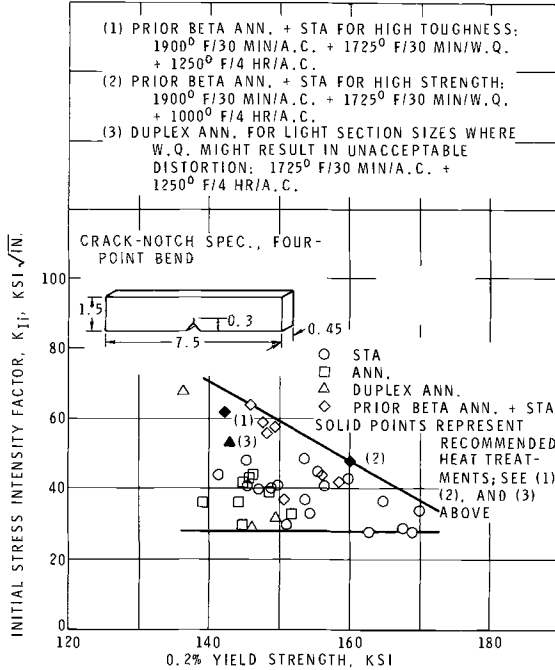


FIG. 16—Stress intensity factor to cause failure in 6 hr in 3.5 per cent sodium chloride solution at room temperature for 0.5-in.-thick Ti-6Al-4V plate given various heat treatments [28]. Solution treated and aged, 1550 to 1850 F, 30 min, water quenched + 1000 to 1250 F, 4 hr, air cooled; duplex annealed, 1500 to 1900 F, 30 min, air cooled + 1000 to 1200 F, 4 hr, air cooled; annealed, 1200 to 1500 F, 2 hr, air cooled; prior beta annealed, 1850 to 2100 F, 30 min, air cooled + 1725 F, 30 min, water quenched + 1000 to 1250 F, 4 hr, air cooled.

in 6 hr was used as an index of relative susceptibility to stress corrosion. Generally this stress intensity value corresponded to K_{Isec} . Sixty-six variations of annealing cycles and solution treating plus aging conditions were investigated. The results for the Ti-6Al-4V alloy are shown in Fig. 16 which gives K_{Ii} to cause failure in 6 hr as a function of yield strength. A summary of the essential features of the heat treating cycles employed is given in the figure legend. In general, there appears to be an advantage to β annealing prior to solution treating and aging. The lowest sensitivities to stress corrosion are obtained at the lower yield

strengths. However, the sensitivity is not a simple function of yield strength but depends on the heat treatment used to obtain a given yield strength level. As shown in Fig. 16, three specific heat treatments were selected by Curtis et al as optimum for conditions of high toughness, high strength, and high strength combined with minimum distortion during heat treatment. The results for the Ti-4Al-3Mo-1V alloy indicated stress corrosion behavior essentially equivalent to that observed for Ti-6Al-4V at the same yield strength levels, providing optimum heat treatments were employed which again involved prior β annealing. Solution annealing above the β transus in these heat treatments results in an acicular $\alpha + \beta$ structure in which the tough beta phase impedes fracture propagation.

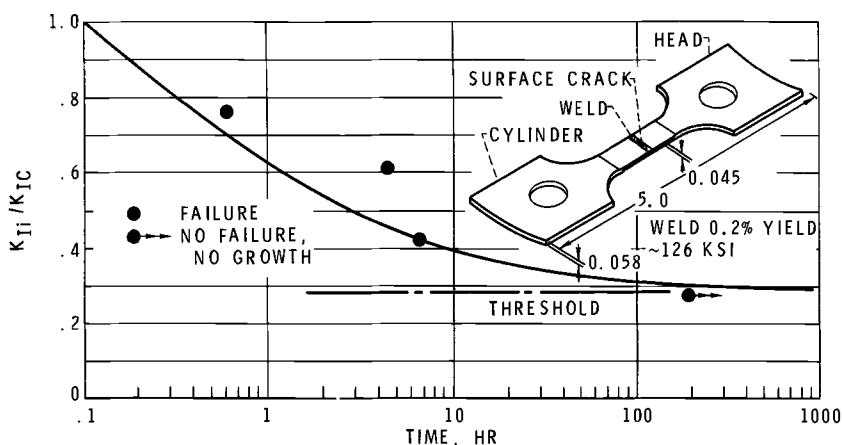


FIG. 17—Delayed failure stress corrosion cracking results at room temperature for Ti-6Al-4V weldments (HAZ) in methanol [31].

It should be noted that while heat treatments producing continuous networks of β phase may improve room temperature toughness and stress corrosion resistance, the low temperature fracture properties may not be similarly improved. Thus, solution treated β titanium is quite brittle at low temperatures [9].

Unusual Environments

Recent experience with Ti-6Al-4V in the Apollo rocket systems has indicated that stress corrosion cracking of storable propellant tanks can occur in the presence of certain fuels and oxidizers as well as with special fluids used to simulate the flow characteristics of the propellants in various ground tests. Difficulties were first encountered with N_2O_4 and very recently with methanol and certain types of Freon. Typical results obtained by Tiffany [31] are shown in Figs. 17 and 18 for surface cracked specimens of Ti-6Al-4V weldments tested in methanol and

Freon MF, respectively. The specimens shown were cut from production tanks (solution treated, welded, and aged) and the cracks were introduced into the weld heat affected zone (HAZ). It is quite evident that delayed failure is encountered in both these environments and that the threshold K_{Ii} values are very much lower than the K_{Ix} values measured in air. Similar tests on Ti-6Al-4V parent metal ($\sigma_{YS} \approx 165$ ksi) in Freon MF also showed a substantial reduction in crack tolerance.

It is much too early to make any observations concerning the effects of composition and heat treatment on the sensitivity of titanium alloys to these unusual environments. In a recent seminar [32] sufficient information was presented to show that many organic solvents and several halogenated hydrocarbons will produce stress corrosion in a number

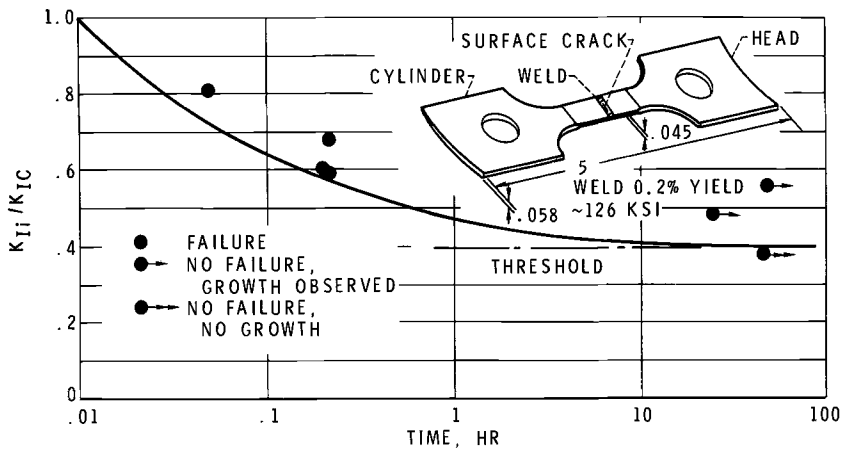


FIG. 18—Delayed failure stress corrosion cracking results at room temperature for Ti-6Al-4V weldments (HAZ) in Freon MF [31].

of titanium alloys. On the basis of the information at hand environmental testing is an essential prerequisite in the selection of titanium alloys for critical applications. What is most needed is general agreement on the type of test to be used. Without standardization in this respect a great amount of time and money will be wasted.

Plane Strain Fracture Toughness

For the past several years the ASTM Committee E-24 on the Fracture Testing of Metals has been struggling with the problems of formulating recommended test methods for determination of the plane strain fracture toughness, K_{Ic} . This has been a difficult task and has required the development of special experimental techniques and data analysis methods coupled with an extensive experimental program designed to explore the limits of applicability of elastic fracture mechanics. The

TABLE 1—Plane strain fracture toughness of three titanium alloys in annealed and heat treated conditions at various test temperatures.

Alloy	Form and (mill analysis, weight per cent)	Condition ^a	Specimen Type	Test Direction	Test Temperature, deg F	σ_{YS} , ksi	Ap-parent K_{IC} , ksi $\sqrt{\text{in.}}$	K_{IC}^2 / σ_{YS}^2	Source	Remarks								
Ti-6Al-6V-2Sn . . .	1-in. plate (5.4Al, 5.5V, 1.9Sn, 0.66Cu, 0.72Fe, 0.026C, 0.025N, 0.007H, 0.159O)	1550 F, 1/2-hr, WQ + 900 F, 4 hr, AC ^d 1550 F, 1/2 hr, WQ + 1000 F, 4 hr, AC ^d 1550 F, 1/2 hr, WQ + 1100 F, 4 hr, AC ^d 1550 F, 1/2 hr, WQ + 1300 F, 4 hr, AC ^d 1650 F, 1 hr, WQ + 1050 F, 4 hr, AC ^d	three-point bend B = 1 in., a = 1 in., W = 2 in.	RW ^b	RT ^c	187	19	0.010	Strawley [33]									
						183	25	0.019										
						173	31	0.032										
						145	39	0.072										
						Ti-6Al-4V	4 1/2 by 4 1/2 in. forging (5.5Al, 5.4V, 1.9Sn, 0.64Cu, 0.65Fe, 0.025C, 0.012N, 0.006H, 0.12O) 1 in. plate (5.33Al, 5.34V, 1.96Sn, 0.65Cu, 0.59Fe, 0.015C, 0.018N, 0.006H, 0.081O) 3 by 9-in. forging (5.7Al, 5.3V, 2.2Sn, 0.75Cu, 0.69Fe, 0.08C, 0.004N, 0.006H, 0.148O) 3-in. forged plate (6.3Al, 4.1V, 0.13 Fe, 0.023C, 0.014N, 0.004H, 0.17O)	1600 F, 1 hr, WQ + 1050 F, 4 hr, AC 1650 F, 1 hr, WQ + 1125 F, 4 hr, AC Annealed: 1300 F, 2 hr, AC 1575 F, 1 hr, WQ + 1200 F, 4 hr, AC 1750 F, 1 hr, WQ + 1000 F, 4 hr ^e			double edge crack B = 0.5 in., 2a = 1 in., W = 3 in. three-point bend B = 0.25 in., a = 0.2 in., W = 0.5 in. center crack B = 1 in., 2a = 3 in., W = 9 in. wedge opening loaded (WOL) B = 2 in., a = 1.8 in., W = 6.2 in.	RW	RT	179	30	0.028	DeSisto & Hickey [35]	ELI grade alloy
														171	34	0.040		
														142	56	0.155		
														172	28	0.026		
														190	26	0.019		
														159	68	0.182		
153	72	0.221																
147	70	0.227																
148	65	0.192																
140	79	0.318																
159	68	0.182	Wessel [37]															
153	72	0.221																
147	70	0.227																
148	65	0.192																
140	79	0.318																

Ti-5Al-2.5Sn.....	2-in.-dia bar (6.2Al, 4.2V, 0.15Fe, 0.025C, 0.013N, 0.0074H, 0.195O)	1775 F, 1 hr (argon), WQ + 925 F, 4 hr ^d	surface crack B = 0.25 in., 0.09 in. < a < B/2, W = 1.5 in.	L	100	133	71	0.285	Randall [38]	ELI grade alloy
					150 RT	127 160	78 31	0.376 0.038		
Ti-5Al-2.5Sn.....	3 by 9-in. forging (6.5Al, 4.1V, 0.18Fe, 0.08C, 0.003N, 0.007H, 0.121O)	1650 F, 1 hr, WQ + 1100 F, 4 hr, AC	center crack B = 1 in., 2a = 3 in., W = 9 in.	RW	-110	176	47	0.071	Boeing Co. [36]	ELI grade alloy
					RT	147	37	0.063	Tiffany [39]	
					-110	176	36	0.042		
					RT ^h	214	52	0.059		
Ti-5Al-2.5Sn.....	0.188-in. sheet (5.2Al, 2.5Sn, 0.007Zr, 0.002Mn, 0.16Fe, 0.025C, 0.016N; 0.005H, 0.07O)	Annealed: AMS 4910 ^g	fatigue crack notch round D = 1.125 in., d = 0.77 in.	L	RT	147	37	0.063	Tiffany [39]	ELI grade alloy
					-110	176	36	0.042		
Ti-5Al-2.5Sn.....	0.5-in. plate (5.0Al, 2.6Sn, 0.006Mn, 0.16Fe, 0.023C, 0.01N, 0.001H, 0.086O)	Annealed: 1500 F, FC ^g	three point bend B = 0.5 in., a = 0.1 in., W = 0.5 in.	RT	-423	207	52	0.063	Carman [40]	ELI grade alloy
					-423	207	52	0.063		

^a WQ = water quenched; AC = air cooled; FC = furnace cooled.

^b RW crack normal to rolling direction, propagation in width direction.

^c RT = room temperature.

^d Specimens heat treated after rough machining.

^e Specimens cut from quenched and aged full section plate.

^f WR crack normal to width direction, propagation in rolling direction.

^g Specimens cut from annealed plate.

^h RT crack normal to rolling direction, propagation in thickness direction.

results of these efforts are summarized in a recent report prepared for E-24 Sub I on High Strength Metallic Materials [3]. Using this report as a background, E-24 Sub I has drafted a "Recommended Practice for Plane Strain Fracture Toughness Testing of High Strength Metallic Materials Using a Fatigue Cracked Bend Specimen" [33]. This practice gives specimen size requirements, methods of specimen preparation, and procedures for data analysis. The general principles described are applicable to other types of specimens, and data obtained in accordance with these principles should have a high probability of representing true K_{Ic} values. Unfortunately, a considerable amount of the published K_{Ic} data on titanium alloys was obtained before all of the details of test technique and data analysis could be satisfactorily resolved. For this reason, with the few exceptions noted, the K_{Ic} values given here must be considered as estimates until confirmed by tests conducted in accordance with the Recommended Practice.

Values of plane strain fracture toughness are given in Table 1 for three titanium alloys in annealed and heat treated conditions [33-40]. This table also provides information concerning the source of data, the type of specimens from which they were obtained, and an indication as to whether the test procedures satisfied the known requirements for a valid K_{Ic} determination. A column giving $(K_{Ic}/\sigma_{YS})^2$ has been added to the table in order to provide a relative measure of the tolerable crack size at the yield strength. In practice, by applying the appropriate coefficient to this quantity, an estimate of the tolerable size of a particular type of flaw in a given body at stresses approaching the yield strength is obtained. For example, $\pi/2$ times this quantity gives the maximum diameter of a buried circular crack in a large body that could be tolerated when the stress remote from the crack plane reaches the yield strength. All of the results presented in Table 1 are illustrated in Fig. 19 where $(K_{Ic}/\sigma_{YS})^2$ is plotted as a function of the yield strength.

Ti-6Al-6V-2Sn

It will be noted from Table 1 that K_{Ic} data known to satisfy all the requirements for a valid test are available from two heats of this alloy. One of these [33] is an early production product, probably not representative of present melting and processing practice, while the other [34] is more recent and probably typical of current production. Data from two additional investigations [35,36] have been added to the table, for which the dates of production are unknown.

Figure 19 presents the crack size parameter $(K_{Ic}/\sigma_{YS})^2$ as a function of the yield strength for all four heats of this alloy. The curve has been established by the data from the earlier production heat. At yield strength levels above about 170 ksi quite limited crack tolerance is indicated. With decreasing strength level the curve describes only a small elevation

in toughness, while two data points from the more recently produced stock offer much more promise. This advantage, however, is apparently lost if the temperature is reduced to -110 F, which raises the yield strength above 170 ksi. In this range all the data agree in describing very low crack tolerance.

Ti-6Al-4V

There is no scarcity of data on this alloy from fracture investigations using sharply notched or fatigue-cracked specimens. However, only a small portion of this information can be identified as possibly useful

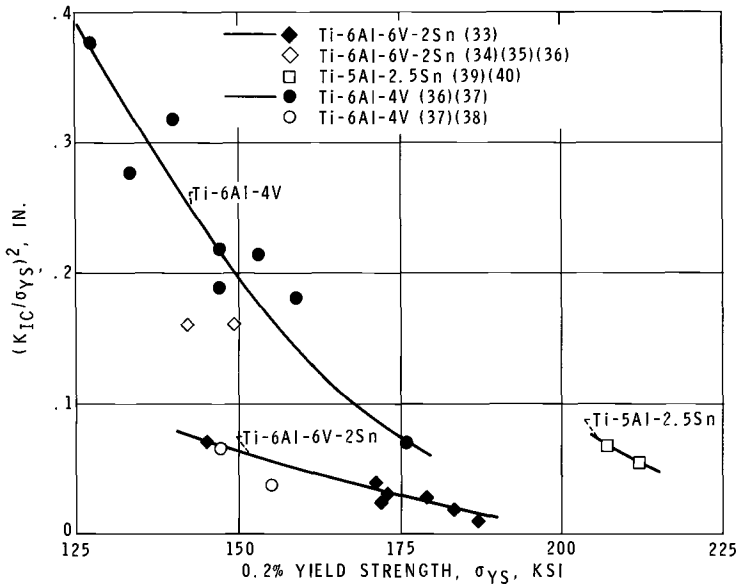


FIG. 19—Crack size parameter $(K_{Ic}/\sigma_{YS})^2$ as a function of the 0.2 per cent yield strength for three titanium alloys (from Table 1).

for K_{Ic} determination. The K_{Ic} values presented in Table 1 and Fig. 19 were obtained from several specimen types, all of which were of adequate size to permit determination of the toughness values reported. However, we do not have sufficient knowledge of the instrumentation or data analysis methods used to compare them with the requirements of the ASTM Draft Recommended Practice.

As might be expected, the plane strain fracture toughness of this alloy in the aged condition is primarily a function of the yield strength. Figure 19 describes a definite increasing trend in $(K_{Ic}/\sigma_{YS})^2$ with decreasing strength level for most of the data. However, at about the 150 ksi yield level two very low data points are observed. In our opinion it is doubtful that such variations in toughness could be explained by

differences in composition or processing history. The data from this alloy illustrate the difficulty one would encounter in assigning a K_{Ic} to Ti-6Al-4V in the aged condition.

In the annealed condition the toughness of Ti-6Al-4V at normal temperatures is very high and correspondingly large specimens would be required for a K_{Ic} evaluation. None of the fracture toughness data available to us on annealed Ti-6Al-4V was obtained using sufficiently large specimens to permit a valid K_{Ic} determination. For example, Goode et al [4] report a K_{Ic} value of 110 ksi $\sqrt{\text{in.}}$ from 1-in.-thick plate having a yield strength of 105 ksi and a value of 151 ksi $\sqrt{\text{in.}}$ from 2-in. plate with a yield strength of 99 ksi. These evaluations were made at the Naval Research Laboratory using 1- and 2-in.-square cross-section bend specimens. However, according to the ASTM Recommended Practice, the required thickness and crack length would be 2.7 and 5 in., respectively. In other words, the plate material is considerably thinner than would be required to make a valid K_{Ic} determination. It should be noted that the Naval Research Laboratory does not depend solely on K_{Ic} tests to evaluate the fracture properties of low strength alloys, but also employs a variety of special methods including tests designed to closely simulate service conditions.

Ti-5Al-2.5Sn

This annealed α alloy at normal test temperatures is as tough or tougher than annealed Ti-6Al-4V, and no data exist to permit even an estimate of the room temperature K_{Ic} value. At liquid hydrogen temperature fracture toughness tests have been made by Tiffany [39] and by Carman [40], and the calculated K_{Ic} values are given in Table 1 and Fig. 19. The values from these two extra low interstitial heats agree quite well but in both cases were determined from specimens having insufficient crack length, and probably should be considered as rough estimates.

Concluding Remarks

Strengthening agents such as cryogenic temperatures, aging treatments, and interstitial element additions were shown to produce low levels of crack tolerance in titanium alloys. Solution treated or underaged structures normally quite tough, become unstable during long-time exposure to elevated temperatures resulting in appreciable embrittlement. This reduction in crack tolerance may occur at temperatures well below those employed in aging and often precede increases in yield strength. A practical example of this type of instability relates to the behavior of spot welds in otherwise stable, overaged sheet exposed for long time periods at elevated temperatures. The spot welds, being essentially solution treated, subsequently age to a brittle condition during exposure.

Reductions in interstitial element contents to levels below those commercially stipulated for the ELI grade compositions can result in further improvements in crack tolerance.

Slow cooling from the annealing temperature of alpha and super-alpha alloys containing high aluminum contents results in the precipitation of Ti_3Al and a corresponding loss in crack tolerance. Rapidly cooled structures in these alloys revert to the slow cooled, brittle structure during elevated temperature exposure.

Moderate amounts of cold work can improve the smooth strength of all-alpha and all-beta alloys with no corresponding loss in crack tolerance. Heavier amounts of cold work or cold working plus aging, on the other hand, produces a considerable loss in crack tolerance.

In the presence of cracks, aggressive liquid environments cause delayed failure under sustained load conditions in a great number of titanium alloys. Among these are aqueous solutions of certain halides, many organic solvents and several halogenated hydrocarbons. Environmental testing has thus become an essential prerequisite in the selection of titanium alloys for critical applications. In this respect, testing standards, preferably ones which will produce results interpretable in terms of linear elastic fracture mechanics, are greatly needed.

There is a dearth of valid plane strain fracture toughness data for titanium alloys. In those few instances where results are available, departure from recommended practice in testing and data analysis methods or disagreement of values obtained or both indicate that the application of fracture mechanics to titanium alloy systems is indeed in an early state of development and further work in this area is sorely needed.

References

- [1] Srawley, J. E. and Brown, W. F., Jr., "Fracture Toughness Testing and Its Applications," *Fracture Toughness Testing and Its Applications, ASTM STP 381*, American Society for Testing and Materials, 1965, p. 133.
- [2] Brown, W. F., Jr., "Fracture Testing and the ASTM," *Materials Research and Standards*, Vol. 7, No. 3, Mar. 1967, pp. 117-120.
- [3] Brown, W. F., Jr., and Srawley, J. E., *Plane Strain Crack Toughness Testing of High Strength Metallic Materials, ASTM STP 410*, American Society for Testing and Materials, 1967.
- [4] Goode, R. J. et al, "Metallurgical Characteristics of High Strength Structural Materials," NRL-6454, Naval Research Laboratory, 1966. (Available from DDC as AD-641262.)
- [5] Tiffany, C. F. and Masters, J. N., "Applied Fracture Mechanics," *Fracture Toughness Testing and Its Applications, ASTM STP 381*, American Society for Testing and Materials, 1965, p. 249.
- [6] Kies, J. A. et al, "Fracture Testing of Weldments," *Fracture Toughness Testing and Its Applications, ASTM STP 381*, American Society for Testing and Materials, 1965, p. 328.
- [7] Christian, J. L. and Hurlich, A., "Physical and Mechanical Properties of Pressure Vessel Materials for Applications in a Cryogenic Environment," ASD-TDR-62-258, Pt. II, General Dynamics/Astronautics, 1963. (Available from DDC as AD-404025.)

- [8] Shannon, J. L., Jr., and Brown, W. F., Jr., "Effects of Several Production and Fabrication Variables on Sharp Notch Properties of 5Al-2.5Sn Titanium Alloy Sheet at Liquid Hydrogen Temperature," *Proceedings, American Society for Testing and Materials*, Vol. 63, 1963, pp. 809-829.
- [9] Espey, G. B., Jones, M. H., and Brown, W. F., Jr., "Sharp-Edge-Notch Tensile Characteristics of Several High-Strength Titanium Sheet Alloys at Room and Cryogenic Temperatures," *Low-Temperature Properties of High-Strength Aircraft and Missile Materials*, ASTM STP 287, American Society for Testing and Materials, 1961, p. 74.
- [10] Blackburn, M. J., "Phase Transformations in the Alloy-Ti:8% Al:1% Mo:1% V," D1-82-0402, Boeing Scientific Research Laboratories, 1965.
- [11] Clark, D., Jepson, K. S., and Lewis, G. I., "A Study of the Titanium-Aluminum Systems up to 40 At.-% Aluminum," *Journal, Institute for Metals*, Vol. 91, No. 6, 1962-63, pp. 197-203.
- [12] Crossley, F. A., "Titanium-Aluminum Equilibrium Diagram," IITRI-B6034-13, IIT Research Inst., 1965. (Available from DDC as AD-474518.)
- [13] Piper, D. E., "Effect of Heat Treatment Variables on the Fracture Toughness of Duplex Annealed 8Al-1Mo-1V-Ti Alloy Sheet," *Materials Technology Summary Report*, Boeing Co., 1965, p. 3.
- [14] Roy, A., Chave, C., and Weiss, V., "Material Evaluation for a Mach III Transport Plane," MET-873-634-QP4A (NASA CR-50553), Syracuse University, 1963.
- [15] Roy, A. and Weiss, V., "Further Material Evaluation for Supersonic Transport Aircraft," MET-E-873-6312-F (NASA CR-53483), Syracuse University, 1963.
- [16] Espey, G. B., Bubsey, R. T., and Brown, W. F., Jr., "A Preliminary Report on the NASA Sheet Alloy Screening Program for Mach 3 Transport Skins," *Proceedings, American Society for Testing and Materials*, Vol. 62, 1962, pp. 837-854.
- [17] Jaffee, R. I., "The Physical Metallurgy of Titanium Alloys," *Progress in Metal Physics*, Vol. 7, Chalmers, B. and King, R., eds., Pergamon Press, New York, 1958, p. 65.
- [18] Holden, F. C., Schwartzberg, F. R., and Ogden, H. R., "Tensile Properties of Titanium Alloys at Low Temperatures," DMIC Report No. 107, Battelle Memorial Institute, 1959. (Available from DDC as AD-207911.)
- [19] Christian, J. L. et al "Effects of Impurity Elements and Cold Rolling on the Mechanical Properties of Titanium-5Al-2.5Sn Alloy at Room and Cryogenic Temperatures," *Proceedings, American Society for Testing and Materials*, Vol. 63, 1963, p. 578.
- [20] Broadwell, R. G. and Wood, R. A., "Titanium Alloys for Cryogenic Service," *Materials Research and Standards*, Vol. 4, No. 10, Oct. 1964, pp. 549-554.
- [21] Sachs, G. and Sessler, J. G., "Effect of Stress Concentration on the Tensile Strength of Heat Treated Titanium Alloy Sheet at Various Temperatures," Final Report (Contract NOas 58-855c), Syracuse University, 1960.
- [22] Repko, A. J. and Brown, W. F., Jr., "Influence of Cold Rolling and Aging on Sharp Notch Properties of β Titanium Sheet," *Proceedings, American Society for Testing and Materials*, Vol. 62, 1962, pp. 869-877.
- [23] Bomberger, H. B., Discussion to Repko and Brown, "Influence of Cold Rolling and Aging on Sharp Notch Properties of β Titanium Sheet," *Proceedings, American Society for Testing and Materials*, Vol. 62, 1962, p. 878.
- [24] Weiss, V. and Sessler, J. G., eds., "Ti-8Al-1Mo-1V Code 3709," *Aerospace Structural Metals Handbook, Vol. II, Non-Ferrous Alloys*, Syracuse University Press, Syracuse, N. Y., 3rd revision, Mar. 1966.
- [25] *Stress Corrosion Cracking of Titanium*, ASTM STP 397, American Society for Testing and Materials, 1966.
- [26] Brown, B. F., "A New Stress-Corrosion Cracking Test for High-Strength Alloys," *Materials Research and Standards*, Vol. 6, No. 3, Mar. 1966, pp. 129-133.
- [27] Brown, B. F. et al, "Marine Corrosion Studies: Stress-Corrosion Cracking,

- Deep Ocean Technology, Cathodic Protection, Corrosion Fatigue," NRL-Memo-1634, Naval Research Labs., 1965. (Available from DDC as AD-621743.)
- [28] Curtis, R. E., Smith, S. H., and Spurr, W. F., "Titanium Alloy Selection Report," D6-19729, Boeing Co. Commercial Supersonic Transport Program, 1965.
- [29] Hatch, A. J., Rosenberg, H. W., and Erbin, E. F., "Effects of Environment on Cracking in Titanium Alloys," *Stress-Corrosion Cracking of Titanium, ASTM STP 397*, American Society for Testing and Materials, 1966, p. 122.
- [30] Lane, I. R., Jr., Cavallaro, J. L., and Morton, A. G. S., "Sea Water Embrittlement of Titanium," *Stress-Corrosion Cracking of Titanium, ASTM STP 397*, American Society for Testing and Materials, 1966, p. 246.
- [31] Tiffany, C. F. and Masters, J. N., "Investigation of the Flaw Growth Characteristics of 6Al-4V Titanium Used in Apollo Spacecraft Pressure Vessels," D2-113530-1 (NASA CR-65586), Boeing Co., 1967.
- [32] Defense Metals Information Center Seminar on Accelerated Crack Propagation of Titanium by Methanol, Halogenated Hydrocarbons and Other Solutions, Battelle Memorial Institute, Columbus, Ohio, Mar. 6, 1967. (To be published.)
- [33] Srawley, J. E., Jones, M. H., and Brown, W. F., Jr., "Determination of Plane Strain Fracture Toughness," *Materials Research and Standards*, Vol. 7, No. 6, June 1967, p. 262.
- [34] Bubsey, R. T., NASA Lewis Research Center, Cleveland, Ohio, unpublished data.
- [35] DeSisto, T. S. and Hickey, C. F., Jr., "Low-Temperature Mechanical Properties and Fracture Toughness of Ti-6Al-6V-2Sn," *Proceedings*, American Society for Testing and Materials, Vol. 65, 1965, pp. 641-653.
- [36] "Thick Section Fracture Toughness," AFML-TDR-64-236, Boeing-North American, 1964.
- [37] Wessel, E. T., Clark, W. G., and Wilson, W. K., "Engineering Methods for the Design and Selection of Materials Against Fracture," Report 66-9B4-315-R1, Westinghouse Research Laboratories, 1966. (Available from DDC as AD-801005.)
- [38] Randall, P. N., "Severity of Natural Flaws as Fracture Origins and a Study of the Surface-Cracked Specimen," AFML-TR-66-204, TRW Systems Group, 1966. (Available from DDC as AD-487986.)
- [39] Tiffany, C. F., Lorenz, P. M., and Hall, L. R., "Investigation of Plane-Strain Flaw Growth in Thick-Walled Tanks," D2-24078-1 (NASA CR-54837), Boeing Co., 1966.
- [40] Carman, C. M., Forney, J. W., and Katlin, J. M., "Plane Strain Fracture Toughness and Mechanical Properties of 5Al-2.5Sn ELI Titanium at Room and Cryogenic Temperatures," FA-R-1796 (NASA CR-54296), Frankford Arsenal, 1966.

Structural Ductility of High Strength Titanium Alloys

REFERENCE: Papirno, Ralph, "Structural Ductility of High Strength Titanium Alloy," *Applications Related Phenomena in Titanium Alloys, ASTM STP 432*, American Society for Testing and Materials, 1968, pp. 64-79.

ABSTRACT: The concept of the ductility ratio was introduced by Gerard in 1961, as a quantitative measure of structural ductility useful design. An experimental technique for determining ductility ratio was established which involved the testing to failure of internally notched tension specimens containing a variety of stress concentration values, and this technique was applied in preliminary tests on high-strength aged beta titanium alloy. In the work reported here, more extensive test programs involving the all beta titanium alloy Ti-13V-11Cr-3Al in several thicknesses of sheet are described. The test materials were aged to give the highest strengths prior to testing. The paper presents the technique for performing the tests, the method of reducing the data, as well as giving the experimental results. The results of a literature survey of notch strength data from which ductility ratio values could be derived are also given, and from this survey the effect of decreasing the temperature in increasing the ductility ratio is demonstrated. The value of the ductility ratio varies from zero for a perfectly plastic material to unity for a perfectly brittle material. For the limited ductility alloys tested in the program the ductility ratio was in the range 0.1 to 0.2. There appeared to be a size effect evident with the thinnest sheet displaying the lowest ductility ratio values (highest ductility). The range of thicknesses tested was from 0.040 to 0.093 in. The test results lend additional experimental verification to the relation delineated by Gerard between the strength/weight ratio and the ductility ratio: $\sigma_{tu}/\rho = 1.6 \times 10^9 e^{1/9}$.

KEY WORDS: titanium alloys, ductility, structural ductility, elastic stress concentrations, strength, notch strength

Introduction

The common measures of ductility such as the elongation or reduction in area in a tension test or the height of cupping in an Erichsen test have long been employed to characterize materials by comparison with acceptance values. The structural designer, however, cannot directly apply such ductility data in a rational quantitative manner in material

¹ Senior scientist, Allied Research Associates, Inc., Concord, Mass.

selection for design of tension structures. If the objective is an efficient, minimum weight design and if the structure contains stress concentrations, there are difficulties in using the common measures of ductility in the structural design process.

If tension structures could be designed and constructed without stress concentrations, ductility would assume a minor role in material selection for efficient design. The major consideration would be the tensile strength/weight ratio of the material modified by economic considerations. However, it has not proven feasible to design practical tension structures of minimum weight where the stress is uniformly the nominal value. Even if such a structure could be designed, it would probably be impossible to construct it without introducing stress concentrations in the construction process.

Stress Concentration Factors

In a general sense the value of a stress concentration factor is directly related to the sharpness of a discontinuity in a structural configuration. As the structure is loaded the stress concentration factor will generally remain constant so long as the deformations are small, that is, so long as the material remains elastic. The effect of ductility is to reduce the sharpness of the discontinuity as the material is stressed beyond the elastic limit and simultaneously reduce the values of the stress concentration factor. In limited ductility materials, the stress concentration reduction is relatively small, and the structure can fail statically at fractions of the ultimate tensile strength of the material.

It has been possible to determine stress concentration values for many common structural discontinuities such as round and elliptical holes, fillets, corners, etc., and these have conveniently been collected and published [1].² The structural designer will generally be able to specify the maximum value of stress concentration factor in his design using the published data or if necessary to determine the value using the techniques of theoretical and experimental stress analysis. Stress concentrations due to fabrication are not easily determined; however, with close control over manufacturing processes, they can usually keep to values less than those inherent in the design.

The structural designer, developing an efficient configuration, must be able to relate the strength of the material of construction to the strength of the designed structure containing stress concentrations. The essential mechanical properties required are the ultimate tensile strength and the strength of the material in the presence of stress concentrations. The latter quantity is related to ductility.

² The italic numbers in brackets refer to the list of references appended to this paper.

Ductility Ratio

Gerard in 1961 introduced the concept of ductility ratio as a material parameter to relate the tensile strength of a material to that of a structure fabricated of the given material and containing stress concentrations [2]. In the following year he presented a number of methods whereby this concept might be applied in structural design with special reference to pressure vessels [3]. It was demonstrated, using a semiempirical analysis, that it was also possible to define ductility ratio in terms of the strength of notched specimens using the following equation:

$$k_p = \frac{1}{k_s} + \left(k_e - \frac{1}{k_s} \right) e \dots \dots \dots (1)$$

where:

- k_p = plastic stress concentration factor (inverse of notch strength),
- k_s = notch strengthening factor,
- k_e = elastic stress concentration factor, and
- e = ductility ratio.

An experimental technique for evaluating ductility ratio was established based upon Eq 1 which involved the testing to failure of internally notched tension specimens where the notch end radii introduced a series of known elastic stress concentration values [4]. The technique was applied in preliminary tests on high-strength aged beta titanium alloy.

Currently Reported Investigation

In the work reported here extensive programs involving the testing of aged titanium alloy Ti-13V-11Cr-3Al at room temperature were accomplished. The test procedure, test results, and the method of reducing the data are given. The results of a literature survey of notch strength data from which ductility ratio values for a number of titanium alloys at various temperatures are also given. The relationship between strength and ductility ratio for a large number of materials is also presented.

Ductility Ratio Experiments

A complete description of the technique for evaluating the ductility ratio experimentally by the use of notched tension specimens is given in Ref 4. The basis of the test is Eq 1 where the test variables are assumed to be k_e and k_p . The quantities k_s and e are assumed to be constant and specific for a given material, in a given condition of fabrication and in a given environment. A brief description of the procedure and the data reduction process is given in the next several paragraphs.

General Description of Test Techniques

A series of internally notched specimens are prepared with varying notch-end radii. The value of k_e for any specimen is predetermined from

the notch dimensions and the chosen notch-end radius. The specimen is fractured and the specimen strength is determined using the net-section area. Separate tests are performed on standard uniform section sheet tension specimens to establish the ultimate tensile strength of the material. The plastic concentration factor for any specimen is then computed by dividing the ultimate tensile strength by the strength of the notched specimen; this value is the inverse of the familiar notch-strength expressed as a fraction of the ultimate tensile strength.

After a series of tests is completed, the $k_e - k_p$ data are plotted on a linear graph with k_e on the abscissa. Under the given assumptions, these data for a material should lie on a straight line whose equation is given by Eq 1. The latter can be put in the familiar slope-intercept form:

$$k_p = ek_e + (1/k_s)(1 - e) \dots \dots \dots (2)$$

where the e represents the slope of the line and the last term on the right hand side is the intercept on the k_p axis. Using a simple least squares analysis on the data it is possible to find the slope and intercept of the best straight line of the form of Eq 2, which fits the data. The slope value is the ductility ratio, and the notch strengthening factor can be computed from the intercept value.

The material properties which determine the value of the notch strengthening factor, k_s , have not yet been delineated. However, notch strengthening may likely be associated with the effects of the triaxial stress field at the root of the notch which develops when necking occurs. Such other factors as the Poisson's ratio values, anisotropy, the ductility ratio itself, and specimen dimensions and configuration may all influence notch strengthening.

Expected magnitudes of the ductility ratio vary from zero for a perfectly ductile material to unity for a material which exhibits no yielding up to fracture. Materials with ductility ratio values of 0.1 and higher may be considered to be limited ductility materials. Notch strengthening factors for most materials are in the range from 1.0 to 2.0. The value of unity connotes no notch strengthening.

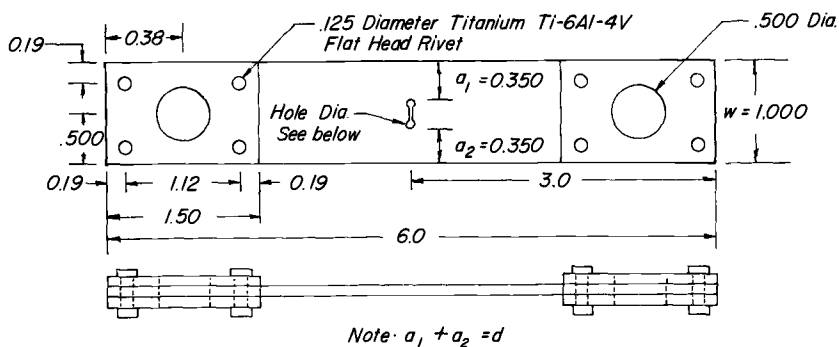
Previous Results

Our previous experiments on three separate thicknesses of aged all beta alloy in Ref 4 showed considerable scatter in the plastic concentration factor results. In these previous tests, single experiments were performed at each elastic concentration value in the range from 4 to 11. In an effort to refine the technique in the currently reported program, duplicate experiments were performed at each elastic stress concentration value, and a larger number of elastic concentration factor levels in the range 4 to 10 were employed so that the current results are considered to be statistically more significant. Ultimate tensile strength data were obtained from uniform section specimens.

Specimen Material

Nominal 0.040-in.-thick sheet of Ti-13V-11Cr-3Al, Heat No. D-1680 was obtained from Titanium Metals Corporation of America in the solution heat treated condition. The composition reported by the manufacturer was as follows:

Carbon.....	0.021 per cent
Iron.....	0.150 per cent
Nitrogen.....	0.020 per cent
Aluminum.....	3.00 per cent
Vanadium.....	13.70 per cent
Chromium.....	11.00 per cent
Hydrogen.....	0.010 per cent
Titanium.....	balance



Nominal Elastic Concentration	Hole Diameter (in)
4	0.0596
5	0.0330
6	0.0210
7	0.0160
8	0.0118
9	0.0098
10	0.0079

FIG. 1—Internally notched specimen configuration.

The stock had been hot rolled and surface conditioned by conventional procedures and was solution heated at $1425\text{ F} \pm 25\text{ F}$ 10 min. After specimen blanks were machined, they were aged at 900 F 72 hr and furnace cooled in vacuum.

Specimens

Two types of specimens were prepared: uniform-section, ultimate tensile strength specimens and internally notched specimens of the configuration and dimensions given in Fig. 1. The notch end holes were precisely located using a jig and were drilled and reamed before the connecting slot was cut using procedures described in detail in Ref 4.

Specimen dimensions are given in Table 1 as determined by measurement. Hole radii were those of the reamer size used in finishing the hole; ligament dimensions were determined using Johansson blocks; all other dimensions were obtained by micrometer caliper.

End plates were riveted in place with titanium rivets for specimens with notch end radii of 0.0298, 0.0165, and 0.0105 in. to prevent premature failure of the specimens through the loading holes. The fracture loads for the remainder of the specimens were sufficiently small to make this procedure unnecessary.

Test Procedure

Specimens were installed in universal joint loading clevises in an Instron 10,000-lb-capacity testing machine. The machine was calibrated

TABLE 1—Notched specimen dimensions.

Specimen No.	Thickness, in.		Ligament, in.		Width, in. <i>w</i>	Hole Radii, in. <i>r</i>
	<i>t</i> ₁	<i>t</i> ₂	<i>a</i> ₁	<i>a</i> ₂		
12.....	0.0371	0.0370	0.3515	0.3522	1.0002	0.0298
10.....	0.0376	0.0382	0.0382	0.3512	1.0003	0.0298
13.....	0.0370	0.0366	0.3505	0.3490	1.0003	0.0165
16.....	0.0372	0.0371	0.3475	0.3505	1.0003	0.0165
14.....	0.0382	0.0382	0.3535	0.3542	1.0003	0.0105
20.....	0.0383	0.0385	0.3529	0.3528	1.0004	0.0105
5.....	0.0385	0.0385	0.0389	0.3589	1.0001	0.0080
33.....	0.0385	0.0385	0.3626	0.3599	1.0002	0.0080
28.....	0.0385	0.0385	0.3600	0.3625	1.0003	0.0059
3.....	0.0380	0.0380	0.3635	0.3612	1.0000	0.0059
8.....	0.0381	0.0378	0.3630	0.3622	1.0002	0.0049
9.....	0.0380	0.0384	0.3545	0.3600	1.0000	0.0049
31.....	0.0382	0.0382	0.3445	0.3449	0.9998	0.0039
11.....	0.0365	0.0368	0.3459	0.3461	0.9999	0.0039

just prior to the tests. All specimens were tested in a single session, and the machine calibration was checked after the tests. There was no change in the calibration. A constant head speed of 0.05 in./min was employed until fracture. Fracture stress was computed from the fracture load and the net section area.

Test Data

Elastic concentration factors for the notched specimens were computed from the relationship:

$$k_e = \left[\frac{d/w}{2 - d/w} \right]^{1/2} [1 + (L/r)^{1/2}] \dots \dots \dots (3)$$

where:

d = total net section width,

w = specimen width,
 $2L$ = notch length, and
 r = hole radius.

The derivation and substantiation by photoelasticity of Eq 3 is given in Ref. 5 Computations based upon Eq 3 can be considerably simplified by eliminating the factor L from the equation, resulting in an expression of the form:

$$k_e = \left[\frac{d/w}{2 - d/w} \right]^{1/2} + \left[\frac{d/w}{2 - d/w} \right]^{1/2} [2 - 2d/w]^{1/2} [w/r]^{1/2} \dots (4)$$

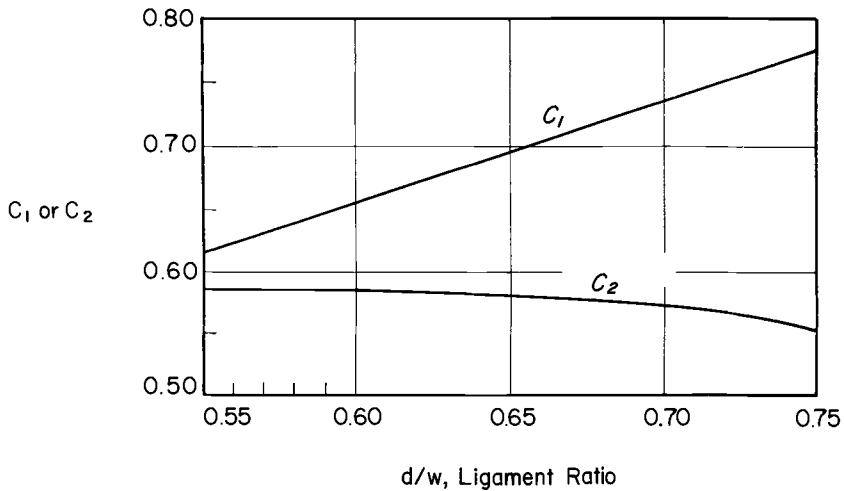


FIG. 2—Values of the constants C_1 and C_2 in the elastic stress concentration relation: $k_e = C_1 + C_2 (W/r)^{1/2}$.

It is possible to express Eq 4 in simplified form as

$$k_e = C_1 + C_2 [w/r]^{1/2} \dots (5)$$

Practical specimens will have a range of d/w values $0.55 < d/w < 0.75$. Shown in Fig. 2 are values of C_1 and C_2 for the range of d/w of interest. It should be noted that Eq 5 together with Fig. 2 can also be used to obtain nominal required values of elastic stress concentration factor in specimen design.

Plastic concentration factors were computed from the notch strength and the ultimate tensile strength according to:

$$k_p = \sigma_{uts} / \sigma_{ns} \dots (6)$$

where σ_{uts} is the ultimate tensile strength obtained from standard uniform section tension specimens and σ_{ns} is the notch specimen strength.

TABLE 2—Elastic and plastic stress concentration factors for internally notched specimens.

Specimen	Elastic Concentration Factor	Notch Specimen Strength, ksi ^a	Plastic Concentration Factor
12.....	4.04	167.2	1.25
10.....	4.04	178.8	1.17
13.....	5.16	165.0	1.27
16.....	5.00	163.7	1.28
14.....	6.26	151.1	1.39
20.....	6.26	139.1	1.50
5.....	6.91	136.2	1.54
33.....	7.00	135.3	1.55
28.....	8.04	128.2	1.63
3.....	8.03	133.8	1.57
8.....	8.74	116.3	1.80
9.....	8.77	119.8	1.75
31.....	9.84	117.8	1.78

^a Based upon net section area.

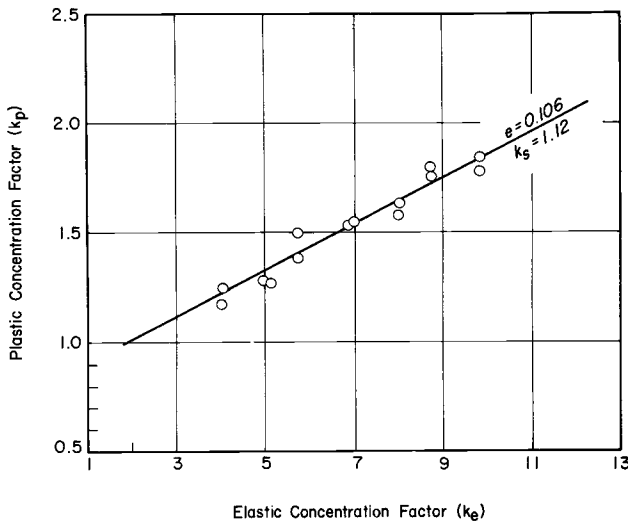


FIG. 3—Experimental results for nominal 0.040-in.-thick sheet of aged titanium alloy Ti-13V-11Cr-3Al.

The ultimate tensile strength of the material from two uniform section specimens gave values of 208.0 and 211.0 ksi. The average value, 209.5 ksi, was employed in computing the plastic stress concentration factor. The data are given in Table 2.

Data Analysis and Discussion

Shown in Fig. 3 are the test results of Table 2 together with a straight line based upon Eq 2 and obtained by a least squares analysis of the data.

The ductility ratio and notch strengthening factor, obtained directly from the analysis, were found to be:

$$e = 0.106 \quad \text{and} \quad k_s = 1.12$$

as shown in the figure. The scatter in the data indicated that a statistical approach should be used to evaluate the ductility ratio. The simple least squares method was the logical choice based upon the anticipated linear behavior of the results from Eq 2.

The actual source of the scatter has not been determined; however, there may be contributions by elements which affect both the elastic and plastic stress concentration factors. The elastic value of the concentration factor is very sensitive to the local radius of curvature at the notch end. Small irregularities in the drilling and reaming procedure may introduce undetectable dimensional changes in the material at the hole periphery such that the radius of the hole at the notch end might not be the same as that of the reamer which was used as a finishing tool. Microscopic inhomogeneities in the material at the notch ends would have a significant effect on the plastic concentration factor. There may be other effects which also tend to cause scatter including small eccentricities in the specimen, small misalignments in the testing machine and loading clevises, and residual stresses in the material. It would appear, therefore, that in the determination of the ductility ratio, numbers of tests at each elastic stress concentration level are essential. The actual minimum number required for a value of e with a particular degree of confidence has not been determined and will require further testing and additional statistical analysis.

Data previously obtained for the same alloy [4] have been compared with the current data in Fig. 4. In the figure the lines marked 2 and 3 were for test results for two thicknesses of material supplied by Crucible Steel (CRUC) and those marked 1 and 4 by Titanium Metals Corporation of America (TMCA). The current data are those of line 4.

The data in Fig. 4 suggest that there is a thickness effect in the ductility ratio with higher ductility ratio for thicker sheet stock. It appears, however, that notch strengthening may not be completely a geometric effect as has been suggested [6] since the values for three sets of data represented by lines 2, 3, and 4 show only a ± 3 per cent variation from an average value of $k_s = 1.15$ while the thickness varies from 0.040 to 0.093 in.

Derived Ductility Ratio Data

Data from a limited number of notch strength tests on titanium specimens with stated elastic stress concentration factors have been published. The author has analyzed these data to determine the values of the ductility ratio and notch strengthening factor using the least squares method.

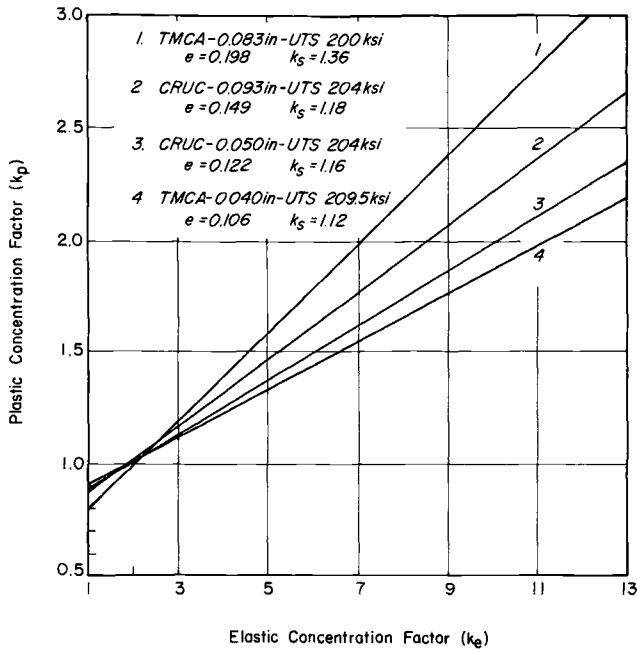


FIG. 4—Comparison of test results for several thicknesses and different heats of aged titanium alloy Ti-13V-11Cr-3Al.

TABLE 3—Ductility data for various titanium alloys at various temperatures

Material	Temperature, deg F	$\bar{\epsilon}$	k_s	σ_{tu} , ksi	σ_{tu}/ρ , in.	Reference
Ti-4Al-3Mo-1V	-320	0.178	1.52	274	1.67×10^6	7
	-100	0.148	1.88	218	1.33	7
	RT ^a	0.100	1.67	184	1.13	7
	+250	0.0705	1.50	160	0.98	7
	+400	0.0484	1.17	155	0.96	7
	+600	0.0336	1.12	150	0.93	7
Ti-13V-11Cr-3Al	-320	0.440	10.58	157	0.90	7
	-100	0.234	2.02	211	1.21	7
	RT	0.123	1.30	200	1.14	7
	+400	0.0825	1.34	189	1.08	7
Ti-13V-11Cr-3Al	RT	0.108	0.98	195	1.11	8
Ti-6Al-4V	RT	0.049	...	170	1.06	8
Ti-5Al-3Cr-1Fe	RT	0.093	...	190	1.16	8

^a RT = room temperature.

In practically all cases the analyses were performed on data from only 3 or 4 tests (as contrasted with 14 tests for the results given in Fig. 3). Considerably less confidence can be placed in the results from the published data than in the results of the experiments reported in this paper,

since there appears to be some uncertainty in the values of the elastic stress concentration factor and since so few tests were performed. However, these published data are the only additional data which are available, and the results have some value in indicating trends although individual values may be erroneous by substantial amounts.

Elastic and plastic stress concentrations for the various titanium alloys are given, together with other pertinent data, in Table 3.

Actual test points for the Ti-4Al-3Mo-1V and the Ti-13V-11Cr-3Al

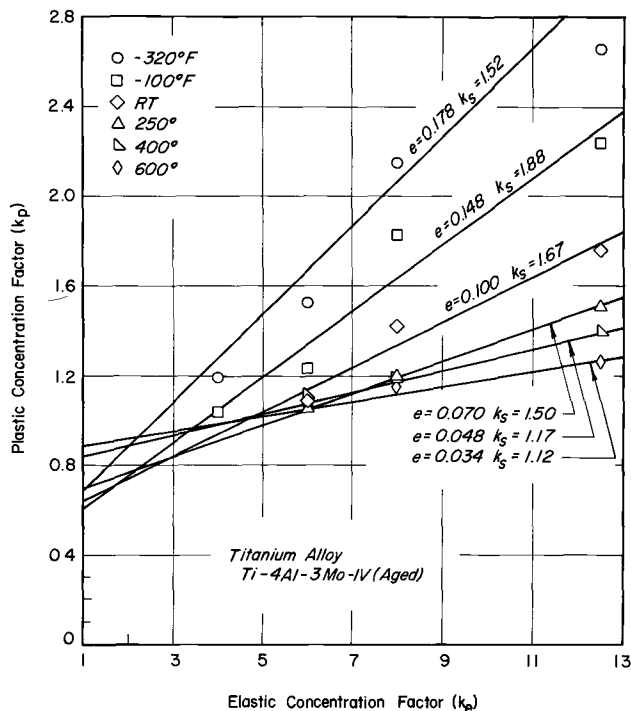


FIG. 5—Notch test data at various temperatures for aged titanium alloy Ti-4Al-3Mo-1V (Ref 7).

from data in Ref 7 are shown in Figs. 5 and 6. It should be noted that the values of elastic stress concentration which were reported were given generally to one significant figure, and this may in part account for the scatter of the data points around the straight line found from the least squares analysis.

Within the limitations of the data, both alloys show an expected increase in ductility ratio with decreasing temperature with the effect being markedly more severe in the Ti-13V-13Cr-3Al alloy. The data also show an increase in notch strengthening with decrease in temperature; however, in this respect, the data for the Ti-4Al-3Mo-1V alloy appear to be more consistent.

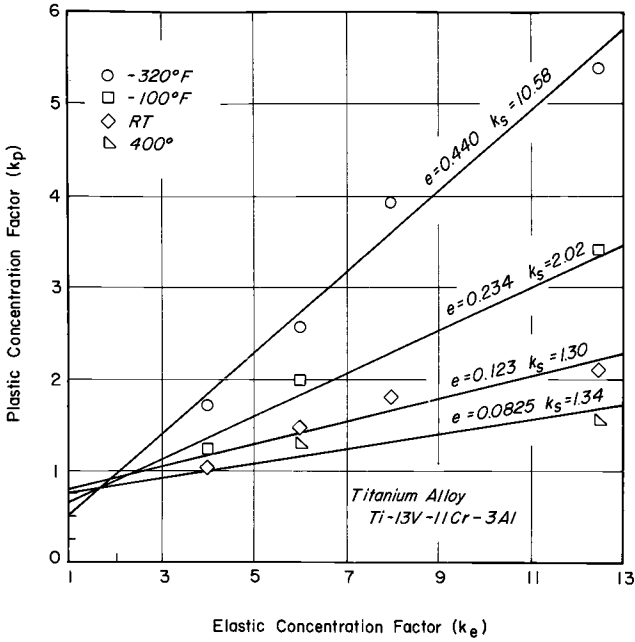


FIG. 6—Notch test data at various temperatures for aged titanium alloy Ti-13V-11Cr-3Al (Ref 7).

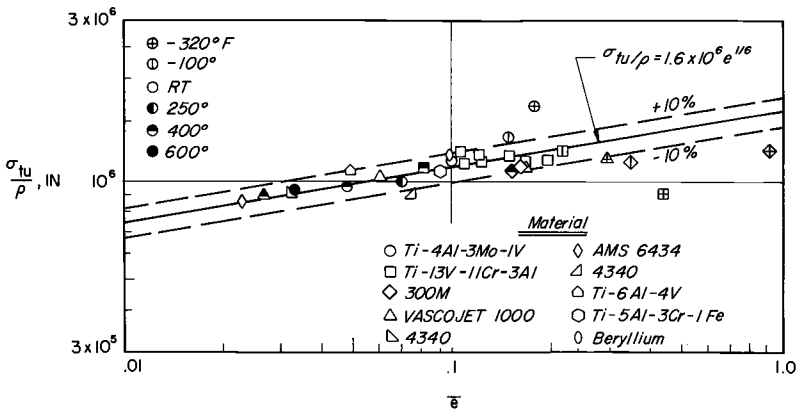


FIG. 7—Material strength/weight ratio as a function of ductility ratio.

Material Behavior

Gerard had previously suggested that the strength/weight ratio of a material may be related to the ductility ratio by an equation of the form

$$\sigma_{tu}/\rho = 1.6 \times 10^6 e^{1/6} \dots \dots \dots (7)$$

Shown in Fig. 7 are strength/weight-ductility data from Table 3, the

results of the current study, and from Refs 3, 4, and 7-10, together with Eq 7 and its ± 10 per cent limits. It is interesting to note that the scatter remains within ± 10 limits of Eq 7 for a large number of materials with the exception of some data at cryogenic temperatures. The reasons for the deviation at the low temperatures are not apparent at this time and must await further experiments with statistically significant numbers of specimens at low temperatures.

Within the limitations of the accuracy of the reviewed data, it can be concluded that Eq 7 is adequate to describe ductility behavior for titanium alloys and other materials at room and elevated temperatures.

These results should be considered tentative until additional ductility ratio data are obtained. At present, we are performing experiments on age hardened titanium alloy Ti-6Al-4V; when the results have been evaluated it may be possible to draw more definite conclusions. In these experiments, approximately six specimens per elastic stress concentration value are being tested so that the data, when treated statistically, should be more representative of the properties of the material. The experimental results will be reported in the near future.

Structural Design Considerations

Discussions of the applications of the ductility ratio concept in structural design are given in Refs 3 and 4. However, as an illustration of one application of such data, Fig. 8 was prepared to compare two titanium alloys for application in room-temperature designs: titanium alloys Ti-4Al-3Mo-1V (Ref 7) and Ti-13V-11Cr-3Al (data from the current investigation).

On the ordinate is structural strength/weight ratio. On the abscissa is elastic concentration factor. The curves represent the upper limit of strength for structures containing the given elastic stress concentrations. Structures with a given elastic stress level must be designed to operate at a stress value lower than that represented by the curve. The implicit assumption made in preparing the curves is that the behavior of a notched tensile strip containing a given elastic stress concentration is representative of all tension structures of the same material and same thickness having the same value of elastic stress concentration. Furthermore, it is assumed that a particular discontinuity is characterized by its value of elastic stress concentration and it is exactly equivalent in terms of its plastic and fracture behavior to all other discontinuities having the same value of elastic concentration regardless of their geometric configuration.

In preparing Fig. 8, test data were not available for elastic concentration values below $k_e = 4$, hence, the curves in the region from $k_e = 1$, representing the ultimate tensile strength of the material and $k_e = 4$ are shown as dashed to indicate the uncertainty in their shape. It is interesting to note, however, that the superior ultimate strength characteristics of the Ti-13V-11Cr-3Al alloy make this material favorable only for struc-

tures with very low elastic concentration factors. The Ti-4Al-3Mo-1V alloy, although it has lower ultimate strength values at room temperature, is superior for structures with elastic concentration factors of approximately three and higher. This is a consequence of its lower ductility ratio (and, hence, higher ductility) and its superior notch strengthening characteristics.

It should be noted that charts similar to that shown in Fig. 8 can be prepared for other alloys and temperatures and can serve both for design and for material comparisons. However, such design charts using

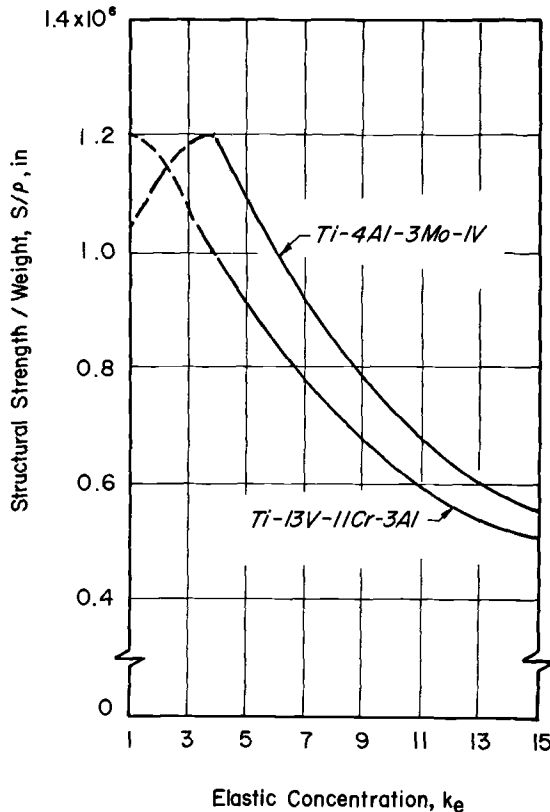


FIG. 8—Strength/weight of tension structures containing elastic stress concentrations of aged titanium alloys Ti-13V-11Cr-3Al and Ti-4Al-3Mo-1V.

notch strength data must be considered tentative and open to change except where sufficient data was available that the ductility properties may be considered statistically significant.

Conclusions

Ductility ratio data on a number of titanium alloys have been obtained both from specially designed experiments in which elastic concentrations factors were precisely determined and from the results of notch-strength

tests by other investigators in which only nominal values of elastic stress concentration factors were available and a limited number of tests were performed.

1. On the basis of ductility ratio experiments performed on aged titanium alloy Ti-13V-11Cr-3Al it can be concluded that reasonable values of the ductility ratio can be obtained when a number of tests at each of a number of precisely determined elastic stress concentration values.
2. Scatter in the test data occurs even with carefully performed experiments, and simple statistical techniques are necessary to process the raw data to obtain values of ductility ratio and notch strengthening factor.
3. Although direct evidence of the cause of data scatter is not available, it is suspected that small geometric or material irregularities may have a significant effect on the test results.
4. For aged titanium alloy Ti-13V-11Cr-3Al sheet, the ductility ratio increases with increasing thickness; however, no quantitative conclusions on the effect can be drawn.
5. The relation $\sigma_{tu}/\rho = 1.6 \times 10^6 e^{1/6}$ can be used to describe material behavior at room temperature and elevated temperatures.
6. It is possible to use ductility ratio and notch strengthening data in a rational structural design process for tension structure which contain elastic stress concentrations.
7. Less confidence can be placed on ductility ratio data and notch strengthening factors when they have been derived from only a limited amount of experimental notch strength data and in which only nominal elastic concentration factors at the notch are given. With this reservation, it can be concluded that there is a significant temperature effect on ductility ratio with lower temperatures resulting in larger values of the ductility ratio.

Acknowledgments

The research reported in this paper was sponsored in part by the U.S. Navy (BuAer) and in part by NASA, Washington. The contributions of the late George Gerard, who originated these studies on ductility, are gratefully acknowledged.

References

- [1] Peterson, R. E., *Stress Concentration Design Factors*, Wiley, New York, 1953.
- [2] Gerard, G., "Structural Significance of Ductility," *Journal of Metals*, Vol. 13, No. 3, March 1961, pp. 201-203.
- [3] Gerard, G., "Structural Significance of Ductility in Aerospace Pressure Vessels," *American Rocket Society Journal*, Vol. 32, No. 8, 1962, pp. 1216-1221.
- [4] Gerard, G. and Papirno, R., "Ductility Ratio of Aged Beta Titanium Alloy," *Transactions Quarterly*, American Society for Metals, Vol. 55, No. 3, Sept. 1962, pp. 373-387.
- [5] Papirno, R., "Stress Concentrations in Tensile Strips with Central Notches of Varying End Radii," *Journal of the Royal Aeronautical Society*, Vol. 65, May 1962.

- [6] See, for example, V. Weiss' comments on Ref 4 in *Transactions Quarterly*, American Society for Metals, Vol. 55, No. 4, 1962, p. 1057.
- [7] Weiss, V. and Sessler, J., "Analysis of the Effects of Test Temperature on the Notch Strength of High Strength Sheet Alloys," Preprint 80d, American Society for Testing and Materials, 1961.
- [8] Sachs, G. and Sessler, J., "Effect of Stress Concentration on Tensile Strength of Titanium and Steel Alloy Sheet at Various Temperatures," American Society for Testing Materials, *Low Temperature Properties of High-Strength Aircraft and Missile Materials*, ASTM STP 287, 1960, pp. 122-137.
- [9] Weiss, V. et al, "The Effect of Several Geometric Variables on the Notch Tensile Strength of 4340 Steel Sheet Heat Treated to Three Strength Levels," WADD TR 60-31, Sept. 1960.
- [10] Crawford, R. F. and Burns, B. A., "Strength and Design Data for Beryllium Structures," ASD TR 61-692, Feb. 1962.

Toughness of Two-Phase 6Al-4V Titanium Microstructures

REFERENCE: Gerberich, W. W. and Baker, G. S., "Toughness of Two-Phase 6Al-4V Titanium Microstructures," *Applications Related Phenomena in Titanium Alloys, ASTM STP 432*, American Society for Testing and Materials, 1968, pp. 80-99.

ABSTRACT: A duplex heat treatment which provides different shapes, sizes, and volume fractions of alpha platelets in 6Al-4V titanium is presented. It is shown that a 40 per cent increase in fracture toughness may be attained without any significant decrease in yield or ultimate strength. With respect to toughness, critical aspects of both the interstitial oxygen content and the shape, size, and spacing of the alpha phase are discussed. Metallographic and fractographic evidence supports the contention that the second-phase alpha in platelet form acts as a crack arrestor and causes a deviation in the crack path, resulting in additional energy absorption. A tentative hypothesis for fracture in two-phase microstructures is presented based upon the theoretical crack tip displacement. Preliminary evidence indicated that the critical toughness, size, and spacing of the second phase may all be related to the crack tip displacement concept.

KEY WORDS: titanium, microstructures, fracture, fracture toughness, fractography, stress-wave detection, crack-tip displacement

Enhancement of fracture toughness and stress corrosion properties of titanium alloys is currently the prime target of titanium research, both basic and applied. During a recent study [1],³ we found that both fracture toughness and resistance to stress-corrosion cracking in distilled water could be enhanced by introducing a platelet-like phase of alpha into a beta matrix of 6Al-4V titanium. This microstructure was obtained in a duplex process which involved an initial slow cool from above the beta transus, followed by a re-resolution anneal just below the beta transus. The mechanical properties obtained on specimens of medium interstitial level are shown in the table herewith.

¹ Engineering specialist, Aerojet-General Corp., Sacramento, Calif.

² Senior engineering specialist, Aerojet-General Corp., Sacramento, Calif.

³ The italic numbers in brackets refer to the list of references appended to this paper.

	0.2% Yield Strength, ksi	Ultimate Strength, ksi	Pre- Cracked Charpy W/A, in-psi	Plane Strain K_{Ic} , ksi-in. ^{1/2}	Stress Corrosion	
					K_I , ksi-in. ^{1/2}	Failure Time, min
Equiaxed alpha.....	160	186	525	43.3	34.4	4
Platelet alpha.....	157	175	770	>53.3	34.4	>4000

It is seen that while strength properties are only decreased about 5 per cent, the toughness is increased by more than 25 per cent and the time to failure, by several orders of magnitude. From examination of the crack path, we surmised that the platelet alpha was acting as a crack arrestor. This observation coupled with some parallel observations in steel microstructures and fiber-reinforced composites led to a critical-displacement fracture concept for two-phase materials [1]. Since the two-phase alpha-beta microstructure gave some interesting mechanical properties and since a relatively uniform dispersion of alpha in beta could be obtained with which to test the proposed fracture criterion, we considered this microstructure in more detail. Such variables as cooling rate and interstitial content were investigated, the former being expected to change the morphology of the alpha and the latter being expected to change the toughness of the alpha. To define morphology, we utilized light microscopy. To define the effect of the second phase on strength and toughness, we used both tensile evaluations and pre-cracked specimens evaluated under impact and slow-rate loading conditions. In conjunction with these tests, both light and electron fractography as well as a stress-wave monitoring technique to detect microflaw growth were utilized to help us define the fracture mechanisms.

Material and Heat Treatments

We obtained three heats of 6Al-4V titanium with the main difference being the interstitial oxygen level. There were, however, increasing amounts of other interstitial elements such as carbon and nitrogen as seen in the following tabulation of chemical compositions.

	O	C	N	Al	V	Fe	H
Low interstitial.....	0.07	0.02	0.01	5.7	4.0	0.07	...
Medium interstitial.....	0.11	0.023	0.016	6.0	4.1	0.13	0.005
High interstitial.....	0.15	0.045	0.020	6.3	4.0	0.17	0.003

The low interstitial heat was purchased as 1-in.-thick plate while the other two were 0.125-in.-thick sheet, all originally being in the mill-annealed condition.

For the heat treatments, we utilized two basic procedures. We obtained the equiaxed condition by solution treating at 1750 F for ½ hr, quenching in water, and again at 1000 F for 8 hr. For the platelet microstruc-

ture, a duplex treatment was involved. First, we beta annealed the specimens at 1840 F for $\frac{1}{2}$ hr, furnace cooled at 50 F/hr to 1200 F, and then air cooled to room temperature. This treatment was then followed by the standard treatment of solution treating at 1750 F for $\frac{1}{2}$ hr, quenching in water and aging at 1000 F. Several deviations from this general procedure were made. We varied furnace cooling rates from 40 to 60 F/hr since previous data had indicated a variation in morphology within these limits. Also, since it might be desirable to apply this treatment to thick sections, we attempted to reproduce the microstructure by air cooling 1-in.-thick sections from the re-solution treatment temperature instead of quenching in water.

Experimental Test Procedures

Since both gross mechanical properties as well as effects of microstructural details on the fracture mechanism were desirable, several different types of mechanical tests and metallographic procedures were utilized.

Mechanical Tests

Standard tensile coupons, 8 in. long with a $\frac{1}{8}$ -in.-thick by $\frac{1}{2}$ -in.-wide gage section, were machined from all heats and evaluated to determine 0.2 per cent offset yield, ultimate strength, and per cent elongation. Pre-cracked Charpy tests were utilized to measure toughness with $\frac{1}{8}$ -in.-thick sheet being evaluated for the medium and high interstitial heats and 0.394-in.-thick specimens being evaluated for the 1-in.-thick, low interstitial heat. The pre-crack was extended about 50 mils below the standard V-notch depth. Besides these standard mechanical tests, we investigated the slow crack growth process of the high interstitial heat with $\frac{1}{8}$ by 3 by 12-in. single-edge notch specimens. The pre-crack was extended 150 mils in tension-tension fatigue at a stress-intensity level of 25 ksi-in^{1/2}. We also evaluated $\frac{1}{8}$ by 2 in. sections with part-through-crack (PTC) surface flaws in bending. In this case, the pre-crack fatigue was performed in cantilever bending. This particular test was desirable since the flaw was located at the surface of maximum stress, thus allowing immediate location of the crack tip for metallographic examination.

Metallographic Procedures

Light metallography was utilized to document the various heat-treatment procedures with a 3 per cent hydrofluoric acid-8 per cent nitric acid reagent being used to etch both equiaxed and platelet microstructures. We examined several PTC specimens tested in bending by unloading prior to failure and sectioning to examine the relationship of the crack tip with the second phase. These specimens were ground and polished to several different levels to obtain an in-depth picture of the

crack front. Also, we took replicas from the pre-cracked Charpy specimen fracture surfaces and examined them at about $\times 10,000$ in a Philips EM-100 electron microscope. Two-stage, plastic-carbon replicas shadowed with chromium at about 20 deg were utilized.

Stress-Wave Monitoring Technique

We equipped the latter two mechanical tests mentioned above with accelerometers to detect stress-waves emanating from the advancing crack. For several steel alloys, this technique has been employed to detect crack initiation and the step-wise movement of the crack front [2,3]. We used essentially an identical system with an accelerometer having a



FIG. 1—Conventional solution treated, water quenched, and aged microstructures of (a) medium and (b) low interstitial heats of 6Al-4V titanium ($\times 250$).

flat response to about 8000 cps being used in conjunction with a charge amplifier to obtain a full-scale response for a 0.1-g acceleration. To remove extraneous noise, we filtered the signal with a low-high pass band filter set at 6000 and 20,000 cps. The signal was then recorded on a FM tape recorder for eventual playback and analysis. The reader is referred to previous investigations [2,3] for further details on the equipment and test techniques for analyzing stress waves.

Results and Discussion

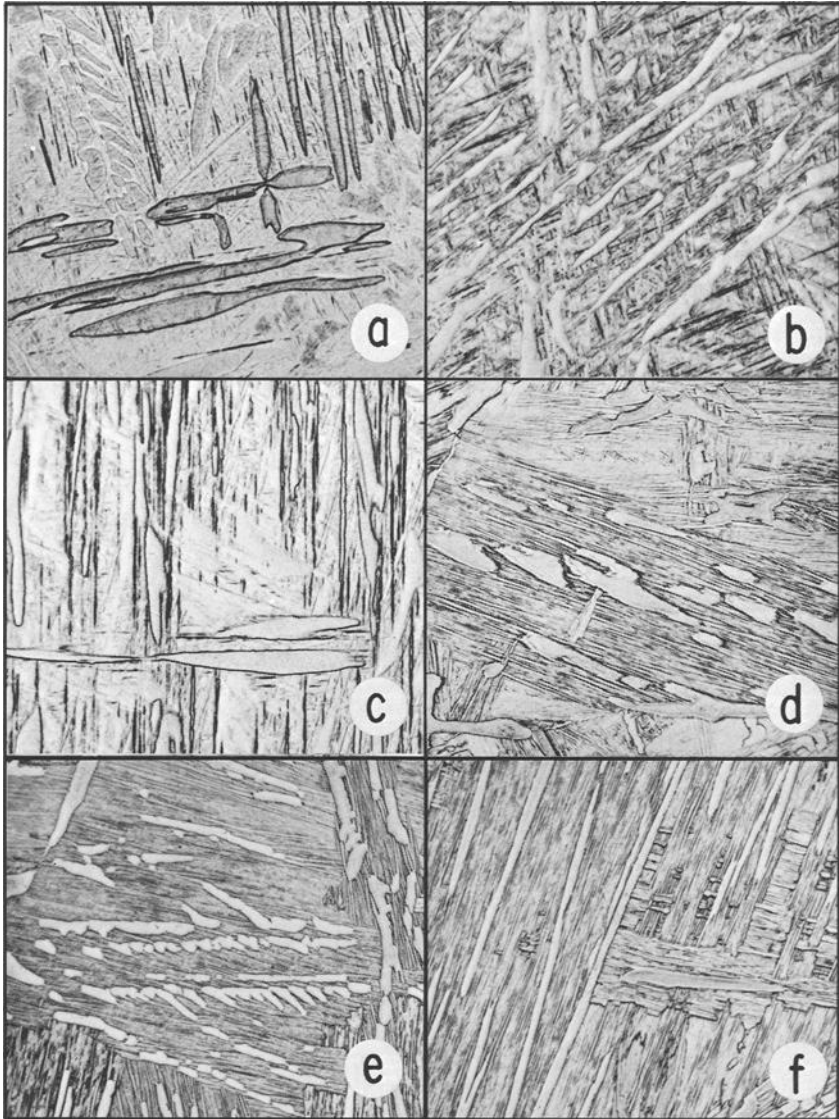
First, we will consider the gross microstructural, strength, and toughness characteristics followed by a detailed discussion of several aspects of toughness. The standard microstructures obtained by a single solution treatment, quench and aging treatment are shown in Fig. 1. Note that the low interstitial heat is more nearly equiaxed. Considering the duplex

heat treatment, we subjected 1 by 2-in. blocks of the low interstitial heat and $\frac{1}{8}$ -in.-thick pre-cracked Charpy blanks of the other two heats to each thermal cycle. Cooling rates at 5-deg intervals from 40 to 60 F/hr were generally utilized. The morphology of the alpha platelets were generally the same being independent of the interstitial content. For example, Figs. 2*a* and *b* show that for similar cooling rates there did not seem to be an appreciable difference in size or spacing of the alpha.

As pertains to cooling rate we observed a tendency for the faster cooling rate to result in delineation of the crystallographic planes with the alpha being somewhat finer. Compare Figs. 2*b* and *c*. In the only experiment where we varied the second step of the duplex treatment, air cooling 1 by 2-in. blocks from 1750 F resulted in the microstructures shown in Figs. 2*d*, *e*, and *f*. Although the alpha is somewhat coarser than that obtained with the water quench, the size and spacing of the platelets is relatively unchanged. We observed that the effect of a faster furnace cooling rate during the first thermal cycle was to give thinner and longer platelets. For example, compare the almost globular shapes obtained at 40 F/hr in Fig. 2*d* to the very long platelets obtained at 60 F/hr in Fig. 2*f*.

Based upon these microstructural observations, we selected several thermal cycles and obtained uniaxial strength and pre-cracked Charpy toughness data for each heat as given in Table 1. These data all involved a water quench from 1750 F and aged at 1000 F. The general trend was for the strength to increase slightly and toughness to decrease drastically with increasing interstitial content. Comparing the conventional and duplex heat treatments, we found similar strengths but about a 40 per cent increase in toughness with the duplex treatment for the low and medium interstitial heats. However, for the high interstitial heat, there was a reversal in the toughness trend with the duplex treatment giving lower toughness values. This apparently anomalous result is discussed in a later section. As pertains to the furnace cooling rates used in the duplex treatment, we found little effect of this variable on either strength or toughness over the range of 40 to 55 F/hr.

Electron fractographs taken from selected Charpy specimen fracture surfaces are shown in Fig 3. The top two fractographs, which consist of large tear dimples, represents the toughest condition, a duplex treatment with a 40 F/hr cooling rate. For the same low interstitial heat, we replicated the fracture surface of a conventionally-treated specimen, the resulting fractographs being shown in Fig 3*b*. Although the tear dimples seem somewhat smaller, the general morphology is the same. We also replicated the lowest toughness condition as indicated in Fig 3*c*. The dimple size was still roughly the same, but these areas were fewer in number, and there was a tendency for them to consist of more nearly equiaxed dimples. The fact that the shape of the dimples changes from an elongated



- (a) Medium interstitial, 45 F/hr, water quenched.
 (b) Low interstitial, 40 F/hr, water quenched.
 (c) Low interstitial, 55 F/hr, water quenched.
 (d) Low interstitial, 40 F/hr, air cooled.
 (e) Low interstitial, 50 F/hr, air cooled.
 (f) Low interstitial, 60 F/hr, air cooled.

FIG. 2—Microstructures of duplex heat treatment, cooling rate in first cycle and quench in second cycle ($\times 250$).

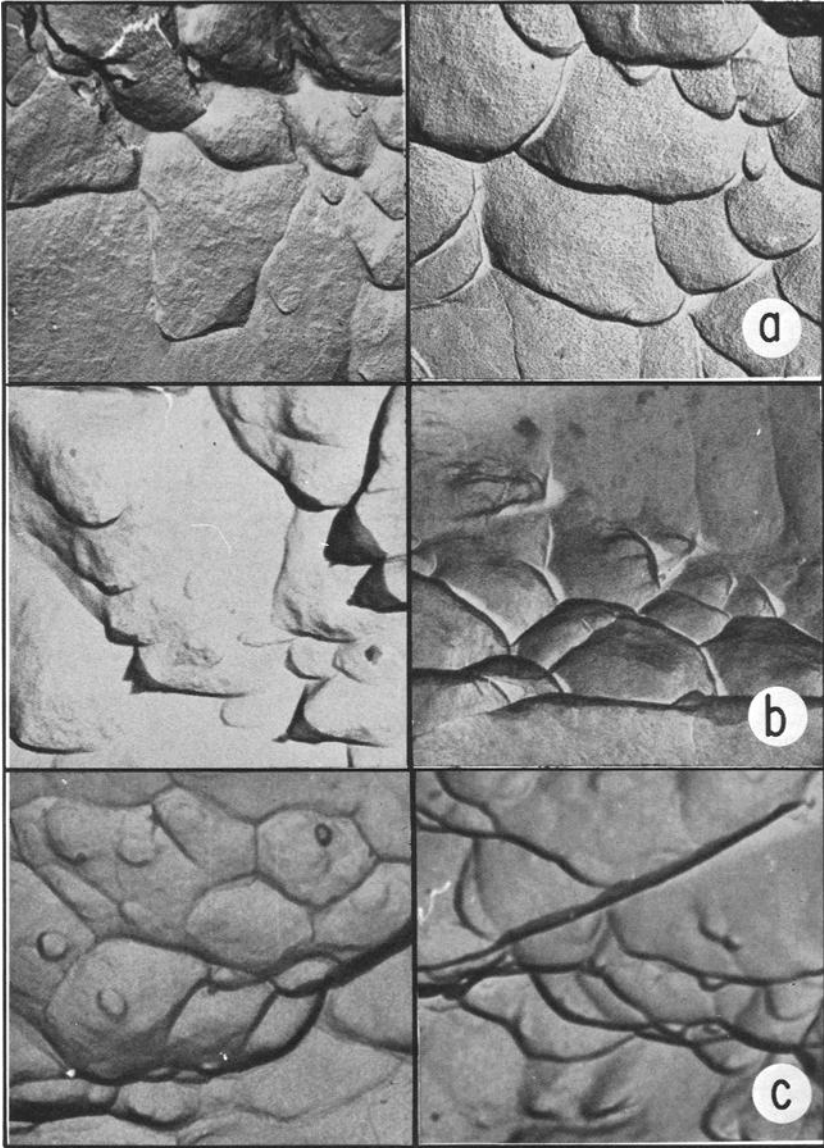
tear type to a relatively equiaxed normal type indicates that the ratio of the maximum principal strains is decreasing from the highest toughness to the lowest toughness conditions. It is now appropriate to consider the detailed effects of oxygen and the morphology of the second phase on toughness.

TABLE 1—*Mechanical properties of 6Al-4V titanium representing several interstitial levels and heat treatments.*

Condition	Interstitial Oxygen Level, weight %	0.2% Offset Yield Strength, ksi	Ultimate Tensile Strength, ksi	Elongation in 1 in., %	Pre-Cracked Charpy Impact, W/A, in-psi
Conventional, solution treated at 1750 F and aged at 1000 F	0.070	128.8	147.4	8.5	1245
		133.2	150.0	12.0	1518
		131.5	151.3	10.5	1519
Beta annealed at 1840 F, 40 F/hr, cooled to 1200 F, plus conventional solution treated, and aged	0.070	130.9	150.0	8.5	2128
		132.5	150.4	5.0	2004
		134.1	150.9	5.0	1911
Beta annealed at 1840 F, 55 F/hr, cooled to 1200 F, plus conventional solution treated, and aged	0.070	131.0	150.8	7.0	1826
		131.2	149.6	6.0	2060
		129.0	148.4	6.5	1938
Conventional, solution treated, and aged	0.110	158	182	...	480
		162	190	...	570
47 F/hr, cooled to 1200 F, plus conventional solution treated, and aged	0.110	160	178	...	720
		154	173	...	815
Conventional, solution treated, and aged	0.150	165.7	187.7	5.4	460
		169.7	187.7	5.4	459
		172.0	190.7	5.4	522
Beta annealed at 1840 F, 40 F/hr, cooled to 1200 F, plus conventional solution treated, and aged	0.150	162.8	175.4	3.0	344
		159.6	178.5	3.1	316
		160.3	177.5	3.1	368
Beta annealed at 1840 F, 55 F/hr, cooled to 1200 F, plus conventional solution treated, and aged	0.150	166.7	184.6	5.2	329
		169.7	185.6	5.2	556
					381

Effect of Oxygen on Toughness

As long as the alpha is low in oxygen it is very tough and the energy required to propagate the crack past the second phase is considerable. With increasing oxygen the alpha phase becomes less tough until it is actually more brittle than the matrix. The effect of oxygen was dramatically shown in several PTC bend tests where contamination at the highly stressed surface represented a high oxygen content. At very low stresses, we observed cracks on the surface as shown at high magnification in Fig. 4a. The crack tends to be predominantly in the alpha phase and in many



(a) Low interstitial, 40 F/hr cooling rate.
 (b) Low interstitial, conventional.
 (c) High interstitial, 55 F/hr cooling rate.

FIG. 3—Electron fractographs taken from 6Al-4V titanium impact specimens representing duplex and conventional heat treatments ($\times 10,000$).

instances cleaves the platelets. From a section through the thickness in Fig. 4b, we found the crack actually jumps past the matrix to a considerable depth in several instances. For comparison, a micrograph taken from the failure origin of a full-scale premature burst of a 6Al-4V titanium

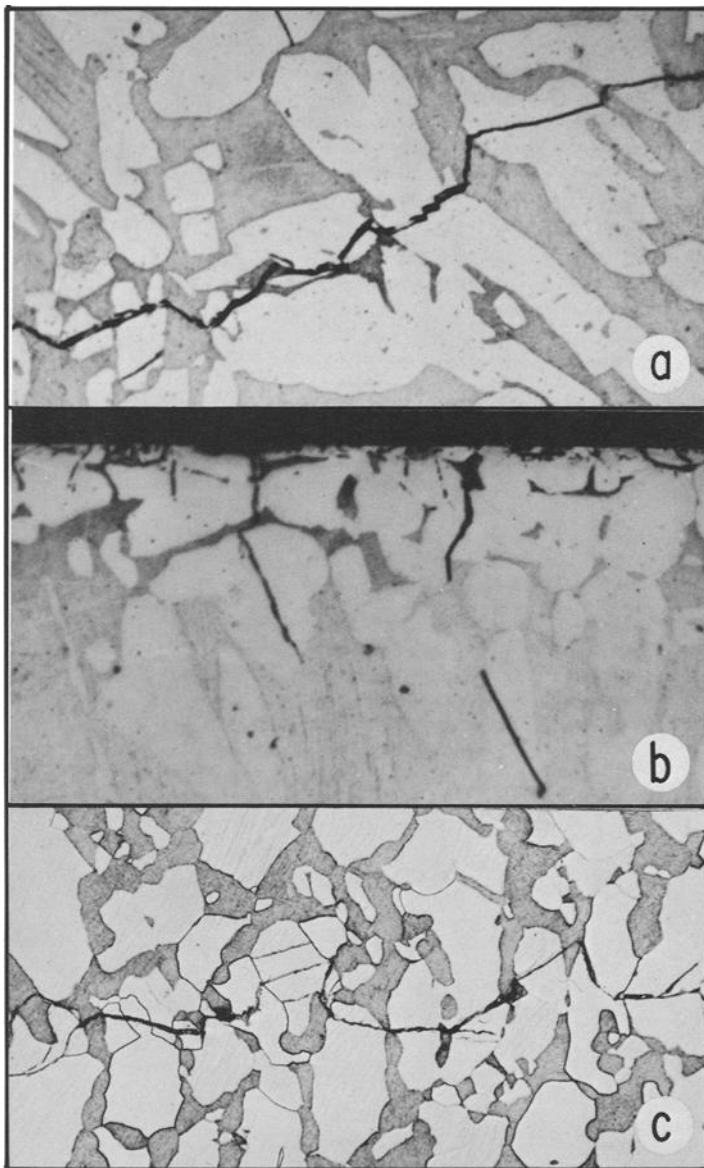


FIG. 4—Effect of oxygen contamination on crack path in 6Al-4V titanium (a) $\times 400$, (b) $\times 475$, and (c) $\times 250$.

chamber is shown in Fig. 4c. This chamber burst at a membrane stress which was 55 per cent of the calculated yield strength. Note that the crack path is very similar to Fig. 4a in that the alpha phase is preferred. Post-failure vacuum fusion analysis indicated that the bulk of the chamber contained 0.19 weight per cent oxygen while the failure origin contained 0.79 weight per cent oxygen.

The PTC bend tests were equipped with accelerometers to detect incipient flaw growth. Typical stress waves that were obtained on rising load are similar to those shown in Fig. 5 which were observed in D6aC steel [3]. As indicated in Table 2, we observed stress-wave emission (SWE) at applied stresses as low as 32 ksi which represented a stress intensity factor of 4.4 ksi-in^{1/2}; this is about an order of magnitude less than the

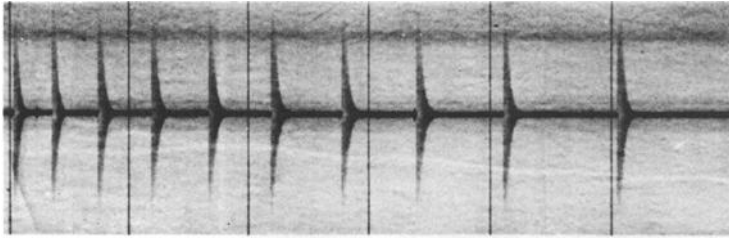


FIG. 5—Typical stress-waves obtained during tests on steel (Ref 3).

TABLE 2—Stress-wave emission data for part-through-crack bend specimens.

Specimen Number	Crack Depth, <i>a</i> in.	Crack Length, <i>2c</i> in.	Applied Surface Stress, σ_0 ksi	Surface Stress ^a Intensity, K_{I_s} ksi-in ^{1/2}	Number ^b of SWE/sec
<i>Surface initially contaminated</i>					
TS-1	0.035	0.206	32	4.4	<1
			70	9.7	~25
			98	13.5	~100
			112	15.5	>100
			112	15.5	~50 ^c
<i>Specimen unloaded and surface ground to remove contamination</i>					
			≥160	≥22.1	first SWE
<i>Surface initially clean</i>					
TS-3	0.039	0.240	55	7.7	only one ^d
			≥160	≥22.6	first SWE ≥ 0.1 g

^a $K_{I_s} = \sigma_0(\pi a^2/c)^{1/2}$.

^b Number of SWE greater or equal to 0.01 g in amplitude.

^c SWE ≥ 0.1 g.

^d Only four SWE ≥ 0.01 g were noted between an applied surface stress of 55 ksi and about yield where the first large SWE was noted.

plane strain fracture toughness. By using a digital counter, we determined the number of SWE greater than a specified amplitude that were occurring on rising load. We found that at stresses nearly one half the yield strength, 25 to 100 SWE were occurring per second. At stresses nearly 70 per cent of yield, greater than 100 SWE/sec were occurring with 50 large SWE/sec being recorded. The specimen was then unloaded and surface ground to remove the contamination. As indicated in Table 2, we found that upon reloading, the first SWE did not occur until the specimen

surface yielded. This behavior was verified by an additional specimen which was initially ground. In this instance, we observed only four small SWE upon raising the load to where the surface yielded. Considering the SWE in the oxygen-contaminated specimens, the smaller pulses probably represented cracks forming within the alpha platelets as indicated in Fig. 4b, while the large pulses represented gross movements of the crack. The numbers of SWE at first were quite puzzling until post-test observation revealed that cracking was not confined to the flaw area but occurred over the entire specimen surface.

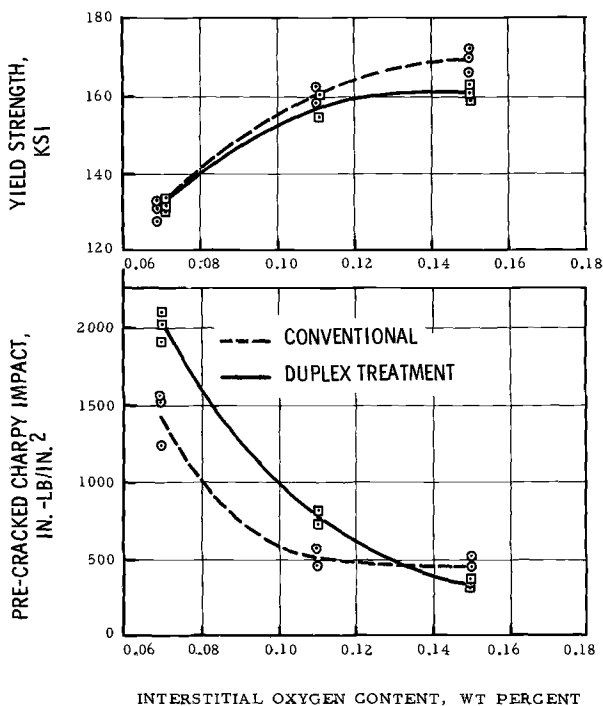


FIG. 6—Effect of oxygen content on strength and toughness of 6Al-4V titanium.

It is an accepted fact that a high level of interstitial oxygen decreases the toughness of alpha titanium in conventionally treated microstructures. From these studies, we verified that oxygen may have a deleterious effect on the toughness of alpha obtained by these duplex heat treatments. It is now possible to explain the anomalous effect encountered in one heat wherein the platelet-alpha microstructure was less tough than the equiaxed microstructure. The data from Table 1 are more clearly seen in Fig. 6 which indicates the trend of strength and toughness with increasing interstitial oxygen content. For both conventional and duplex heat treatments, the increase in strength and the decrease in toughness with increasing oxygen is as expected. We did not anticipate the crossover in

toughness, however, which occurred near 0.13 weight per cent oxygen. As the oxygen content increases, the platelet alpha becomes more brittle and at some point can no longer effectively arrest the crack. But does not the equiaxed alpha in the conventionally-treated specimens also become embrittled? The crossover in toughness is explained by considering the relative role and amount of alpha in the two conditions. The duplex treatment gains its enhanced toughness from the platelet alpha which requires the crack to deviate from its normal path. If the alpha were not tougher than the beta because of a high oxygen content, then there would be no barrier to crack propagation. In fact, since the platelet alpha represents a larger volume fraction of the specimen (Fig. 2) as compared to the equiaxed alpha (Fig. 1), one would expect a crossover in toughness when the alpha became more brittle than the beta phase. We must conclude that alpha titanium is not tough unless the interstitial oxygen is less than 0.13 weight per cent. Of course, this oxygen level may vary with strength level and alloy content, but the fact that most commercial grades contain greater than 0.13 weight per cent oxygen may be of concern to specialty users which require considerable toughness.

Effect of the Alpha Phase on Toughness

The previous discussion inferred that the alpha phase in platelet form could act as a crack arrestor and actually cause the crack to deviate from its normal path. Confirmation of this was obtained in one specimen of the medium interstitial heat where a 45 F/hr cooling rate was utilized in the duplex heat treatment. Upon polishing through the thickness of a part-through-crack bend specimen, the crack appeared to progress normal to the applied stress, as indicated in Fig. 7a. Upon polishing a little further, we observed that the crack had interacted with a group of alpha platelets, as indicated in Fig. 7b. It appeared as though the crack had made two sharp turns and had actually jumped passed the second phase, as indicated in Fig. 7c. In 7c, we also noted that the crack tended to follow a path about midway between the platelets rather than at an alpha-beta interface. Further polishing revealed in Fig. 7d that the crack was actually continuous and that it had deviated through the thickness to avoid the second phase. Finally, in Figs. 7e and f, we found that the crack had taken several more sharp turns as it threaded its way through the second-phase alpha platelets.

It should be obvious that the crack arrest or change in the crack path by the alpha platelets or both would enhance the toughness. The change in the crack path was more clearly detailed by an electron fractograph. From one of the specimens of the low interstitial heat subjected to a duplex treatment involving a 55 F/hr cooling rate, a fractograph of the impact fracture surface is shown in Fig. 8. We surmised that the lenticular shape in the middle of the fractograph was a cross section of a fractured

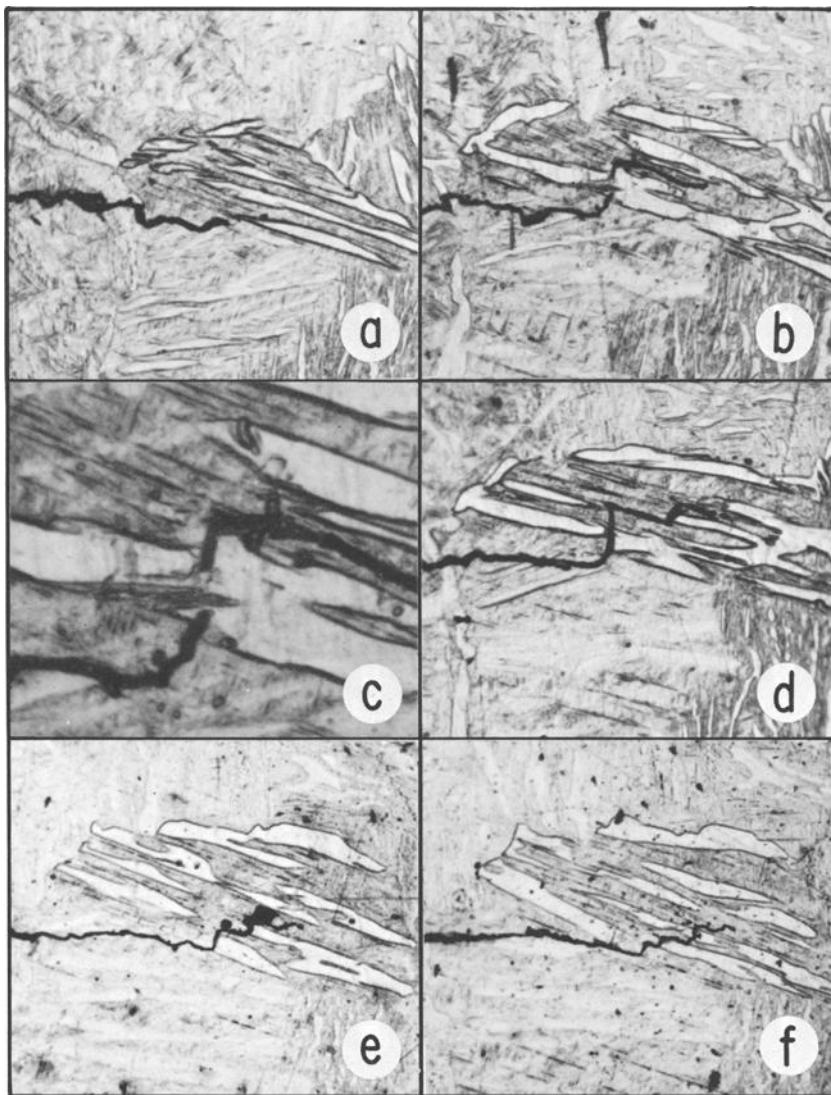


FIG. 7—Effect of platelet alpha on the crack path in 6Al-4V titanium subjected to a duplex heat treatment, (a) $\times 160$, (b) $\times 160$, (c) $\times 475$, (d) $\times 160$, (e) $\times 160$, and (f) $\times 160$.

alpha platelet. From the same heat, the identical thermal treatment produced the microstructure in Fig. 2c, which indicates the finer alpha platelets to be 1 to 4 μ in width. This corresponds favorably to the lenticular shape in Fig. 8 which is about 2 μ in width.

In Fig. 8, we noted a considerable number of small striations within the alpha platelet which may be due to the sharp turn the crack takes as it crosses the second phase. That is, if the slip and fracture planes involved



FIG. 8—*Electron fractograph of crack path through and around alpha platelet ($\times 13,000$).*

in the two phases are sufficiently different, a number of small crack steps may be the preferred fracture path through the second phase. It is significant that as the crack makes an abrupt change in its path, similar to those shown in Fig. 7, the matrix surrounding the second phase must also accommodate the change. We suspect that this accommodation accounts for the number of large steps surrounding the second phase alpha in Fig. 8. From Figs. 7 and 8 it is apparent that a great deal of fracture surface would be exposed as the crack moves through these two-phase materials. The more surface area that is exposed during crack propagation, the more energy that may be absorbed by the specimen. Thus, we would expect that on both a microscopic and macroscopic scale that the change in crack path would produce greater toughness. On top of this, one must add the effect of requiring a greater energy to reinitiate an arrested crack so that the sum total of the two effects could be considerable. We are now in a position to consider an approximate model for crack propagation in this type of microstructure.

Fracture Mechanism

Hahn and Rosenfield [4] have presented a simple fraction criterion for homogenous materials based upon the displacement at the crack tip. They have shown the equivalence of the critical displacement to fracture toughness by

$$K_c = (2\nu^*\sigma_{ys}E)^{1/2} \dots \dots \dots (1)$$

where:

- K_c = plane stress fracture toughness, ksi-in^{1/2},
- $2\nu^*$ = critical crack tip displacement, in.,
- σ_{ys} = yield strength, ksi, and
- E = modulus of elasticity, ksi.

This analysis has been extended to describing the crack extension process in two-phase materials [1]. This latter concept is schematically shown in Fig. 9. As may be inferred from Eq 1, the crack tip displacement $2\nu_c$, at any point in the loading sequence would be dependent upon the applied stress intensity, K . Thus, $2\nu_c$ would increase as K increases either through an increase in crack length or applied stress. At some point, the crack tip displacement, $2\nu_c$, would be greater than $2\nu_{M_1}^*$ which is the critical crack tip displacement for the brittle phase. Thus, as the material is loaded, when $2\nu_c > 2\nu_{M_1}^*$ the crack moves from Position 1 to Position 2 where it encounters a tough second phase. This is indicated in Fig. 9. If $2\nu_{c_2} < 2\nu_{M_2}^*$, then the crack will be arrested providing the width of the M_2 phase is sufficiently large. This condition is necessary since the displacement at Position 2 has increased due to the longer crack length. Thus, the displacement at the distance x (representing the dimension of the second phase) in front of the crack may be larger than the critical displacement for failure in the brittle material. If $2\nu_x > 2\nu_{M_1}^*$, then failure will proceed in the brittle material. The value of $2\nu_x$ may be calculated by knowing the plastic zone size and utilizing the result of Goodier and Field [5] for the displacement distribution.

It was observed [1] that this concept explains some features of the fracture process in both macrostructural composites and two-phase microstructures. We will now consider it in terms of the specific case encountered in the duplex heat treatment of 6Al-4V titanium. Considering the angle the main crack (that which is normal to the applied stress) makes with the alpha platelets, from Fig. 7, we measured it to range from 11 to 38 deg with the average being 24 deg. Based upon this average, a schematic diagram is shown in Fig. 10. We also measured the width of the fractured alpha platelets for this particular condition to average 0.00046 in. or 11.7 μ . For an angle of 24 deg, the distance $x_{(1)}$ in front of the crack at which the beta phase would be encountered would be 28.3 μ . Following the discussion above, it is pertinent to ask if fracture could have proceeded in the beta phase.

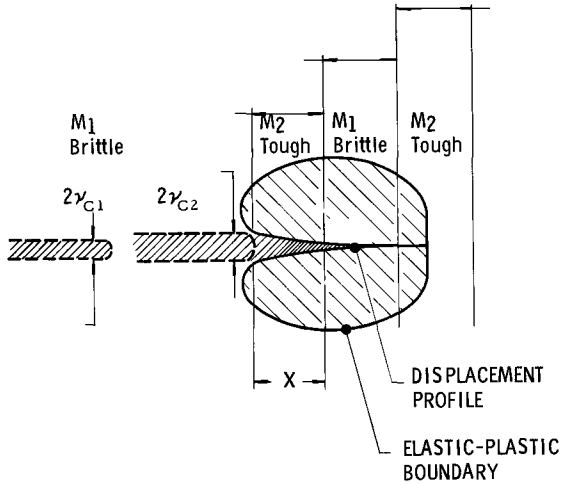


FIG. 9—Schematic of crack displacements and plastic zone in a two-phase material.

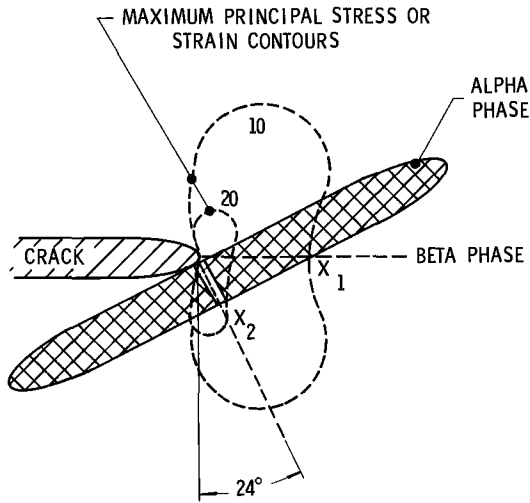


FIG. 10—Schematic of crack encountering second phase alpha at an angle of 24 deg.

Considering the plane strain plastic zone size to be approximated by

$$2r_p \sim (\frac{1}{3}\pi)(K/\sigma_{ys})^2 \dots \dots \dots (2)$$

and using values of K_{Ic} to be 53 ksi-in^{1/2} for the platelet alpha and the yield strength to be 160 ksi leads to a calculated zone size of 0.0116 in. or 294 μ . From Eq 1, the crack tip displacement may be calculated⁴ to

⁴This is a plane stress calculation. The crack was actually more in a plane strain situation, and thus the calculated displacement might be about one half this value. However, it is only the relative values that are important in determining whether fracture ensues in the brittle matrix.

be 27μ for the same values of K and σ_{ys} . According to Hahn and Rosenfield [4], at a distance of 28.3μ in front of the crack, the displacement, $2\nu_{x_1}$, would be 16.2μ . All that is needed is an estimate of the critical displacement for the beta matrix, $2\nu_M^*$, in order to determine if cracking will proceed. A rough approximation of $2\nu_M^*$ may be made from the equiaxed microstructure assuming an equiaxed phase does not make crack propagation much more difficult. In the introduction, we indicated K_{Ic} for the equiaxed microstructure to be $43 \text{ ksi-in}^{1/2}$. Using this value in Eq 1 leads to $2\nu_M^*$ being 17.6μ . Since $2\nu_{x_1} < 2\nu_M^*$, we would not expect cracking to continue along the line of the crack passed the second phase.

Why then would the material crack at such a steep angle to the second phase as indicated in Fig. 7? It may be inferred from both experimental [6] and calculated [7] strains and elastic-plastic stresses in finite thickness plates with some degree of work hardening, that the displacement off the line of the crack may be somewhat greater than the displacement along the line of the crack. In Fig. 10, the angle the secondary crack makes with respect to the main crack axis is 66 deg . According to the elastic stress distribution, this angle would roughly coincide with the maximum principal stress and strain. As indicated by the dotted contours in Fig. 10, the relative stress or strain at x_2 might be a factor of two greater than that at x_1 . Thus, whether a displacement, stress, strain, or energy criterion is invoked, it might be expected that the crack would traverse the second phase in the manner observed in Fig. 7 rather than to continue straight ahead.

There is one disturbing feature of this model. Why does the crack not progress along the second phase interface or, for example, proceed along an angle of 66 deg entirely in the beta matrix? The obvious explanation is that this is only a small slice of a three-dimensional array and that a much larger group of second phase alpha platelets may be requiring the crack to progress away from the matrix at this point. Another factor might be that there is a preferred crystallographic plane along which cracking occurs.

The above discussion gives a potential framework for analyzing how the size of the alpha might effect the toughness. However, it gives little insight into how the spacing of the alpha might effect the fracture process. Of course, the more second-phase alpha there is the more toughness one would expect, but this would be at the expense of strength. There is probably some combination where the microstructure is optimized⁵ with respect to strength and toughness. It would be desirable to know the spacing of the tough second phase which would give the greatest increase in toughness with the smallest decrease in strength. As the second phase becomes further apart statistically, the number of times the crack tip may

⁵ A microstructure would only be optimized in terms of a particular application where the thickness or strength and toughness requirements or both are stipulated.

be arrested and effectively blunted would decrease. If the minimum distance over which the crack propagated were known and a second phase could be arbitrarily placed at this point, it might be expected that an efficient microstructure would be attained. On the average, this might be possible. Of course, it would be necessary to know the structural unit over which the crack would normally travel.

Recently, Wells [8] postulated that there was a region in front of the crack tip, ρ_s , over which plastic instability occurred and that this region was roughly equal in size to the crack tip displacement. Cotterell [9] and Teleman [10] hypothesized that this region of plastic instability was a prerequisite for cleavage fracture. Independently, Gerberich and Hartbower [2, 3, 11] found that the distance, ρ_s , over which the crack would jump was on the average numerically equal to the crack tip displacement. These findings were made possible through monitoring of stress waves associated with frontal movement of the crack. By dividing the number of these stress waves into a macroscopic crack increment as detected by a displacement gage, the value of ρ_s was experimentally determined. Following this procedure, we loaded two single-edge-notch specimens with an equiaxed alpha microstructure. In the first specimen, 0.067 in. of cracking was observed from an applied stress intensity factor of 33 to 61.6 ksi-in.^{1/2}. Forty-six SWE were observed in this interval so that on the average one SWE would represent a ρ_s of 0.00146 in. Considering the average stress intensity factor of 47.3 ksi-in.^{1/2}, the crack tip displacement would be 0.00089 in. which is very close to ρ_s . Similarly, in a second specimen where slow crack growth was observed from 37.8 to 59.6 ksi-in.^{1/2}, 0.052 in. of growth was represented by 44 SWE which gives a ρ_s of 0.00118 in. Again, this is very close to the calculated average value of the crack tip displacement which is 0.00095 in. Thus, in these cases the crack tip displacement gave a reasonable estimate of the average crack jump taking place in the slow crack growth process.

Consider this with respect to the microstructure with the platelet alpha. At the critical stress intensity factor, the crack tip displacement for the microstructure shown in Fig. 7 was calculated to be 27 μ . If one were to use a plane strain estimate, the crack tip displacement would be about 13.5 μ . It is significant that the spacing of the alpha platelets in Fig. 7 is about 0.0005 in. or 12.7 μ . In either case, the spacing of the alpha phase is extremely close to the theoretical crack tip displacement. It would be interesting if an increase or decrease in the volume fraction of the alpha phase would produce a corresponding increase or decrease in the critical crack tip displacement. This could be evaluated with a slight variation in the duplex heat treatment. We have found that the amount of alpha retained upon re-resolution treating is sensitive to how close one approaches the beta transus. The normal process has been to re-resolution treat about 50 F below the beta transus. By re-resolution treating about 20 F below the

beta transus, more than twice as much alpha was taken back into solution resulting in a much lower volume fraction. Thus, a range of volume fractions could be obtained by adjusting the re-solution treatment temperature.

Conclusions

1. A duplex heat treatment for 6Al-4V titanium which involves controlled cooling from above the beta transus in the first cycle followed by water or air quenching from below the beta transus in the second cycle provides the following morphological characteristics: (a) platelet alpha may be attained by cooling near 50 F/hr on the first cycle, (b) the platelet shape may be varied from almost globular to nearly acicular by sufficiently varying the cooling rate, and (c) the volume fraction of the alpha phase may be controlled by re-solution treating at various temperatures approaching the beta transus.

2. The alpha platelet microstructure provides a 40 per cent increase in toughness over the equiaxed microstructure without any significant decrease in strength. We find that this improvement is only attained if the interstitial oxygen content is low, the critical oxygen level being near 0.13 weight per cent.

3. We find that the effect of the platelet alpha is to cause crack arrest and require the crack to deviate from its normal fracture path, thus allowing more energy to be absorbed during crack propagation.

4. We found that incipient flaw growth could be detected in these materials with an accelerometer technique that monitors stress waves which are emitted when the crack moves.

5. This stress-wave technique was utilized to determine the number of crack jumps that were occurring during the slow crack growth process. These observations indicate that the structural unit involved in fracture was on the average numerically equal to the theoretical crack tip displacement.

6. We propose a tentative fracture hypothesis for two-phase microstructures based upon a critical crack tip displacement being exceeded to induce local fracture. Although this concept is only one of several that could be proposed, we find that both critical size and spacing of the second phase may be described in terms of the crack tip displacement.

Acknowledgment

The work reported herein was performed under contract N600-(61533)-65927 to the Navy Marine Engineering Laboratory. The authors would like to thank J. Nieman, P. P. Crimmins and C. E. Hartbower for making much of the data available for use in this paper. We would also like to acknowledge S. Carpenter and G. Faulkner who originally developed this heat-treatment procedure for 6Al-4V titanium.

References

- [1] Gerberich, W. W., "Some Observations on Crack Extension in Two-Phase Materials," *Transactions, American Institute of Mining, Metallurgical, and Petroleum Engineers*, Vol. 239, 1967, p. 753.
- [2] Hartbower, C. E., Gerberich, W. W., and Crimmins, P. P., "Characterization of Fatigue-Crack Growth by Stress-Wave Emission," Final Report, Contract NASA-4902, Aerojet-General Corp. for Langley Research Center, June 1966.
- [3] Hartbower, C. E., Gerberich, W. W., and Crimmins, P. P., "Investigations of the Metallurgical Nature of Slow Crack Growth," First Year Summary Report, Contract AF 33(615)-2788, Aerojet-General Corp. for AFML, Jan. 1967.
- [4] Hahn, G. T. and Rosenfield, A. R., "Plastic Energy Dissipation in Crack Propagation," *Acta Metallurgica*, Vol. 13, 1965, p. 293.
- [5] Goodier, J. N. and Field, F. A., "Plastic Energy Dissipation in Crack Propagation," *Fracture of Solids*, Drucker and Gilman, ed., Interscience, New York, 1963, p. 103.
- [6] Gerberich, W. W., "Plastic Strains and Energy Density in Cracked Plates," *Proceedings, Society for Experimental Stress Analysis*, Vol. 21, No. 2, 1964, p. 335.
- [7] Swedlow, J. L., Williams, M. L., and Yang, W. H., "Elasto-Plastic Stresses and Strains in Cracked Plates," *Proc. First Int. Conf. on Fracture*, Yokobori, Kawasaki, and Swedlow, eds., Sendai, Japan, Vol. 1, 1966, p. 259.
- [8] Wells, A. A., "Application of Fracture Mechanics at and Beyond General Yielding," *British Welding Journal*, Vol. 10, 1963, p. 563.
- [9] Cotterell, B., "A Possible Macro-Mechanism for Cleavage Fracture Initiation in Mild Steel," *Proceedings, First International Conference on Fracture*, Yokobori, Kawasaki, and Swedlow, eds., Sendai, Japan, Vol. 3, 1966, p. 1663.
- [10] Teleman, A. S. and Rau, C. A., Jr., "The Effect of Small Drilled Holes on the Notch Toughness of Iron Base Alloys," *First International Conference on Fracture*, Yokobori, Kawasaki, and Swedlow, eds., Sendai, Japan, Vol. 2, p. 691.
- [11] Gerberich, W. W., "A Discussion of Slow Crack Growth Associated with Plane-Strain Instability," *Transactions, American Society for Metals*, Vol. 59, No. 4, 1966, p. 899.

Relation of Strength and Toughness to Fine Structures in a Beta Titanium Alloy

REFERENCE: Banerjee, B. R., Hauser, J. J., and Capenos, J. M., "Relation of Strength and Toughness to Fine Structures in a Beta Titanium Alloy," *Applications Related Phenomena in Titanium Alloys*, ASTM STP 432, American Society for Testing and Materials, 1968, pp. 100–123.

ABSTRACT: Although a great deal of mechanical properties data on titanium alloys have appeared in the literature, no attempt has been made to relate the fine structures in beta titanium alloys to strength and fracture toughness. Therefore, strength and fracture toughness properties of B-120VCA—obtained through a variety of thermal and thermomechanical treatments—were related to fine structures by transmission electron microscopy, electron fractography, etc. Effects of (1) prior solution-treating temperatures, (2) cold working after solution treating, and (3) cold working both before and after solution treating were evaluated in terms of strength and fracture toughness, and parallel fine structure studies. The double cold-work treatment, without aging, produced σ_t with a fracture toughness of 115 ksi $\sqrt{\text{in.}}$ and may be promising for certain high-strength applications. Also short aging times produce unique combinations of strength and fracture toughness ($\sigma_t \approx 190$ ksi, $K_{Ic} \approx 70$ ksi $\sqrt{\text{in.}}$). The kinetics of $\beta \rightarrow \alpha$ transformation were characterized and related to fracture toughness and strength properties. Precipitation of omega was suggested in the solution-annealed material during cooling to room temperature; further growth of this phase upon prolonged aging at 600 F was established. At 900 F, omega growth was limited, being replaced by alpha precipitation first in a discontinuous and later in a general dispersion.

KEY WORDS: titanium alloys, mechanical properties, fracture toughness, dynamic structural analysis, electron microscopy, electron fractography, aging, mechanical treatments, transformation

The all-beta titanium alloy, Crucible B-120VCA, [1]³ is of considerable technological interest because of its high strength potential of over 200 ksi—obtainable through age-hardening and thermomechanical treatments—its high strength-to-weight ratio of more than 1 million

¹ Associate director of research, Hunter Research Laboratories, Crucible Steel Co., Pittsburgh, Pa.

² Staff scientists, Hunter Research Laboratories, Crucible Steel Co., Pittsburgh, Pa.

³ The italic numbers in brackets refer to the list of references appended to this paper.

inches, and its excellent formability in the as-quenched, β , condition. The beta phase is stabilized in this alloy through additions of vanadium, which has complete miscibility with titanium, and chromium, which is a eutectoid former. Enough of the alpha-stabilizer aluminum is added to produce the desired aging kinetics [2]. Solid-state transformations were studied [3] in this alloy by X-ray diffraction, optical metallography, and hardness measurements. Based on these studies, the hardening mechanism was concluded to be an age-hardening reaction involving both the transition phase, ω , and the stable transformation product, α , at aging temperatures of 800 F up to 1050 F. Above 1050 F, the alpha phase directly precipitated from the parent beta; prolonged aging and very high aging temperatures yielded alpha and titanium chromide (TiCr_2)

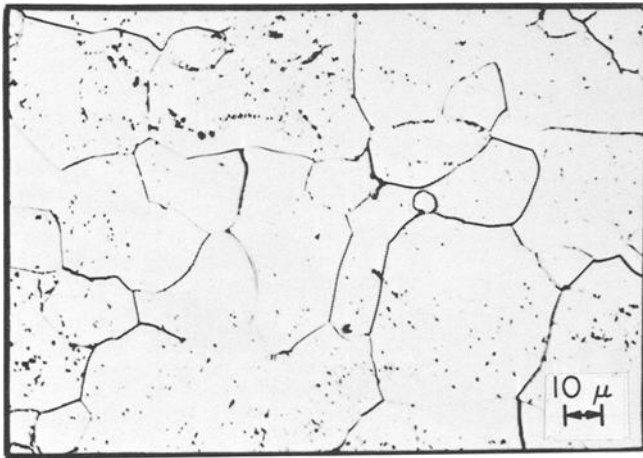


FIG. 1—As-received B-120VCA titanium alloy.

as the precipitates. However, another investigator [4] differed from this viewpoint on the basis of similar investigations and concluded that the transition phase, ω , was observable only at temperatures up to 662 F; while between 752 and 1202 F the reaction sequence was $\beta \rightarrow \beta + \alpha \rightarrow \beta + \alpha + \text{TiCr}_2$. But, in a later investigation by the same author [5], using X-ray diffraction and surface replica electron microscopy, the evidence seemed to indicate the presence of ω as a "mottled" unresolved-general precipitate upon aging at 900 F. Clearly, the transformation kinetics in this alloy system needs better definition. In the area of fracture properties, while some sharp-edge notch tensile data on this alloy exist in the literature [6,7], fatigue-cracked sheet-tensile data have not yet been systematically related to fine structural parameters.

Therefore, the isothermal transformation kinetics in the critical strengthening region of the B-120VCA alloy were followed by hardness,

strength and fracture toughness measurements, while the structural transitions were characterized by transmission electron microscopy, and other complementary fine-structural techniques [8].

Materials and Methods

The starting material consisted of vacuum-annealed 0.180-in. sheets, from a double consumable-arc vacuum-melted heat of B-120VCA, of the following composition:

C	Cr	V	Al	Fe	B	N	O
0.02	11.5	14.0	3.2	0.25	0.004	0.018	0.11

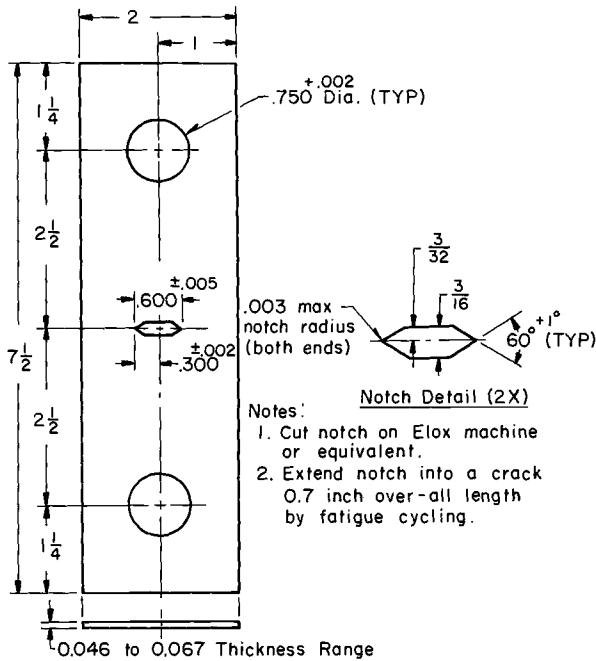


FIG. 2—Center notch sheet tension specimen.

The vacuum-annealed (as received) material had a beta matrix grain structure with a small amount of generally precipitated alpha (see Fig. 1). Also ghost boundaries, representing vestigial remains of a previous grain boundary network, were observed. These networks became more prominent after aging, because of preferred precipitation at these sites.

The sheets were first cold reduced about 65 per cent by rolling to a nominal 0.067 in. thickness. In addition to the 65 per cent cold reduction, some material was twice cold reduced (50 per cent each time) with a

standard ¼ hr, 1450 F solution anneal⁴ between reductions; this resulted in 0.046 in. thickness.

To determine the possible role of reactions at the fatigue crack during heat treating, notched tension specimens were fatigue cracked both before and after solution treating. After the 900 F/72-hr aging, transverse test data showed no significant difference: Net fracture stress with fatigue cracking before SA = 39 ksi; after SA = 40 ksi. Therefore, fatigue cracking before the solution anneal was used.

Test specimens (see Fig. 2) were rough machined and center notched

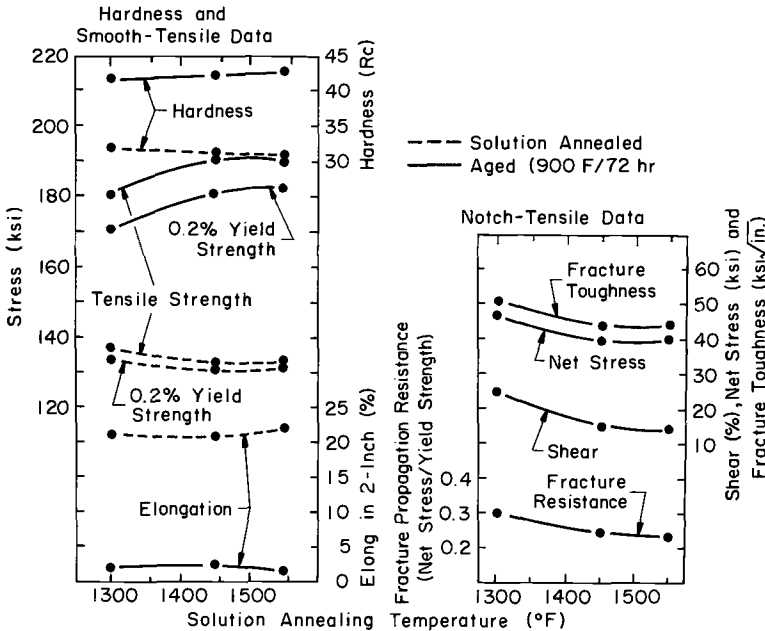


FIG. 3—Hardness and longitudinal tensile properties of B-120VCA as a function of solution annealing (SA) temperature.

by spark-discharge machining, and fatigue cracked by tension-tension cycling; the specimens were degreased, heat treated, and finish machined to final dimensions. After some preliminary testing, premature failure at pinholes led to designing smooth-tension specimens without pinholes and using file grips in the tensile machine. Predesiccated argon provided an inert atmosphere for all heat treatments in a sealed-off stainless steel tube within the furnace; specimens were cooled by withdrawing the sealed tube from the furnace. All specimens were solution treated at 1450 F for ¼ hr except as noted. They were aged at temperatures of 600 and 900 F, and for times up to 500 hr. Metallographic specimens

⁴ For simplicity, solution anneal will often be abbreviated as SA.

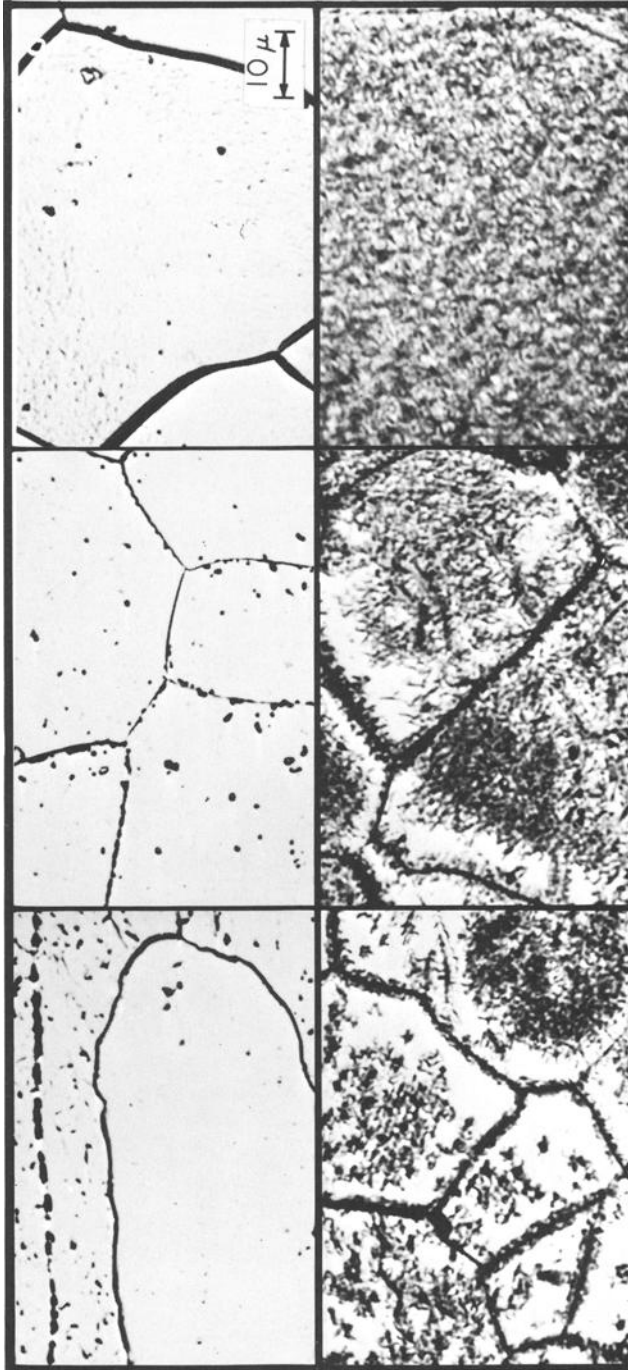


FIG. 4—Light micrographs showing effects of ($\frac{1}{4}$ hr) solution annealing at the indicated temperatures, (top) annealed structures and (bottom) aged (900 F/72 hr) structures.

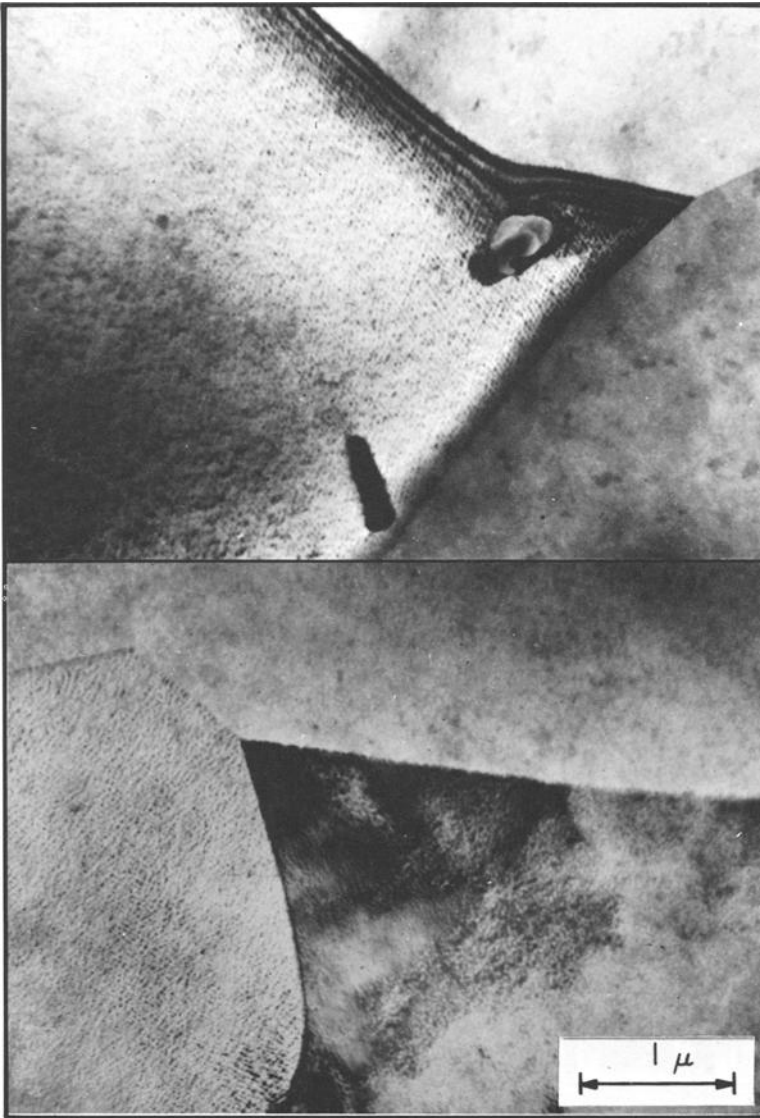


FIG. 5.—Transmission electron micrographs of solution annealed structures of B-120VCA suggesting incipient precipitation of omega.

were electropolished on a Disapol unit, using the A-3⁵ electrolyte; 0.5 to 1.0 per cent hydrofluoric acid (HF) in water was used as etchant. Thin sections were prepared for transmission electron microscopy, from pre-rolled thin foils (about 1 mil) which were electrolytically polished in the

⁵ Disapol A-3 electrolyte: 6 per cent perchloric acid, 59 per cent methanol, 35 per cent ethylene glycol monobutyl ester, 0.2 per cent Inhibitor X (patented).

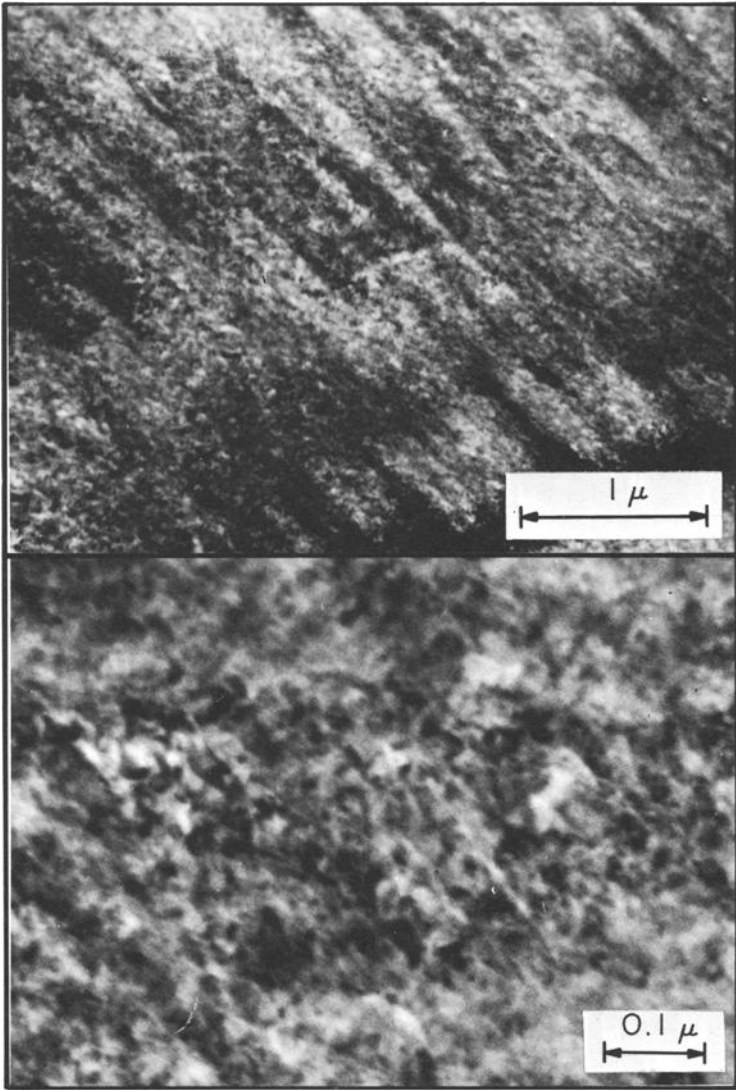


FIG. 6—Transmission electron micrographs of (600 F/462 hr) aged B-120VCA, showing unresolved fine dispersion of omega precipitate.

A-3⁵ electrolyte at 15 to 18 v. A Bollmann electrode arrangement was used in a stirred and ice-chilled bath.

Solution Treating

The effect of solution treating on the hardness, strength, and fracture properties of B-120VCA beta titanium alloy are shown in Fig. 3. The

hardness and strength of the unaged alloy decreases slightly with increasing solution-treating temperatures from 1300 to 1550 F (1/4 hr). The unaged fracture toughness was high enough to cause fracturing at the pinholes outside the specimen gage length and was therefore not measured. Light metallography (see Fig. 4, top row), after 1300 F solutionizing, showed persistent elongated cold-worked grains in a partially recrystallized or equiaxed matrix, and many ghost boundaries. Solutionizing at 1450 F produced (Fig. 4) a mixed grain size with some ghost boundaries, suggesting complete recrystallization but still not an equilib-

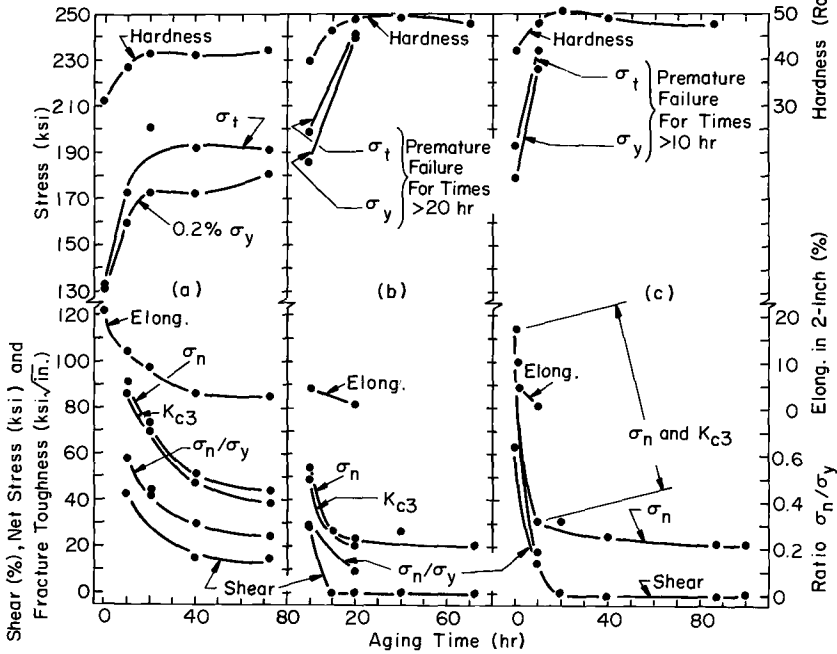
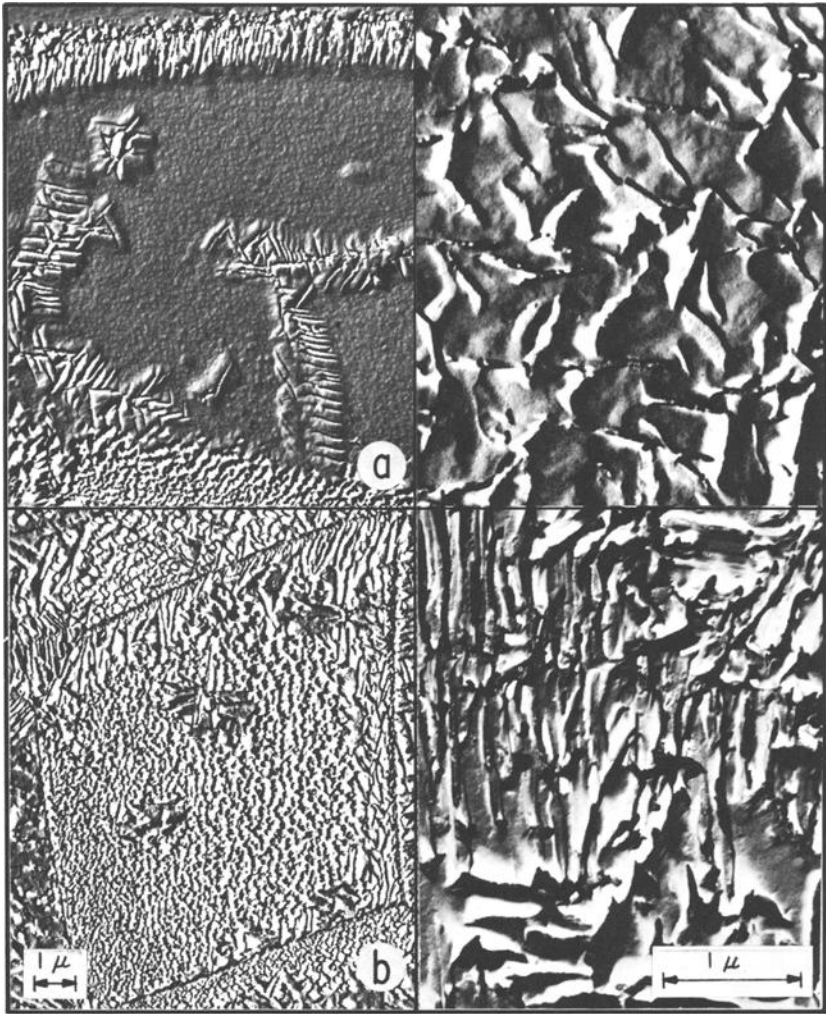


FIG. 7—Hardness and longitudinal sheet tensile properties of B-120VCA as a function of aging time at 900 F.

rium grain structure. After 1550 F solutionizing, the grains coarsened, and the ghost boundaries were removed (Fig. 4). Thus, the smaller structural units from the lower solutionizing treatments (cold-worked grains and substructures) provide some strengthening in the unaged condition; while at the higher solution annealing temperatures, the strength decreases with increasing grain size and progressive elimination of substructures. The effect of solution annealing temperature on the unaged strength properties is simple and direct.

On the other hand, after aging at 900 F for 72 hr, this relationship is reversed, and the strength properties increase, while the toughness parameters decrease with increasing solution annealing temperatures (see



(a) Aged 10 hr.
 (b) Aged 72 hr.

FIG. 8—Surface replica electron micrographs showing precipitation kinetics at 900 F after 65 per cent cold rolling and solution annealing at 1450 F.

Fig. 3). This may be qualitatively explained in terms of the aging kinetics; the bottom row of Fig. 4 shows light micrographs of aged (72 hr/900 F) structures of the 1300, 1450, and 1550 F solutionized matrices. With the 1300 F solutionizing pretreatment alpha precipitates in a highly discontinuous manner (Fig. 4), and the accelerated grain-boundary precipitation leaves adjacent solute denuded zones that are precipitate free. With increasing solutionizing temperatures (as more solutes are taken into solu-

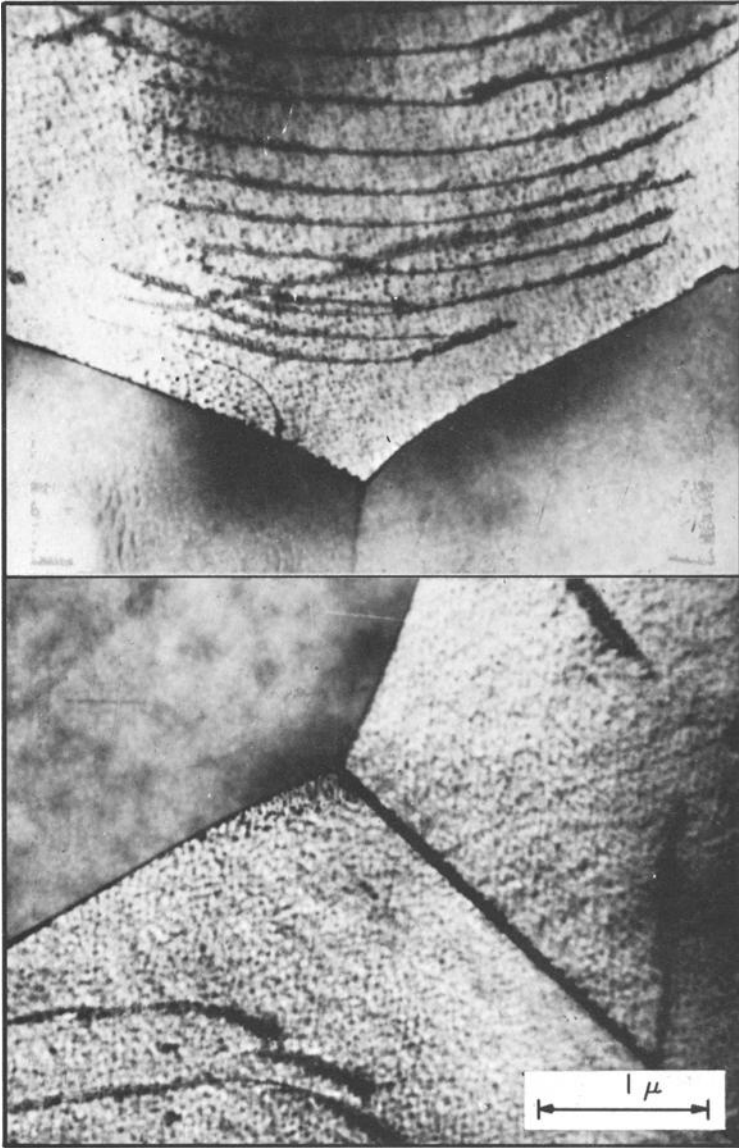


FIG. 9—Transmission electron micrographs of (900 F/2 hr) aged B-120VCA, showing dispersed omega precipitate; also nucleation at dislocations and grain boundaries.

tion), the precipitate becomes more continuous and has a finer dispersion. This aging characteristic explains the increased age strengthening and the corresponding toughness decline, observed after solutionizing at higher temperatures.

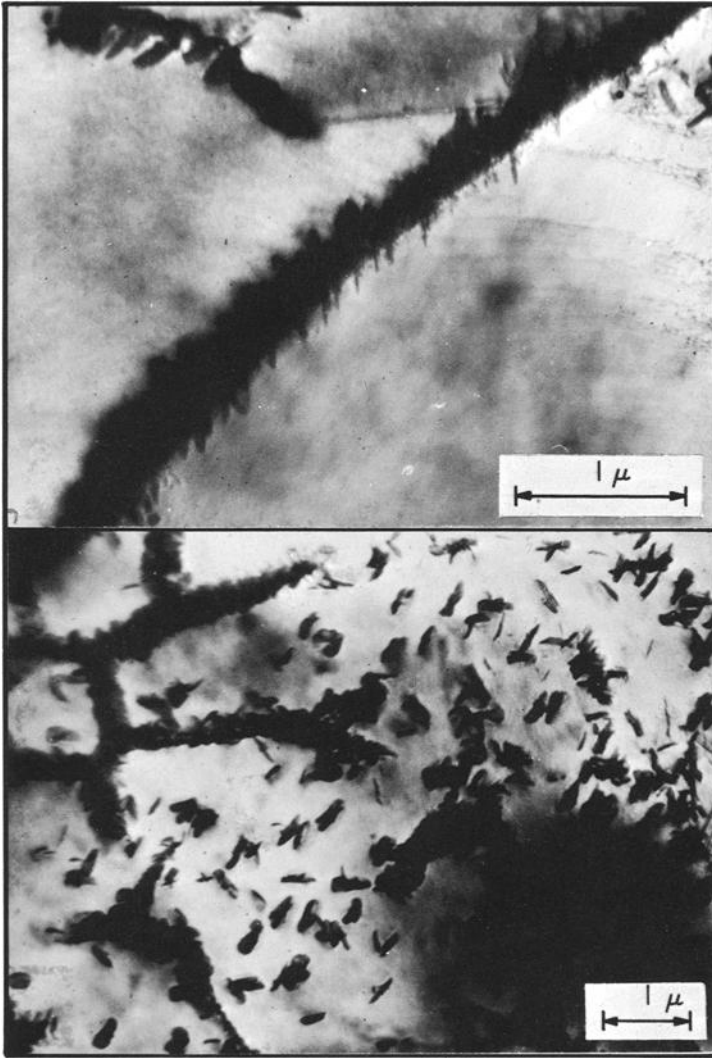


FIG. 10—Transmission electron micrographs of (900 F/4 hr) aged B-120VCA, showing alpha nucleation at grain and sub-boundaries, as well as some intragranular nucleation.

Transmission microscopy of the 1400 F solution annealed material showed mainly beta grains, but some of the beta grains suggest (Fig. 5) a very finely dispersed unresolved precipitate. In earlier observations [8] this surface effect was attributed to a Moiré pattern, suspected to have been caused by double diffraction from a thin surface-oxide film. However, observations on a more advanced stage of this effect on specimens aged at 600 F have led to the conclusion that the solution-annealed ma-

terial probably contains a fine dispersion of the same precipitate, ω , that is produced upon aging at 600 F, even though no diffraction evidence of this was obtained in the SA condition. Thus, some omega seems to precipitate during cooling from the solution-anneal treatment.

600 F Aging

Prolonged aging treatments (462 hr) at 600 F, with either a solution



FIG. 11—Transmission electron micrograph of (900 F/8 hr) aged B-120VCA, showing alpha precipitates with Moiré fringe contrast.

annealing or a cold rolling pretreatment, produced high hardness and strength but were accompanied by low notch strength:

	Hardness, R _c	σ_t , ksi	σ_n , ksi
65% CR + 1450 F SA + 462 hr at 600 F.....	52.5	196	18.8
50% CR + 1450 F SA + 50% CR + 462 hr at 600 F.....	52.9	220	16.7

Transmission electron microscopy (Fig. 6) demonstrates growth of the finely dispersed precipitate originally observed in the SA condition, with some grain boundary side plate extensions from the boundary on the right-hand bottom (upper micrograph). The lower micrograph in Fig. 6, at a higher magnification, still fails to clearly resolve individual precipi-

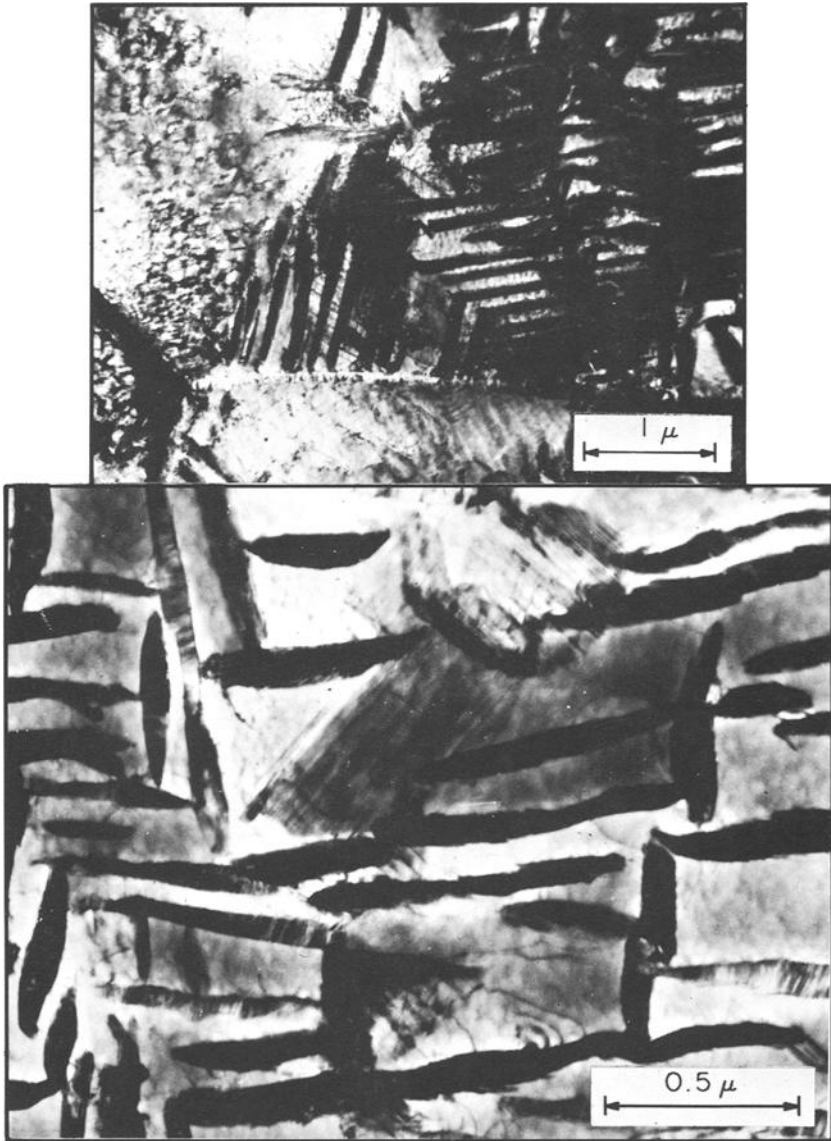
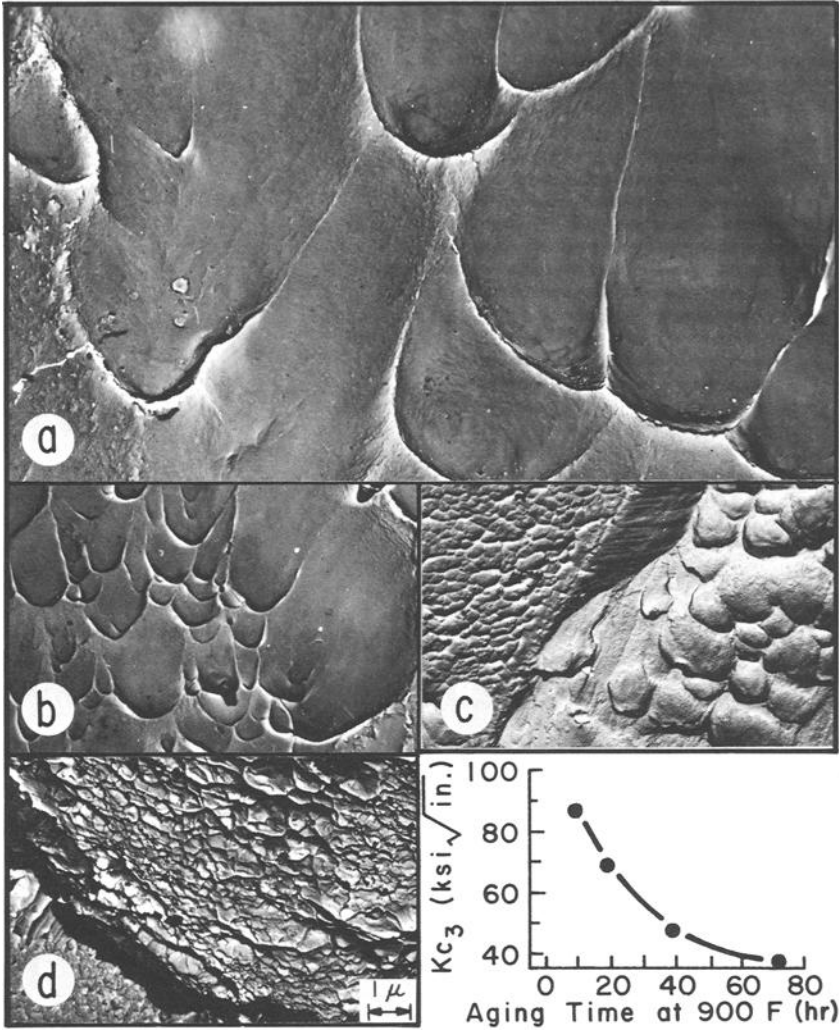


FIG. 12—Transmission electron micrographs of (900 F/72 hr) aged B-120VCA, showing general alpha precipitation; lower micrograph shows Moiré fringe contrast.

tate particles within the beta grain. However, selected-area electron diffraction data from regions of high precipitation density showed the presence of two reflections: the $11\bar{2}2$ at $d = 1.202$ Å, and the $30\bar{3}2$ at $d = 0.967$ Å, which uniquely characterize the omega, ω , precipitate. The broad and diffuse beta reflections tend to obscure a unique identifi-



(a) Solution annealed.
 (b) Aged 10 hr.
 (c) Aged 20 hr.
 (d) Aged 72 hr.

FIG. 13—Relationship of fractographic appearance with precipitation hardening and decreasing ductility in B-120VCA.

cation of this fine precipitate by X-ray diffraction techniques. But the $1\bar{2}10$ omega reflection at $d = 2.28 \text{ \AA}$ was partially resolved from the 110 beta reflection at 2.26 \AA in the electron diffraction pattern.

Thus, the extreme hardness, high tensile strength, and low fracture strength of the 600 F aged material is explained in terms of a fine ω precipitate, generally dispersed throughout the beta matrix.

900 F Aging

Isothermal aging kinetics of B-120VCA at 900 F were characterized in terms of three different initial or pretreatments: (1) 65 per cent cold reduction plus solution anneal at 1450 F for $\frac{1}{4}$ hr, (2) 65 per cent cold reduction by rolling, and (3) 50 per cent cold reduction plus solution anneal at 1450 F for $\frac{1}{4}$ hr plus 50 per cent cold rolling. Figure 7 shows the hardness, strength, and fracture properties of these materials, as a function of subsequent aging treatments. Before aging, Pretreatment 1



FIG. 14—Surface replica electron micrograph of 65 per cent cold-rolled and -aged (900 F/72 hr) specimen showing finely dispersed alpha precipitate.

naturally produces the lowest strength, but the highest fracture toughness. Pretreatment 3 provides intermediate strength but excellent toughness, while Pretreatment 2 produces the highest strength but the lowest fracture toughness. After aging for various times at 900 F, the strength increases, but the toughness declines most rapidly for the material which received Pretreatment 3 and least rapidly for Pretreatment 1, Pretreatment 2 being intermediate.

Pretreatment 65 Per Cent Deformation + Solution Anneal

A pretreatment consisting of 65 per cent cold rolling plus 1450 F SA, produces (Fig. 7) the lowest strength but highest toughness in the unaged

condition; tensile and yield strengths of 130 ksi are combined with 20 per cent elongation. The aged tensile strength and hardness are also the lowest of the three pretreatments, but the aged toughness is higher than with the other two pretreatments; tensile strength of 191 ksi and yield

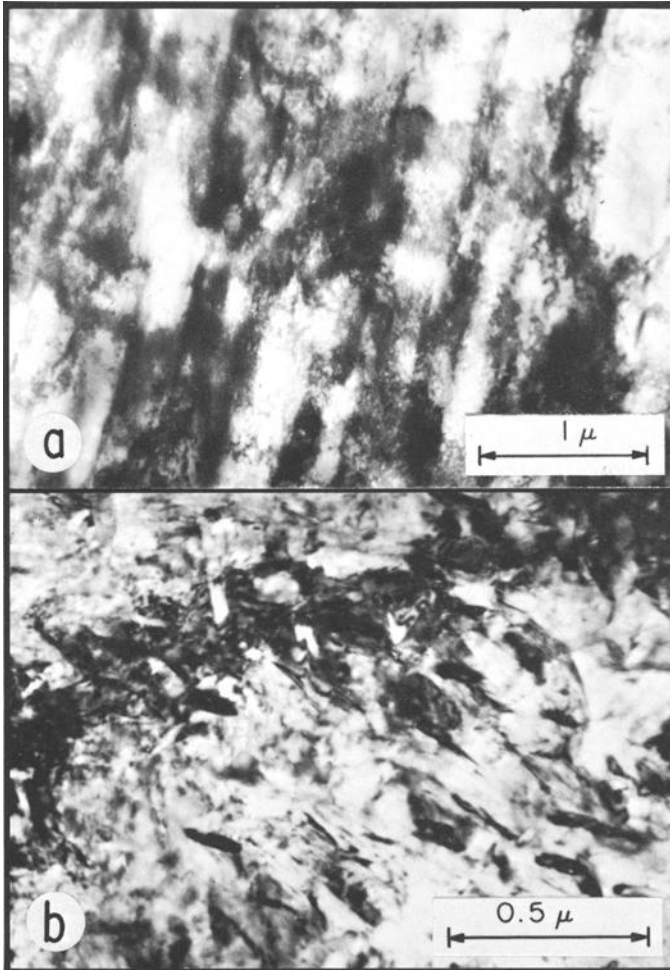


FIG. 15—Transmission electron micrographs of (a) cold rolled and (b) aged 900 F/72 hr structures, showing structural fragmentation with working, and finer alpha precipitate upon aging.

strength of 181 ksi are combined with a fracture toughness, K_{c3} of 39 ksi $\sqrt{\text{in.}}$, after 72-hr aging at 900 F. Also, as shown in Fig. 7, strength and ductility can be optimally combined through shorter aging times at 900 F. Thus, aging 20 hr at 900 F produces more than 190 ksi ten-

sile strength and 173 ksi yield, along with fracture toughness, K_{Ic} , of 70 ksi $\sqrt{\text{in.}}$

In the solution-treating studies, electron metallography had suggested a beta matrix, with some incipient omega precipitation, after solution-annealing at 1450 F for $\frac{1}{4}$ hr. The subsequent aging kinetics upon 900 F aging were studied by surface replica and thin-section transmission electron microscopy.

The surface replica electron micrographs in Fig. 8 show the progress of precipitation at 900 F. Figure 8a (10-hr aging) shows that α initially precipitates at grain and subgrain boundaries, with occasional nucleation in the grain center. While after aging 72 hr (Fig. 8b), general precipitation occupies nearly the entire matrix.

The precipitation kinetics at 900 F were established in considerable detail by transmission electron microscopy. After short aging times, such as 2 hr at 900 F, the omega, ω , precipitate (see Fig. 9) is more clearly visible as a generally dispersed precipitate. This dispersed precipitate was identified by electron diffraction in the 600 F/462-hr aged material as omega. In addition to the finely dispersed ω precipitate background, nucleation of a second precipitate is suggested (see Fig. 9) along the beta grain boundaries and dislocation lines. This is believed to be the beginning of the alpha precipitation. This tentative identification of early alpha is based on morphological considerations, because no discrete diffraction evidence was obtainable. After 4 hr of aging at 900 F, Fig. 10 shows further growth of the grain boundary side plates, as well as general nucleation at specific sites within the beta grains; also, several instances of sympathetic nucleation may be seen. Accelerated nucleation at subgrain boundaries tend to produce a network of alpha precipitate stringers, seen in the lower micrograph of Fig. 10.

After 8 hr of aging at 900 F, both the grain boundary alpha side plates and the alpha precipitates within the grains have achieved dimensions in the order of some thousand angstroms (see Fig. 11). The alpha precipitates exhibit Moiré fringes due to the superposition of the precipitate and matrix lattices, and the consequent double diffraction phenomena as the electron waves pass through these lattices during transmission through the specimen.

After prolonged aging at 900 F, for example, 72 hr, the general precipitation of alpha has progressed throughout the grains, along with considerable growth of the grain boundary side plates (see Fig. 12). Boundary side plates are also seen emanating from subboundaries, as in the top micrograph of Fig. 12. At a higher magnification, the lower micrograph in Fig. 12 shows distinct Moiré fringes in the alpha precipitates. Some of the partially coherent alpha precipitates, when suitably oriented, reveal Moiré fringe contrast from the array of structural dislocations or Van Der Merwe nets, at the precipitate matrix interfaces.

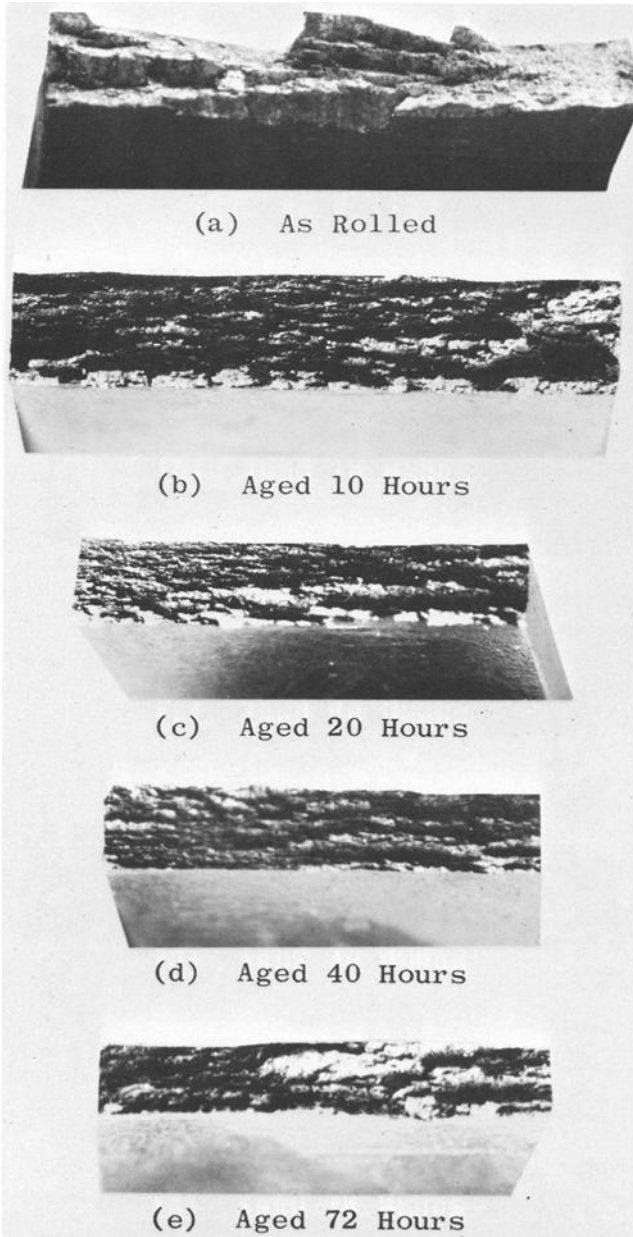
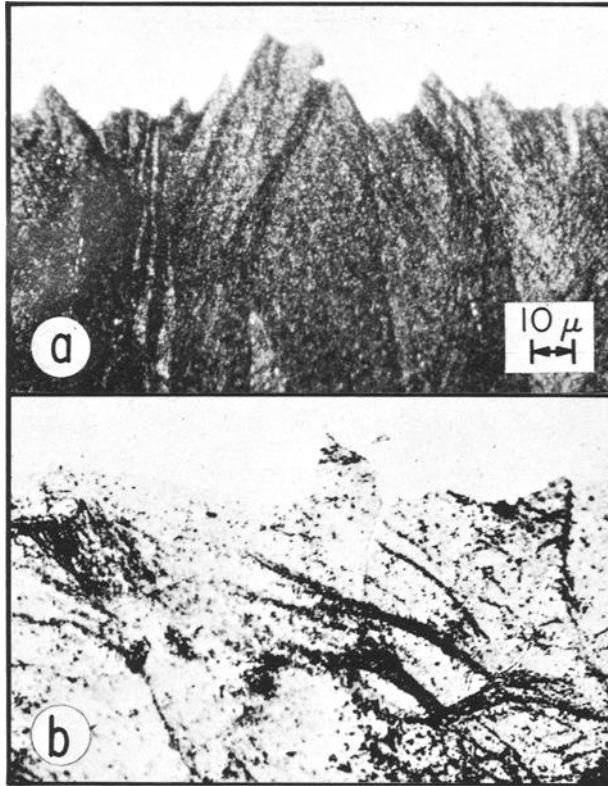


FIG. 16—Fractographs of tension specimens illustrating rapidly decreasing toughness with aging time at 900 F.

Interaction of these interface dislocations with dislocations originating within the beta matrix may be occasionally observed.

Electron fractography was used to study the detailed progress of fracture in broken tension specimens in the aged condition (various aging times at 900 F). Figure 13 shows the solution-annealed (1450 F/¼ hr)



(a) Edge view.
(b) Sheet normal view.

FIG. 17—Nickel-plated fracture edges viewed from the sheet edge and sheet normal on a longitudinal tension specimen in the 65 per cent cold-rolled and -aged (900 F/72 hr) condition. Etchant: 1 per cent hydrofluoric acid.

material to have huge ductile-shear dimples, measuring up to tens of microns in diameter (Fig. 13a). Correspondingly, this material had the highest fracture toughness, with 21 per cent elongation in the smooth tension test. Upon aging for 10 hr, the elongation drops to 12 per cent, and the fracture toughness is 86 ksi $\sqrt{\text{in.}}$; in Fig. 13b, ductile dimples are still seen, but they are much smaller (4 to 5 μ maximum diameter). Upon aging for 20 hr ($K_{cs} = 70$ ksi $\sqrt{\text{in.}}$), in addition to the still smaller dimples, some flat intercrystalline fracture is encountered (Fig. 13c).

After 72-hr aging ($K_{c3} = 39 \text{ ksi } \sqrt{\text{in.}}$), intercrystalline fractures and small dimpled fractures are seen in Fig. 13d.

Pretreatment 65 Per Cent Deformation

Figure 7 showed high tensile (199 ksi) and yield (186 ksi) strengths, but much lower fracture toughness ($< 50 \text{ ksi } \sqrt{\text{in.}}$) for the cold-reduced, unaged condition. This increased strengthening in the unaged condition may be understood in terms of the stored cold-work energy. After aging, a finely dispersed alpha precipitate (see Fig. 14) increases the strength to 240 ksi tensile and yield strengths (see Fig. 7); but the fracture toughness, K_{c3} drops to about $20 \text{ ksi } \sqrt{\text{in.}}$

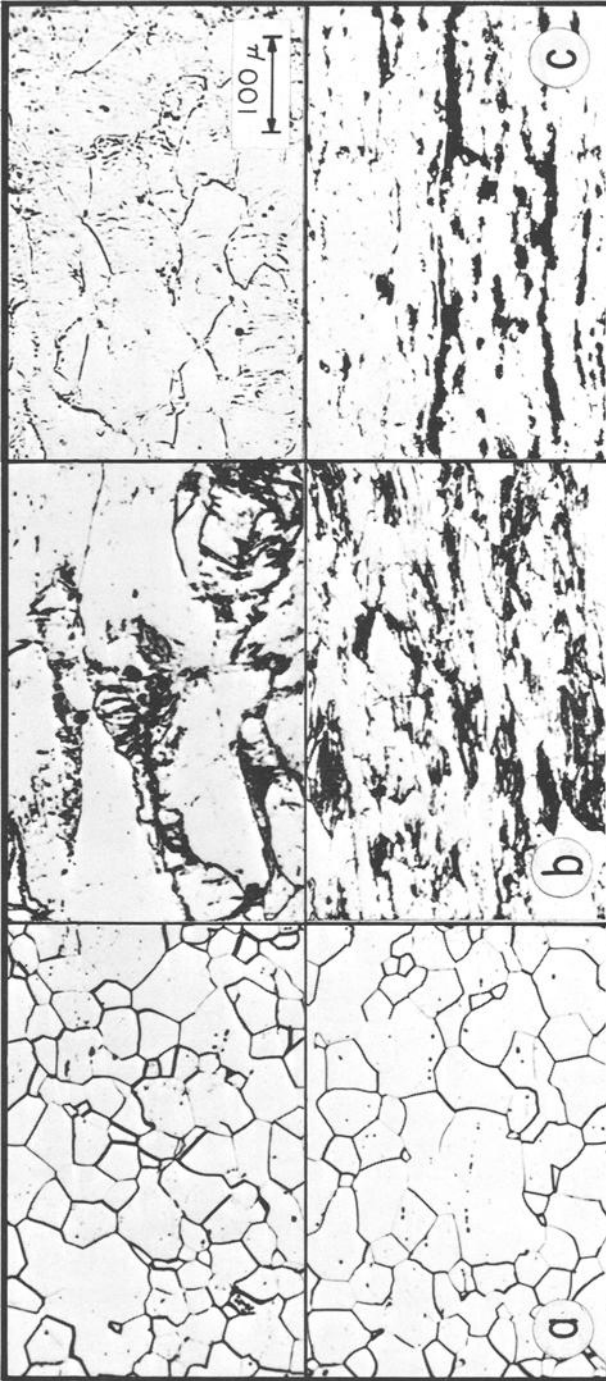
The top micrograph in Fig. 15 shows the transmission electron microstructure of a cold-rolled matrix—which is heavily deformed and highly fragmented, and reveals little structural details. After 72 hr aging at 900 F, the alpha needles (Fig. 15, lower micrograph) are seen to be substantially smaller than those found in the SA + aged material.

The cold-reduced materials show deep internal shear lips in their macroscopic fracture appearance (Fig. 16), which relates to their low fracture toughness. Upon aging, even for as short a time as 10 hr, a nearly flat fracture is seen. To explain the internal shear-fracture lips, Fig. 17a shows the sheet edge in a nickel-plated fractograph at $\times 500$. The fracture path follows steps along deformation bands, inclined about 30 deg to the tension axis. Figure 17b shows the fracture edge viewed normal to the sheet surface, and again the parallelism of the fracture path to the deformation banding is evident. Also, Fig. 17 reveals the ribbon shape of the deformation bands produced by cold rolling. Thus, the brittleness of the cold worked material seems to be related to weaknesses at the boundary regions of the coarse deformation bands.

Pretreatment 50 Per Cent Deformation + Solution Anneal + 50 Per Cent Deformation

The initial 50 per cent cold rolling was designed to produce a grain refinement upon solution-anneal, while the final 50 per cent cold rolling introduced matrix strain before aging. In the unaged condition, this pre-condition produced 193 ksi tensile and 180 ksi yield strengths, with a fracture toughness, K_{c3} , of $115 \text{ ksi } \sqrt{\text{in.}}$ (see Fig. 7); but after aging, the toughness rapidly decreases to ($K_{c3} \approx 20 \text{ ksi } \sqrt{\text{in.}}$), while the yield and tensile strengths steeply rise ($\sigma_t, \sigma_y \approx 230 \text{ ksi}$). The high strength and toughness combinations of the unaged 50-SA-50 material may hold particular promise for high-strength ambient and cryogenic applications, where thermal stability is not required.

The cold-work energy in the material—with an intermediate anneal—which was twice 50 per cent cold-reduced is not appreciably greater than that in the material cold-rolled 65 per cent, judging by the similarity in



- (a) 65 per cent cold rolled and solution annealed.
- (b) 65 per cent cold rolled.
- (c) 50 per cent cold rolled and solution annealed, plus 50 per cent cold rolled.

FIG. 18—Micrographs showing effect of various treatments on grain size and shape of B-120VCA (top) viewed on rolling plane and (bottom) viewed on longitudinal edge.

their tensile and yield strengths (Fig. 7). However, the 50-SA-50 treatment produces a finer grain size than the direct rolling (65 per cent), which merely elongates the original coarse grains (compare Figs. 18c and b). Correspondingly, the 50-SA-50 unaged material is tougher than the 65 per cent cold-rolled, unaged material. The K_{c3} toughness for the twice cold-reduced material is more than double that of the 65 per cent cold-rolled material. But aging causes preferential alpha precipitation along the deformed regions in the cold-worked material, producing favorable paths for crack initiation and propagation. Thus, fracture toughness, K_{c3} , rapidly drops to less than 20 ksi $\sqrt{\text{in}}$.

Discussion and Summary

Strength and fatigue-cracked center-notched sheet fracture-toughness, K_{c3} , properties were related to fine-structural characteristics of B-120-VCA beta titanium alloy in a variety of conditions produced through thermomechanical treatments.

In the unaged condition, solution treating temperatures had a simple direct effect on strength properties related to extent of recrystallization and grain coarsening. Thus strength properties declined with increasing solution-annealing temperatures. However, after aging (900 F/72 hr), this relation was reversed, namely, the strength properties increased at higher solutionizing temperatures but the toughness declined. These observations are explained in terms of the finely dispersed precipitate, which forms upon aging after solutionizing at higher temperatures.

Prolonged aging at 600 F produced a finely dispersed general precipitate, which was identified by electron diffraction as the omega, ω , phase. By morphological analogy, a finely dispersed omega is believed to form also during cooling from the solution-annealing treatment.

Aging kinetics at 900 F were studied in terms of three different initial pretreatments: (1) 65 per cent cold reduction plus solution-anneal at 1450 F for $\frac{1}{4}$ hr, (2) 65 per cent cold reduction by rolling, and (3) 50 per cent cold reduction plus solution-anneal at 1450 F for $\frac{1}{4}$ hr plus 50 per cent cold reduction by rolling.

Before aging, Pretreatment 1 produces the lowest strength properties but the highest fracture toughness; tensile and yield strengths of about 130 ksi are combined with 20 per cent elongation. Pretreatment 3 provides higher strength and excellent toughness: 193 ksi tensile and 180 ksi yield strength are combined with fracture toughness of 115 ksi $\sqrt{\text{in}}$. Thus, the 50-SA-50 unaged condition may hold promise for high-strength ambient and cryogenic applications where thermal stability is not required. Pretreatment 2 produces the highest strength, namely, 199 ksi tensile strength and 186 ksi yield strength, but the fracture toughness falls to less than 50 ksi $\sqrt{\text{in}}$.

After aging for various times at 900 F, the strength increases and

correspondingly the toughness declines most rapidly for Treatment 3, and least rapidly for Treatment 1, Treatment 2 being intermediate. Isothermal aging at 900 F of the SA material revealed that unique combinations of strength and notch toughness can be obtained through short aging times. Thus, 20 hr at 900 F produces more than 190 ksi tensile strength, and 173 ksi yield strength along with fracture toughness of 70 ksi $\sqrt{\text{in}}$. This contrasts with 191 ksi tensile strength, 181 ksi yield strength, and 39 ksi $\sqrt{\text{in}}$ fracture toughness obtained through the commercial 72-hr aging. Thus, short-aging treatments may prove useful for near ambient applications where high strength and toughness must be combined.

Fine structural study of the aging kinetics suggested limited growth of the omega precipitate at 900 F, but alpha plates begin to discontinuously nucleate as side plates upon grain boundaries and dislocation lines within 2 hr of aging at 900 F. As the alpha plates grow, they exhibit Moiré fringe contrast through double diffraction between the precipitate plates and the matrix. After prolonged aging (72 hr), general nucleation of the alpha precipitate covers the entire matrix. With a cold work (65 per cent chromium) pretreatment, aging produces a finer dispersion of smaller alpha needles which accounts for its high strength; the low fracture toughness of this material seems to be related to weakness at the boundary regions of the coarse deformation bands, formed upon deformation. If an intermediate annealing step is introduced (as in the 50-SA-50 pretreatment), the structure is further refined and narrow deformation bands produce improved toughness along with high strength in the unaged condition, but aging causes precipitation along the band interfaces and produces favorable crack paths which reduce the toughness to low values. No TiCr_2 nor other intermetallic precipitates were observed under these aging conditions. TiCr_2 was observed after considerable overaging at 1000 F. Thus, the observed strength and fracture properties produced by a variety of treatments may be understood in terms of the fine-structural parameters of this alloy.

References

- [1] U. S. Patent, 3,147,115, Sept. 1, 1964.
- [2] Petersen, V. C., Bomberger, H. B., and Vordahl, M. B., "An Age Hardening Titanium Alloy," *Metal Progress*, Vol. 76, No. 6, 1959, p. 119.
- [3] Rawe, R. A., Dupouy, J. J., and Bever, M. B., "The Aging Characteristics of the Ti-13V-11Cr-4Al Alloy," *Transactions Metallurgical Society*, American Institute of Mining, Metallurgical, and Petroleum Engineers, Vol. 218, 1960, p. 821.
- [4] Tanner, L. E., "The Isothermal Transformation of Ti-13V-11Cr-3Al," *Transactions*, American Society for Metals, Vol. 53, 1961, p. 407.
- [5] Tanner, L. E., Boyd, J. E., and Coyne, J. E., Jr., "The Electron Metallographic Examination of Transformation Structures in the Ti-13V-11Cr-3Al Alloy," *Transactions Metallurgical Society*, American Institute of Mining, Metallurgical, and Petroleum Engineers, Vol. 224, 1962, p. 872.
- [6] Espey, G. B., Jones, M. H., and Brown, W. F., Jr., "Sharp-Edge-Notched Ten-

sile Characteristics of Several High-Strength Titanium Sheet Alloys at Room and Cryogenic Temperatures," *Low Temperature Properties of High Strength Aircraft and Missile Materials*, ASTM STP 287, American Society for Testing and Materials, 1961, p. 74.

- [7] Repko, A. J., Jones, M. H., and Brown, W. F., Jr., "Influence of Sheet Thickness on Sharp-Edge-Notch Properties of a Beta Titanium Alloy at Room and Low Temperature," *Evaluation of Metallic Materials in Design for Low Temperature Service*, ASTM STP 302, American Society for Testing and Materials, 1962, p. 213.
- [8] Banerjee, B. R. and Hauser, J. J., "Fracture Micromechanics in High Strength Steels and Titanium," MLTDR-64-182, Wright-Patterson Air Force Base, Ohio, July 31, 1964.

Plane Strain Fracture Toughness and Mechanical Properties of 5Al-2.5Sn ELI and Commercial Titanium Alloys at Room and Cryogenic Temperatures

REFERENCE: Carman, C. M. and Katlin, J. M., "Plane Strain Fracture Toughness and Mechanical Properties of 5Al-2.5Sn ELI and Commercial Titanium Alloys at Room and Cryogenic Temperatures," *Applications Related Phenomena in Titanium Alloys, ASTM STP 432*, American Society for Testing and Materials, 1968, pp. 124-144.

ABSTRACT: An investigation was performed to determine the engineering properties and plane strain fracture toughness characteristics at cryogenic temperatures for $\frac{1}{4}$, $\frac{1}{2}$, and 1-in.-thick plates of 5Al-2.5Sn ELI (extra low interstitial) and commercial grade titanium alloys. These results were then translated into design information data applicable to liquid-fueled rocket booster tanks for service at -320 and -423 F. The tensile properties of these materials were determined at room temperature, -110 F, -320 F, and -423 F using small round tension specimens. The plane strain fracture toughness was determined using an instrumented precracked bend specimen. The dimensions of these specimens were such that the criterion (crack length and specimen thickness are equal to $2.5 (K_{Ic}/\sigma_{ys})^2$) was met at testing temperatures of -320 and -423 F. These data may be considered valid values of plane strain fracture toughness. The commercial 5Al-2.5Sn titanium alloy gave values of K_{Ic} of approximately 25,000 and 24,000 psi $\sqrt{\text{in.}}$ at testing temperatures of -320 and -423 F, respectively. On the other hand, the 5Al-2.5Sn ELI titanium alloy gave values of K_{Ic} of 65,000 and 55,000 psi $\sqrt{\text{in.}}$ at these testing temperatures, respectively. These data show a superiority of approximately 1.5 in terms of critical crack size for the ELI grade. The relative level of texture hardening in this material was estimated by measuring the R values of these plates. The predicted biaxial yield strength of tanks fabricated from this material was compared with experimental data.

KEY WORDS : aluminum alloys, tin alloys, titanium alloys, cryogenic testing, fracture mechanics, metals, mechanical treatments

Nomenclature

a Notch depth or $\frac{1}{2}$ crack length

¹ Metallurgists, Pitman-Dunn Research Laboratories, Frankford Arsenal, Philadelphia, Pa.

B	Specimen thickness
d	Beam depth
e	Engineering strain
K	Parameter describing the local elevation of the elastic stress field ahead of a crack
K_{Ic}	Plane strain fracture toughness
\ln	Natural logarithm
LD	Specimen longitudinal to rolling direction and crack propagating into the thickness direction of the plate
LS	Specimen longitudinal to rolling direction and crack propagating parallel to the rolling plane
M	Bending moment
Q	Form factor
R	Ratio of width to thickness strain
TD	Specimen transverse to rolling direction and crack propagating into the thickness direction of the plate
TS	Specimen transverse to rolling direction and crack propagating parallel to the rolling plane
β	Relative plastic zone size
ϵ	True strain
σ	Gross section stress
σ_{ys}	0.2 per cent offset uniaxial yield stress

Subscripts

c	Critical value of a parameter
I	First, or opening, mode of fracture

In the past, the majority of liquid-fueled rocket booster tanks have been constructed of either aluminum alloys or cold rolled stainless steel. The minimum operating temperature for these tanks has been that of the liquid oxygen contained in them, namely, -297 F. However, future upper-stage rockets will use liquid hydrogen as a fuel, and, therefore, the propellant tanks will operate at -423 F. It is doubtful if the presently used materials will operate efficiently at this temperature, due to either low strength or a deficiency in fracture toughness.

Because of the weight limitations in the upper-stage structures of these new rockets, it would be desirable to employ materials possessing very high strength-to-density ratios, provided the material properties were satisfactory at the minimum operating temperatures. The aluminum alloys and cold rolled stainless steels used previously for rocket booster tanks have strength-to-density ratios of approximately 650,000 in. at room temperature and 850,000 in. at -297 F.

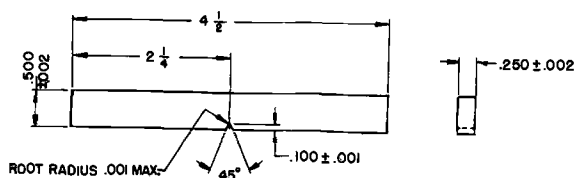
Data presented at the 1960 ASTM Symposium on Low Temperature

Properties of High Strength Aircraft and Missile Alloys [1]² showed that these strength-to-density values can be exceeded substantially by some materials. Based on this published information, it appears that three types of alloys offer the promise of achieving high strength in combination with adequate toughness at -423 F. These materials are: (1) cold worked stable and metastable austenitic stainless steels, (2) annealed alpha titanium alloys, and (3) certain aluminum alloys of the copper-bearing series.

The annealed alpha titanium alloys offer the most promise in terms of high strength in conjunction with good fracture toughness. Of these

TABLE 1—Composition of 5Al-2.5Sn titanium alloy.

Thickness, in.	Grade	Per Cent							
		C	Fe	N	Al	H	Sn	Mn	O
1/4.....	ELI	0.023	0.16	0.010	5.0	0.009	2.6	0.006	0.080
1/2.....	ELI	0.023	0.16	0.010	5.0	0.001	2.6	0.006	0.086
1/2.....	commercial	0.023	0.34	0.015	5.1	0.017	2.3	0.006	...
1.....	ELI	0.026	0.14	0.16	5.1	0.003	2.4	0.004	.0.101



Note: Specimen to be Fatigue cracked prior to testing.

FIG. 1—Small notched bend specimen.

alloys, the best one appears to be 5Al-2.5Sn titanium alloy. Since the toughness of the annealed alpha titanium alloys is dependent on the interstitial content of the material, it was decided to concentrate this study on the ELI (extra low interstitial) material in the 1/4, 1/2, and 1 in. thickness. The commercial grade of 5Al-2.5Sn titanium alloy in the 1/2 in. thickness was used for comparison.

The basic material parameters used for evaluating the 5Al-2.5Sn titanium alloys were: (a) tensile properties at room and cryogenic temperatures, (b) plane strain fracture toughness at room and cryogenic temperatures, and (c) *R* values measured at room temperature.

² The italic numbers in brackets refer to the list of references appended to this paper.

Materials

The chemical composition of the 5Al-2.5Sn titanium alloy plates are given in Table 1. The commercial alloy has a higher content of iron and hydrogen. These plates were annealed by furnace cooling from 1500 F.

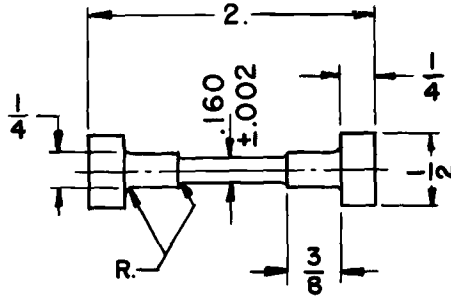


FIG. 2—Small round tension specimen.

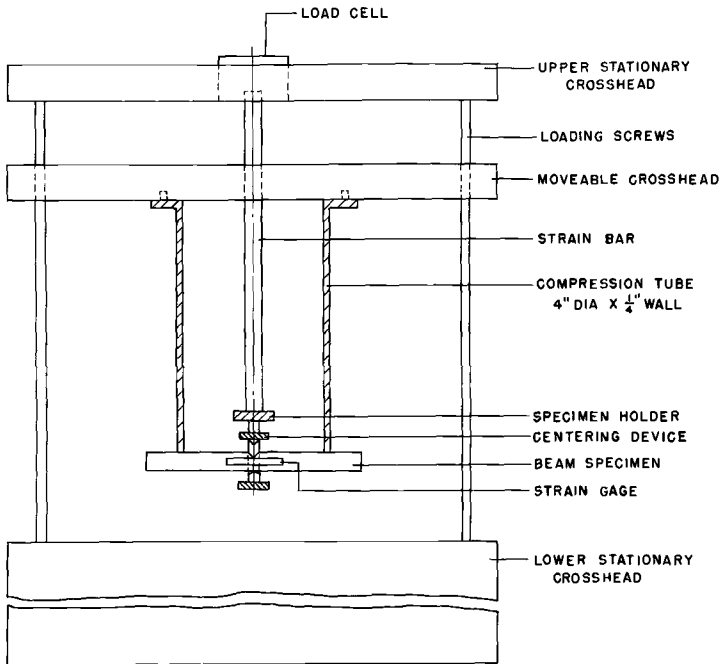


FIG. 3—Schematic of loading notched bend specimens.

Experimental Procedure

Size is an important factor in selecting specimens for cryogenic testing. Large specimens require excessive amounts of costly cryogenic liquids to cool them. Consequently, it is desirable to use as small a speci-

men as possible and still be consistent with the experimental condition for obtaining valid fracture toughness measurements. Therefore, a small precracked notched bend specimen was selected for this study. The dimensions of the specimen are given in Fig. 1.

This specimen offers the advantage of small size and minimum break-

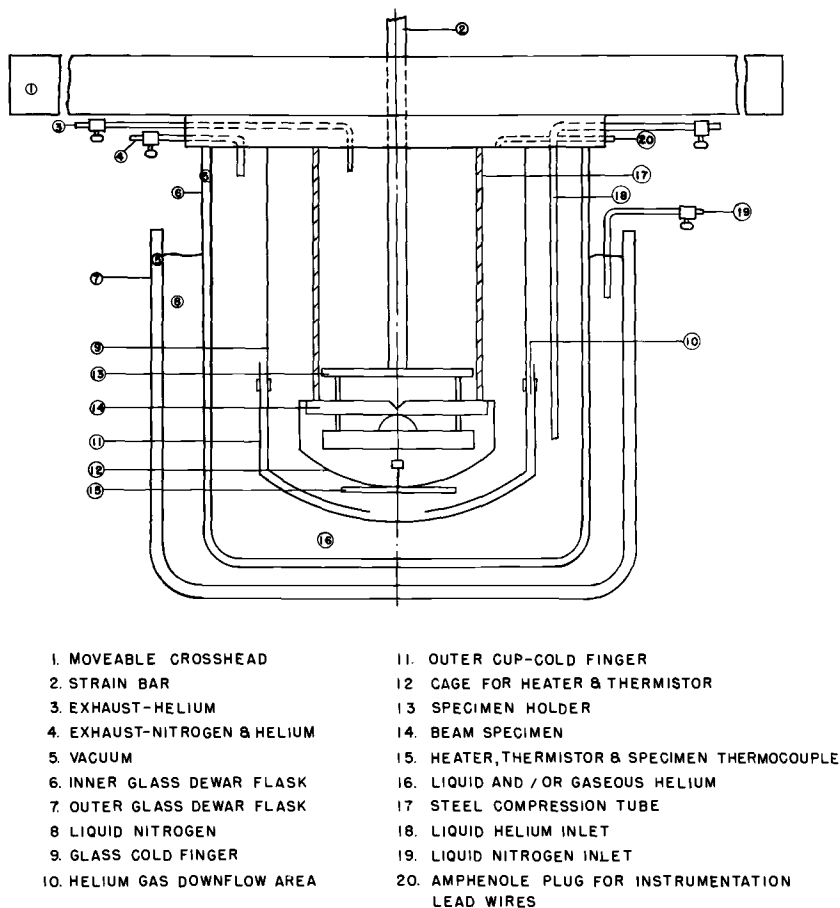


FIG. 4—Schematic of cryostat and associated apparatus used for tests conducted at -423 F .

ing load. By using the “pop-in” [2] technique, it may be possible to further reduce the specimen size. Unpublished work at Frankford Arsenal has shown that the load at pop-in may be readily detected by a small high-elongation strain gage placed at the crack tip. With the advent of suitable techniques for attaching and using strain gages at these low temperatures, this method of pop-in detection should give reliable data without incorporating an additional large mass requiring greater cooling capacity.

As previously discussed, large consumptions of cryogenic coolants as well as the mechanical limitations of the testing equipment necessitated the use of small specimens for plane strain fracture toughness measurements. This also holds true for the measurement of the tensile properties.

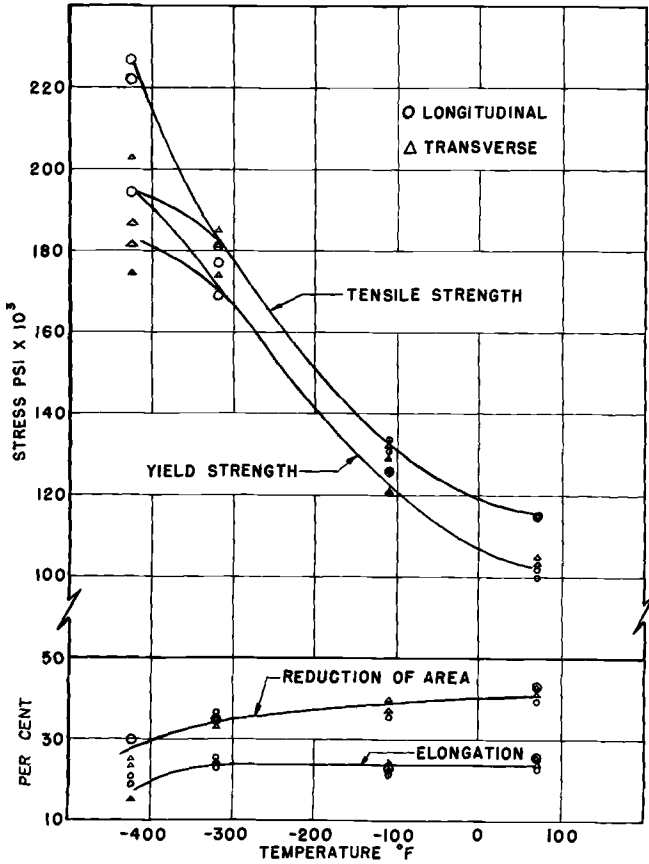


FIG. 5—Tensile properties of ¼-in.-thick 5Al-2.5Sn ELI titanium alloy plate as a function of testing temperature.

Therefore, a small round tension specimen (0.160 in. diameter), as shown in Fig. 2, was used for these studies. Small strain gages were used to determine the strain of the specimen.

The tension and notched bend tests were conducted on an Instron tension testing machine. The method of loading is shown in Fig. 3. The notched bend specimens were tested in three-point loading. The end loads were reacted against a compression column which was attached to the movable crosshead of the Instron. The central load was applied by means of a tension bar and loading saddle, which pass up the center of the compression column and are attached to the load cell of the machine.

The loading was accomplished by driving the movable crosshead downward.

For the tests conducted at ambient temperature, the specimens were broken in air at approximately 70 F. Tests at -110 and -320 F were conducted by immersing the compression column, specimen, and asso-

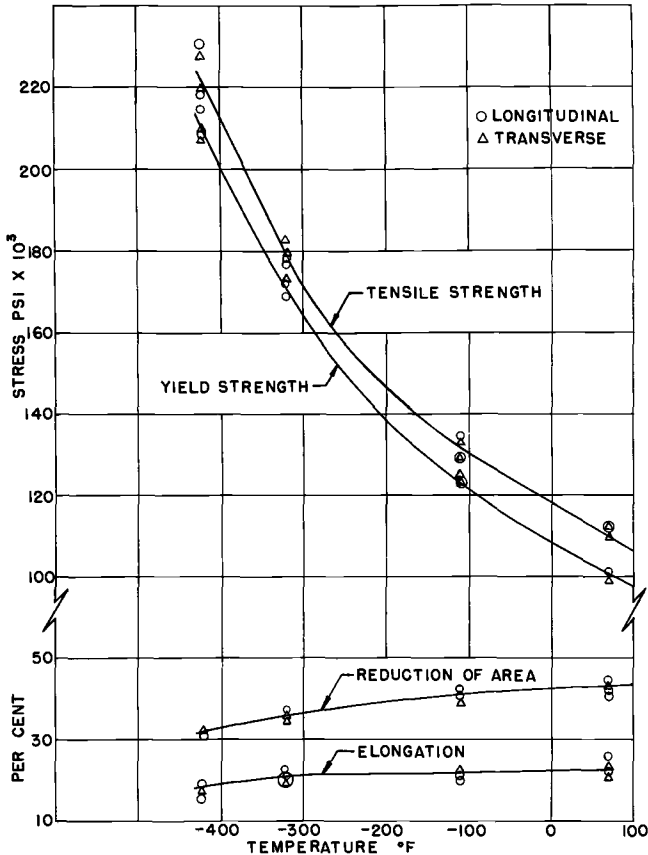


FIG. 6—Tensile properties of $\frac{1}{2}$ -in.-thick 5Al-2.5Sn ELI titanium alloy plate as a function of testing temperatures.

ciated apparatus in a mixture of dry ice and alcohol and in liquid nitrogen, respectively.

Since it was not practical, from a safety standpoint, to use liquid hydrogen in the laboratory, a system had to be developed whereby testing could be accomplished at -423 F. The method devised utilized the evaporating gas of liquid helium (-452 F) as the cryogenic medium. The cold gas passed over an electrical resistance heater controlled so that the emerging stream of heated gas maintained the test specimen at

liquid hydrogen temperature. A schematic of the cryostat and associated apparatus used is shown in Fig. 4. After placing the specimen in position in the holder, making all electrical connections, and sealing the cryostat to the testing machine, liquid nitrogen was introduced into the outer dewar until the proper level was maintained. This served as a shield for

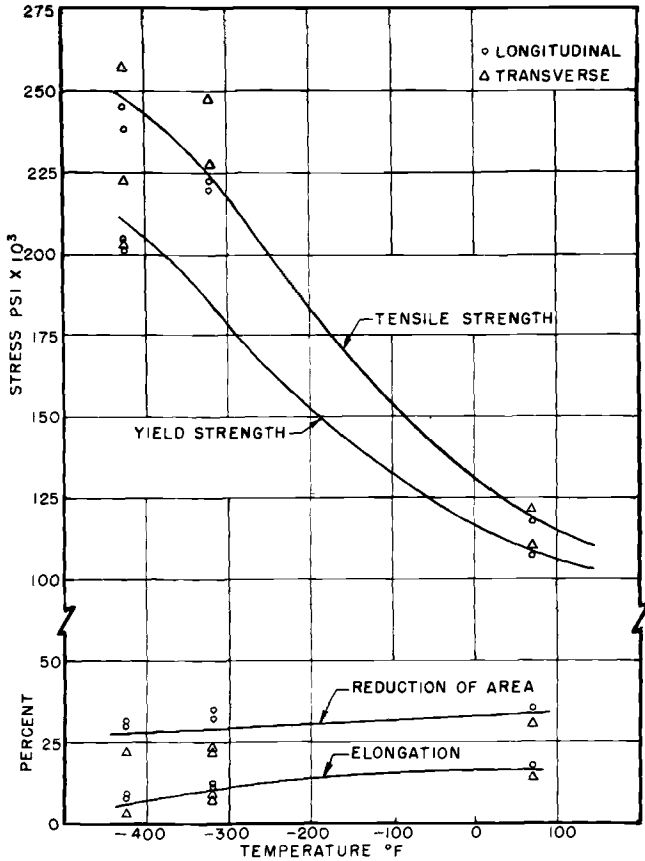


FIG. 7—Tensile properties of 1-in.-thick 5Al-2.5Sn ELI titanium alloy plate as a function of testing temperature.

the liquid helium system. Liquid nitrogen was then slowly introduced through inlet ⑮ into the inner dewar and allowed to boil. The boil-off gas filled the region ⑯ and then dropped down into cup ⑰ through opening ⑩. The gas then travelled up through the opening at the bottom of the cold finger ⑨, over the heater and thermistor, over the specimen and out the exhaust ④. Excess pressure was bled off by exhaust valve ④. Cooling with liquid nitrogen was continued until the specimen temperature was approximately -250 F. The system was purged with helium gas,

and then liquid helium was transferred into the inner [®] dewar. The path of the cold helium gas was the same as that of the nitrogen gas. However, when the temperature of the cold helium gas stream was below -423 F, the heater coil was energized to condition the gas stream to liquid hydro-

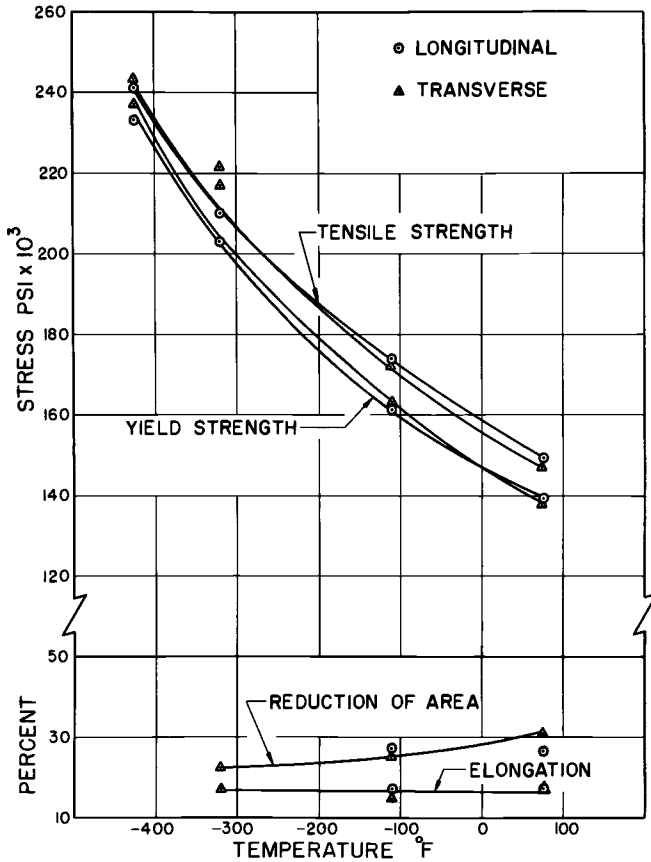


FIG. 8—Tensile properties of 1/2-in.-thick 5Al-2.5Sn commercial titanium alloy plate as a function of testing temperature.

gen temperature. The temperature of the specimen was determined by means of a differential thermocouple.

Experimental Results and Discussion

Tensile Properties

The tensile properties of the 1/4, 1/2, and 1-in.-thick plates of 5Al-2.5Sn ELI titanium alloy are shown as a function of testing temperature

in Figs. 5, 6, and 7. The tensile properties of the commercial grade are shown in Fig. 8.

Both the ELI and commercial titanium alloys exhibit a high degree of sensitivity of strength to temperature and show an increase in yield strength from 100,000 psi at room temperature to over 200,000 psi at -423 F. The increase was accomplished with only a minor loss in the

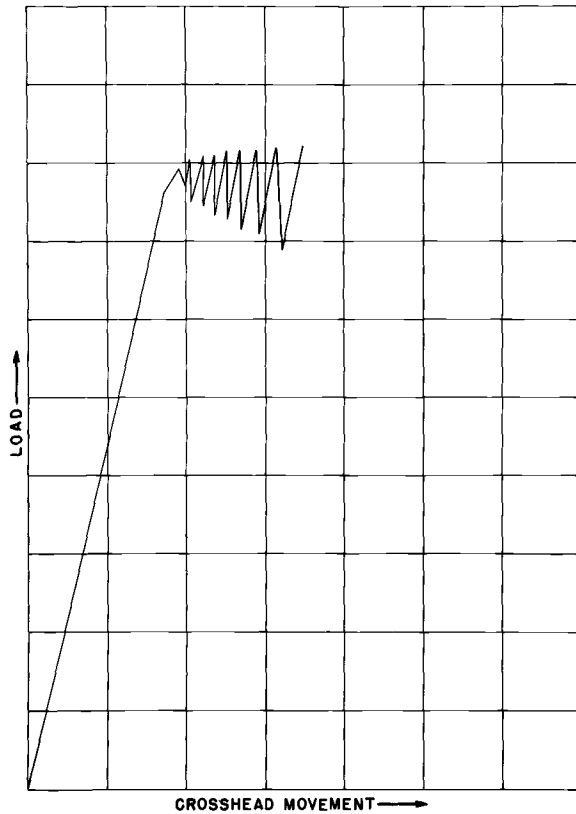


FIG. 9—Load deflection curve for 5Al-2.5Sn ELI titanium alloy tested at -423 F.

commonly accepted ductility parameters, namely, elongation and reduction of area.

No high degree of anisotropy was observed in the ordinary engineering tensile properties as shown by the uniformity of results between the longitudinal and transverse specimens.

The stress-strain curves for these materials when tested at cryogenic temperatures show a serrated type plot (Fig. 9). This behavior has been discussed by Kula and De Sisto [3]. They have shown that these serra-

tions are caused by adiabatic heating and can occur independently of the deformation mechanism. At cryogenic temperatures, thermal softening becomes so large that maximum load is exceeded and discontinuous yielding occurs. During yielding, cooling occurs reducing the thermal softening, and serration ceases.

Plane Strain Fracture Toughness

Of particular interest to the investigator and practical importance to the designer is possible variation of the plane strain fracture toughness with respect to crack orientation. In the thicker plates ($\frac{1}{2}$ and 1 in. thick) it is possible to study the anisotropy of the material with respect to the

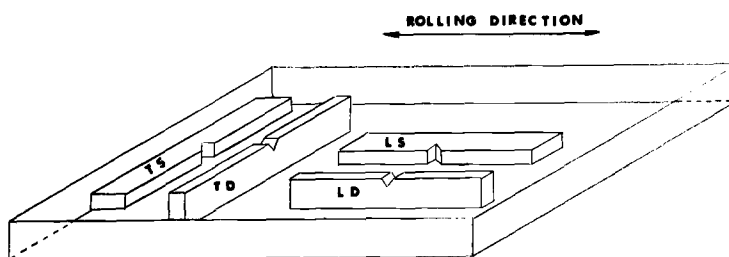


FIG. 10—Orientation of specimens machined from $\frac{1}{2}$ -in. or thicker plate.

TABLE 2— K_{Ic} specimen measuring capacities.

Test Temperature, deg F	Approximate Maximum Valid K_{Ic} Values, psi $\sqrt{\text{in.}}$		
	$\frac{1}{4}$ -in. Specimens	$\frac{1}{2}$ -in. Specimens	1-in. Specimens
+80	30 000	45 000	60 000
-110	40 000	60 000	80 000
-320	50 000	75 000	100 000
-423	60 000	90 000	120 000

plane strain fracture toughness. The orientation of the various specimens is shown in Fig. 10. In this designation the L and T nomenclature give the orientation of the specimen relative to the rolling direction of the plate. In the S series of specimens, the direction of crack propagation is parallel to the rolling plane; in the D series, the specimens are so oriented that the path of crack propagation is perpendicular to the rolling plane.

The plane strain fracture toughness of these specimens was calculated from the load at pop-in and initial crack length using a stress analysis developed by Bueckner [4].

To obtain valid plane strain fracture toughness values, certain minimum specimen dimensions must be met. Brown and Srawley [5] have developed the criterion that the minimum specimen thickness and crack length be equal to $2.5 (K_{Ic}/\sigma_{ys})^2$. This size requirement is of primary importance to obtain valid plane strain fracture toughness data. Using these

TABLE 3—Summary of plane strain fracture toughness values at cryogenic temperatures of 1/4-in.-thick 5Al-2.5Sn ELI grade titanium alloy.

Specimen			Test Temperature, deg F	σ_{ys} , psi	a, in.	P, lb	K_{Ic} , psi $\sqrt{\text{in.}}$
Type	Size, in.	Direction					
Bend bar	1/4 by 1/2	LS	-320	170 500	0.148	820	62 000
Bend bar	1/4 by 1/2	LS	-320	170 500	0.140	855	61 400
Bend bar	1/4 by 1/2	LS	-320	170 500	0.150	830	63 200
Bend bar	1/4 by 1/2	TS	-320	174 500	0.132	800	49 300
Bend bar	1/4 by 1/2	TS	-320	174 500	0.135	815	57 200
Bend bar	1/4 by 1/2	TS	-320	174 500	0.141	800	58 000
SEN	1/4 by 1	LS	-320	170 500	0.349	4240	61 000
SEN	1/4 by 1	LS	-320	170 500	0.349	4490	64 600
SEN	1/4 by 1	LS	-320	170 500	0.358	4355	64 500
SEN	1/4 by 1	LS	-320	170 500	0.367	4420	67 900
SEN	1/4 by 1	TS	-320	174 500	0.372	3935	60 900
SEN	1/4 by 1	TS	-320	174 500	0.371	4220	66 000
SEN	1/4 by 1	TS	-320	174 500	0.400	3400	58 600
SEN	1/4 by 1	TS	-320	174 500	0.342	4560	64 000
Bend bar	1/4 by 1/2	LS	-423	195 000	0.127	863	56 400
Bend bar	1/4 by 1/2	LS	-423	195 000	0.117	775	54 000
Bend bar	1/4 by 1/2	LS	-423	195 000	0.143	702	51 600
Bend bar	1/4 by 1/2	TS	-423	181 000	0.156	621	48 800
Bend bar	1/4 by 1/2	TS	-423	181 000	0.145	660	49 800
Bend bar	1/4 by 1/2	TS	-423	181 000	0.170	490	41 800

TABLE 4—Summary of plane strain fracture toughness values at cryogenic temperatures of 1/2-in.-thick 5Al-2.5Sn ELI grade titanium alloy.

Specimen			Test Temperature, deg F	σ_{ys} , psi	a, in.	P, lb	K_{Ic} , psi $\sqrt{\text{in.}}$
Type	Size, in.	Direction					
Bend bar	1/4 by 1/2	LS	-320	175 000	0.098	1190	67 000
Bend bar	1/4 by 1/2	LS	-320	175 000	0.099	1230	69 800
Bend bar	1/4 by 1/2	LS	-320	175 000	0.099	1070	60 800
Bend bar	1/4 by 1/2	TS	-320	174 500	0.113	860	52 800
Bend bar	1/4 by 1/2	TS	-320	174 500	0.105	790	46 400
Bend bar	1/4 by 1/2	TS	-320	174 500	0.131	750	51 500
Bend bar	1/4 by 1/2	LD	-320	175 000	0.109	910	55 200
Bend bar	1/4 by 1/2	LD	-320	175 000	0.107	980	58 000
Bend bar	1/4 by 1/2	LD	-320	175 000	0.113	910	55 000
Bend bar	1/4 by 1/2	TD	-320	174 500	0.103	950	55 200
Bend bar	1/4 by 1/2	TD	-320	174 500	0.107	995	58 400
Bend bar	1/4 by 1/2	TD	-320	174 500	0.108	930	54 200
Bend bar	1/4 by 1/2	LS	-423	205 500	0.098	912	51 400
Bend bar	1/4 by 1/2	LS	-423	205 500	0.099	1055	59 600
Bend bar	1/4 by 1/2	LS	-423	205 500	0.098	965	54 400
Bend bar	1/4 by 1/2	TS	-423	209 000	0.100	860	48 800
Bend bar	1/4 by 1/2	TS	-423	209 000	0.105	924	54 000
Bend bar	1/4 by 1/2	TS	-423	209 000	0.101	945	54 200
Bend bar	1/4 by 1/2	LD	-423	205 500	0.109	890	53 600
Bend bar	1/4 by 1/2	LD	-423	205 500	0.098	970	54 600
Bend bar	1/4 by 1/2	LD	-423	205 500	0.109	780	47 200
Bend bar	1/4 by 1/2	TD	-423	209 000	0.111	1010	60 000
Bend bar	1/4 by 1/2	TD	-423	209 000	0.103	1115	63 600
Bend bar	1/4 by 1/2	TD	-423	209 000	0.109	985	59 200

criteria, Table 2 gives the K_{Ic} measuring capacity for the various plate thicknesses investigated.

Based on these calculations, it may be concluded that those values of plane strain fracture toughness determined at -320 and -423 F are valid measurements. These values are summarized in Tables 3, 4, 5, and 6. They show that the higher nitrogen and iron contents of the commercial 5Al-2.5Sn titanium alloy result in a significant loss of plane strain fracture toughness at the lower temperatures. The use of another speci-

TABLE 5—Summary of plane strain fracture toughness values at cryogenic temperatures of 1-in.-thick 5Al-2.5Sn ELI grade titanium alloy.

Specimen			Test Temperature, deg F	σ_{ys} , psi	a , in.	P , lb	K_{Ic} , psi $\sqrt{\text{in.}}$
Type	Size, in.	Direction					
Bend bar	$\frac{1}{2}$ by 1	LS	-320	176 000	0.336	3790	56 900
Bend bar	$\frac{1}{2}$ by 1	LS	-320	176 000	0.339	3470	52 100
Bend bar	$\frac{1}{2}$ by 1	LS	-320	176 000	0.335	3175	46 400
Bend bar	$\frac{1}{2}$ by 1	TS	-320	176 000	0.321	3230	46 000
Bend bar	$\frac{1}{2}$ by 1	TS	-320	176 000	0.337	3425	50 700
Bend bar	$\frac{1}{2}$ by 1	LD	-320	176 000	0.344	4200	59 500
Bend bar	$\frac{1}{2}$ by 1	LD	-320	176 000	0.332	4470	61 300
Bend bar	$\frac{1}{2}$ by 1	LD	-320	176 000	0.337	3775	53 000
Bend bar	$\frac{1}{2}$ by 1	TD	-320	176 000	0.327	4720	64 200
Bend bar	$\frac{1}{2}$ by 1	TD	-320	176 000	0.325	5500	74 600
Bend bar	$\frac{1}{2}$ by 1	TD	-320	176 000	0.335	4350	60 400
Bend bar	$\frac{1}{2}$ by 1	LS	-423	203 000	0.333	3010	45 000
Bend bar	$\frac{1}{2}$ by 1	LS	-423	203 000	0.330	4370	63 700
Bend bar	$\frac{1}{2}$ by 1	LS	-423	203 000	0.320	4020	57 000
Bend bar	$\frac{1}{2}$ by 1	TS	-423	203 000	0.330	3225	46 700
Bend bar	$\frac{1}{2}$ by 1	TS	-423	203 000	0.321	3900	55 500
Bend bar	$\frac{1}{2}$ by 1	TS	-423	203 000	0.325	3850	55 200
Bend bar	$\frac{1}{2}$ by 1	TS	-423	203 000	0.322	3860	55 300
Bend bar	$\frac{1}{2}$ by 1	LD	-423	203 000	0.330	3540	46 000
Bend bar	$\frac{1}{2}$ by 1	LD	-423	203 000	0.336	4050	55 600
Bend bar	$\frac{1}{2}$ by 1	TD	-423	203 000	0.337	4425	61 000
Bend bar	$\frac{1}{2}$ by 1	TD	-423	203 000	0.326	5650	76 300
Bend bar	$\frac{1}{2}$ by 1	TD	-423	203 000	0.324	4760	64 200

men geometry to measure the plane strain fracture toughness would supply supporting data. Small single-edge notch specimens (Fig. 11) were machined from the $\frac{1}{4}$ -in. plate in the LS and TS directions. These specimens were precracked in fatigue, instrumented with strain gages to detect the pop-in load, and tested in tension at -320 F. Comparison of the data obtained (Table 3) shows that essentially the same values of plane strain fracture toughness were obtained using both specimens.

Texture Hardening

The textures of rolled sheets of hexagonal close packed (HCP) materials cause high yield strengths under biaxial tension, thus making some

of these materials especially suitable for pressure vessels. Under combined stress loading, anisotropic continuum theory of yielding and plastic flow predict striking deviations from the von Mises criterion. In particular, the resistance of a sheet to thinning under stresses in its plane has much influence on the form of the two-dimensional yield locus as discussed by Hosford and Backofen [6].

One simple measure of the thinning resistance of sheet metal is the ratio, R , of the width to thickness strain found in the tension test on a strip. In an isotropic material, the width and thickness strains are equal,

TABLE 6—Summary of plane strain fracture toughness values at cryogenic temperatures of 1/2-in.-thick 5Al-2.5Sn commercial grade titanium alloy.

Specimen			Test Temperature, deg F	σ_{ys} , psi	a , in.	P , lb	K_{Ic} , psi $\sqrt{\text{in.}}$
Type	Size, in.	Direction					
Bend bar	1/4 by 1/2	LS	-320	203 000	0.115	480	30 200
Bend bar	1/4 by 1/2	LS	-320	203 000	0.117	410	26 000
Bend bar	1/4 by 1/2	LS	-320	203 000	0.115	360	22 700
Bend bar	1/4 by 1/2	TS	-320	204 000	0.108	970	58 400
Bend bar	1/4 by 1/2	TS	-320	204 000	0.114	735	45 900
Bend bar	1/4 by 1/2	LD	-320	203 000	0.110	670	40 900
Bend bar	1/4 by 1/2	LD	-320	203 000	0.110	650	39 700
Bend bar	1/4 by 1/2	LD	-320	203 000	0.115	390	24 500
Bend bar	1/4 by 1/2	TD	-320	204 000	0.113	408	25 300
Bend bar	1/4 by 1/2	TD	-320	204 000	0.108	455	27 400
Bend bar	1/4 by 1/2	TD	-320	204 000	0.114	358	22 400
Bend bar	1/2 by 1/2	LS	-423	233 000	0.108	325	19 600
Bend bar	1/4 by 1/2	LS	-423	233 000	0.108	445	26 800
Bend bar	1/4 by 1/2	LS	-423	233 000	0.111	445	27 400
Bend bar	1/4 by 1/2	TS	-423	237 000	0.115	845	53 100
Bend bar	1/4 by 1/2	TS	-423	237 000	0.107	460	27 500
Bend bar	1/4 by 1/2	LD	-423	233 000	0.119	750	48 000
Bend bar	1/4 by 1/2	LD	-423	233 000	0.110	520	31 700
Bend bar	1/4 by 1/2	LD	-423	233 000	0.109	321	19 400
Bend bar	1/4 by 1/2	TD	-423	237 000	0.117	345	21 900
Bend bar	1/4 by 1/2	TD	-423	237 000	0.103	400	23 300
Bend bar	1/4 by 1/2	TD	-423	237 000	0.107	355	21 200

so $R = 1$. A particular straightforward example is a balanced biaxial tension in the plane of a sheet. Such a stress system is equivalent to a uniaxial through-thickness compression plus a hydrostatic tension. Therefore, yielding under the balanced tension can occur only when the tensile stresses reach a value equal to the compressive yield strength in the through-thickness direction.

In an isotropic material, the tensile and compressive yield strengths are identical so that yielding under the balanced tension begins when the uniaxial yield strength is reached. For anisotropic materials, however, the uniaxial tensile and through-thickness compressive strength may differ considerably. In (0001) textured sheets of HCP metals, for ex-

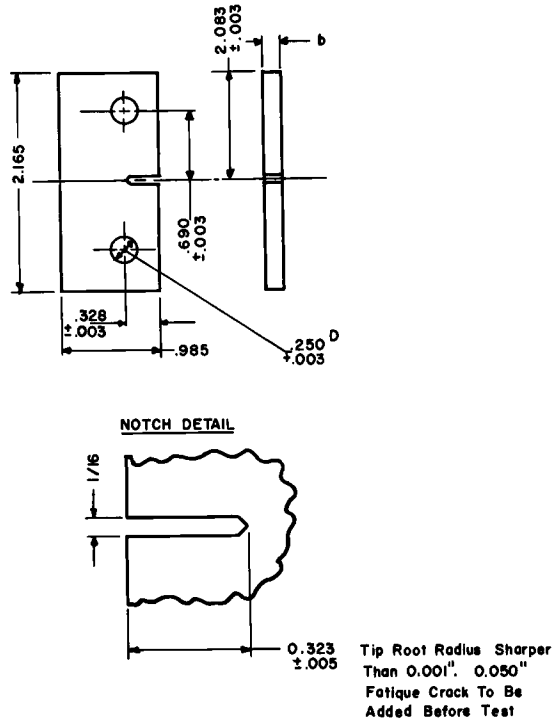


FIG. 11—Small single-edged notched specimen.

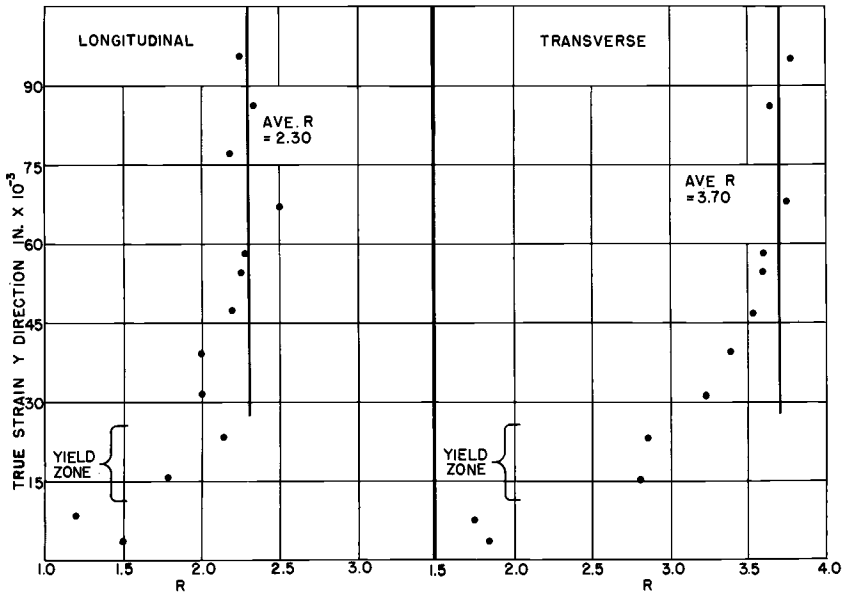


FIG. 12—*R*-value versus true strain in *y* direction for 1/4-in.-thick 5Al-2.5Sn ELI titanium alloy plate.

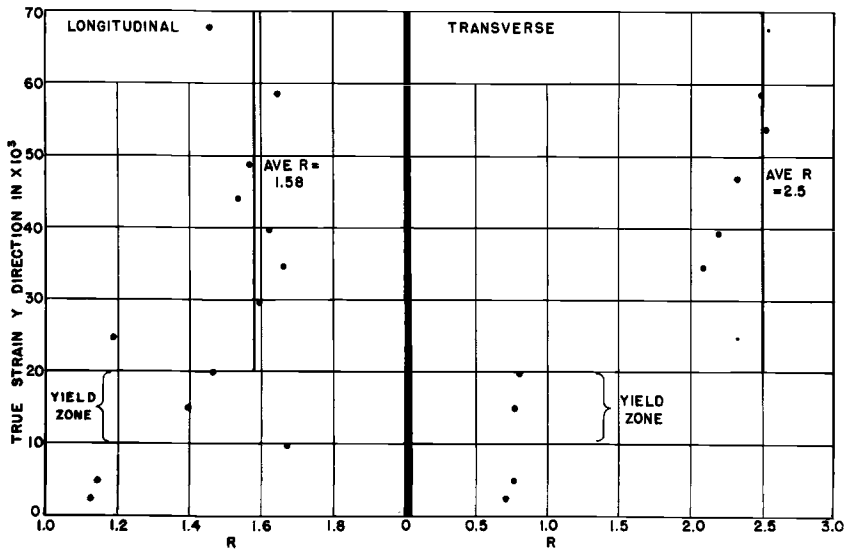


FIG. 13.—*R*-value versus true strain in *y* direction for 1/2-in.-thick 5Al-2.5Sn ELL titanium alloy plate.

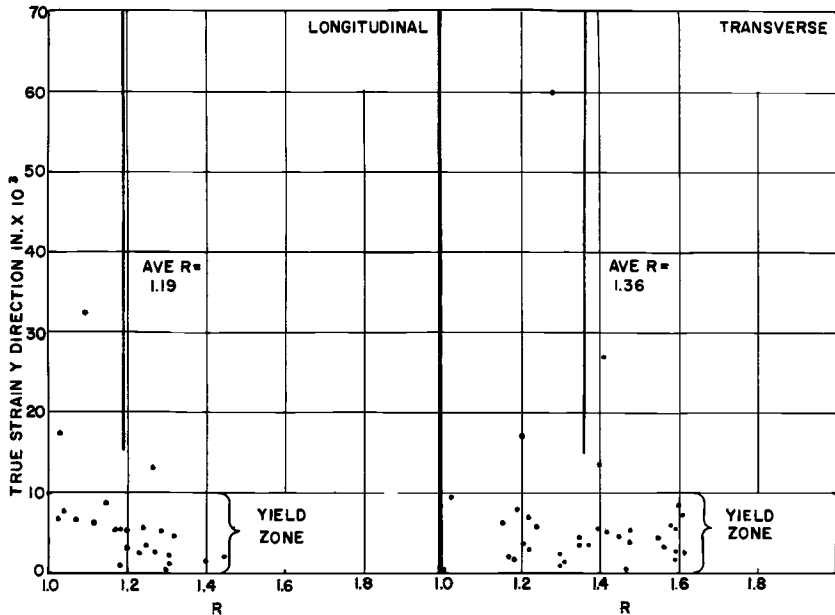


FIG. 14.—*R*-value versus true strain in *y* direction for 1-in.-thick 5Al-2.5Sn ELL titanium alloy plate.

ample, the lack of slip systems suitably oriented to allow thinning may be responsible for high compressive yield strengths in the through-thickness direction and a combined strengthening that may be identified as “texture hardening.”

As discussed previously, measurement of the R value of the material is a good indication of the degree of texture hardening. Since R is defined as the ratio of the width-to-thickness strains, then a strip type tension specimen provides a simple and convenient method of determining R . In the example of thin sheets, it is possible to measure the strains in the x and y directions and compute the z strain using the constancy of volume relationship. However, measurement of the strains in the x , y , and z directions, using plate specimens, permits direct determination of the R value. The latter method was used here.

Since it is desired to measure an average value of R for the 5Al-2.5Sn ELI titanium alloy, full thickness strip type tension specimens were machined from the plates. High elongation metafilm strain gages were applied to the specimen in the x , y , and z directions of the specimen. Strain gage readings were taken at regular load increments, using a digital read-out strain indicator. Readings were taken up to at least 10 per cent strain in the y direction.

The texture hardening effect is developed only in the plastic range. In order to conform to the constancy of volume requirements for plastic flow, it is necessary to convert the engineering strains to true strains. The relationship used is

$$\epsilon = \ln (e + 1) \dots \dots \dots (1)$$

The R values were determined by dividing the width strain by the thickness strain.

The R values so determined are plotted as a function of the true strain in the y direction for the three ELI plates in Figs 12, 13, and 14. It will be observed that the R value is relatively low in the elastic range. At the yield point of the material, the R value is indeterminate. This is presumably due to the gradual change in Poisson's ratio from 0.30 to 0.50 for plastic deformation. However, once the yield point has been exceeded, the R value rises to a maximum value and remains constant with increasing strain. Basically, the R versus ϵ relation expresses the difference between elastic anisotropy and plastic anisotropy for the materials. The elastic anisotropy has to do with the variation of the elastic constants, while the plastic anisotropy has to do with the shear strengths of the operative slip system and their work hardening behavior. The magnitude of the anisotropy exhibited is also dependent, of course, on the intensity of the texture.

The highest R values were found for the 1/4-in.-thick plate followed by the 1/2-in.-thick plate and the 1-in.-thick plate. This would be anticipated since the higher percentage of hot work in the thinnest plate would offer more opportunity for preferred orientation. It should also be noted that the transverse results were higher than the longitudinal results.

Design Considerations

Of the many considerations to which the designer must devote attention, those discussed in this paper are: (a) yield stress, (b) plane strain fracture toughness, and (c) texture hardening. These topics will be reviewed in that order.

The data for the yield stress at the various test temperatures are self-explanatory.

The plane strain fracture toughness may be used to calculate the size and geometry of defects which will become unstable under a given stress. Irwin [7] has defined a parameter, β , as

$$\beta = \frac{K^2}{B\sigma_{ys}^2} \dots\dots\dots (2)$$

It has been shown that $\beta_c = 2\pi$ or its equivalent $\beta_{Ic} = 1.5$ will cause arrest of a $2t$ crack. If one assumes a K_{Ic} value of 120,000 psi $\sqrt{\text{in.}}$ for the 5Al-2.5Sn ELI titanium alloy at room temperature [8], then the maximum β_{Ic} are given in Table 7.

TABLE 7—Maximum β_{Ic} values for 5Al-2.5Sn ELI titanium alloy.

Test Temperature, deg F	Maximum β_{Ic}
70.....	5.6
-320.....	0.532
-423.....	0.254

These calculations show that the fracture toughness of this material is sufficiently great so that at room temperature a $2t$ crack will be arrested. However, at -320 and -423 F, “part-through” plane strain defects may become unstable and cause failure.

The geometry of the part-through defect and the gross section stress required to produce failure have been related by Irwin [9] in the following equation

$$K_I = 1.1 \sigma \left(\frac{\pi a}{Q} \right)^{1/2} \dots\dots\dots (3)$$

In Fig. 15, the crack depth for instability is plotted as a function of gross section stress for a crack having a surface length two times its depth (semicircular) using this equation. The range of K_{Ic} values shown here was obtained from this investigation. Examination of the curves for the different yield strengths, which result from the various operating temperatures, shows that the stress for instability at a given flaw size varies by only 5 per cent.

This type of plot may be used to establish inspection standards or limit the design stress to account for the minimum size of defect which can be

found by nondestructive testing. An example of the use of this figure as an engineering design tool follows.

If a structure were to be fabricated from the $\frac{1}{2}$ -in.-thick 5Al-2.5Sn ELI titanium alloy used in this investigation for service at -340 F, the K_{Ic} in the direction of interest would be determined from the appropriate chart (for example, TS, $K_{Ic} = 50,000$ psi $\sqrt{\text{in.}}$). If the service stress were approximately 127,000 psi (tensile strength/1.4) then the maximum allowable flaw size (as seen from Fig. 15) would be 0.093 in. If the structure were fabricated from the $\frac{1}{4}$ -in.-thick material to be used at -423 F and

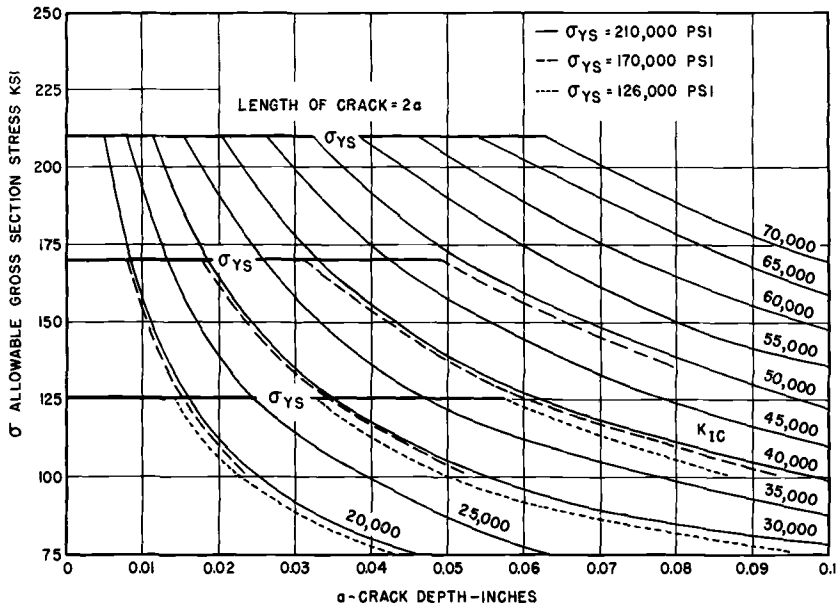


FIG. 15—Variation of critical crack depth for instability as a function of applied stress for several K_{Ic} -values.

the direction of interest was transverse to the original direction of rolling, the K_{Ic} would be 48,000 psi $\sqrt{\text{in.}}$ If the minimum crack depth which could be reliably detected by nondestructive means were 0.040 in., the a in Fig. 15 would be 0.040 in., and the maximum allowable stress which the structure could be used would be approximately 190,000 psi.

It is at the lower testing temperatures that the superiority of the extra low interstitial material becomes evident. The commercial grade of 5Al-2.5Sn titanium alloy exhibits an average value of K_{Ic} of 30,000 psi $\sqrt{\text{in.}}$ Assuming a service stress of 127,000 psi, then the maximum allowable defect which could be tolerated (as seen from Fig. 15) would be 0.033 in. as compared with 0.093 in. for the ELI grade.

Texture hardening may be used to obtain elevated yield strengths in

pressure vessel applications. The biaxial yield strength for a cylindrical pressure vessel may be calculated from Eq 4.

$$\sigma = \sigma_{ys} \left[\frac{4(R + 1)}{5 + R} \right]^{1/2} \dots \dots \dots (4)$$

Using the *R* value for the 1/4-in.-thick longitudinal specimen of 5Al-2.5Sn ELI titanium alloy, the elevation of the biaxial yield stress was calculated to be 33 per cent.

Having established a theoretical basis for the biaxial strengthening of textured metals, it would be desirable to obtain experimental verification of this strengthening effect. Data for small cylindrical pressure vessels made from 5Al-2.5Sn titanium alloy reported by Babel et al [10] support this analysis. The alloy used for their study exhibited an *R* value of 2.56. Using Eq 4, an elevation of the biaxial yield strength of 1.37 was predicted. The experimental data showed an elevation of the biaxial yield strength of 1.25. The experimental data also show an elevation of the cylindrical ultimate strength over uniaxial tensile strength of 1.53. The experimental and predicted biaxial yield strengths are in good agreement.

Conclusions

It may be concluded that:

1. The tensile properties of 5Al-2.5Sn titanium alloy are sensitive to testing temperature. The tensile yield strength varies from 100,000 psi at room temperature to approximately 200,000 psi at -423 F.
2. The plane strain fracture toughness of the 5Al-2.5Sn ELI titanium alloy is considerably greater than that of the commercial grade. These differences are more pronounced at the lower testing temperatures.
3. The 5Al-2.5Sn ELI titanium alloy exhibits essentially an isotropic behavior in regard to plane strain fracture toughness.
4. The plane strain fracture toughness of this material does not appear to be affected by the amount of reduction in the plate. The *K_{Ic}* values for the 1/4, 1/2, and 1-in.-thick plates are essentially the same at the cryogenic temperatures when reliable data could be obtained.
5. The 1/4-in.-thick plate exhibits higher *R* values than the 1/2 and 1-in.-thick plate and, consequently, a greater potential for elevation of the biaxial yield strength.

Acknowledgment

The authors wish to acknowledge the support of the Lewis Research Center of the National Aeronautics and Space Administration. This work was conducted under NASA Purchase Order C-6860A with G. T. Smith and R. Johnson serving as project engineers. The complete details of the

ELI titanium investigation are given in NASA Contractor's Report (CR) 54296.

References

- [1] Espy, C. B., Jones, M. H., and Brown, W. F., Jr., "Factors Influencing Fracture Toughness of Sheet Alloys for Use in Lightweight Cryogenic Tankage," *Evaluation of Metallic Materials in Design for Low Temperature Service, ASTM STP 302*, American Society for Testing and Materials, 1961.
- [2] Boyle, R. W., Sullivan, A. M., and Krafft, J. M., "Determination of Plane Strain Fracture Toughness with Sharply Notched Sheets," *Welding Journal*, Vol. 41, No. 9, Research Supplement, 1962, pp. 428-s-432-s.
- [3] Kula, E. and De Sisto, T., "Plastic Behavior of Metals at Cryogenic Temperatures," *Behavior of Metals at Cryogenic Temperatures, ASTM STP 387*, American Society for Testing and Materials, 1966.
- [4] Bueckner, H. F., internal reports of the General Electric Co., Schenectady, N.Y.
- [5] Brown, W. F., Jr., and Srawley, J. E., "Current Status of Plane Strain Crack Toughness Testing," NASA Technical Memorandum TMX-52209, National Aeronautics and Space Administration.
- [6] Hosford, W. F., Jr., and Backofen, W. A., "Strength and Plasticity of Textured Metals," *Fundamentals of Deformation Processings*, Proceedings of Ninth Sagamore Conference, Syracuse University Press, Syracuse, N.Y., 1964.
- [7] Irwin, G. R., "Relation of Crack Toughness to Practical Applications, Welding Journal Research Supplement, Nov. 1962.
- [8] Tiffany, C. F., Lorenz, P. M., and Hall, L. R., "Investigation of Plane Strain Flaw Growth in Thick Walled Tanks," NASA CR-54837, National Aeronautics and Space Administration.
- [9] Irwin, G. R., "Crack Extension for a Part-Through Crack in a Plate," *Journal of Applied Mechanics*, Vol. 29, *Transactions*, American Society of Mechanical Engineers, Vol. 84, Series E, 1962.
- [10] Babel, H. W., Eitman, D. A., and McLives, R. W., "The Biaxial Strengthening of Textured Titanium," ASME Paper 66-Met-6, American Society of Mechanical Engineers.

Fracture Toughness in Aqueous Saline Environments

Metallurgical and Mechanical Aspects of the Sea-Water Stress Corrosion of Titanium*

REFERENCE: Lane, I. R. and Cavallaro, J. L., "Metallurgical and Mechanical Aspects of the Sea-Water Stress Corrosion of Titanium," *Applications Related Phenomena in Titanium Alloys*, ASTM STP 432, American Society for Testing and Materials, 1968, pp. 147-169.

ABSTRACT: Results of concentrated investigations on the sea-water stress corrosion of titanium indicate that the behavior is dependent on certain mechanical factors and on the metallurgical structure. The mechanical factors include a requirement that localized plastic deformation induce the formation of a coarse slip step. A possible further requirement is that the slip step occurs under crevice conditions. Recent work on the titanium-aluminum system, including kinetics of reactions occurring in the system, add to the evidence that stress corrosion is associated with the presence of the coherent Ti₃Al precipitate. The most effective method for control of stress corrosion in titanium alloys containing aluminum is inhibition of the formation of Ti₃Al by control of composition and heat treatment.

KEY WORDS: titanium alloys, stress corrosion, embrittlement

In late 1964 it was discovered that under certain conditions some titanium alloys were susceptible to an apparent stress corrosion effect in sea water [1].² This discovery was found in the laboratory before in-service failures had occurred. The opposite situation has generally prevailed for other structural materials. In-service failures usually are the basis for laboratory investigations which involve development of suitable testing procedures for a study to find the cause and cure. The absence of in-service failures raised the still unanswered question as to the extent to which the conditions involved in the laboratory test would be encountered

* The opinions or assertions made in this paper are those of the authors and are not to be construed as official or reflecting the views of the Department of the Navy or the naval service at large.

¹ Physical metallurgists, Naval Alloys Div., Marine Engineering Laboratory, Annapolis Div., Naval Ship Research and Development Center, Annapolis, Md.

² The italic numbers in brackets refer to the list of references appended to this paper.

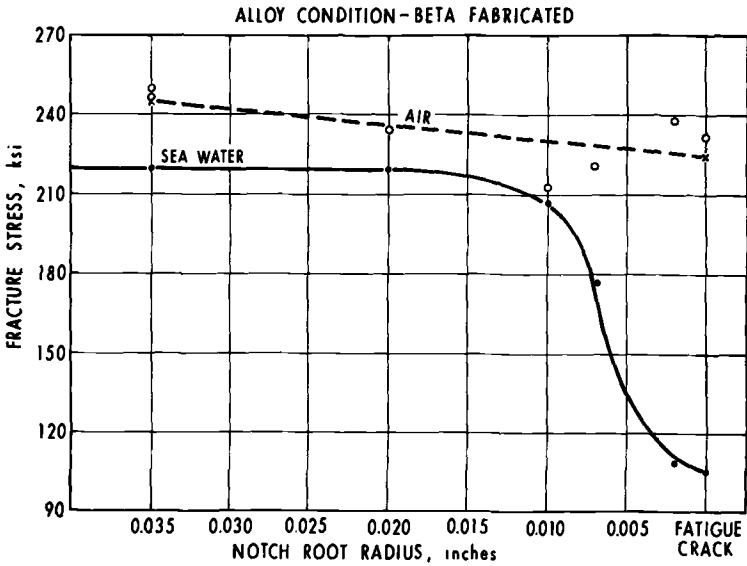


FIG. 2—Effect of notch acuity on nominal breaking stress.

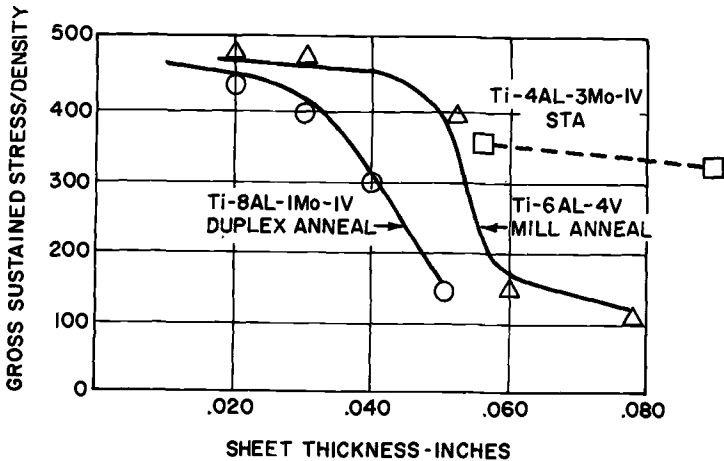


FIG. 3—Effect of sheet thickness on stress corrosion.

thermal history. It was therefore concluded that sea-water stress corrosion in titanium can be eliminated or reduced by compositional control and careful attention to thermal treatment.

The purpose of this paper is to survey the information that has been developed on the sea-water stress corrosion of titanium. Particular emphasis is given to the physical metallurgy aspects of the problem because experimental evidence has shown that the underlying factors that lead to stress corrosion in titanium are structure dependent. The logical approach

to complete elimination of the effect is control of the structure to eliminate the embrittling constituents.

Mechanical Factors

A necessary requirement for environment-sensitive behavior in laboratory sea-water stress corrosion tests on titanium is the presence of a stress concentration in the specimen. This stress concentration is in the form of a sharp notch usually a fatigue crack. Tests can be conducted to generate curves similar to the one shown in Fig. 1. There is a threshold stress below which stress corrosion action will not take place, even if the specimen is held under stress for long periods. This threshold nominal bending stress is dependent on mechanical factors (notch acuity and specimen configuration) and on the material characteristics (stress corrosion sensitivity as the result of composition and heat treatment).

The results of MEL studies on the effect of notch on stress corrosion of one heat of a Ti-7Al-2Cb-1Ta (Ti-721) alloy are shown in Fig. 2. Notch acuities ranging from a 0.035 in. root radius to a fatigue crack had essentially no effect on the nominal breaking stress of the alloy specimens in air. However, a transition from "insensitive" to "sensitive" behavior in sea water occurred at about a 0.010 in. root radius and reached a minimum nominal bend stress to fracture at about a 0.002 in. radius. There was essentially no difference in nominal breaking stress between the 0.002-in. root radius notch and the fatigue crack. There has been found to be a difference for alloys less sensitive to sea-water stress corrosion, and it is suspected that the transition is shifted to the right for these less sensitive alloys.

A dependency on specimen thickness for stress corrosion sensitivity has been shown by Wald [3] and Feige and Murphy [4]. Typical curves are shown in Fig. 3. Transition from insensitive to sensitive stress corrosion behavior is displayed by Ti-6Al-4V and Ti-8Al-1Mo-1V alloys with increasing thickness. This difference in behavior is attributed to plane strain conditions that develop as the result of increasing thickness.

These data indicate that the necessary mechanical requirement for sea-water stress corrosion in titanium is that the plastic zone at the base of the notch, in contact with the corrosive environment, undergoes a certain degree of plastic deformation.

From a mechanical standpoint it may be possible to circumvent stress corrosion failure in titanium alloys through design control. One approach would be to ensure that there are no tensile stresses developed at or above the threshold stress level for the "susceptible" alloys. This would permit the presence of stress concentrations, including defects. The other approach would be to eliminate stress concentrations. This would also preclude existence of "stress concentration" defects or development of such defects.

Theoretical Aspects

The corrosion resistance of titanium in seawater is unsurpassed by any other structural metal. Although titanium is a very reactive metal, it has excellent corrosion resistance due to the presence of a passive film on its surface. The film is extremely difficult to break, and if broken by mechanical action, such as abrasion, repair in sea water is so rapid that corrosive action does not take place. Sea-water stress corrosion therefore must involve a breakdown of the passive film plus some condition that prevents repair of the film.

A corrosion crack must first initiate then propagate through the structure of the metal. Three mechanistic aspects of interest are:

1. How the action initiates.
2. How it propagates.
3. Identification of the element in the environment that reacts with titanium to initiate and propagate stress corrosion cracks.

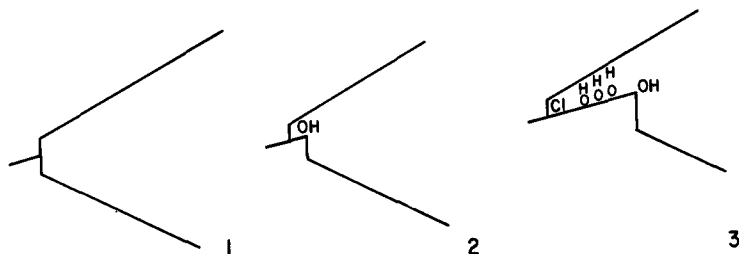


FIG. 4—Proposed stress corrosion initiation mechanism.

MEL and others who have investigated sea-water stress corrosion in titanium have found that not all titanium alloys are susceptible to stress corrosion but that the action is dependent on the presence of an embrittling constituent in the structure, such as the coherent Ti_3Al precipitate. Sanderson and Scully [5] have observed that in those titanium alloys susceptible to stress corrosion, dislocations form long coplanar arrays, whereas in nonsusceptible pure titanium dislocations are formed in tangled arrays. The long coplanar arrays are favorable for producing a wide slip step which could rupture the passive film.

Scully's proposed mechanism for initiation of stress corrosion cracking [6] in stainless steel may be applicable to titanium. Figure 4 illustrates how corrosive action could initiate in a susceptible alloy according to this proposed mechanism. A coarse slip step emerging, 1, at the stress concentration reacts preferentially with OH^- ions to passivate the surface, 2. The long slip step exhausts the supply of OH^- ions in the liquid which is in contact with the surface. The last part of the slip step, 3, reacts with the available Cl^- ions and initiates the stress corrosion process. The attack at the root of a stress concentration may be influenced by the

“crevice” conditions of the notch. That is, the supply of passivating ions might be used up faster than they can be replenished by diffusion into the close quarters of the crevice.

An alternate argument can also be made that the emerging slip step reacts with the aqueous environment to decompose the water to OH^- and H^+ and the hydrogen then reacts with titanium to induce premature failure. However, experimental evidence tends to discount a hydrogen mechanism.

Stress corrosion cracking, once initiated, may possibly proceed through the structure by dissolution, dissolution plus mechanical fracture, adsorption, or adsorption plus mechanical fracture.

The following significant observations have been made by various investigators in stress corrosion of titanium in sea water:

1. Crack propagation is rapid and generally transgranular [7].
2. Failure is by brittle fracture mode with the fracture surface displaying striated quasi-cleavage facets [8,9].
3. There is no apparent pitting, etching, or development of corrosion products.
4. The stress corrosion process can be suppressed by cathodic protection [11].
5. Inhibitors such as silver nitrate, potassium nitrate, and sodium sulfate are effective in suppressing stress corrosion [12] if the chloride ion concentration is low.
6. No sound emission has been detected during the stress corrosion process although it is possible that emissions are of such a low level that special techniques are necessary for their detection [11].

The crack growth rate during sea-water stress corrosion cracking of titanium has been measured at 0.17 in./min (25 cm/hr) [7]. This fast rate appears to rule out dissolution as the sole mechanism³, even though cathodic protection is an effective suppressor. Cathodic protection has been reported to be effective in other metal systems where the mechanism was determined to be other than dissolution. One example of this is alpha brass in oxygenated aqueous ammonia containing large concentrations of the cupric complex ion $\text{Cu}(\text{NH}_3)_5^{+2}$ [12].

It seems possible that all of the observations on titanium stress corrosion characteristics could be satisfied by a “film rupture-adsorption dependent mechanism” similar to that proposed by Westwood [14] and Westwood and Kamdar [15] for liquid metal embrittlement and for the embrittlement of silver chloride in aqueous environments [16]. Westwood suggests that the embrittlement is caused by the adsorption and interaction of specific species with strained bonds, causing a localized reduction in cohesive strength and hence allowing rupture at reduced stress levels.

³ Unpublished work by E. N. Pugh, Research Institute for Advanced Studies.

Sea-water stress corrosion of titanium could involve the adsorption of the Cl^- ion which causes a reduction in cohesive strength. The proposed mechanism of initiation discussed previously and which involved the action of the Cl^- ion fits very well with this hypothesis. Titanium alloys which are susceptible to stress corrosion in sea water have also been shown to be susceptible to stress corrosion in distilled water [1,2]. Beck [12] believes that residual Cl^- ion concentration present in titanium may be leached out by distilled water and become active in the stress corrosion process. He has also noted slight increases in crack ve-

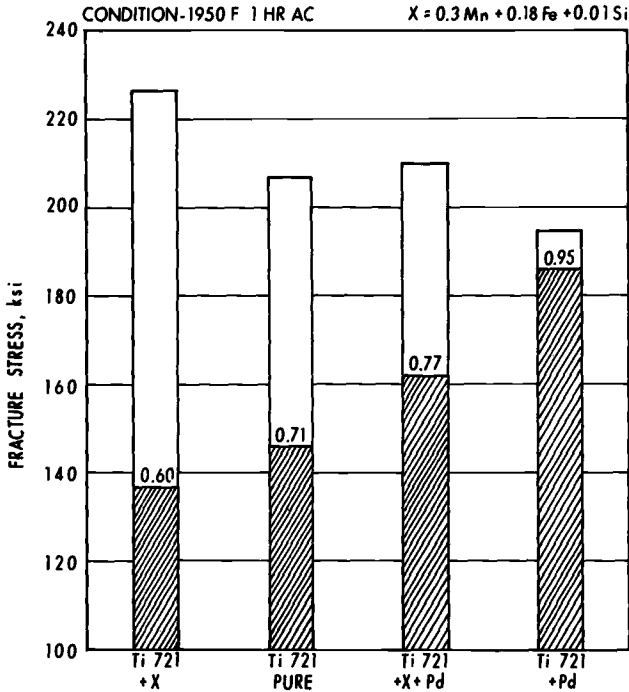


FIG. 5—Effect of palladium on stress corrosion of Ti-721.

locity with additions of sodium chloride to the water. It is possible that the concentration of Cl^- ions, within some concentration limit, may effect the extent to which the cohesive strength of the material is lowered.

It appears from the information developed up to this time that a film-rupture adsorption-dependent mechanism could be responsible for stress corrosion of titanium in sea water and that it is very likely that the Cl^- ion is the adsorbing species. The work now being conducted toward understanding the mechanism should confirm or refute this proposed mechanism within a few years.

From a mechanistic standpoint, several routes could be taken to inhibit sea-water stress corrosion in titanium alloys. These include cathodic

protection, addition of an inhibitor to the environment, or addition of an inhibitor or passivator as an alloying element to the metal. In some applications any one of these might be feasible. However, for most applications the only practical approach would be addition of an inhibitor as an alloying element.

MEL investigated the use of palladium as an inhibitor for the stress corrosion sensitive Ti-721 alloy. Figure 5 shows the effect of 0.075 weight per cent palladium on the stress corrosion properties of relatively pure Ti-721 and on Ti-721 containing small percentages of iron and manganese as impurities. These data show that palladium enhances the

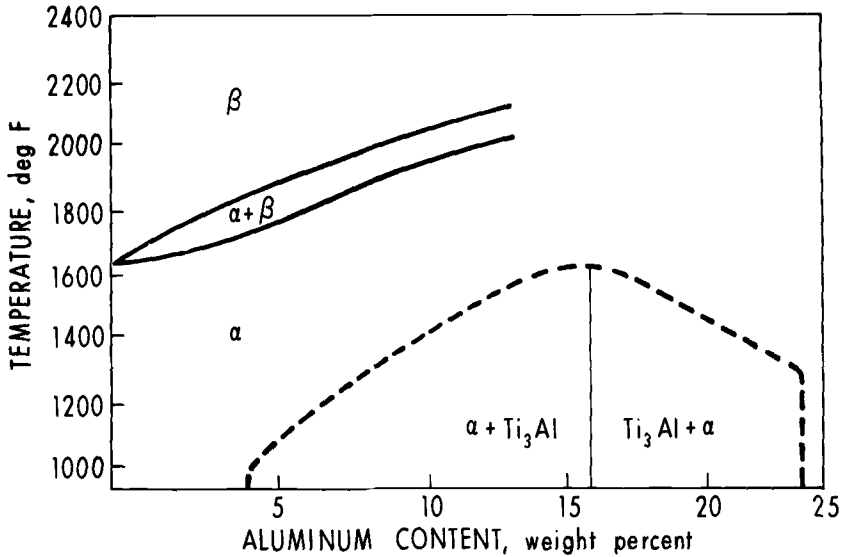


FIG. 6—Titanium-aluminum equilibrium diagram by Crossley.

corrosion resistance of the Ti-721 alloy. However, iron and manganese serve to make palladium less effective possibly by reducing the solubility of palladium in the alloy. Palladium has very little solubility in alpha titanium, and lower temperature anneals would probably result in the precipitation of palladium, and thus its effectiveness as a corrosion inhibitor would be decreased. It is believed that palladium must be in solid solution in titanium to be an effective stress corrosion inhibitor.

Metallurgical Aspects

As mentioned previously, the most significant factors influencing stress corrosion in titanium are those related to structure. The logical means of controlling stress corrosion in titanium is control of the structure to eliminate the embrittling constituents that cause stress corrosion.

Titanium-Aluminum Alloys

The data developed by MEL and other investigators strengthen the conviction that there is a relationship between formation of the embrittling Ti_3Al phase and stress corrosion susceptibility. Although there are other embrittlors, the practical importance of the aluminum-containing alloys for structural applications emphasizes the urgency of understanding the titanium-aluminum influence on stress corrosion. MEL has therefore concentrated on correlating the metallurgical variables in the titanium-aluminum system with sea-water stress corrosion.

The titanium-aluminum system is the most important alloy system in

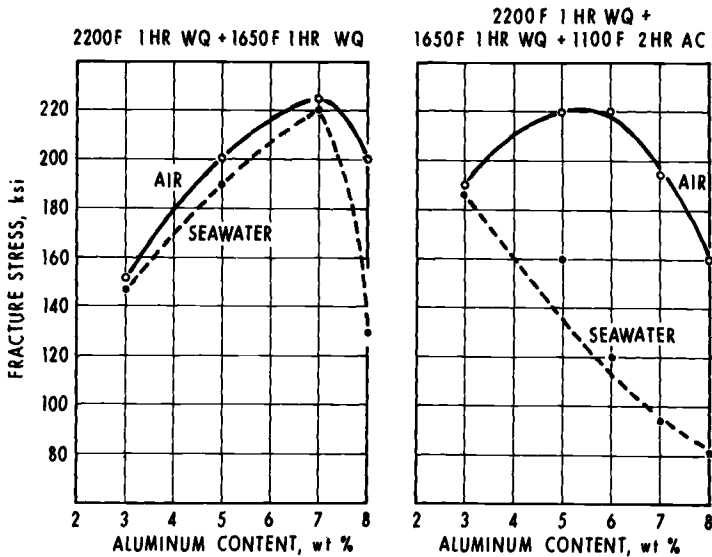


FIG. 7—(left) stress corrosion of quenched Ti-Al alloys and (right) stress corrosion of aged Ti-Al alloys.

the metallurgy of titanium. MEL sponsored a research contract with IIT Research Institute (IITRI) to attempt to resolve the controversies as to the location of the phase boundaries in the titanium-aluminum system. A new diagram, Fig. 6, was developed by Frank Crossley [17]. Two significant points concerning this diagram are:

1. The region of the embrittling phase, Ti_3Al , extends further into the titanium-rich end of the diagram than previous investigators have shown.
2. Crossley found that the partitioning of aluminum which occurs in the alpha plus beta field due to thermal history within this region is extremely difficult to erase by subsequent thermal treatment at lower temperatures.

Another important finding of Crossley was the evidence that the embrittler is a coherent Ti_3Al precipitate rather than an ordered struc-

ture. This point is still not definitely settled, but the evidence for a coherent Ti_3Al precipitate is convincing. This is based on indications that long term aging in the alpha plus Ti_3Al field results in loss of coherence. Both the coherent precipitate and an ordered structure act in the same manner, that is, they produce lattice strains in the structure which lead to the formation of coarse slip steps when the metal is deformed.

MEL has sponsored additional work at IITRI to investigate the effect of ternary additions on the titanium-aluminum system [18]. It has been found that ternary additions affect the extent of the alpha plus Ti_3Al field, the kinetics of reactions involving the formation of Ti_3Al , and possibly the magnitude of the Ti_3Al coherence strains.

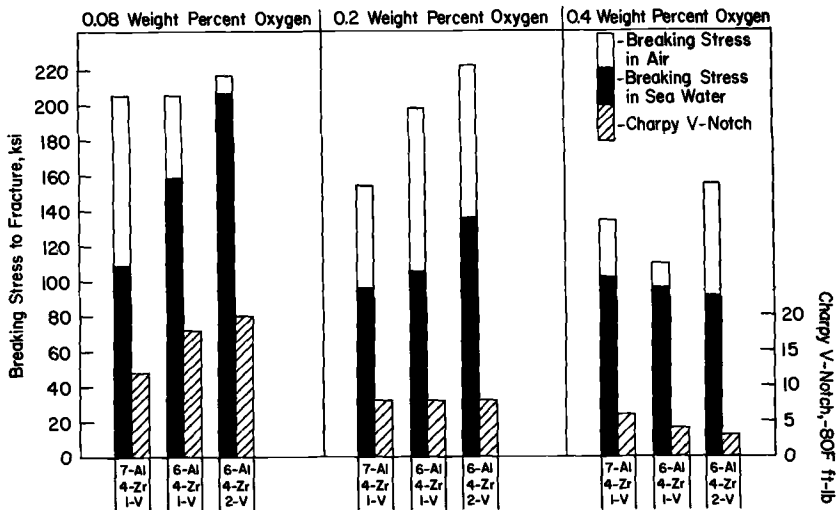


FIG. 8—Effect of aluminum and vanadium on stress corrosion of Ti-Al-Zr-V alloys.

Compositional Effects—MEL has conducted investigations on a number of titanium alloy compositions to correlate stress corrosion results with metallurgical variables in the titanium-aluminum system.

A series of binary titanium-aluminum alloys containing 3, 5, 6, 7, and 8 weight per cent aluminum were homogenized by an anneal in the beta field at 2200 F (1477 K), water quenched, annealed at 1650 F (1172 K), and water quenched. The 1650 F (1172 K) anneal is above the alpha plus Ti_3Al field and fast cooling through this region should suppress the formation of Ti_3Al . The results of sea-water stress corrosion tests on these alloys are shown in Fig. 7 (left). Alloys containing 3 through 7 per cent aluminum were insensitive to sea-water stress corrosion, and the fracture strength in both air and sea water increased with aluminum content up to 7 per cent aluminum. However, at 8 per cent

aluminum there was a decrease in fracture stress in both air and sea water with the low fracture stress in sea water, indicating stress corrosion. Crossley [17] found that for titanium containing 8.4 weight per cent aluminum, Ti_3Al formation could not be suppressed on quenching but appeared as a martensitic structure. It is suspected that this occurred in the 8 weight per cent aluminum alloy in this investigation and thus led to loss in toughness in air and to sea-water stress corrosion susceptibility. This same series of alloys was aged at 1100 F (866 K), after the higher temperature anneals, to promote the formation of Ti_3Al . Referring to the titanium-aluminum diagram, Fig. 6, the 3 per cent aluminum alloy should contain no Ti_3Al . The alloys containing 5 per cent through 8 per cent

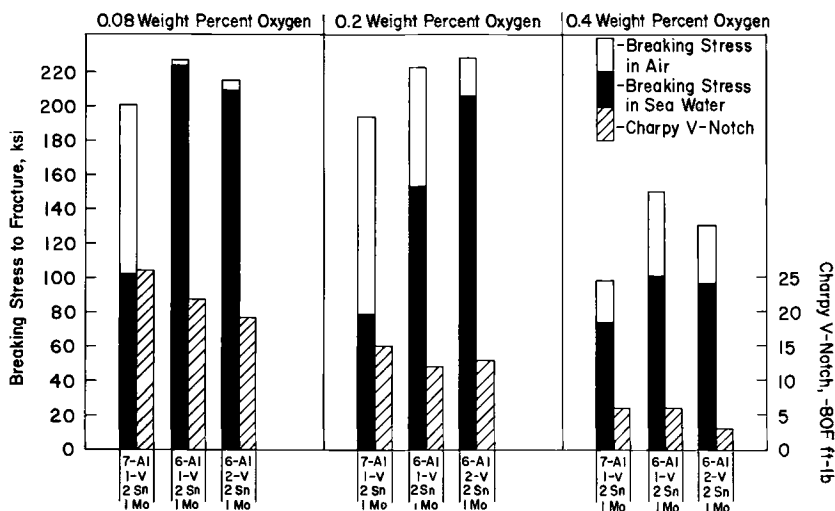


FIG. 9—Effect of aluminum and vanadium on stress corrosion of Ti-Al-Sn-Mo-V alloys.

aluminum should each contain Ti_3Al in an amount proportional to the aluminum content. Results of stress corrosion tests on these alloys are shown in Fig. 7 (right). The 3 per cent aluminum alloy was found to be insensitive to stress corrosion. The sea-water stress corrosion sensitivity of the other alloys was proportional to the aluminum content. The breaking stress in air was proportional to the aluminum content up to 6 per cent. Alloys containing greater than 6 per cent aluminum were reduced in notch strength due to the presence of Ti_3Al . The data developed in these tests support a correlation of stress corrosion sensitivity with presence of Ti_3Al .

MEL has investigated the effect of aluminum content, isomorphous beta stabilizer content, and oxygen content on the sea-water stress corrosion susceptibility of titanium alloys.

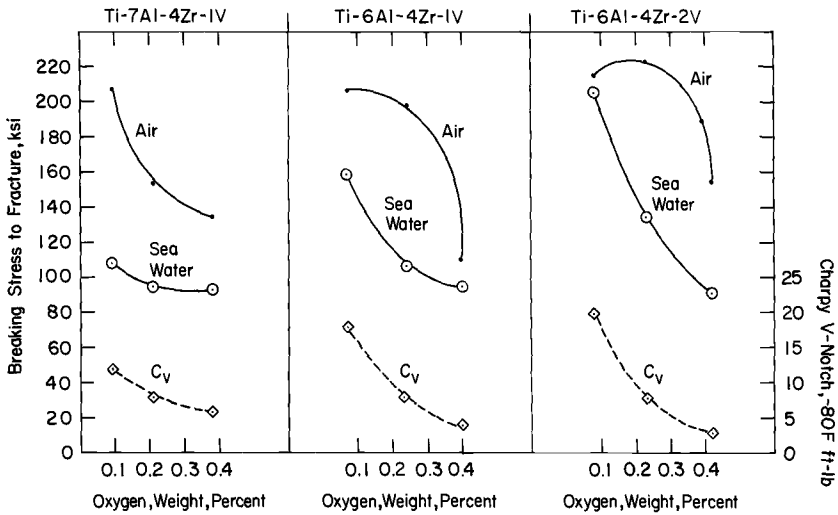


FIG. 10—Effect of oxygen on stress corrosion of Ti-Al-Zr-V alloys.

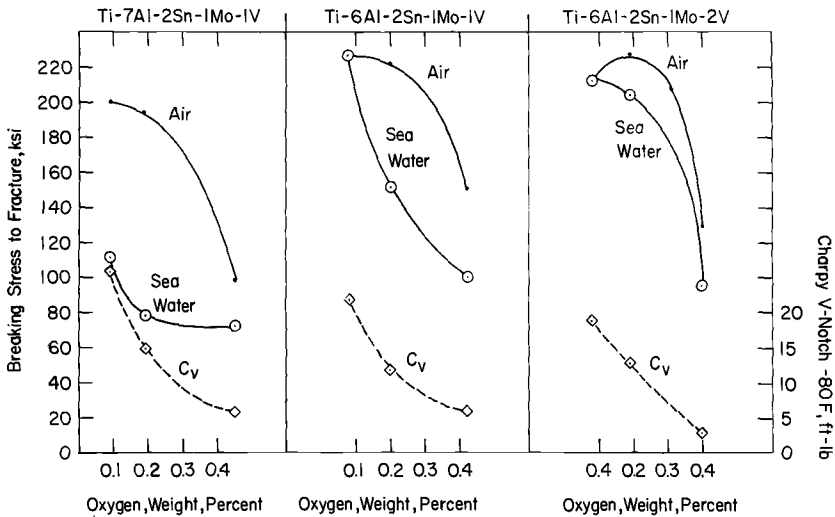


FIG. 11—Effect of oxygen on stress corrosion of Ti-Al-Sn-Mo-V alloys.

A series of titanium-aluminum-vanadium-zirconium alloys and titanium-aluminum-tin-molybdenum-vanadium alloys were evaluated for the effect of aluminum content and vanadium content at three different oxygen levels, 0.08, 0.2, and 0.4 weight per cent. The alloys were first given a homogenizing vacuum anneal above the beta transus at 1950 F (1339 K) and cooled in helium.

The results of cantilever-beam tests on specimens run in air and in sea

water and of Charpy V-notch tests at -80 F (211 K) are shown for the Ti-Al-Zr-V alloys in Fig. 8. At 0.08 weight per cent oxygen, a reduction in aluminum content from 7 to 6 weight per cent resulted in improvement of both stress corrosion and toughness properties. The addition of 1 per cent vanadium further improved these properties. At the 0.2 per cent oxygen level, the same compositional variations had the same effect on stress corrosion. However, these variations had no effect on the Charpy V-notch properties. At the 0.4 per cent oxygen level, the compositional variations were not effective in reducing stress corrosion susceptibility nor in increasing toughness. This indicates that oxygen alone probably affected the structure to such a degree that it masked any effect that

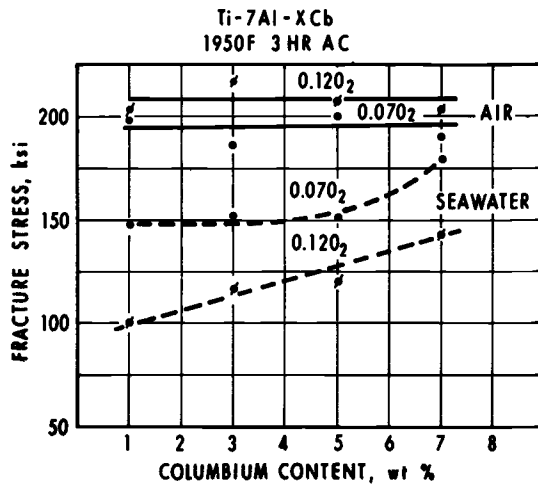


FIG. 12—Effect of columbium on stress corrosion of Ti-7Al alloy.

Ti₃Al had. Earlier work by MEL [2] showed that high-oxygen unalloyed titanium was sensitive to sea-water stress corrosion. Further work by Reactive Metals, Inc.⁴ indicated that there may be a transition from insensitive to sensitive behavior at approximately 0.25 weight per cent oxygen.

Figure 9 shows the effect of aluminum and vanadium content on the stress corrosion and Charpy V-notch properties of Ti-Al-Sn-Mo-V alloys at three oxygen levels. At an oxygen content of 0.08 weight per cent, a reduction in aluminum content from 7 to 6 per cent changed the alloy from "susceptible" to "insusceptible" to sea-water stress corrosion. There was no effect on stress corrosion by the addition of 1 per cent vanadium. The effect of compositional variation on Charpy V-notch properties was opposite that on the stress corrosion properties. A reduction in aluminum

⁴ Private communication, Reactive Metals, Inc.

content and an increase in vanadium content reduced the toughness. In other words, an increase in beta stabilizing equivalency increased stress corrosion resistance but reduced toughness. At the 0.2 per cent oxygen level, these compositional variations resulted in an increase in resistance to stress corrosion susceptibility with no effect on toughness. At 0.4 per cent oxygen, the effect of oxygen was similar to that in Ti-Al-Zr-V alloys. That is, the effect of oxygen, *per se*, masked the effect of Ti_3Al .

The data presented in Figs. 8 and 9 on the Ti-Al-Zr-V alloys and the Ti-Al-Sn-Mo-V alloys are presented in different form in Figs. 10 and 11 to show the effect of oxygen on strength and toughness in these alloys. In

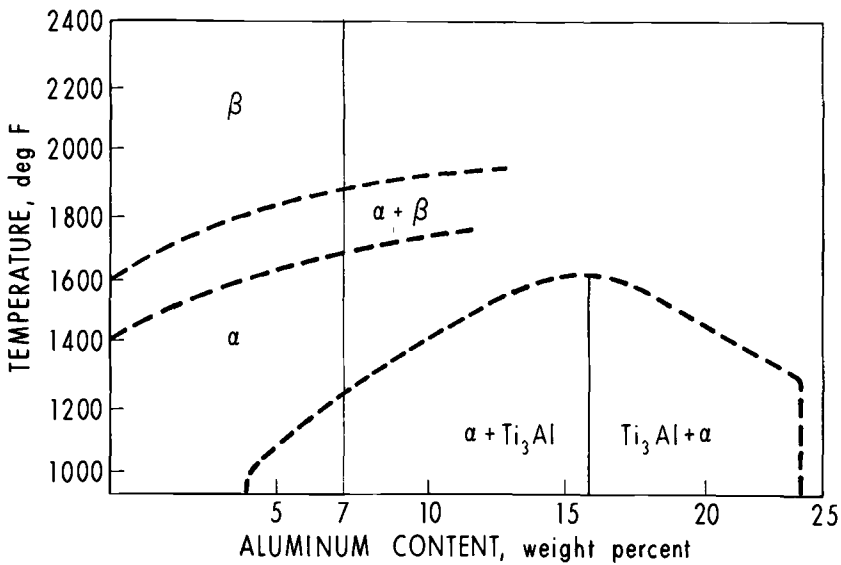


FIG. 13—Estimated vertical section of Ti-Al-Cb diagram at 2.5 columbium.

all cases, increased amounts of oxygen resulted in degradation of both stress-corrosion properties and Charpy V-notch properties.

The effect of columbium content on the stress corrosion properties of a 7 per cent aluminum alloy at oxygen levels of 0.07 and 0.12 per cent is shown in Fig. 12. These alloys were homogenized at 1950 F (1339 K) for 3 hr. An increase in oxygen level served to increase the breaking stress in air. At 0.07 per cent oxygen, columbium had no effect on stress corrosion resistance until 7 weight per cent was added. At 0.12 per cent oxygen stress corrosion resistance was proportional to columbium content. An increase from 0.07 per cent to 0.12 per cent oxygen resulted in lower stress corrosion resistance for all columbium levels.

These data on Ti-Al-X compositions correlate well with the observation of Crossley [18] on compositional effects in the titanium-aluminum

system. The amount of Ti_3Al present, if thermal history is held constant, is related to the aluminum content and the presence of additional alloying elements. The isomorphous beta stabilizers columbium, vanadium, and molybdenum decrease the amount of Ti_3Al principally due to their effect on the kinetics of formation of Ti_3Al . Oxygen increases the amount of Ti_3Al formed because of its effect on kinetics. The data developed in this phase of the sea-water stress corrosion investigation correlated with the compositional effects with respect to amounts of Ti_3Al formed. It is concluded that stress corrosion susceptibility is related to the amount of Ti_3Al present in the structure of titanium.

Heat Treatment Effects—The effect of heat treatment on the sea-

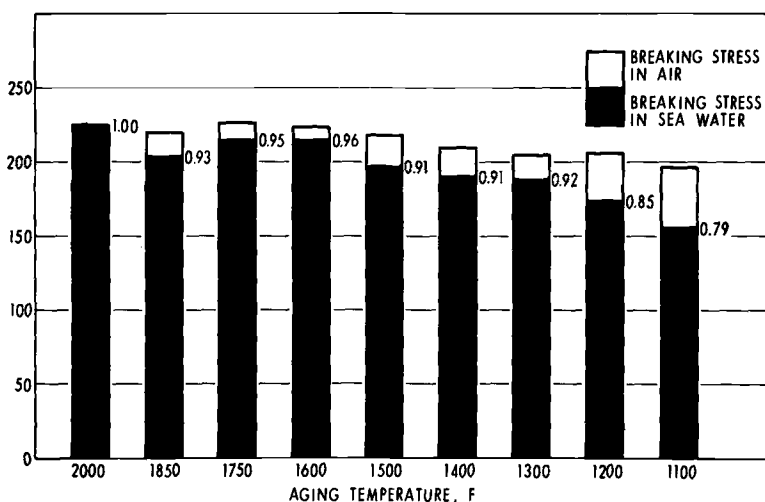


FIG. 14—Stress corrosion of quenched Ti-721.

water stress corrosion properties of Ti-721 was investigated for one heat of the alloy.

The first step in this phase of the investigation was to construct a vertical section of the Ti-Al-Cb diagram at the 2.5 per cent columbium level to locate the phase fields of the Ti-721 system with respect to aluminum content and temperature. The diagram as shown in Fig. 13 was drawn based on the known location of the beta transus and the alpha transus for the Ti-2.5 columbium binary alloy [19] and the alpha and beta transus for the Ti-721 alloy. The alpha plus Ti_3Al field was assumed to be the same as for the titanium-aluminum binary system. Crossley [18] has indicated it may be expanded slightly by the addition of columbium.

It was found in the first phase of the MEL stress corrosion investigation [2] that water quenching of the Ti-721 alloy from above the beta

transus resulted in immunity to sea-water stress corrosion. It is now apparent that the formation of Ti_3Al is responsible for stress corrosion in titanium-aluminum alloys. Therefore, a fast cool through the alpha plus Ti_3Al region from any temperature above it should prevent the formation of Ti_3Al . Specimens were water quenched from 2000 F (1366 K) in the beta field; from 1850 (1283) and 1750 F (1227 K) in the alpha plus beta field; from 1600 (1144), 1500 (1089), 1400 (1033), and 1300 F (977 K) in the alpha field; and from 1200 (922) and 1100 F (866 K) in the alpha plus Ti_3Al field. Formation of Ti_3Al should be suppressed by quenching from all temperatures except 1200 and 1100 F (866 K). The results of stress corrosion tests are shown in Fig. 14. A

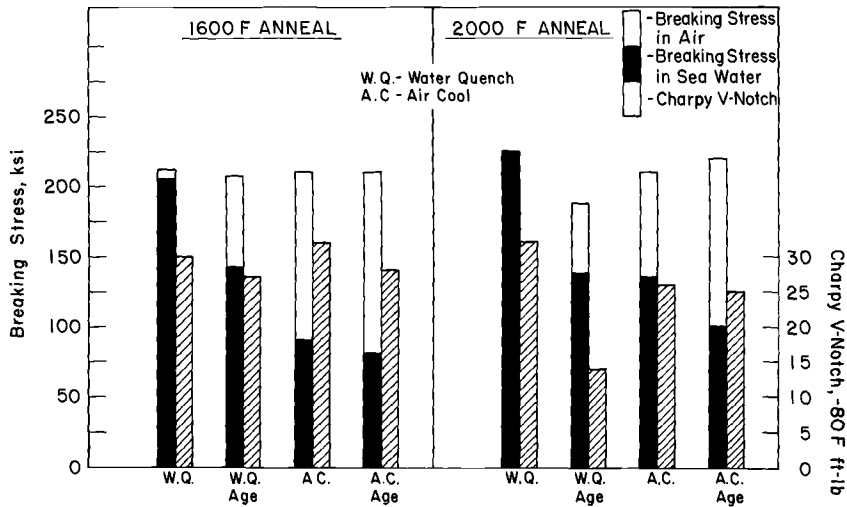


FIG. 15—Stress corrosion of Ti-721 annealed at 1600 and 2000 F.

stress corrosion ratio, (nominal breaking stress in sea water)/(nominal breaking stress in air) of 0.9 and above is considered by MEL and others [20] to indicate insensitivity to sea-water stress corrosion. In these tests, quenching from 1300 F (977 K) and above resulted in a stress corrosion ratio above 0.9. Specimens quenched from 1200 (922) and 1100 F (866 K) showed a stress corrosion effect. However, the stress corrosion susceptibility of the alloy quenched from either temperature was not as great as the starting material which had a stress corrosion ratio of 0.72. It is suspected that this behavior can be attributed to quenching strains developed in the structure. These strains probably interact with the coherence strains to make them less severe and thus reduce their effect on the stress corrosion process.

The Ti-721 alloy was annealed for 1 hr in the alpha field at 1600 F (1144 K) and in the beta field at 2000 F (1366 K). It was evaluated for

stress corrosion resistance and for Charpy V-notch impact toughness after water quenching, water quenching and aging, air cooling, and air cooling and aging. The aging treatment was a 3-hr anneal at 1100 F (866 K). The results of these tests are shown in Fig. 15. The alloy quenched from either 1600 (1144) or 2000 F (1366 K) was insensitive to stress corrosion, but aging at 1100 F (866 K) for 3 hr resulted in sen-

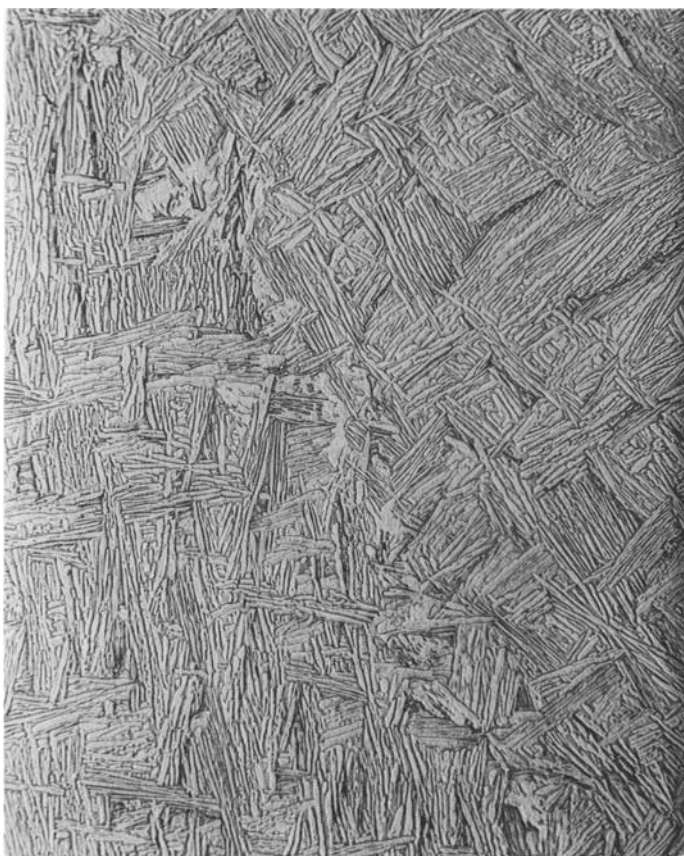


FIG. 16—*Typical microstructure of Ti-721 annealed at 1850 F.*

sitivity comparable to the starting material. The air cool and the air cool plus aging resulted in a high degree of sensitivity after the anneal at both 1600 (1144) and 2000 F (1366 K). The stress corrosion resistance of the alloy annealed at 2000 F (1366 K) and air cooled was slightly greater than that of the alloy annealed at 1600 F (1144 K) and air cooled. It is suspected that the air cool through the alpha plus beta field after the 2000 F (1366 K) anneal resulted in partitioning of the alloying elements. This lowered the aluminum content of the matrix, reduced the amount

of Ti_3Al formed in the matrix and improved the corrosion resistance. The -80 F Charpy V-notch toughness was good for all the heat treated alloys with the exception of the 2000 F (1366 K) quenched and aged material. Aging of the metastable martenistic structure results in development of products that are detrimental to toughness. The martenistic transformation and "tempering" of martensite in titanium has received



FIG. 17—*Typical microstructure of Ti-721 annealed at 1750 F.*

very little attention and is not yet fully understood. Aging of both water quenched and air cooled Ti-721 annealed at 1600 (1144) and 2000 F (1366 K) resulted in degradation in toughness, but the effect of Ti_3Al on toughness was not as drastic as it was on stress corrosion resistance.

Ti-721 was annealed in the alpha plus beta field at two temperatures, 1750 (1227) and 1850 F (1283 K). The effect of water quenching, air cooling, and aging the water quenched and air cooled alloy at 1100 F (866 K) for 3 hr was investigated. The 1850 F (1283 K) anneal was high

in the two phase field. The microstructure for the air cooled material is shown in Fig. 16. It consisted of primary alpha platelets richer in aluminum and leaner in columbium and tantalum than the nominal composition. The matrix consisted of transformed alpha, leaner in aluminum and richer in the beta stabilizers than the nominal composition. The 1750 (1227 K) anneal was lower in the alpha plus beta field. The structure shown in Fig. 17 is for the air cooled material. The matrix was essentially all transformed alpha higher in aluminum content and lower in columbium and tantalum content than the nominal composition. The results of stress corrosion tests and Charpy V-notch tests at -80°F (211 K) are shown in Fig. 18. Ti-721 quenched from both 1750 (1227)

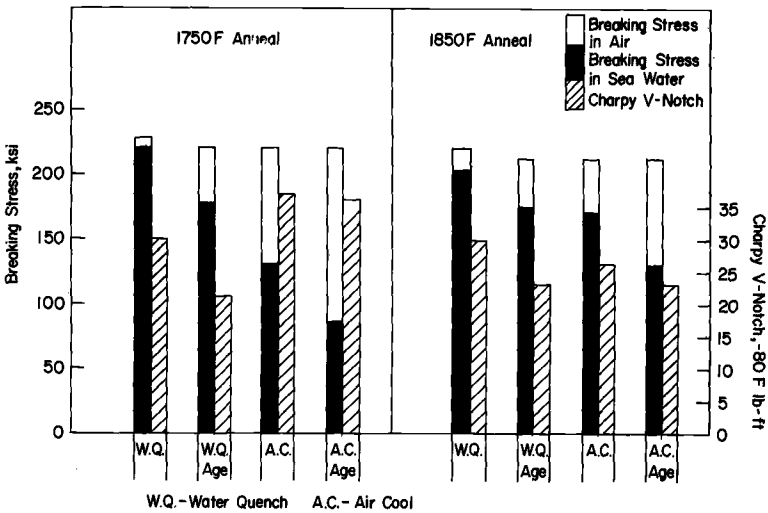


FIG. 18—Stress corrosion of Ti-721 annealed at 1750 and 1850 F.

and 1850 F (1283 K) was not susceptible to sea-water stress corrosion. A 3-hr age at 1100 F (866 K) increased stress corrosion susceptibility slightly. The toughness was the same for either annealing temperature and was reduced to the same degree by the age. The 1750 F (1227 K) anneal and air cool and the air cool plus aging resulted in a high degree of stress corrosion susceptibility. However, the toughness as the result of these treatments was excellent. The stress corrosion resistance of the alloy air cooled from 1850 F (1283 K) was better than for any of the air cool treatments, and the aged material was likewise better than for any of the air cooled and aged treatments. Although the toughness was still fairly good, it was not comparable to the 1750 F (1227 K) annealed alloy. It is concluded, therefore, that the best stress corrosion resistance is obtained in a structure that has a matrix leaner in aluminum and higher in isomorphous beta stabilizer content than the nominal composi-

tion. It is also evident that distribution of Ti_3Al in the structure influences the corrosion resistance of an alloy.

Discussion

Some investigators have been puzzled by the absence of a correlation between stress corrosion cracking and any other mechanical property such as toughness. Experimental evidence has shown that the presence of Ti_3Al leads to both loss in toughness and to loss in stress corrosion resistance. The degree of loss in each case appears to be related to the amount of Ti_3Al present. If both properties are related to the same factor it seems logical that they should be related to each other. That is, a toughness test such as the Charpy V-notch impact test should give an indication as to the degree of stress corrosion sensitivity a titanium alloy would display. However, investigations by MEL and by others [7] have shown that there is no correlation between stress corrosion behavior and toughness for titanium alloys. An understanding of the metallurgical factors which influence each property makes the reason for the lack of correlation quite obvious. The presence of coherent Ti_3Al does adversely affect toughness, but there are other factors which also lead to loss in toughness and either do not affect stress corrosion resistance or serve to improve it. These include solid solution alloying elements which are either soluble in the alpha phase or which promote stabilization of the beta phase. Isomorphous beta stabilizers, as shown by the investigation of the Ti-Al-Sn-Mo-V alloys (Fig. 9), improved stress corrosion resistance by suppressing the formation of Ti_3Al , but their alloying effect generally reduced toughness. Also, heat treatment of Ti-721 in the alpha plus beta field showed a similar effect through the creation of mixed structures of two different compositions. A high aluminum, low beta stabilizer content matrix had good toughness but low resistance to stress corrosion. A low aluminum high beta stabilizer content matrix had good stress corrosion resistance but low toughness. Stress corrosion of low oxygen content aluminum-containing titanium alloys is related essentially to only one variable, the presence of Ti_3Al . Toughness in these alloys is related to at least two variables, the presence of Ti_3Al and the presence of other alloying elements. Therefore, it is impossible to have a correlation between two properties if the variables affecting each are not the same.

Crossley [18] observed that ternary additions to titanium-aluminum alloys possibly affect the magnitude of Ti_3Al coherence strains. It appears logical that additions of substitutional or interstitial elements should affect the magnitude of Ti_3Al coherence strains due to the changes they induce in the lattice parameters of the alpha matrix, the coherent Ti_3Al precipitate, or both. The effect of hydrogen on stress corrosion behavior as observed by Howe and Goode [21] could be associated with its effect

on the coherency strains of Ti_3Al . Margolin and Portisch [22] have reported that hydrogen results in expansion of Ti_3Al . As noted previously in this investigation, the interaction of strains induced by quenching with coherence strains may have an effect on stress corrosion behavior. Time and temperature of aging in the alpha plus Ti_3Al field has an effect on the magnitude of coherency strains and probably also has an effect on stress corrosion similar to the effect on toughness observed by Crossley [18].

On the basis of the present knowledge concerning the titanium-aluminum system and its stress corrosion behavior, there are three significant variables that affect stress corrosion in this system. These are:

1. Amount of Ti_3Al present.
2. Distribution of Ti_3Al in the structure.
3. Magnitude of coherence strains due to Ti_3Al .

The logical approach to control of stress corrosion in titanium is control of the structure to eliminate formation of the embrittling constituents that cause stress corrosion action. This can be accomplished through composition control and heat treatment. This approach has been used in the development of a stress-corrosion resistant compositional variation of the Ti-721 alloy. The new stress-corrosion resistant alloy is Ti-6Al-2Cb-1Ta-0.8Mo. The reduction in aluminum content and the addition of 0.8 weight per cent molybdenum has resulted in an alloy that is stress corrosion resistant after the most severe thermal treatments that should promote this behavior. This alloy has been evaluated in production size heats and is now ready for use in marine structural applications [23].

Summary and Conclusions

Sea-water stress corrosion in titanium alloys is dependent on mechanical factors and on the metallurgical structure. The mechanical aspects include the presence of a stress concentration and application of sufficient stress so that the plastic zone at the base of the stress concentration in contact with the environment undergoes a degree of plastic deformation. An embrittling constituent must be present in the structure to restrict slip so that it occurs in coarse steps. A possible further requirement is that crevice conditions prevail at the stress concentration so that depletion of the passivating ions occurs faster than they can be replaced by diffusion of fresh ions from the bulk of the liquid environment.

It is possible that a number of structural influences can restrict slip in titanium and cause stress corrosion, but the one of most concern is that which occurs in titanium alloys containing aluminum. This structural embrittler is the coherent Ti_3Al precipitate. The formation of Ti_3Al can be controlled by composition, heat treatment, or both. The most effective

method for control of stress corrosion in titanium alloys is control of the metallurgical structure.

References

- [1] Brown, B. F., "A New Stress-Corrosion Cracking Test Procedure for High Strength Alloys," *Materials Research & Standards*, Vol. 6. No. 3, March 1966.
- [2] Lane, I. R., Jr., et al, "Sea-Water Embrittlement of Titanium," *Stress Corrosion Cracking of Titanium, ASTM STP 397*, American Society for Testing and Materials, 1966.
- [3] Wald, G. G., "Effect of Heat Treatment on Salt Water Delayed Fracture of Titanium Alloys," paper presented at 96th American Institute of Mining, Metallurgical, and Petroleum Engineers' meeting, Los Angeles, Calif., Feb. 19-23, 1967.
- [4] Feige, N. G. and Murphy, T., "Fracture Behavior of Titanium Alloys in Aqueous Environment," paper presented at WESTEC Conference, Los Angeles, Calif., 1966.
- [5] Sanderson, G. and Scully, J. C., "Some Observations on the Stress-Corrosion Cracking of Titanium Alloys," *Proceedings, Conference on Environment-Sensitive Mechanical Behavior*, Baltimore, Md., 1965 (in press).
- [6] Scully, J. C., "The Characteristics of Transgranular Stress Corrosion Cracking," *British Corrosion Journal*, to be published.
- [7] Lennox, T. J. et al, "Marine Corrosion Studies," NRL Memorandum Report 1711, Naval Research Laboratory, May 1966.
- [8] Brown, B. F. et al, "Marine Corrosion Studies," NRL Memorandum Report 1634, Naval Research Laboratory, July 1965.
- [9] Judy, R. W. et al, "Fractographic Analysis of Ti-721 and Ti-6Al-4V Fractures Developed in Wet Fatigue," NRL Report 6330, Naval Research Laboratory, July 1965.
- [10] Cavallaro, J. L., "Stress Corrosion of Titanium in Sea Water," NSRDC R&D Phase Report, 2483, Oct. 1967.
- [11] Williams, D. N. et al, "Studies of the Mechanism of Crack Propagation in Salt-Water Environments of Candidate Supersonic Transport Titanium Alloy Materials," Final Report on Contract No. FA-SS-66-1, Jan. 1966.
- [12] Beck, T. R., "Stress Corrosion of Titanium Alloys Heat Treatment Effects, SCC Velocity in Various Solvents and Electrochemical Kinetics with Ti:8-1-1 Alloy," Quarterly Progress Report No. 2 on Contract NAS 7-489, Jan. 1967.
- [13] Pugh, E. N., "On the Mechanism(s) of Stress Corrosion Cracking," First brittlement, Particularly of Zinc Monocrystals by Mercury," *Philosophical Magazine*, Vol. 9, 1963.
- [14] Westwood, A. R. C., "Effects of Environment on Fracture Behavior," *Fracture of Solids*, Interscience, New York, 1963.
- [15] Westwood, A. R. C. and Kamdar, M. H., "Concerning Liquid Metal Embrittlement, Particularly of Zinc Monocrystals by Mercury," *Philosophical Magazine*, Vol. 9, 1963.
- [16] Westwood, A. R. C. et al, "Fracture Behavior of AgCl in Aqueous NaCl," *Acta Metallurgica*, Vol. 13, 1965.
- [17] Crossley, F. A., "Titanium-Rich End of the Titanium-Aluminum Equilibrium Diagram," *Transactions, American Institute of Mining, Metallurgical, and Petroleum Engineers*, Vol. 236, Aug. 1966.
- [18] Crossley, F. A., "Research and Development of Physical Metallurgy of Titanium," Final Report on Contract No. Nonr-4766(00) with NSRDC, April 1967.
- [19] Maykuth, D. J. et al, "The Effects of Alloying Elements in Titanium," Volume A. Constitution, DMIC Report 136A, Sept. 1960.
- [20] Seeley, R. R. et al, "Effect of Heat Treatment and Microstructure on the

- Aqueous Stress-Corrosion Cracking of Titanium-Base Alloys," paper presented at 96th American Institute of Mining, Metallurgical, and Petroleum Engineers' meeting, Los Angeles, Calif., Feb. 19-23, 1967.
- [21] Howe, D. G. and Goode, R. J., "The Effects of Vacuum Heat Treatment on the Stress-Corrosion-Cracking Resistance of Alloys of Titanium," paper presented at 96th American Institute of Mining, Metallurgical, and Petroleum Engineers' meeting, Los Angeles, Calif., Feb. 19-23, 1967.
- [22] Margolin, H. and Portisch, H., "Expansion of Ti-Al Alloys by Hydrogen," paper presented at 96th American Institute of Mining, Metallurgical, and Petroleum Engineers' meeting, Los Angeles, Calif., Feb. 19-23, 1967.
- [23] Cavallaro, J. L., "Ti-6Al-2Cb-1Ta-0.8Mo Titanium Alloy as a Structural Material for Marine Applications," MEL R&D Phase Report 506/66, Jan. 1966.

S. R. Seagle,¹ R. R. Seeley,² and G. S. Hall³

The Influence of Composition and Heat Treatment on the Aqueous-Stress Corrosion of Titanium

REFERENCE: Seagle, S. R., Seeley, R. R., and Hall, G. S., "The Influence of Composition and Heat Treatment on the Aqueous-Stress Corrosion of Titanium," *Applications Related Phenomena in Titanium Alloys, ASTM STP 432*, American Society for Testing and Materials, 1968, pp. 170-188.

ABSTRACT: Chemical composition and heat treatment were found to have an effect on the aqueous-stress corrosion of titanium. Aluminum contents greater than 5 per cent and oxygen contents greater than about 0.3 per cent caused appreciable sensitivity to stress corrosion. The additions of beta-isomorphous type alloying elements, such as molybdenum, were beneficial for titanium-aluminum alloys but showed no improvement for titanium-oxygen alloys. The amount of oxygen that could be tolerated was reduced substantially by the addition of aluminum.

Heat-treatment effects were very pronounced and not similar for the alloy systems investigated. The heat-treatment temperature for maximum sensitivity to stress corrosion increased from 1000 F for Ti-6Al alloys to 1200 F for Ti-8Al alloys. This corresponds to about 150 F below the estimated Ti₃Al transus. The stress-corrosion resistance of Ti-6Al-4V alloy was reduced as a result of long annealing times prior to exposure in the Ti₃Al region. Long annealing times also promoted stress corrosion in titanium-oxygen alloys. Microscopic examination did not reveal significant changes with annealing time. This finding indicates the metallurgical factors affecting the stress corrosion resistance are related to submicroscopic changes.

KEY WORDS: stress corrosion, titanium alloys, embrittlement, heat treatment, fracture toughness

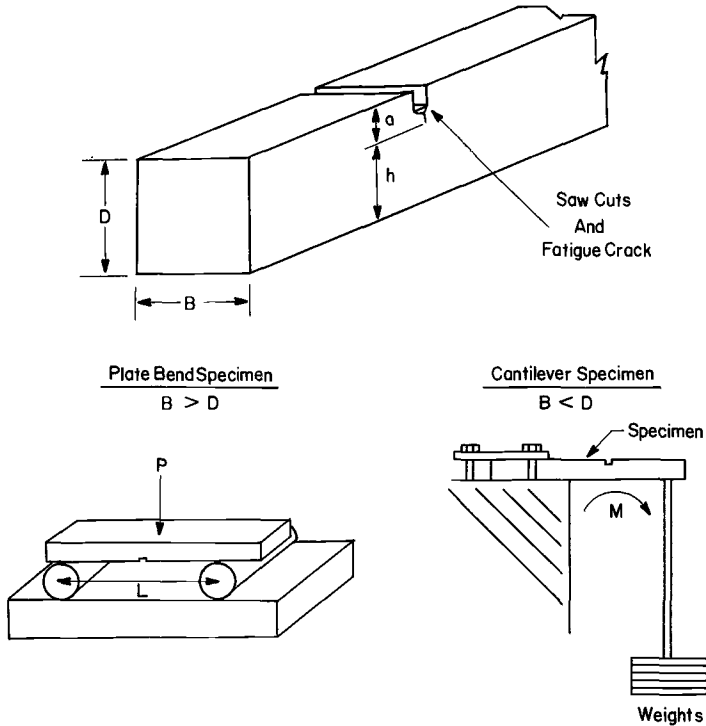
Several investigations have been conducted in the past two years in an attempt to clarify the aqueous-stress corrosion of titanium. These studies have revealed that only some alloys are susceptible to this type of stress corrosion and that the degree of susceptibility varies considerably. Several

¹ Supervisor, Physical Metallurgy, Research and Development Department, Reactive Metals, Inc., Niles, Ohio.

² Research metallurgist, Research and Development Department, Reactive Metals, Inc., Niles, Ohio.

³ Graduate student, Lehigh University, Bethlehem, Pa.

laboratories [1-3]⁴ showed the stress-corrosion resistance of titanium could be improved through chemistry modifications, heat treatment, and processing. This surprisingly large variation in sensitivity indicated several possibilities might exist for improving the stress-corrosion resistance of current commercial alloys. Many of these possibilities were explored



Crack Tip Stress:

$$S = \frac{1.5 PL}{B h^2}$$

Sa or Ka = air test

Ssw or Ksw = sea water test

Stress Intensity:

$$K_c = \frac{4.12 M \sqrt{(1/\alpha^3) - \alpha^3}}{B D^{3/2}}$$

M = moment at crack tip

$\alpha = 1 - a/D$

FIG. 1—Test specimen and equipment.

in our studies conducted at Reactive Metals, Inc. (RMI) and are discussed in this presentation.

Procedure

Two testing methods, cantilever-beam and bend, were used in this study. Figure 1 shows the specimen and equations necessary for stress calculations.

⁴The italic numbers in brackets refer to the list of references appended to this paper.

Bend Test

Specimen blanks were cut with a band saw and then heat treated. Again using a band saw, a notch was cut across the width of the specimen to a predetermined depth. The specimen was washed in hot water to remove the water soluble cutting oil left from the sawing operation. A fine notch was placed at the bottom of the saw cut with a 0.015-in.-thick saw blade. A fatigue crack was initiated and propagated by cycling from 0 to about 90 ksi under three-point loading. The fatigue crack was propagated to the desired length after 1000 to 2000 cycles. The total crack depth including saw cuts was maintained between 25 to 35 per cent of the specimen thickness.

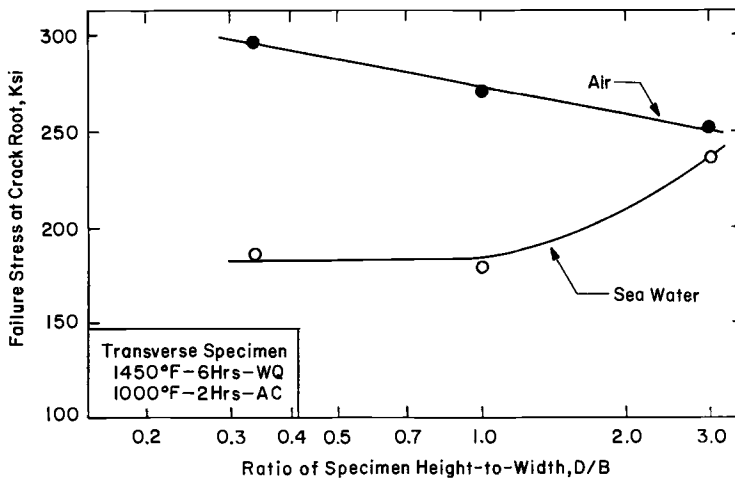


FIG. 2—Effect of specimen geometry on the aqueous-stress corrosion of Ti-6Al-4V 0.75-in.-thick plate.

After a fatigue crack had been established, the specimen was placed on a titanium testing jig under the compression head of a screw-type tensile machine. The specimen was loaded to approximately 50 per cent of the estimated breaking stress and then continuously loaded at 6 ksi/min until failure occurred. Tests in sea water were conducted by immersing the complete specimen and testing rig in a titanium tank containing the solution. Synthetic sea water according to ASTM Specification for Substitute Ocean Water (D 1141 - 52) was used for all aqueous tests. The sea water was constantly agitated to reduce the possibility of localized solution concentrations.

The nominal failure stress at the root of the original fatigue crack was calculated from the ultimate load using beam equations. Stress corrosion was evident by a lower failure stress in sea water than in air. A ratio of the sea water-to-air fracture stress was used as a measure of the ma-

terial's stress-corrosion resistance. A high ratio such as 0.9 indicates good resistance. In addition, stress corrosion can be confirmed by a different fracture texture adjacent to the original fatigue crack.

Cantilever-Beam Test

The cantilever-beam method and equation suggested by B. F. Brown [4] were used for a few of the studies. The specimens were prepared in a manner similar to the bend test specimens; however, the testing procedure was slightly different. The specimens were loaded to approximately 50 per cent of the estimated failure stress. The load was then increased about 10 per cent every 5 min until failure. Using the failure load and specimen dimensions, the stress intensity, K , was calculated. Again a ratio of sea water-to-air values was used to determine degree of susceptibility.

Specimen Geometry

Valid fracture-toughness tests require compliance to specified height-to-width ratios. However, our work showed that specimens not meeting compliance were generally more susceptible to stress corrosion. This is illustrated in Fig. 2. Ti-6Al-4V 0.75-in.-thick plate was used in this study. The specimens were 0.75 in. high (D) by widths (B) of 2.5, 0.75, and 0.25-in., with D/B ratios of 0.3, 1.0, and 3.0, respectively. Figure 2 shows that, as the D/B ratio increases, the fracture stress in air decreases, while the fracture stress in sea water increases. Little difference exists between air and sea water fracture stresses at a D/B ratio of 3.0; thus, stress corrosion is not so evident when compliance is approached, that is, at a D/B ratio of 3.0.

All of the bend test data were obtained from specimens with a D/B ratio of 0.33 with the height, D , being the plate thickness. Although this geometry does not meet compliance, it accentuates stress corrosion and is useful in this type of qualitative study.

The cantilever test data were obtained from specimens with a D/B ratio of 1 to 2. The fatigue crack was perpendicular to the plate surface so that the width dimension, B , was the plate thickness. All bend and cantilever beam testing was conducted on longitudinal specimens taken from plates with a thickness of 0.5 to 1.0 in.

Effect of Composition

Aluminum

The high-aluminum titanium alloys have been particularly susceptible to aqueous-stress-corrosion cracking. Results from an evaluation of binary titanium-aluminum (Ti-Al) alloys, Fig. 3, show that this sensitivity is encountered at aluminum contents between 5 and 6 per cent.

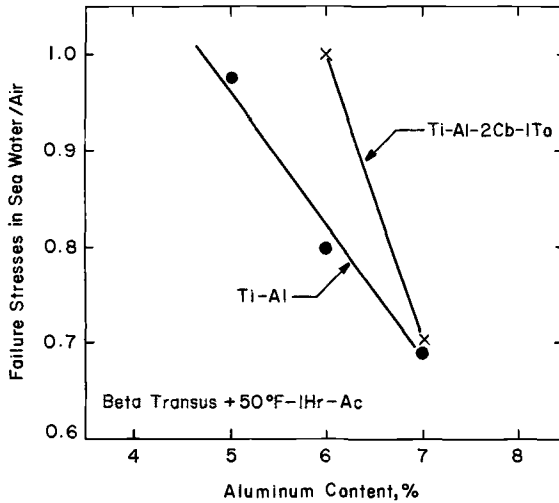


FIG. 3—Effect of aluminum content on the aqueous-stress corrosion of titanium plate.

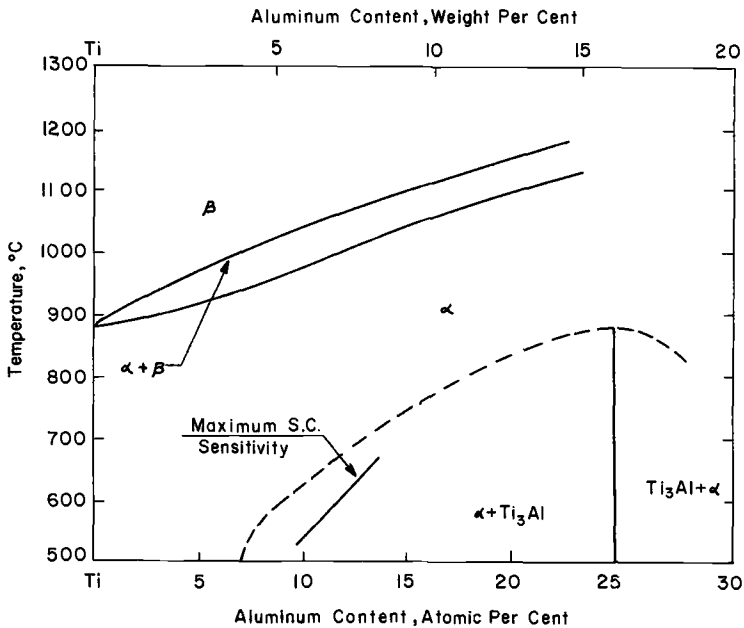


FIG. 4—Titanium-aluminum phase diagram (after Crossley [5].)

This aluminum threshold for sensitivity agrees fairly well with the formation of Ti_3Al , as suggested by Crossley [5] and shown in Fig. 4. The data in our study were obtained from beta-annealed specimens. Since these heat treatments resulted in air cooling through the suggested Ti_3Al

range, slower cooling, or equilibration anneals at temperatures below the Ti_3Al transus, might result in a shift in sensitivity to slightly lower aluminum contents.

Figure 3 also shows the threshold aluminum content is increased from 5 to 6 per cent by the addition of 2 per cent columbium + 1 per cent tantalum. Since this addition of a weak beta-isomorphous element

TABLE 1—Influence of alloying elements on the aqueous-stress corrosion of Ti-7Al-2Cb-1Ta.

Addition to Base	Addition Type	Failure Stress, ksi ^a		Failure Stress Ratio, Sea Water Test/Air Test
		in Air	in Sea Water	
Base (7Al-2Cb-1Ta).....	...	223	152	0.68
0.13 Si.....	active eutectoid	238	145	0.61
0.2 Pd.....	active eutectoid	254	152	0.60
0.8 Mn.....	sluggish eutectoid	201	157	0.78
0.5 Mo.....	β isomorphous	247	245	0.99
1.0 Mo.....	β isomorphous	220	215	0.98

^a Beta annealed, 1 hr, air cooled.

TABLE 2—Influence of oxygen on the aqueous-stress corrosion of titanium.

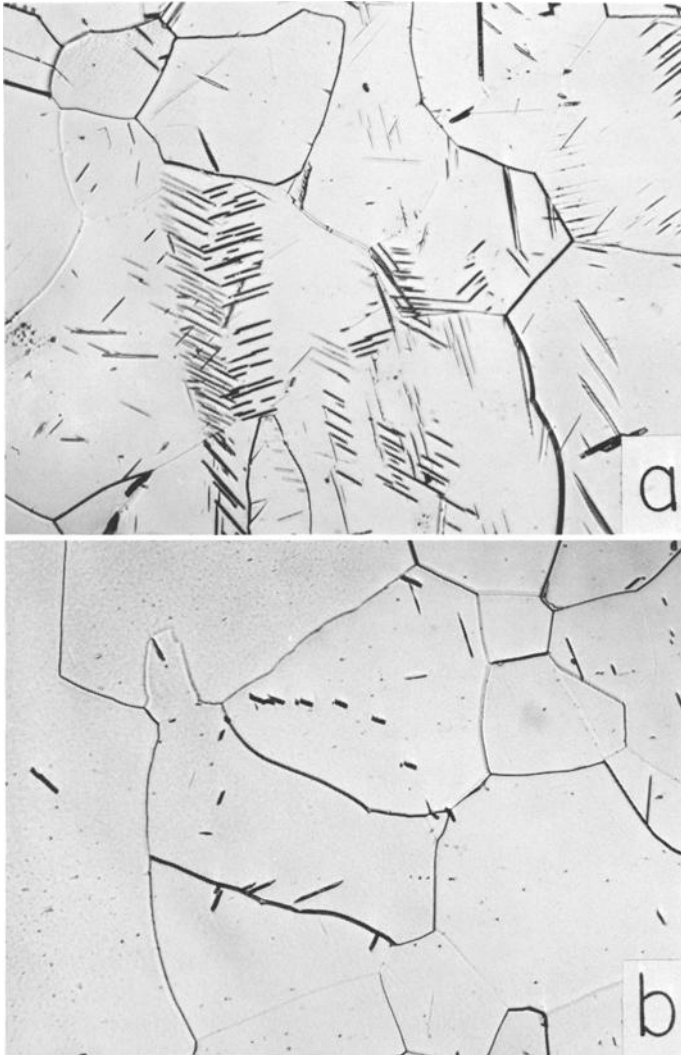
Composition	Failure Stress-Intensity K , ksi $\sqrt{\text{in.}}$		Sea Water Test/Air Test
	in Air	in Sea Water	
Ti-0.060%O ^a	52.9	51.4	0.97
Ti-0.20%O ^a	72.3	68.0	0.94
Ti-0.40%O ^a	90.3	53.3 ^c	0.59
Ti-0.40%O + 1.0%Mo ^a	99.4	62.5 ^c	0.63
Ti-6%Al-4%V-0.08%O ^b	93	88	0.95
Ti-6%Al-4%V-0.18%O ^b	92	60 ^c	0.65

^a Annealed: 1300 F, 7 hr, vacuum cooled.

^b Annealed: 1450 F, 8 hr, furnace cooled.

^c Fracture texture showed stress corrosion.

improved stress-corrosion resistance, other additions were evaluated. Table 1 shows the influence of several types of beta stabilizers on the stress-corrosion resistance of a susceptible Ti-7Al-2Cb-1Ta base. The addition of silicon, an active eutectoid former, resulted in essentially no change in resistance. Palladium was evaluated because of its beneficial effect in titanium nonoxidizing chloride media. Again, no improvement was noted. Manganese, a sluggish eutectoid former, showed some indication of improvement but not enough to pursue further. The addition of the strong beta-isomorphous element molybdenum, resulted in excellent resistance to stress corrosion at both 0.5 and 1.0 per cent molybdenum levels.

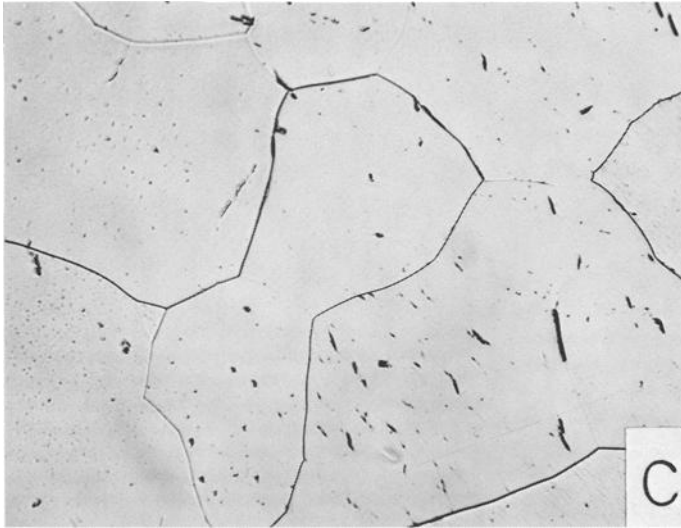


(a) Titanium-0.06 per cent oxygen (44 ppm hydrogen), good stress-corrosion resistance.
(b) Titanium-0.20 per cent oxygen (52 ppm hydrogen), good stress-corrosion resistance.

FIG. 5—Microstructures of titanium-oxygen alloys ($\times 250$).

Oxygen

The susceptibility of commercially pure titanium to stress corrosion has been unclear. Our studies show the resistance is related to both the oxygen content and heat treatment and is discussed later. The influence



(c) Titanium-0.40 per cent oxygen (51 ppm hydrogen), poor stress-corrosion resistance.

FIG. 5—Continued.

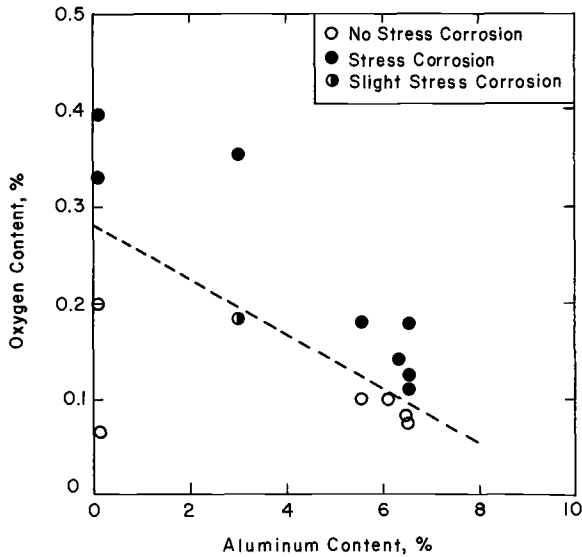


FIG. 6—Influence of oxygen and aluminum content on stress-corrosion incidents.

of oxygen content on stress-corrosion sensitivity is shown in Table 2. A transition from a resistant to a susceptible condition occurs between 0.2 and 0.4 per cent oxygen. This was quite unexpected since the transition does not correspond with any known phase changes.

Figure 5 contains the microstructures of commercially pure titanium with oxygen contents between 0.060 and 0.40 per cent. The microstructure of the low-oxygen material exhibits considerable evidence of twinning which is not present in the other two structures. All three structures show evidence of a second phase which is believed to be titanium hydride. The occurrence of stress corrosion, however, could not be related to any microstructural features.

Molybdenum additions proved beneficial for improving the stress-corrosion resistance of Ti-Al alloys. However, a 1 per cent molybdenum addition (Table 1) did not improve the low stress-corrosion resistance of the high-oxygen alloy.

TABLE 3—Effect of cooling rate on the aqueous-stress corrosion of Ti-7Al-2Cb-1Ta plate.

Heat Treatment	Failure Stress at Crack Root, ksi		Sea Water Test/Air Test
	in Air	in Sea Water	
1950 F, 1 hr, FC ^a	240	138	0.57
1950 F, 1 hr, AC ^b	242	167	0.69
1950 F, 1 hr, WQ ^c	253	222	0.88
1650 F, 1 hr, FC	244	143	0.59
1650 F, 1 hr, AC	248	173	0.70
1650 F, 1 hr, WQ	254	195	0.77

^a FC = furnace cooled.

^b AC = air cooled.

^c WQ = water quenched.

Aluminum Plus Oxygen

Oxygen was found to be detrimental not only in the binary alloys but also in Ti-Al alloys. Table 2 contains an example of the influence of oxygen on Ti-6Al-4V. Increasing the oxygen from 0.08 to 0.18 per cent results in a change from good resistance to appreciable susceptibility. These results suggest a relationship between oxygen and aluminum content on the stress-corrosion resistance of titanium. This is illustrated in Fig. 6. As the aluminum content increases, less oxygen can be tolerated for good stress-corrosion resistance.

Effect of Heat Treatment

Ti-7Al-2Cb-1Ta

The preceding data on the effect of composition indicate corrosion susceptibility is related to the formation of the phase Ti₃Al. This was further investigated on Ti-7Al-2Cb-1Ta by studying the influence of cooling rate from a temperature above the beta transus and the esti-

mated Ti_3Al transus. These results, in Table 3, clearly show that stress corrosion is promoted by slow cooling below 1650 F through the Ti_3Al region. Rapid cooling, such as water quenching, was not sufficiently rapid to suppress the Ti_3Al formation.

Ti-8Al-1Mo-1V

The kinetics of the Ti_3Al transformation were indirectly observed by the use of the stress-corrosion test. Specimens of resistant Ti-8Al-1Mo-1V were heated for several time-temperature combinations and air

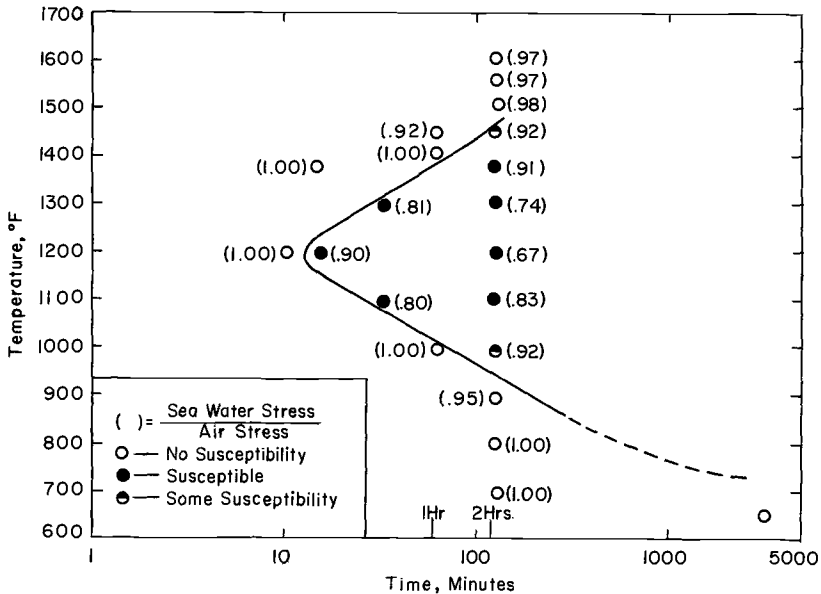


FIG. 7—Effect of heat-treating temperature and time on stress-corrosion incidents in Ti-8Al-1Mo-1V plate (air cooled).

cooled. The results are shown in Fig. 7. These data show a time-temperature stress-corrosion relationship similar to metallurgical time-temperature-transformation diagrams. The most severe exposure and knee of the curve was at 1200 F. The upper boundary for stress corrosion appears to be near 1500 F, the estimated Ti_3Al transus for the aluminum content. Although appreciable changes in stress-corrosion susceptibility were observed, optical microscopy did not reveal significant differences.

The reversibility of stress-corrosion susceptibility was evaluated by annealing a susceptible specimen of Ti-8Al-1Mo-1V at 1550 F above the estimated Ti_3Al transus. Table 4 shows that complete immunity was not achieved although some improvement was noted. Complete stress-corrosion resistance was restored only after annealing at 1800 F or

TABLE 4—Effect of time at 1550 F on the aqueous-stress corrosion of Ti-8Al-1Mo-1V plate.

Heat Treatment	Failure Stress at Crack Root, ksi		Sea Water Test/Air Test
	in Air	in Sea Water	
As received.....	246	174	0.71
1550 F, 1 hr, AC ^a	248	223	0.90
1560 F, 63 hr, AC.....	243	210	0.86
1675 F, 1 hr, AC.....	267	247	0.92
1700 F, 1 hr, AC.....	252	235	0.93
1750 F, 1 hr, AC.....	250	229	0.92
1800 F, 1 hr, AC.....	245	245	1.00
1850 F, 1 hr, AC.....	258	258	1.00

^a AC = air cooled.

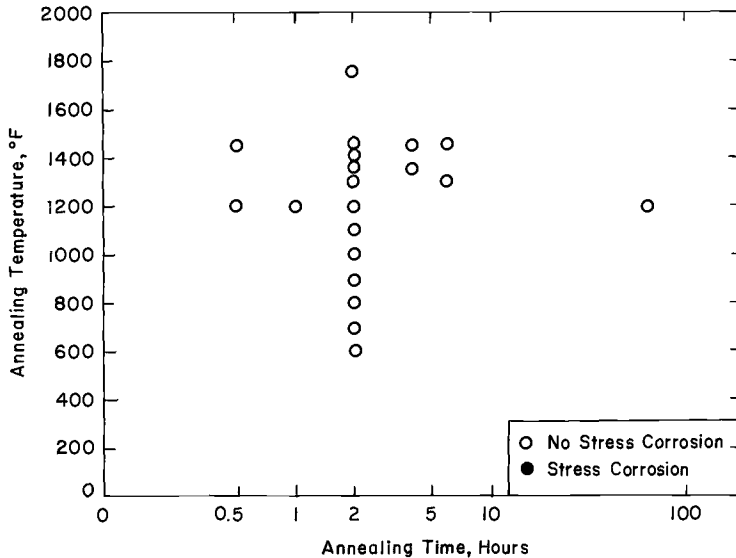
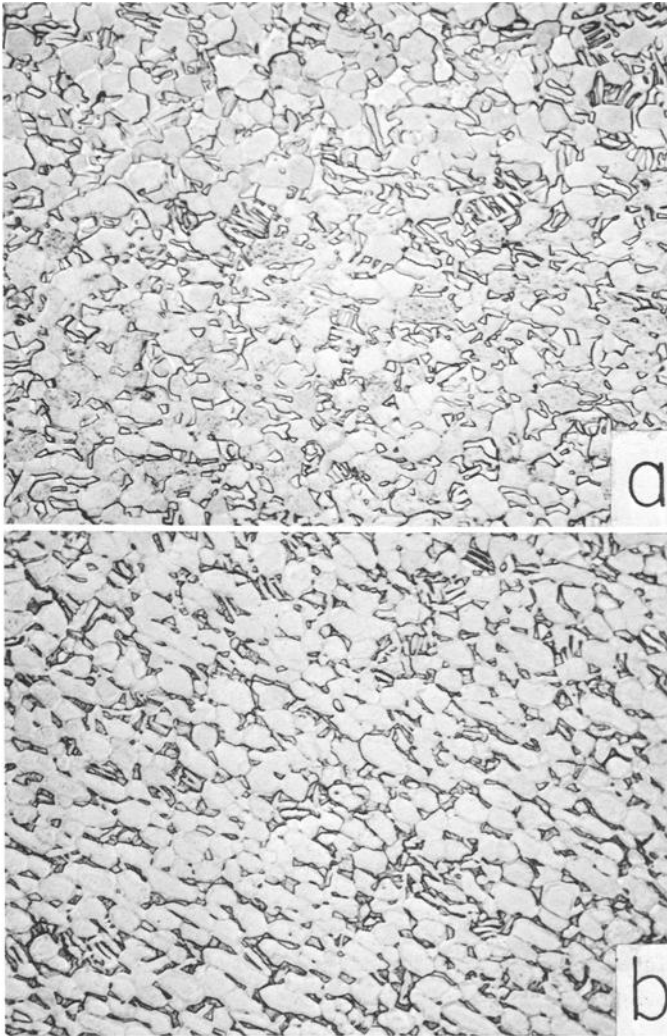


FIG. 8—Effect of heat-treating temperature and time on stress-corrosion incidents in Ti-6Al-4V plate (air cooled).

higher. This illustrates the sluggishness of redissolving or dispersing of the damaging species and it agrees indirectly with Crossley's [5] observation that exceptionally long times are required to redissolve Ti₃Al after it has once been formed.

Ti-6Al-4V

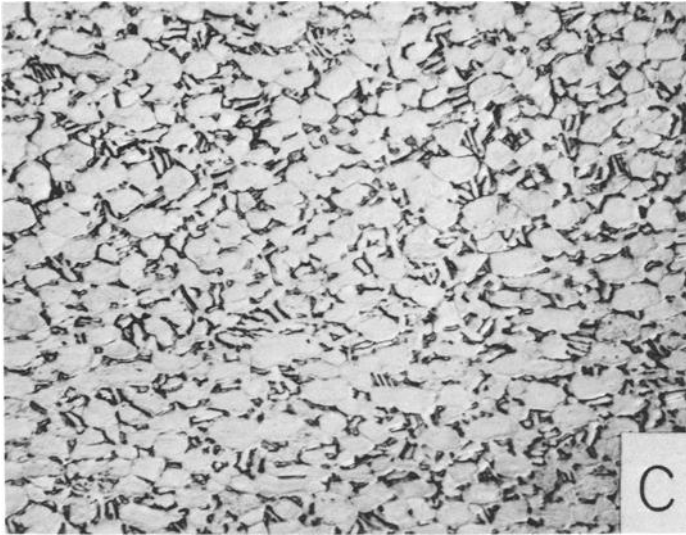
The heat-treatment approach used in the evaluation of Ti-8Al-1Mo-1V was applied to Ti-6Al-4V. The results were somewhat different. Several low temperature-time heat-treatment combinations were investigated. All the conditions tested and shown in Fig. 8 did not cause



	Ultimate Tensile Strength, ksi	0.2% Yield Strength, ksi	Elonga- tion, %	Reduc- tion of Area, %	Sea Water Test/ Air Test
(a) 1450 F, 6 hr, water quenched..	143	129	15	34	0.99
(b) 1450 F, 6 hr, air cooled.....	143	129	14	33	0.87

FIG. 9—Influence of cooling rate on the microstructure and properties of Ti-6Al-4V plate.

significant stress corrosion. These initial results were not anticipated since the Ti-6Al-4V alloy was known to have some sensitivity to stress corrosion. Further study showed that the Ti-6Al-4V alloy, like other high-aluminum content alloys, was sensitive to cooling rate. Figure 9 contains data from tests on plate after water quenching, air cooling, and



(c) 1450 F, 6 hr, furnace cooled ... 145 135 13 25 0.54
 FIG. 9—Continued.

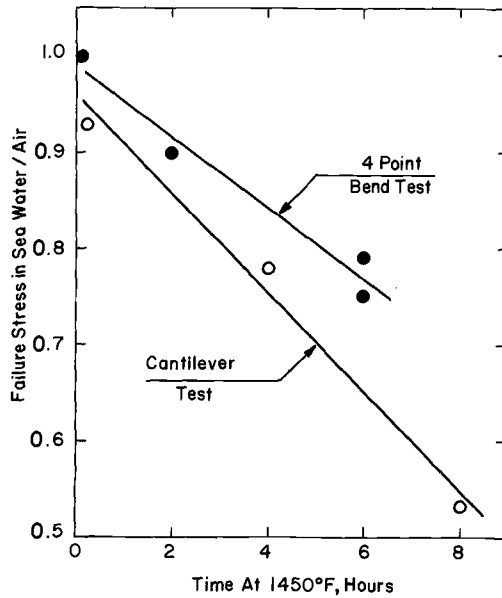
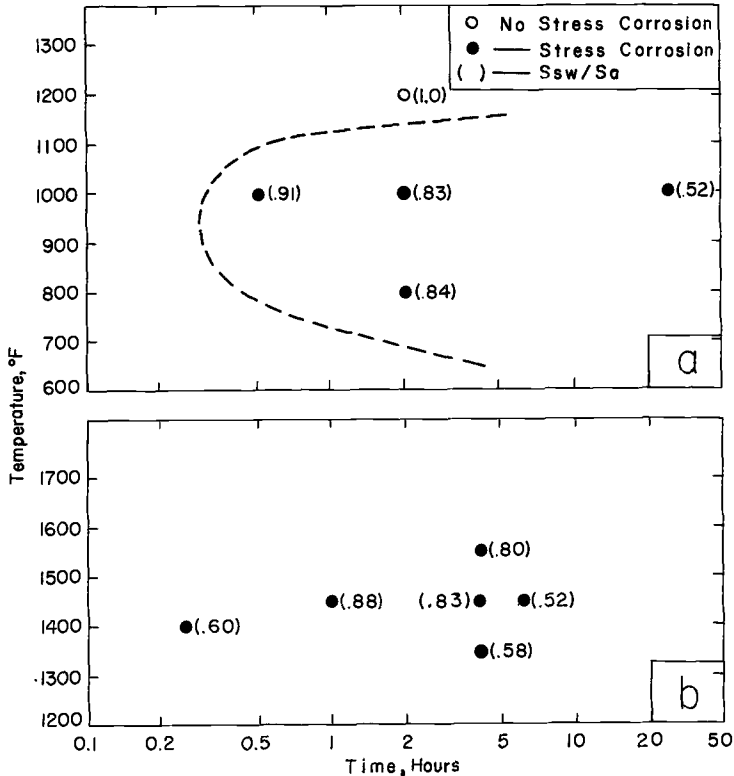


FIG. 10—Effect of annealing time at 1450 F followed by furnace cooling on the stress corrosion of Ti-6Al-4V plate.

furnace cooling from 1450 F. No indication of stress corrosion was observed for air-cooled or water-quenched specimens, while furnace-cooled specimens showed a nearly 50 per cent decrease in the fracture stress in sea water. This decrease in stress-corrosion resistance was also accompanied by a moderate increase in strength and a decrease in ductility.



(a) 1450 F, 4 hr, water quenched, plus indicated heat treatment followed by air cooling.

(b) Indicated heat treatment followed by water quenching, plus 1000 F, 2 hr, air cooled.

FIG. 11—Effect of duplex thermal treatments on the stress corrosion of Ti-6Al-4V.

Examination of microstructures showed a slight increase in the amount of the alpha phase in the furnace-cooled specimen.

Further studies were conducted on the effect of time at 1450 F followed by furnace cooling. The results are shown in Fig. 10 for two different heats of Ti-6Al-4V. The resistance to stress corrosion is greatly reduced as annealing time at this temperature is increased.

These results suggest a dual heat treatment is necessary to induce stress corrosion in Ti-6Al-4V. Holding for long times near 1450 F

apparently establishes a condition that promotes stress corrosion only after a reheat treatment at a lower temperature. This was accomplished as illustrated in the preceding data by slow cooling after holding at 1450 F for 4 to 8 hr.

This dual concept of heat treatment was evaluated in a more systematic manner by first heat treating the alloy at 1450 F for 4 hr, followed by water quenching, and then exposing the material at low temperatures (800 to 1200 F) for various times (0.5 to 25 hr). The results are shown schematically in Fig. 11a.

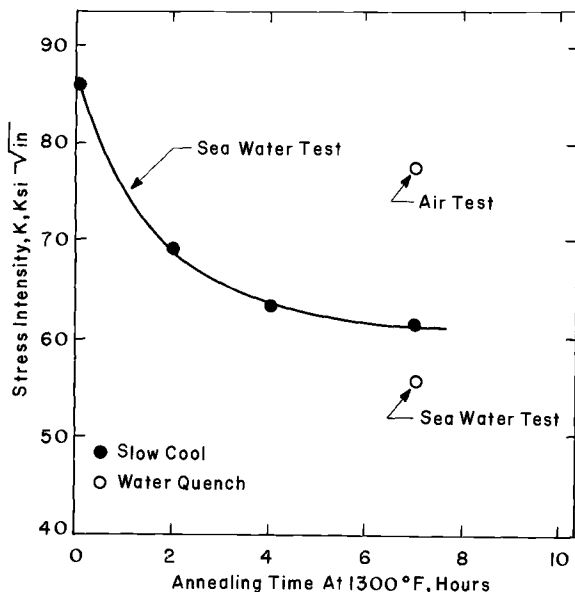


FIG. 12—Effect of annealing time followed by furnace cooling on the stress corrosion of Ti-0.33O-0.30Fe.

Low-temperature exposures at 800 and 1000 F caused stress corrosion with increased susceptibility at longer exposure times. No stress corrosion was noted after 2 hr at 1200 F. This was not unexpected since the Ti_3Al transus is estimated at 1170 F. The area of sensitivity is likely to shift if a different pretreatment is used.

Further studies were conducted on the effect of the pretreatment on stress-corrosion susceptibility. Temperatures of 1350 to 1550 F for 0.5 to 6 hr followed by a water quench were investigated. Each cycle was followed by a 2-hr exposure at 1000 F and air cooling. The results in Fig. 11b show that all the pretreatments resulted in stress corrosion after the 1000 F exposure. The most severe cases were encountered at 1450 F for long times and for shorter times at 1350 F and 1400 F.

The heat-treatment temperature for maximum sensitivity to stress corrosion appears to vary with alloy content. This is illustrated in Fig. 4. The temperature for maximum sensitivity decreases with decreasing aluminum content and appears to be approximately 150 F below the estimated T_{3Al} transus.

Titanium-Oxygen Alloy

The influence of heat treatment on the stress corrosion of Ti-0.33O-0.030Fe alloy was evaluated. Figure 12 shows the influence of annealing time at 1300 F on the failure stress in sea water. Like Ti-6Al-4V, increased annealing time promoted stress corrosion. The microstructures of the two extreme conditions are not appreciably different and do not indicate the cause of stress corrosion.

Although these data were obtained from furnace-cooled specimens, cooling rate does not appear too important. A specimen held for 7 hr and water quenched (Fig. 12) also exhibited a similar decrease in fracture strength in sea water. This indicates the dual-type treatment observed for Ti-6Al-4V is not operative in titanium-oxygen (Ti-O) alloys.

Discussion

Several mechanisms have been suggested for the stress corrosion of metals. Work conducted at Battelle [6] strongly suggests the mechanism in titanium is electrochemical in nature. Active paths by which dissolution occurs must be available. Work reported on copper [7] indicates that transgranular-stress corrosion occurs by dissolution of planar arrays of dislocations. Sanderson and Scully [8] have shown that long pileups of dislocations in Ti-5Al-2.5Sn are chemically more reactive than the matrix. This planar arrangement of dislocations offers a short path for accelerated dissolution, which produces a series of microcracks. Stress concentrations at the microcracks result in ductile tearing of the material between these microcracks. This causes a combined quasi-cleavage and ductile-type fracture which is characteristic of the stress corroded areas [9].

For dissolution to occur, a potential difference must exist between the dislocation and the matrix. Tromans and Nutting [7] have calculated the potential difference between a clean dislocation (no solute atoms present) and the matrix of pure copper. Their results (<0.01 v) indicate the potential difference is not sufficient to account for preferential dissolution at a dislocation. They suggest a potential difference of 0.1 v or greater is necessary. A potential difference of this magnitude is likely to arise only from segregation of solute atoms to a dislocation. This is known to occur extensively in metal systems.

The strong influence of annealing time on the stress corrosion of Ti-

6Al-4V and Ti-O alloys suggests a diffusion-related mechanism. In the case of Ti-6Al-4V, holding at temperatures (1450 F) above the Ti_3Al transus could result in diffusion of aluminum to preferred sites such as dislocations. Reheating of this material below the Ti_3Al transus might result in precipitation of Ti_3Al predominately at dislocation sites. Preliminary studies conducted at RMI indicate a potential difference in synthetic sea water of about 0.2 v between Ti_3Al (Ti-15.8Al) and the matrix phase (Ti-3.5Al) with the Ti_3Al phase being anodic. These results would indicate sufficient potential exists for electrochemical dissolution.

These observations on the stress corrosion of Ti-6Al-4V are similar to a phenomenon noted by Crossley [5] for a Ti-7.8Al alloy. This alloy, aged at 1472 F, appeared to be single phase; however, with the use of an etchant (20 per cent nitric acid, 20 per cent hydrofluoric acid, balance glycerin), a profusion of etch pits was developed. Crossley suggests that this possibly reflects clustering in the solid solution or some other pre-precipitation phenomenon. This same alloy when annealed at 1112 F for 1000 hr developed a two-phase structure consisting of alpha and Ti_3Al .

The role played by oxygen in stress corrosion is not clearly defined since it is reported to have considerable solubility in the alpha phase. The dependency of stress corrosion of Ti-O alloys on annealing time again suggests diffusion of oxygen to preferred sites such as dislocations. Studies of austenitic stainless steels [10,11] show that the interstitial carbon and nitrogen promote stress corrosion by diffusion to dislocations.

High-temperature treatments have been found beneficial for improving stress-corrosion resistance. This is apparently due to an improvement in the intrinsic fracture toughness and the redistribution or redissolving of damaging phases or microsegregation.

The beneficial influence of beta-isomorphous alloying elements on stress corrosion is not clear. Other workers [12] suggest that these elements segregate to dislocations and since they have excellent resistance to chloride attack, they will not preferentially dissolve. This beneficial influence was not noted for pure titanium. Perhaps this suggests that additions such as molybdenum are altering the phase relationship or Ti_3Al kinetics in the high-aluminum containing alloys thus preventing or decreasing the rate of precipitation of Ti_3Al .

Conclusions

The aqueous-stress-corrosion resistance of titanium can be altered substantially by both heat treatment and small changes in chemical composition.

Aluminum contents greater than 6 per cent promoted stress corrosion. The addition of manganese, silicon, and palladium were not beneficial.

However, molybdenum, columbium, and tantalum did improve substantially the resistance of high-aluminum titanium alloys.

Oxygen contents greater than about 0.3 per cent in binary titanium-oxygen alloys result in stress-corrosion susceptibility. The addition of molybdenum in this case, was not beneficial. The amount of oxygen required for stress corrosion decreased as the aluminum content increased.

The stress-corrosion susceptibility of Ti-6Al-4V, Ti-7Al-2Cb-1Ta, and Ti-8Al-1Mo-1V was indirectly related to Ti_3Al formation. A dual heat treatment based on a long time anneal above the Ti_3Al transus (1450 F) followed by a low temperature exposure in the Ti_3Al region was necessary to induce stress corrosion in Ti-6Al-4V.

The stress corrosion of both Ti-6Al-4V and Ti-O alloys was promoted by long annealing times and suggests a mechanism based on diffusion of critical elements to preferred sites such as co-planar dislocations. These preferred sites could become the paths for electrochemical dissolution. Light microscopy did not indicate significant changes that could be related to stress-corrosion observations. This indicates the changes are taking place on an atomic scale and will require more sophisticated studies, such as thin-film microscopy, before the metallurgical relationship to the mechanism can be accurately established.

Acknowledgment

The authors wish to thank several of their co-workers at Reactive Metals, Inc. who contributed to this program. These include: L. J. Bartlo, L. F. Plock, O. Berteau, H. B. Bomberger, and C. L. Dohogne.

References

- [1] Lane, I. R., Jr., Cavallaro, J. L., and Morton, A. G. S., "Sea Water Embrittlement of Titanium," *Stress-Corrosion Cracking of Titanium, ASTM STP 397*, American Society for Testing and Materials, 1966, p. 246.
- [2] Seeley, R. R., Seagle, S. R., and Berteau, O., "Development of a Titanium-Base Alloy for Sea Water Environments," Fall Meeting, American Institute of Mining, Metallurgical, and Petroleum Engineers, Oct. 1966.
- [3] Hatch, A. J., Rosenberg, H. W., and Erbin, E. F., "Effects of Environment on Cracking in Titanium Alloys," *Stress-Corrosion Cracking of Titanium, ASTM STP 397*, American Society for Testing and Materials, 1966, p. 122.
- [4] Brown, B. F., "A New Stress-Corrosion Cracking Test Procedure for High Strength Alloys," *Materials Research and Standards*, Vol. 6, No. 3, March 1966.
- [5] Crossley, F. A., "Titanium-Rich End of the Titanium-Aluminum Diagram," *Transactions, American Institute of Mining, Metallurgical, and Petroleum Engineers*, Vol. 236, No. 8, 1966.
- [6] Williams, D. N. et al, "Studies of the Mechanism of Crack Propagation in Salt Water Environments of Candidate Supersonic Transport Alloy Material," Battelle Memorial Institute, Final Report, Contract No. FA-SS-66-1, Jan. 1966.
- [7] Tromans, D. and Nutting, J., "Stress-Corrosion Cracking of Face-Centered-Cubic Metals," *Corrosion*, Vol. 21, May, 1965, p. 143.
- [8] Scully, J. C. and Sanderson, G., "The Role of Yielding in Stress Corrosion

- Cracking," Annual Conference of the Stress Analysis Group of the Institute of Physics, 1966.
- [9] Judy, R. W., Jr., et al, "Low-Cycle Fatigue-Crack Propagation and Fractographic Investigation of Ti-7Al-2Cb-1Ta and Ti-6Al-4V in Air and Aqueous Environments," *Transactions, American Society for Metals*, Vol. 59, 1966, p. 195.
- [10] Uhlig, H. H. and White, R. A., "Some Metallurgical Factors Affecting Stress Corrosion Cracking of Austenitic Stainless Steels," *Transactions, American Society for Metals*, Vol. 52, 1960, p. 830.
- [11] Uhlig, H. H., *Corrosion and Corrosion Control*, Wiley, New York, 1963, p. 280.
- [12] Feige, N. G. and Murphy, T., "Fracture Behavior of Titanium Alloys in Aqueous Environment," WESTEC Conference, 1966.

Effects of Heat Treating Environmental Conditions on the Stress-Corrosion Cracking Resistance of Several Titanium Alloys

REFERENCE: Howe, D. G. and Goode, R. J., "Effects of Heat Treating Environmental Conditions on the Stress-Corrosion Cracking Resistance of Several Titanium Alloys," *Applications Related Phenomena in Titanium Alloys, ASTM STP 432*, American Society for Testing and Materials, 1968, pp. 189-201.

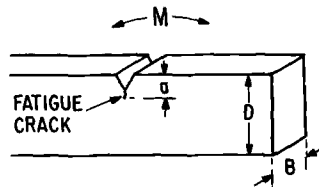
ABSTRACT: The effects of heat treating environmental conditions on the stress-corrosion-cracking resistance of several titanium alloys have been studied. The alloys studied in this investigation were the Ti-8Al-1Mo-1V, Ti-7Al-1Mo-1V, Ti-6Al-4V, and Ti-7Al-2.5Mo alloys. Precracked cantilever type specimens were heat treated in either an inert atmosphere or in vacuum and tested in a 3.5 per cent salt water solution. A comparison of the stress intensity required for failure in salt water with that required for "dry" mechanical fracture indicates that all of these alloys become essentially insensitive to the aqueous environment when vacuum solution annealed and helium gas cooled. Similar heat treatments in argon or helium developed a wide range in level of stress-corrosion-cracking resistance for these alloys; the level was dependent upon the temperatures used. The environmental conditions associated with aging treatments at 1200 F following the solution anneal appear to have little effect on the stress-corrosion-cracking resistance of these alloys. Comparison of the stress-corrosion-cracking data with hydrogen content before and after treatment indicates a close connection between stress-corrosion-cracking sensitivity and hydrogen content in the material even at very low hydrogen levels. These results suggest that hydrogen contained in the metal may play an important role in the stress-corrosion cracking process of titanium alloys.

KEY WORDS: titanium alloys, stress corrosion cracking, heat treatment, vacuum annealing, mechanical properties, fracture toughness, process variables

High-strength titanium alloys have been the subject of a broad based research program at the Naval Research Laboratory. The program is directed to: (1) establishing their usefulness for large, complex structures;

¹ Research physical metallurgists, Metallurgy Div., U.S. Naval Research Laboratory, Washington, D. C. Mr. Goode is a personal member ASTM.

(2) developing guidelines for optimizing their properties through alloy development, processing procedures, and quality control; (3) developing methods by which reliable predictions of structural performance can be made; (4) providing guideline information for materials selection in failure-safe design; and most important, (5) establishing the underlying principles that affect the properties of these alloys and then utilizing them to advance the titanium technology. This program is based upon the philosophy that large, complex structures cannot be fabricated, tested, and put into service for any length of time without having flaws present in critically stressed regions. Therefore, the failure-safe design of such structures must take into account the crack propagation characteristics



$$K_I = \frac{4.12 M \sqrt{\frac{1}{\alpha^3} - \alpha^3}}{BD^{3/2}} \quad (\text{Eq. 1})$$

$$\alpha \equiv 1 - \frac{a}{D}$$

(a)

CANTILEVER SPECIMEN

FIG. 1—Cantilever specimen and cantilever bend equation for stress intensity parameter.

of these alloys in terms of fracture toughness, low-cycle and corrosion fatigue, and stress-corrosion cracking.

This paper summarizes present results of an investigation concerning the effects of heat treatment environmental conditions on the salt water stress-corrosion cracking resistance of several alloys of the Ti-Al-Mo-V system. In addition, data are presented showing the effectiveness of the heat treating atmosphere in removing interstitial hydrogen as well as showing at least a conjunctive relation between interstitial hydrogen and stress-corrosion cracking resistance. Detailed reports covering most segments of this study can be found in Refs 1-4.

Materials and Procedures

The alloys studied in this investigation were Ti-8Al-1Mo-1V, Ti-7Al-1Mo-1V, Ti-6Al-4V, and Ti-7Al-2.5Mo in the form of 1 to 1.25-

in.-thick plate. These plates are representative of commercial practice, and the nominal chemical compositions include a maximum oxygen content of 0.08 per cent by weight and interstitial hydrogen content of 60 to 130 ppm.

A specimen configuration was used similar to that of Brown and Beachem [5],² with the fracture direction in the RT and WT orientation [6]. A schematic of the specimen is shown in Fig. 1. In the RT orientation, the specimen length is along the rolling direction of the plate and the direction of propagation in the fracture plane is through the thickness of the plate. In the WT orientation, the specimen length is normal to the rolling direction and the direction of propagation in the fracture plane is also through the thickness of the plate. Type A specimens were $\frac{3}{8}$ in. wide, 1 in. high, 5 in. long, and side notched to a depth of $\frac{1}{16}$ in. Type B specimens were $\frac{1}{2}$ in. wide, 1 in. high, 5 in. long, and side notched to a depth of $\frac{1}{32}$ in. Type C specimens were $\frac{1}{2}$ in. wide, $1\frac{1}{4}$ in. high, 5 in. long, and side notched to a depth of $\frac{1}{32}$ in. All specimens were machined, side notched, and fatigued until the fatigue crack had propagated approximately $\frac{1}{8}$ in. from the root of the notch. The specimens were then degreased using methyl ethyl ketone in place of other degreasing solvents which contain chlorides which might be detrimental to the stress corrosion cracking (SCC) resistance of the material. After degreasing, the specimens were washed with analytical grade acetone and dried in air before heat treatment. The atmospheres used in heat treating were vacuum, helium, and argon. In several cases, specimens were fatigued after heat treatment, and the test results were the same as those fatigued before heat treatment.

An Inconel muffle was used for the heat treatments conducted in argon where air cooling and water quenching were applied. A "cold-wall" vacuum furnace was used for the vacuum, helium, and argon environmental heat treatments where furnace cooling or helium cooling was applied.

The cantilever stress-corrosion cracking (SCC) test method [5] was used to determine the effect of heat treatment on the stress-corrosion cracking resistance of the titanium alloys in a 3.5 per cent sodium chloride (NaCl) solution. In this procedure the specimen is stressed in cantilever bending with the precracked zone surrounded by a plastic container holding the 3.5 per cent NaCl solution. A moment M is imposed upon the precracked notch by weights at the end of the lever arm which is clamped to the specimen, and the time is noted for final fracture. If subcritical crack growth is not accomplished due to the corrosive environment at the preselected load, the moment is increased. This procedure is repeated in step-wise fashion until crack extension does occur

² The italic numbers in brackets refer to the list of references appended to this paper.

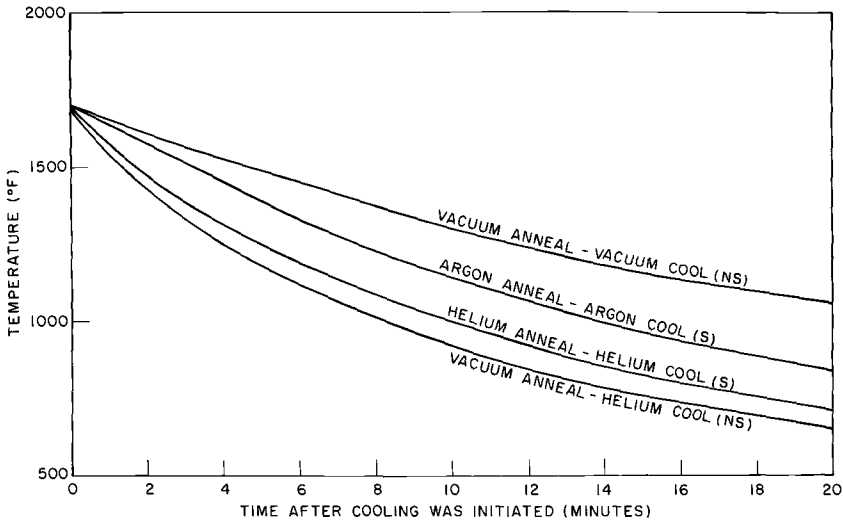


FIG. 2—Cooling curves for the Ti-7Al-1Mo-1V alloy under several different environmental conditions after a 1700 F solution anneal.

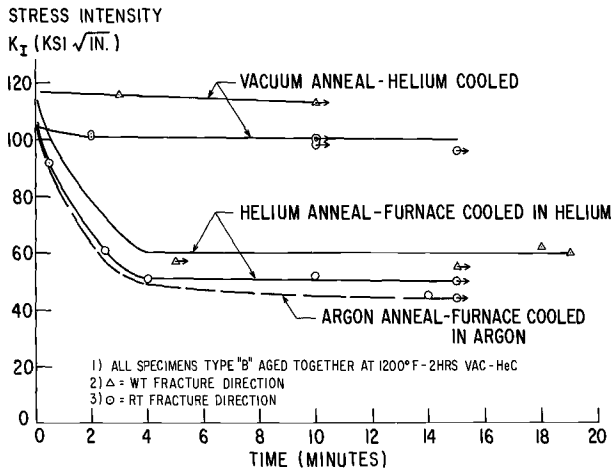


FIG. 3—SCC resistance of Ti-7Al-1Mo-1V alloy resulting from different environmental conditions during a 1 hr/1700 F solution anneal.

eventually failing the specimen. The time at maximum load before failure is then recorded. The times at each specific loading are plotted in graphical form versus the calculated stress intensity of the applied loads.

The torque M and specimen dimensions are converted to the stress intensity parameter K_I through the use of an equation (Fig. 1) developed by Joseph Kies of the Mechanics Division at the U.S. Naval Research Laboratory (NRL) [7]. The minimum value of K_I which is observed to

TABLE 1—Effects of several heat treatments on the resistance of the alloy Ti-7Al-1Mo-1V (T-88) to stress-corrosion-cracking in a 3.5 per cent sodium chloride solution.

Solution Heat Treatment	Aging Heat Treatment	Specimen Type	$K_{I_{sec}}$, ksi $\sqrt{in.}$	Hydrogen Content, ppm by weight
1950 F, 1 hr vacuum, helium cooled	1200 F, 2 hr vacuum, helium cooled	A	115	8
1950 F, 1 hr vacuum, helium cooled	1200 F, 2 hr argon, air cooled	A	109	8
1950 F, 1 hr vacuum, helium cooled	1200 F, 2 hr argon, air cooled	B	109	8
1950 F, 1 hr vacuum, helium cooled	1200 F, 2 hr argon, water quenched	A	118	7
1950 F, 1 hr vacuum, helium cooled	1200 F, 2 hr argon, water quenched	B	105	7
1700 F, 1 hr vacuum, helium cooled	1200 F, 2 hr vacuum, helium cooled	A	117	...
1700 F, 1 hr vacuum, helium cooled	1200 F, 2 hr vacuum, helium cooled	B	112	23
1700 F, 1 hr vacuum, helium cooled	1200 F, 2 hr argon, air cooled	A	101	...
1700 F, 1 hr vacuum, helium cooled	1200 F, 2 hr argon, air cooled	B	109	19
1700 F, 1 hr vacuum, helium cooled	1200 F, 2 hr argon, water quenched	A	118	...
1700 F, 1 hr vacuum, helium cooled	1200 F, 2 hr argon, water quenched	B	114	23
1700 F, 1 hr argon, air cooled	1200 F, 2 hr vacuum, helium cooled	A	68	38
1700 F, 1 hr argon, air cooled	1200 F, 2 hr argon, air cooled	A	64	44
1700 F, 1 hr argon, air cooled	1200 F, 2 hr argon, water quenched	A	66	46

TABLE 2—Effects of heat treating environmental conditions on several properties of the Ti-7Al-1Mo-IV alloy.^a

Solution Heat Treatment	0.2% Yield Strength, ksi	Ultimate Tensile Strength, ksi	Reduction of Area, %	Elongation, %	Specimens	K_{Ic} , no break, ksi $\sqrt{\text{in.}}$	Time, Min	K_{Isc} , ksi $\sqrt{\text{in.}}$	Time, Min	K_{Ic} , dry break, ksi $\sqrt{\text{in.}}$
As-received condition...	121.3(RW)	131.6	26.5	14.2	Type D 0.313 in. dia tensiles	80	...	111
1700 F, 1 hr vacuum, helium cooled.....	125.7(WR)	135.0	23.0	11.2	Type D 0.313 in. dia tensiles
1700 F, 1 hr vacuum, helium cooled.....	120.1(RW)	128.0(RW)	44.3	16.4	Type D 0.313 in. dia tensiles	98(RT) 104(RT)	90 15	105(RT)	1	105(RT)
1700 F, 1 hr vacuum, helium cooled.....	119.1(WR)	127.0(WR)	38.9	15.7	Type D 0.313 in. dia tensiles	101(WT) 106(WT) 108(WT)	60 30 20	112(WT)	3	112(WT)
1700 F, 1 hr helium, helium cooled.....	122.8(RW)	127.7	35.8	16.3	Type M-1 0.250 in. dia tensiles	50(RT)	15	51(RT)	4	105(RT) est.
1700 F, 1 hr helium, helium cooled.....	117.6(WR)	123.4	38.2	16.5	Type M-1 0.250 in. dia tensiles	55(WT)	15	58(WT)	8	113(WT) est.
1700 F, 1 hr vacuum, vacuum cooled.....	115.6(RW)	121.6	35.7	16.3	Type M-1 0.250 in. dia tensiles	103(RT)	15	105(RT)	1	105(RT)
1701 F, 1 hr vacuum, vacuum cooled.....	111.8(WR)	117.8	43.3	17.3	Type M-1 0.250 in. dia tensiles	111(WT)	10	114(WT)	1	114(WT)

NOTE: All heat treated specimens were given aging treatment at 1200 F for 2 hr in vacuum followed by helium cooling. SCC specimens are Type B.

^a Fine grained microstructure in the as-received condition.

cause SCC is designated $K_{I_{SCC}}$. The value K_{I_x} is the stress intensity associated with failing the specimen dry in air.

The interstitial hydrogen contents were determined using a vacuum extraction method described in Ref 8.

Experimental Results

It has been observed in practice that slow cooling after final rolling or heat treating generally promotes low resistance to SCC. Therefore, it was desirable to sort out the effect of the cooling rates involved in this investigation from the effects of the heat treating atmospheres. The

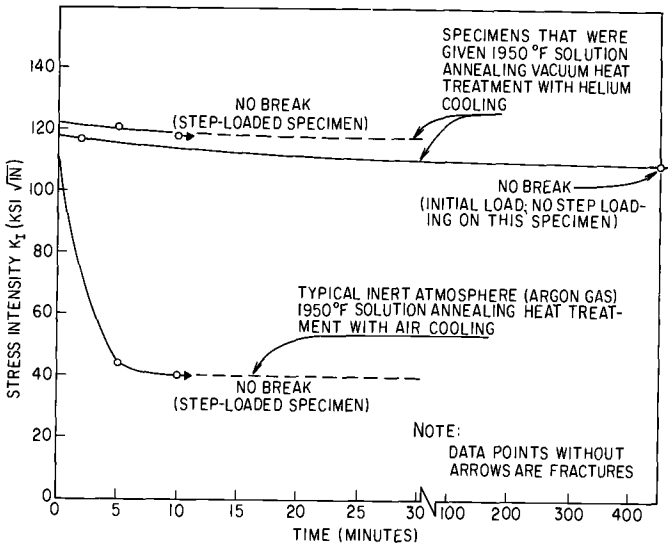


FIG. 4—Stress intensity versus time curves for the alloy Ti-8Al-1Mo-1V in several heat treated conditions (tested in 3.5 per cent sodium chloride solution).

Ti-7Al-1Mo-1V alloy was used to establish the cooling rates involved in solution annealing at 1700 F and in subsequent cooling to about 1000 F or less. These curves are shown in Fig. 2. The designations NS and S represent nonsusceptible and susceptible to SCC, respectively. Cooling in a static argon or helium atmosphere was, respectively, about two and three times faster than cooling in vacuum. The helium cool following the vacuum anneal (lowest curve) initially was in a flowing atmosphere of room temperature helium gas. The flowing gas purge was continued for about the first 3 min (required to backfill the vacuum chamber) after which a static condition was maintained. However, as will be seen from the experimental results, the cooling rates used in this study did not have any measurable effect on the SCC resistance of the alloys investigated.

All specimens annealed in vacuum were essentially immune to SCC regardless of cooling rate.

The effects of a solution anneal at 1700 F in vacuum, argon, and helium followed by a 1200 F age in vacuum and helium cool are shown in Fig. 3. Vacuum solution annealing resulted in a material essentially immune to SCC as indicated by the high K_{Isc} values, whereas the material solution annealed in argon and helium had a fairly low resistance to SCC. Compared to solution annealing the 1200 F aging treatment does not appear to have been of much significance with regards to SCC resistance. Additional specimens vacuum annealed at 1700 F for 1 hr followed by a vacuum cool (no age) had the same high K_{Isc} values as the vacuum anneal-helium cool.

The effect of vacuum solution annealing above and below the β transus (1840 F) of the Ti-7Al-1Mo-1V alloy is shown in Table 1 along with the resultant interstitial hydrogen content. The results show that for the two temperatures used vacuum annealing results in a material with high resistance to SCC. Contrasted to this are the results obtained for the same material with a 1700 F anneal in argon-air cool which showed only moderate resistance to SCC. The 1200 F age treatments again did not appear to be of significance. Vacuum annealing is seen to be most effective in removing interstitial hydrogen with the resultant level of hydrogen content dependent upon temperature at a constant time.

The effects of heat treating environmental conditions on several properties of the Ti-7Al-1Mo-1V alloy are shown in Table 2. Type D (0.313 in. diameter) tensile data were obtained where sufficient specimen length would permit. On the specimens with a shorter length, Type M-1 (0.250 in. diameter), tensile data were obtained.

The effect of solution annealing above the β transus (1885 F) in vacuum and in argon on the SCC resistance of a Ti-8Al-1Mo-1V alloy is shown in Fig. 4. Here again the highly SCC resistant material is associated with the vacuum anneal, whereas the β solution anneal in an inert atmosphere resulted in material with the expected low resistance to SCC.

The data for the vacuum annealed Ti-8Al-1Mo-1V alloy also serve to indicate that problems did not arise which could be associated with blunting of the fatigue crack as a result of step loading the specimens. The step-loaded specimen broke in the salt water at a K_I value of about $121 \text{ ksi}\sqrt{\text{in}}$. A second specimen was then given an initial load to correspond to a K_I of $110 \text{ ksi}\sqrt{\text{in}}$, which was held for 450 min without any crack extension. The stress intensity was then increased to $117 \text{ ksi}\sqrt{\text{in}}$, with failure occurring in 2 min. It should be emphasized that for titanium alloys these high values represent mechanical fracturing.

Results of a 1700 F vacuum solution anneal followed by a 1200 F age in vacuum on the SCC resistance of the Ti-6Al-4V and Ti-7Al-2.5Mo alloys are shown in Tables 3 and 4. These alloys were only moderately

TABLE 3—Effects of vacuum heat treatment on the resistance of the alloy Ti-6Al-4V (T-27)^a to stress-corrosion cracking in a 3.5 per cent sodium chloride solution.

	Solution Annealing Time in Vacuum at 1700 F., helium Cooled, hr	Aging Time in Vacuum at 1200 F., helium Cooled, hr	C ₀ ft.-lb. at +32 F	0.2% Yield Strength, ksi	Ultimate Tensile Strength, ksi	Elongation, %	Reduction of Area, %	K _{Isc} , ksi√in.	K _{Isc} , ksi√in.	Hydrogen, ppm by weight
As-received condition	26(RW)	115.5(RW)	126.0	12.7	29.4	72(WT)	105(WT)	61
1	26(WR)	120.2(WR)	128.8	11.6	28.1
1	2	2	33(WR)	119.8(WR)	125.5	15.0	32.8	...	105(WT)	23
1	2	2	33(WR)	120.4(WR)	125.3	15.0	28.1	106(WT)	...	28
1	37(WR)	118.8(WR)	124.2	15.0	31.3	113(WT)	...	34
1	36(WR)	119.7(WR)	124.6	12.0	27.5	98 ^b (WT)
4	...	2	38(WR)	116.4(WR)	121.9	17.0	33.3	...	116(WT)	14
4	...	2	36(WR)	117.0(WR)	123.2	15.0	39.7	114(WT)	...	19

NOTE: Type B SCC specimens.

Type M-1 0.250 in. diameter tensiles.

Stress-corrosion cracking tests were conducted 2 months after vacuum heat treatment.

^a Fine grained microstructure in the as-received condition.

^b Stress-corrosion cracking tests were conducted 9 months after vacuum heat treatment. No visible evidence of SCC in vacuum solution annealed specimens.

TABLE 4—Effects of vacuum heat treatments on the resistance of the alloy Ti-7Al-2.5Mo (T-94)^a to stress-corrosion cracking in a 3.5 per cent sodium chlorite solution.

Solution Annealing Time in Vacuum at 1700 F, Helium Cooled, hr	Aging Time in Vacuum at 1200 F, Helium Cooled, hr	C ₀ ft.-lb at +32 F	0.2% Yield Strength, ksi	Ultimate Tensile Strength, ksi	Elongation, %	Reduction of Area, %	K _{Isc} , ksi√in.	K _{Ic} , ksi√in.	Hydrogen, ppm by weight
As-received condition	...	27 (RW)	119.2 (RW)	133.2	8.6	24.1	80 (WT)	101	70
1	...	30 (WR)	120.5 (WR)	134.8	8.6	20.2
1	2	31 (WR)	126.4 (WR)	133.6	16.0	25.4	...	109 (WT)	28
1	2	33 (WR)	126.2 (WR)	133.6	14.0	29.5	95 (WT)	...	25
1	...	44 (WR)	124.5 (WR)	132.0	15.0	30.8	110 (WT)	...	30
1	...	44 (WR)	123.4 (WR)	130.8	14.0	36.0	100 ^b (WT)	...	20

NOTE: Type C SCC specimens.

Type M-1 0.250 in. diameter tensiles.

Stress-corrosion cracking tests conducted 2 months after vacuum heat treatment.

^a Fine grained microstructure in the as-received condition.

^b Stress-corrosion cracking tests conducted 9 months after vacuum heat treatment. No visible evidence of SCC in vacuum solution annealed specimens.

sensitive to salt water SCC in the as-received condition. The limited data indicate that for these alloys solution annealing in vacuum promotes high SCC resistance to the material. The data (Tables 3 and 4) also indicate that the aging treatment contributed little towards promoting low levels of interstitial content. Not unexpectedly, the lowest hydrogen contents were associated with the longest annealing times.

A summary of the K_{Isc} values obtained as a result of various heat treatments compared to the residual interstitial hydrogen contents for all four of the alloys investigated is shown in Fig. 5. It is interesting to note that for these alloys where the hydrogen contents were at very low

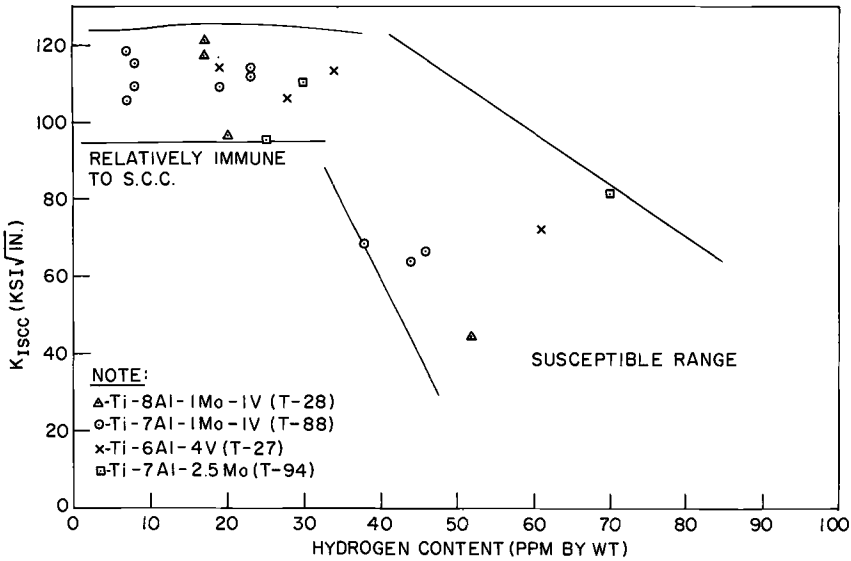


FIG. 5—SCC resistance of several titanium alloys.

values the material was highly resistant to SCC. For the higher levels of hydrogen content, varying degrees of SCC susceptibility were observed. To some, this would appear to indicate that the interstitial hydrogen present in the alloy plays a significant role in the salt water SCC and possibly it does, but the data reported here are not considered sufficient to support this causal relationship. In any case, the data show that vacuum heat treating at solution annealing temperatures promotes significant improvement to the SCC resistance of the alloys considered in this investigation and that there is at least a conjunctive relationship between SCC resistance and interstitial hydrogen content.

Conclusions

It has been shown that vacuum solution annealing is effective in essentially eliminating the SCC susceptibility of the alloys Ti-7Al-1Mo-1V,

Ti-8Al-1Mo-1V, Ti-6Al-4V, and Ti-7Al-2.5Mo. Associated with this high resistance is a lowering of interstitial hydrogen content to very low levels. Solution annealing in inert gas atmospheres was not generally very effective in promoting high SCC resistance to the alloys studied and neither was it as effective in lowering the interstitial hydrogen content of the material. The aging treatments did not appear to have much influence on the level of SCC resistance attained in any of the alloys as a result of solution annealing atmosphere or temperature. A conjunctive relationship has been established between the interstitial hydrogen content and SCC resistance of these titanium alloys, providing unequivocal proof of the existence of a causal relationship between the two was beyond the scope of this investigation, but the data suggest that such a relationship might exist in which case a threshold level may also exist (Fig. 5) for the interstitial hydrogen (may be characteristic for each alloy) above which decreasing resistance to SCC can be expected and below which the alloys are essentially immune to SCC in salt water. This threshold value may very well fall at a level well below the solubility limit of the alloy. A permanent high resistance to SCC would be dependent upon not having additional hydrogen absorbed into the structure during actual service conditions. In this regard, vacuum heat treated alloys shelf-stored for as long as nine months in normal laboratory air have not shown any evidence of becoming susceptible to SCC due to the environment.

Acknowledgments

The authors are grateful to E. J. Chapin and B. F. Brown for their interest and helpful discussions concerning this investigation. The hydrogen analyses were performed by W. A. Fraser, and many of the heat treatments were performed by R. W. Scott and C. R. Forsht. The authors also owe their gratitude to R. L. Newbegin who aided in conducting several of the tests as well as to the Advanced Research Project Agency for sponsoring this work under ARPA Order 878.

References

- [1] Howe, D. G., "Effects of Heat Treatment on the Stress-Corrosion-Cracking Resistance of Several Ti-Al-Mo-V Alloys," Report of NRL Progress, Naval Research Laboratory, Feb. 1966, pp. 14-18.
- [2] Howe, D. G., "Properties of Ultrahigh Strength Alloys (Effects of Heat Treatment on the Stress-Corrosion-Cracking Resistance of Several Ti-Al-Mo-V Alloys)," Report of NRL Progress, Naval Research Laboratory, July 1966, pp. 20-21.
- [3] Howe, D. G., "Properties of Ultrahigh Strength Alloys (Effects of Heat Treatment on the Stress-Corrosion-Cracking Resistance of Several Ti-Al-Mo-V Alloys)," Report of NRL Progress, Naval Research Laboratory, Sept. 1966, pp. 25-27.
- [4] Howe, D. G., "Effects of Heat Treating Environmental Conditions on the

- Stress-Corrosion-Cracking Resistance of Several Titanium Alloys," Report of NRL Progress, Naval Research Laboratory, Feb. 1967, pp. 32-35.
- [5] Brown, B. F. and Beachem, C. D., "A Study of the Stress Factor in Corrosion Cracking by Use of the Pre-Cracked Cantilever Beam Specimen," *Corrosion Science*, Vol. 5, No. 11, 1965, pp. 745-750.
- [6] The ASTM Committee on Fracture Testing of High-Strength Metallic Materials, "The Slow Growth and Rapid Propagation of Cracks," (Second Report), *Materials Research & Standards*, Vol. 1, No. 5, May 1961.
- [7] Kies, J. A. et al, "Fracture Testing of Weldments," *Fracture Toughness Testing and Its Applications*, ASTM STP 381, American Society for Testing and Materials, 1965.
- [8] Eborall, R., "Vacuum Extraction Method," Iron and Steel Institute Special Report No. 68, 1960, p. 192.

Environmental Related Phenomena

The Initiation of Hot-Salt Stress Corrosion Cracking of Titanium Alloys*

REFERENCE: Rideout, S. P., "The Initiation of Hot-Salt Stress Corrosion Cracking of Titanium Alloys," *Applications Related Phenomena in Titanium Alloys, ASTM STP 432*, American Society for Testing and Materials, 1968, pp. 205–217.

ABSTRACT: The initial stages of hot-salt stress corrosion cracking of titanium alloys were studied using hot-stage microscopy and cinematography. An incubation period for cracking was observed, the duration of which depends on exposure temperature, salt composition, and alloy composition. For Ti-8Al-1Mo-1V exposed to sodium chloride (NaCl) the incubation period decreased from about 96 hr at 475 F, to 20 hr at 500 F, to 1½ hr at 650 F, to only 10 min at 850 F. This same alloy cracked severely in only 20 min at 475 F when exposed to tin chloride (SnCl₂) indicating that the apparent "threshold temperature" for cracking is strongly influenced by chemical environment. At 650 F the incubation period for NaCl cracking of four alloys containing aluminum increased with decreasing aluminum content. Cracks appeared abruptly and propagated rapidly for a short distance, then apparently paused for additional corrosion-embrittlement to occur. Moisture was demonstrated to be a vital ingredient in hot-salt attack, and the presence of absorbed hydrogen in salt-corroded areas has been demonstrated using radiotracer tritium (H³). These results support the hypothesis that absorption of corrosion-produced hydrogen promotes embrittlement and crack initiation.

KEY WORDS: titanium alloys, stress corrosion, hot-salt cracking, hot-stage microscopy, crack initiation

Rapid advancements in the technology of titanium alloys have been made during the past five years, and there has been a sharp increase in the use of these alloys in the production of jet engines and airframes. A number of problems remain, however, that may hinder further increases in applications of titanium alloys. Among these problems, the phenomenon known as "hot-salt stress corrosion cracking" is of interest to the aircraft industry. This form of stress corrosion damage can occur when certain halide salts are present as surface contaminants on titanium alloys that are stressed and exposed to elevated temperatures. Fortunately,

* Work performed under NASA Purchase Order No. R-124, issued to the United States Atomic Energy Commission.

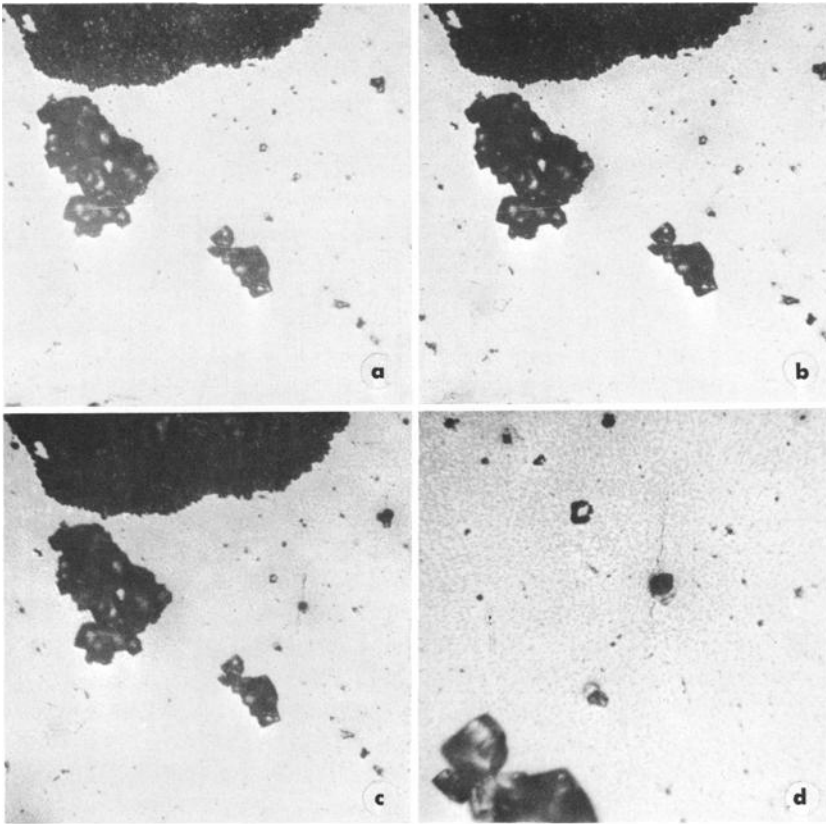
¹ Savannah River Laboratory, E. I. du Pont de Nemours and Co., Aiken, S. C.

this phenomenon was first revealed by laboratory tests rather than by a rash of service failures. Some cases of cracking have occurred during fabrication heat treatments [1].² The threat of hot-salt cracking in service is of great concern because salt contamination of aircraft is certain to occur in coastal airports.

Extensive laboratory investigations of hot-salt cracking have been performed, and the results of these were reviewed at a recent symposium [2]. Although much has been learned about the conditions under which cracking can occur, many aspects of the phenomenon are not adequately understood. For example, it has been reported that cyclic heating from room temperature to 550 F causes much less stress corrosion damage than continuous heating at 550 F [3,4]. This implies that some time at temperature is required for corrosion reactions to produce conditions that lead to cracking. It has been suggested that absorption of corrosion-produced hydrogen causes embrittlement, and radiotracer studies have shown that hydrogen is present in salt-corroded areas of the metal [5]. Another suggestion is that some crack-promoting phase is generated by the salt reactions, and that this phase is converted to a harmless product during the cooling portions of cyclic exposures [4]. Various crack-promoting phases have been suggested, including liquid [1], gaseous [6], and solid [7]. The concept of a crack-promoting phase has also been advanced in connection with a hypothesis that there is a threshold temperature for hot-salt cracking which corresponds to the minimum temperature for formation of the critical phase. However, the minimum temperature for hot-salt cracking depends on several variables such as stress level and alloy composition [8], and a specific threshold temperature has not been identified. Because of these and other uncertainties, the mechanism of hot-salt cracking has remained in doubt.

A program of research to develop fundamental knowledge about the mechanism of hot-salt cracking is in progress at the Savannah River Laboratory under the sponsorship of the National Aeronautics and Space Administration. This paper presents the results of a part of that program in which the initial stages of cracking were studied using hot-stage microscopy and cinematography. The specific objectives of these studies were to observe the nature of hot-salt attack on the metal surface, looking especially for any relationship between visible corrosion products and crack initiation, and to determine the effects of alloy composition and exposure temperature on the initiation of cracks. Several important features of the cracking process were revealed which help to explain the different effects of cyclic versus static exposures. Also, additional evidence was obtained supporting a hypothesis advanced in a previous

² The italic numbers in brackets refer to the list of references appended to this paper.



(a) Salt deposit at room temperature ($\times 320$).
 (b) Same as (a) after reaching 650 F ($\times 320$).
 (c) Same as (b) after 80 mm ($\times 320$).
 (d) Same as (c) enlarges to $\times 800$.

FIG. 1—Hot-stage microscopy of sodium chloride cracking of Ti-8Al-1Mo-1V at 650 F.

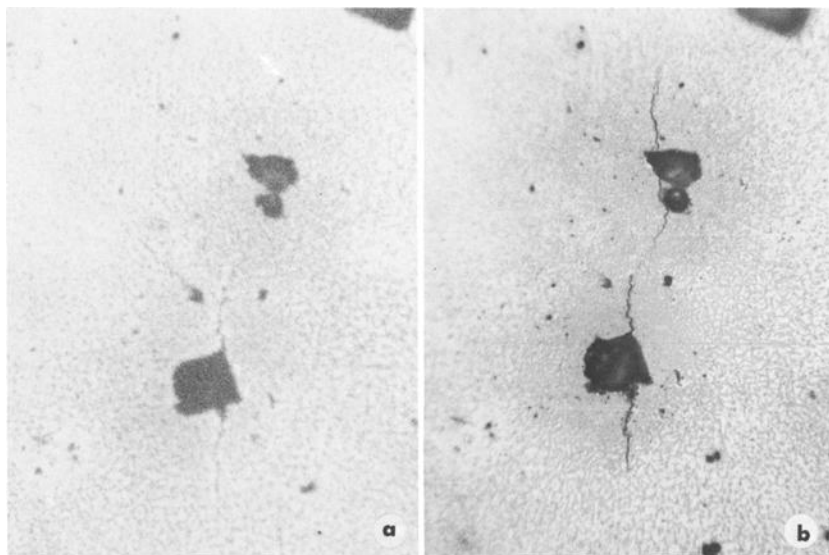
paper [5] that moisture is a critical ingredient in hot-salt attack and that absorption of corrosion-produced hydrogen promotes cracking.

Experimental Procedures

All specimens were strips $\frac{3}{4}$ by 3 in. with metallographically polished surfaces. The specimens were stressed in four-point loading fixtures to a calculated fiber stress of 100,000 psi at room temperature, which caused them to yield slightly when heated to test temperatures. For experiments to determine the time to initiate cracking, deposits of sodium chloride (NaCl) were applied in the area of maximum stress by evaporating three drops of saturated aqueous solution on the specimens at room temperature. (A few tests were performed using other chloride

salts, as indicated in the discussion.) This procedure produced a fairly dense deposit of coarse crystals covering a spot about $\frac{1}{2}$ in. in diameter. Multiple specimens were then heated isothermally in stagnant air using a small electric oven. Specimens were removed at intervals, and, after removing the salt deposits, the surfaces were microscopically examined for evidence of cracking.

In order to permit direct observation of salt reactions on specimens examined by hot-stage microscopy, droplets of a very dilute salt solution

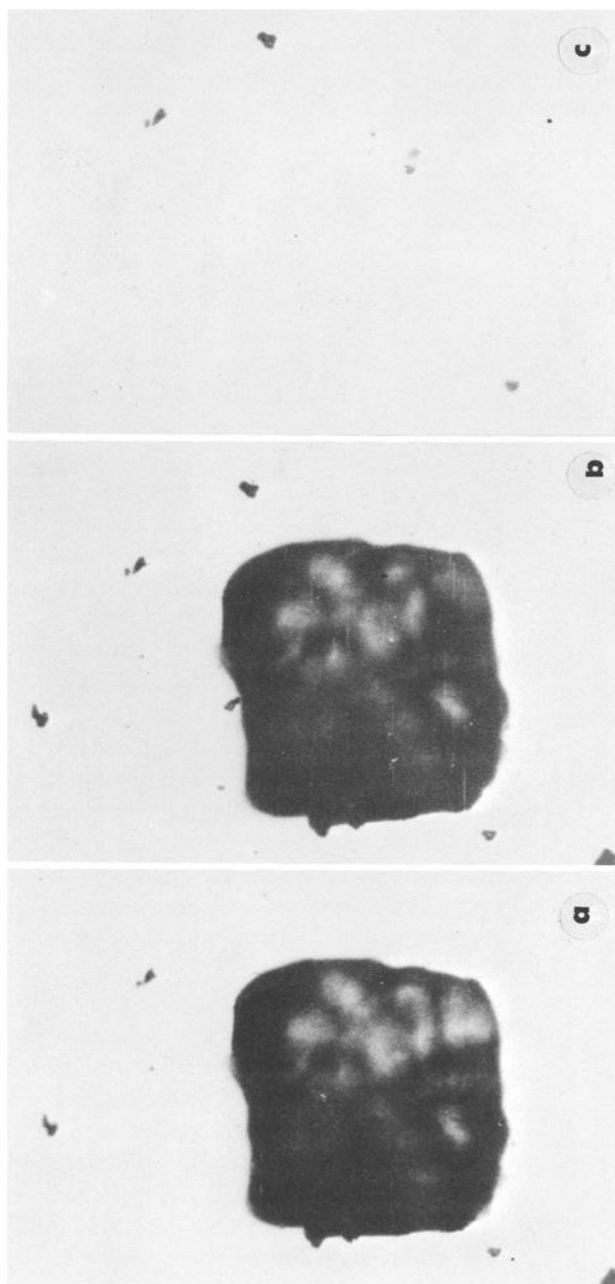


(a) 85 min after reaching 650 F.
(b) 185 min after reaching 650 F.

FIG. 2—Hot-stage microscopy of sodium chloride cracking of Ti-8Al-1Mo-1V at 650 F ($\times 720$).

were evaporated on the pre-polished surfaces. The resulting salt crystals were small enough to be viewed with a conventional metallurgical microscope. Specimen heating was accomplished by placing a tiny, hand-made coil of resistance wire against the underside of the specimen and adjusting the current with a powerstat. Asbestos cloth was used to insulate the specimen loading fixture, which was positioned directly on the microscope stage.

The temperature in the area of the salt deposit was measured with a fine-wire thermocouple held in contact with the surface. Although the temperature control was not precise, this simple arrangement proved to be quite satisfactory, and the times observed for initiation of cracking at any given temperature agreed reasonably well with those determined by



(a) Room temperature.
(b) Same as (a) after 90 min at 650 F.
(c) Same as (b) after cooling to room temperature and removal of salt crystal.

FIG. 3—Hot-stage microscopy of Ti-8Al-1Mo-1V exposed to predried sodium chloride at 650 F ($\times 300$).

the isothermal oven tests. Photomicrographs at magnifications up to $\times 720$ were obtained with a 35-mm camera. Movies of the hot-salt stress corrosion process were made through the microscope at magnifications up to $\times 200$ using a 16-mm camera equipped with a single frame attachment for speeds down to one frame per second.

Results and Discussion

Hot-Stage Microscopy of Ti-8Al-1Mo-1V

The relationship between corrosion and the initiation of cracking by NaCl was studied first on specimens of Ti-8Al-1Mo-1V at 650 F. The direct, hot-stage microscopic observations revealed that corrosion stains began to develop within minutes after the specimen surface reached 650 F, but cracking did not begin until about $1\frac{1}{4}$ to $1\frac{1}{2}$ hr later.

Initially, the corrosion stains appeared as microscopic speckles that developed on the metal around the salt crystals. The number of speckles increased with time, Fig. 1*a*, *b*, and *c*, and gradually formed a fairly continuous stain around the salt. However, the stains did not appear to form by surface diffusion of reaction products spreading out from salt-metal contact areas, and the initiation of cracking occurred before the stain became continuous, Fig. 1*d*.

Cracks appeared abruptly, propagated rapidly for a short distance, and then apparently paused for additional corrosion-embrittlement to occur. Further propagation also appeared to occur by abrupt extensions. Although cracks always originated at points of salt contact, there was no apparent relationship between the size of the salt crystals and the size of the cracks. Many cracks were initiated at extremely small salt crystals. At various intervals after the first cracks appeared, additional cracks were initiated at other sites. In many cases, these sites were close together and the cracks connected to form larger cracks. An example of this is shown in Fig. 2.

The speckled corrosion stain has not been identified, but it has been shown to be a very thin, nonadherent flaky substance which tends to spall off as the specimens cool to room temperature and which is completely removed by a water rinse. It was concluded that the speckled stain is produced by reactions with constituents (probably chloride ions and moisture) adsorbed on the specimen surface. In order to prove that the speckles were not produced by reactions with constituents in the air, specimens that had not been wetted with salt water were heated with and without predried salt crystals on their surfaces. No corrosion stains were produced in either case, which indicated that adsorbed constituents caused the stains and also demonstrated that moisture is a vital ingredient in the hot-salt corrosion process, Fig. 3. Previous work [5] with radiotracer tritium (H^3) in the solutions from which salt was deposited on specimens showed that hydrogen is absorbed in salt-corroded areas.

The combined results of the radiotracer studies and hot-stage microscopic observations support the hypothesis that absorption of corrosion-produced hydrogen promotes crack initiation.

Effects of Temperature on Cracking of Ti-8Al-1Mo-1V by NaCl

The effect of exposure temperature on the incubation period for crack initiation in Ti-8Al-1Mo-1V is shown in Fig. 4. The incubation period

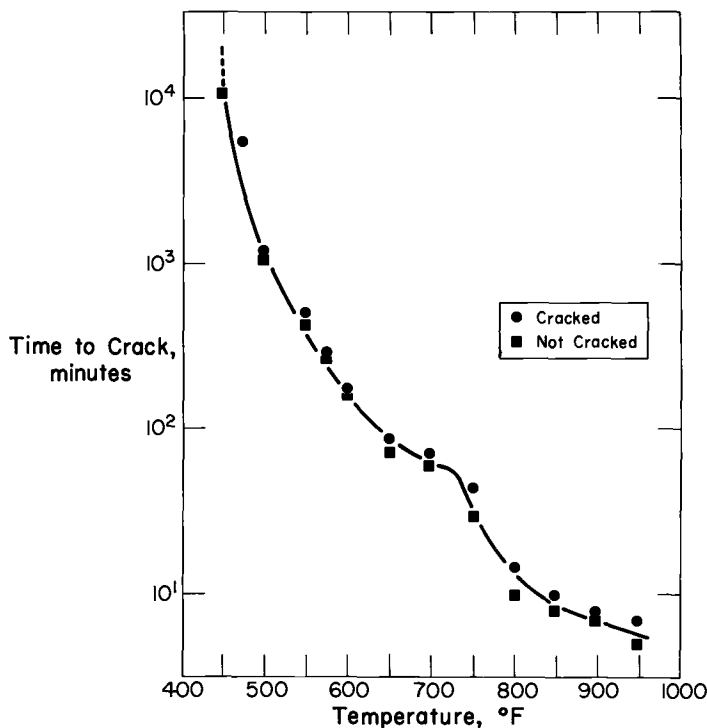
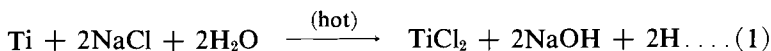


FIG. 4—Time to initiate cracking by sodium chloride in Ti-8Al-1Mo-1V versus temperature.

decreased from about 96 hr at 475 F to 20 hr at 500 F to about 1 hr at 700 F. An obvious inflection occurred in the incubation-temperature curve between 700 and 750 F. From 750 to 950 F the incubation period decreased from about 45 min to only about 6 min. These results indicate two significant points for discussion: (1) the long incubation periods at the lower temperatures provide an explanation for previous reports that cyclic heating to 550 F caused less stress corrosion damage than continuous heating at the same temperature [3,4], and [2] the inflection in the incubation time-temperature curve indicates a change in the salt stress corrosion process between 700 and 750 F.

During cyclic exposures in which the time at temperature is less than

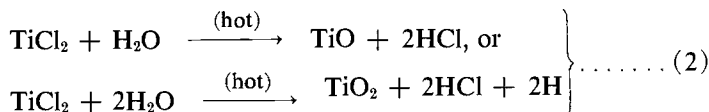
the incubation period, the initiation of cracking either will not occur or will require some number of cycles before sufficient corrosion-embrittlement occurs to produce cracking. Pride and Woodward [3] have demonstrated that increasing the time-at-temperature portion of cyclic exposures does increase the extent of damage in residually stressed specimens. Piper and Fager [4] used a 3-hr cycle between room and 500 F temperatures with rewetting in salt solutions after each cycle, and they reported no damage in dead-weight loaded tension specimens after a total time of 2000 hr. Their time-at-temperature during each cycle was 2½ hr, which is considerably shorter than the incubation period (about 10 hr) at 550 F shown in Fig. 4. Piper and Fager [4] suggested that some detrimental corrosion product generated at 550 F might be washed off or converted to a harmless form during the room-temperature portion of their cycle. This is a definite possibility, especially if the corrosion reactions occur in the sequence previously suggested [5]:



or



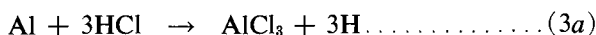
or both;



or



or both;

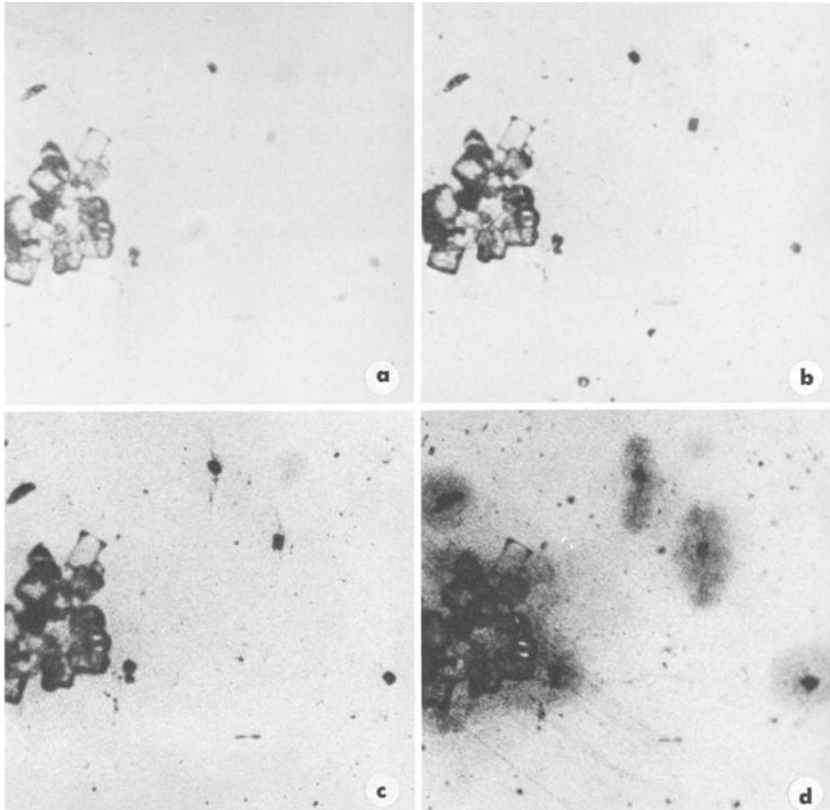


(Repeat reactions 2, 2a, and 3, 3a.)

Cooling to room temperature and rewetting with salt solution before significant progression of these reactions would hydrolyze the initial corrosion products (metal chlorides) and produce oxide phases which would tend to block further reactions on reheating. This would also retard absorption of corrosion-produced hydrogen and possibly prevent buildup to a concentration that would promote further cracking.

The inflection in the incubation time-temperature curve between 700

and 750 F suggests some sort of a change in the corrosion process, possibly through formation of either a liquid or gaseous phase(s). Hot-stage microscopy at temperatures above 750 F showed corrosion stains developing very rapidly over the specimen surface for a short distance around NaCl crystals, but no liquid was actually observed. The stains darkened



- (a) Salt deposit at room temperature.
- (b) Same as (a) after 14.5 min at temperature.
- (c) Same as (a) after 15 min.
- (d) Same as (a) after 17 min.

FIG. 5—Hot-stage microscopy of sodium chloride cracking of Ti-8Al-1Mo-IV at 800 F ($\times 650$).

very rapidly and appeared as a solid corrosion product. It has not been established that the mechanism of cracking requires a liquid phase, or that the mechanism changes at higher temperature. In tests with NaCl there was no evidence of a liquid phase at temperatures below 700 F, and at temperatures above 750 F crack initiation was detected before the corrosion stains were fully developed. An example of this is illustrated in Fig. 5, which shows several frames of a movie taken at one frame per

second during heating of a specimen to 800 F. Cracks were faintly visible after 14½ min (Fig. 5b) and became clearly visible after 15 min (Fig. 5c). Dark stains then developed around the cracks after 17 min. (Fig. 5d). The inflection in the incubation time-temperature curve may be due to melting at the salt-metal interface on a scale that cannot be resolved by hot-stage microscopy. Further work is needed to clarify this point.

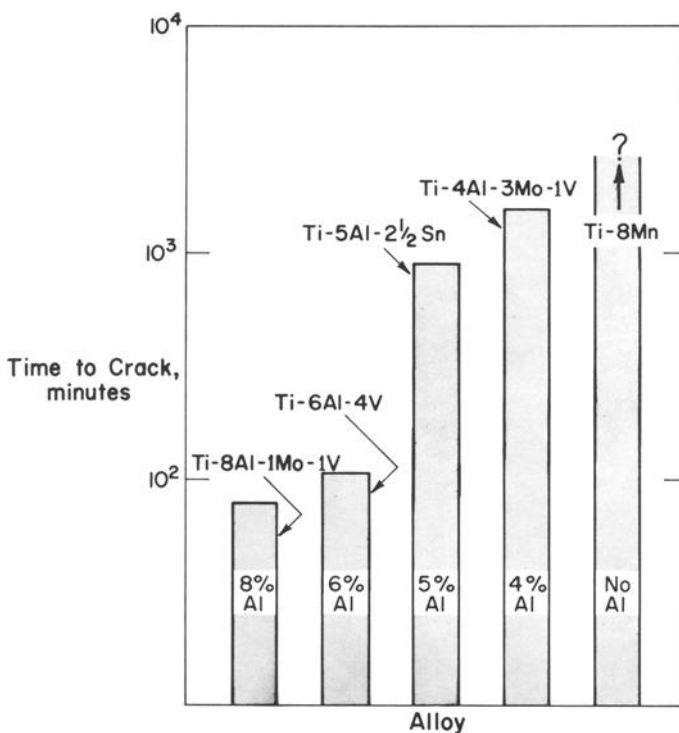
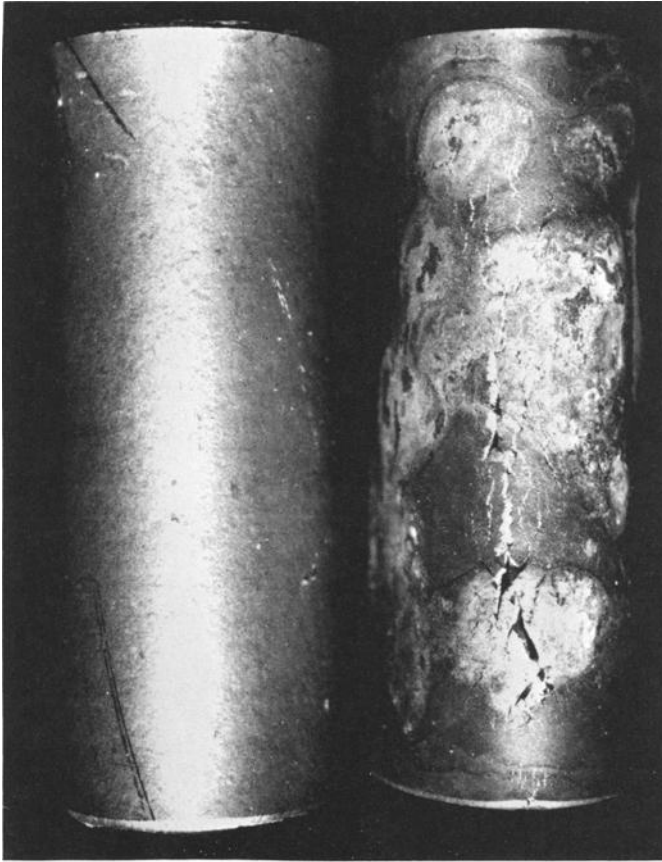


FIG. 6 EFFECT OF ALLOY COMPOSITION ON TIME TO INITIATE CRACKING BY NaCl AT 650°F

FIG. 6—Effect of alloy composition on time to initiate cracking by sodium chloride at 650 F.

Effect of Salt Composition on Crack Initiation

It was reported previously that different halide salts cause various degrees of cracking in Ti-8Al-1Mo-1V at 650 F [5]. Therefore, the incubation time-temperature curve in Fig. 4 is valid only for sodium chloride deposited on metallographically polished specimens of this alloy. A detailed study is now in progress to determine the effects of various salts on the cracking process, and complete results will be reported later. A few preliminary data, presented herewith, demonstrate that the type of salt has a strong influence.



(left) Salt exposed.
(right) Unexposed.

FIG. 7—Corrosion-embrittlement of Ti-8Mn alloy (×5). Cracks were not visible after exposure of stressed specimen with tin chloride deposit at 650 F for 91 hr. Cracks were produced by bending the specimen at room temperature after the salt was washed off.

Type of Salt	Salt Melting Point, deg F	Time to Initiate Cracking, min	
		450 F Exposure	475 F Exposure
NaCl.....	1470	no cracking after 11,200 min	5760
CuCl.....	792	no cracking after 6000 min	45
SnCl ₂	475	1800	17

The melting points of these salts differ widely, but as yet there is no direct relationship between melting point and ability to promote cracking. Melting of the initial salt deposit should accelerate the stress corrosion process, as in the case of tin chloride (SnCl₂). However, salt melting does not appear to be essential for crack initiation. The possi-

bility that the different salts have different amounts of retained moisture, or that they affect the amount of corrosion-produced hydrogen absorbed by the metal, is being investigated.

The rate of crack propagation is also affected by the type of salt. In the case of SnCl_2 , propagation is so rapid that hydrogen diffusion into the metal ahead of an advancing crack seems to be precluded as a mechanism for propagation. However, this does not preclude the possibility that propagation occurs by a stress-sorption mechanism, and that corrosion produced hydrogen is the sorbed species.

Effect of Alloy Composition on Crack Initiation

The time to initiate cracking by NaCl at 650 F in four aluminum-bearing alloys increased with decreasing aluminum content, as shown in Fig. 6. Ti-8Al-1Mo-1V was the most susceptible and cracked in $1\frac{1}{4}$ to $1\frac{1}{2}$ hr, whereas Ti-4Al-3Mo-1V cracked after 28 hr. Specimens of Ti-8Mn were not cracked after 48-hr exposure. Stressed specimens of Ti-8Mn were also exposed at 650 F with SnCl_2 deposits, previously shown to be much more aggressive than NaCl. Although no cracks were visible after 91 hr, specimens cracked during bending at room temperature after the salt was washed off, showing that corrosion embrittlement had occurred, Fig. 7.

The susceptibility to cracking was not directly related to the extent of salt corrosion. Severe attack occurred on the Ti-8Mn and the Ti-4Al-3Mo-1V, which were the most resistant. This indicates that cracking probably is not caused by contact with a specific liquid or solid phase generated during corrosion. However, the degree of susceptibility to cracking may be related to various degrees of tolerance for hydrogen in different alloys.

It was reported previously [5] that aluminum is preferentially attacked during hot-salt corrosion of Ti-8Al-1Mo-1V. The possible role of preferential attack of alloy and impurity elements in the stress corrosion mechanism is an area that requires further work.

Conclusions

Hot-salt cracking of titanium alloys occurs after an incubation period which is influenced by exposure temperature, salt composition, and alloy composition. The initiation of cracks is not related to the extent of salt corrosion which occurs, and therefore the cracking probably is not caused by contact with a specific liquid or solid phase in the corrosion products. Moisture seems to be the most critical ingredient in the corrosion process. This, coupled with the observation that cracks appear abruptly, indicates that crack initiation occurs as a result of hydrogen embrittlement.

The long incubation periods for cracking by NaCl at the lower temperatures provide an explanation for previous reports that cyclic heating

to 550 F caused less stress corrosion damage than continuous heating at the same temperature. During cyclic exposures in which the time at temperature is less than the incubation period, the initiation of cracking either will not occur or will require some number of cycles before sufficient corrosion-embrittlement occurs to produce cracking.

References

- [1] Boyd, W. K. and Fink, F. W., "The Phenomenon of Hot Salt Stress Corrosion Cracking of Titanium Alloys," NASA CR-117, Battelle Memorial Institute, Columbus, Ohio, Oct. 1964.
- [2] *Stress-Corrosion Cracking of Titanium, ASTM STP 397*, American Society for Testing and Materials, 1966.
- [3] Pride, R. A. and Woodward, J. M., "Salt-Stress-Corrosion Cracking of Residually Stressed Ti-8Al-1Mo-1V Brake-Formed Sheet at 550 F," NASA TMX-1082, National Aeronautics and Space Administration, April 1965.
- [4] Piper, D. E. and Fager, D. N., "The Relative Stress-Corrosion Susceptibility of Titanium Alloys in the Presence of Hot Salt," *Stress-Corrosion Cracking of Titanium, ASTM STP 397*, American Society for Testing and Materials, 1966, p. 31.
- [5] Rideout, S. P., Louthan, M. R., and Selby, C. L., "Basic Mechanisms of Stress-Corrosion Cracking of Titanium," *Stress-Corrosion Cracking of Titanium, ASTM STP 397*, American Society for Testing and Materials, 1966, p. 137.
- [6] Petersen, V. C. and Bomberger, H. B., "The Mechanism of Salt Attack on Titanium Alloys," *Stress-Corrosion Cracking of Titanium, ASTM STP 397*, American Society for Testing and Materials, 1966, p. 80.
- [7] Kirchner, R. L. and Ripling, E. J., "The Diffusion of Corrosion Products in Hot-Salt Stress-Corrosion Cracking of Titanium," *Stress-Corrosion Cracking of Titanium, ASTM STP 397*, American Society for Testing and Materials, 1966, p. 230.
- [8] Heimer, G. J. et al, "Salt Stress Corrosion of Ti-8Al-1Mo-1V Alloy Sheet at Elevated Temperatures," *Stress-Corrosion Cracking of Titanium, ASTM STP 397*, American Society for Testing and Materials, 1966, p. 194.

Crevice Corrosion of Titanium

REFERENCE: Jackson, J. D. and Boyd, W. K., "Crevice Corrosion of Titanium," *Applications Related Phenomena in Titanium Alloys, ASTM STP 432*, American Society for Testing and Materials, 1968, pp. 218–226.

ABSTRACT: Crevice attack of titanium and its alloys has been observed in high-temperature chloride solutions, chlorine gas, and certain acid environments. In chloride solutions, the attack becomes more severe as concentration and temperature increase. For chlorine gas, water is found to be an effective inhibitor.

KEY WORDS: crevice corrosion, titanium, titanium alloys

The absence of attack under conditions which cause rapid corrosion of stainless steels, such as under barnacles in seawater, led many to believe that titanium was immune to crevice corrosion [1,2,3,4,5].² More recently, however, several examples of titanium-crevice corrosion have occurred in salt solutions, particularly at elevated temperatures.

It is the purpose of this paper to review the occurrences of titanium-crevice corrosion, possible causes, and means of prevention. Incidents of pitting of titanium are also cited for several environments, since the occurrence of this type of attack may suggest a similar susceptibility to crevice corrosion.

Occurrences of Crevice Corrosion in Seawater and Other Chloride Solutions

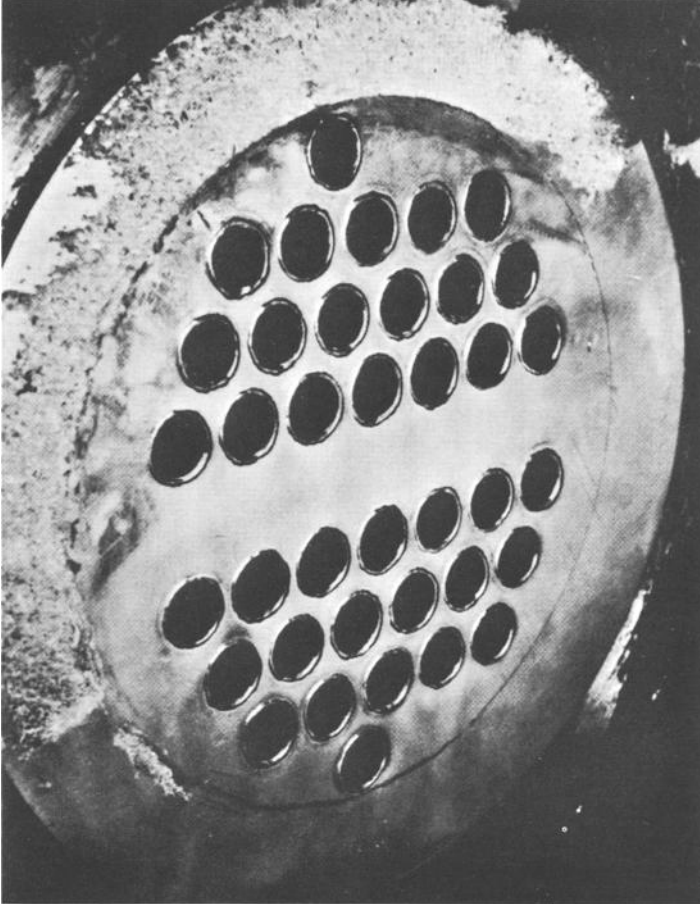
Crevice attack of titanium under an asbestos gasket was encountered by the authors during a corrosion study in a hot seawater loop for the Office of Saline Water [6]. Penetration of $\frac{1}{8}$ -in. cladding of titanium required only eight months' service at 200 to 250 F (93 to 121 C) in de-aerated neutral seawater.

Photographs of the corrosion in the area under the asbestos gasket are presented in Figs. 1, 2, and 3. The titanium tubes themselves were in excellent condition, evincing little or no attack. Metallographic sec-

¹ Research chemical engineer and division chief, respectively, Corrosion Research Div., Battelle Memorial Institute, Columbus, Ohio.

² The italic numbers in brackets refer to the list of references appended to this paper.

tions of the corroded titanium areas revealed excessive attack and hydrogen pickup as evidenced by extensive hydride formation. The results of analysis of the metal confirmed the observed hydrogen pickup. The hydrogen content of the corroded areas was found to be 300 ppm, com-



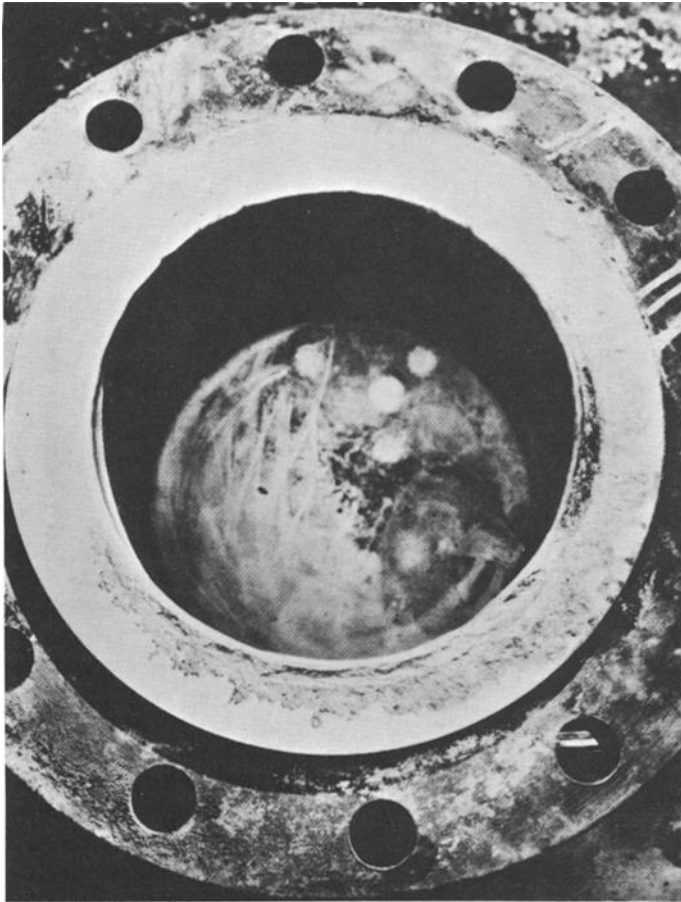
NOTE—Part of the gray area is corrosion products, the rest is asbestos-gasket material which did not part free.

FIG. 1—South end of titanium heat exchanger showing tube sheet after eight months service in hot, deaerated sea water.

pared to 50 ppm for the unattacked metal. The observation of the hydride formation and then subsequent attack of the hydrides is consistent with those reported by Oak Ridge [7] and Titanium Metals Corporation of America,³ who have also observed crevice corrosion of titanium in saline waters at elevated temperatures.

³ Private communication.

Sodium-chloride solutions of 1 and 2 *M* concentration can also initiate crevice corrosion of titanium at temperatures of 212 F (100 C) and above [7]. Both metal-to-metal and metal-to-Teflon crevices are susceptible.



NOTE—Dark area in the flange on left side of picture is where the steel under the corroded titanium has started to corrode.

FIG. 2—Water box at south end of titanium heat exchanger.

Synthetic seawater and seawater-loop exposures at 265 to 285 F (130 to 141 C) result in similar attack of crevices in simulated tube and tube-sheets [7].

Boiling 42 per cent magnesium-chloride solutions promote crevice attack of titanium whether metal-to-metal or metal-to-Teflon crevices are employed [8]. The incubation period of about 10 to 100 hr can be

decreased when the solution is acidified by additions of 0.001 to 0.01 mole per liter of hydrochloric acid (HCl). This effect of pH will be discussed later.

Crevice attack of unalloyed titanium also occurs in 62 per cent calcium-chloride solutions at 310 F (154 C) [9].

Boiling solutions of ammonium, cupric, or ferric chloride initiate crevice attack of titanium when the solutions are greater than 20 per cent concentrations [8].

It is interesting to note these chloride solutions which cause crevice attack of titanium also promote pitting. For example, localized corro-

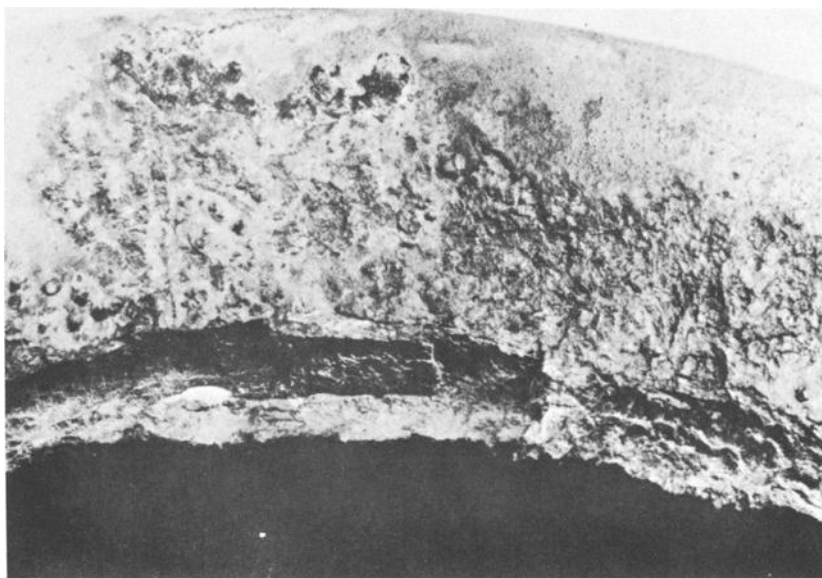


FIG. 3—Same flange area as Fig. 2 after removal of corrosion products and asbestos-gasket residue.

sion has resulted from exposures in boiling 25 per cent sodium chloride (NaCl) [10], 5 and 20 per cent magnesium chloride ($MgCl_2$) at 212 F (100 C) [10], boiling 42 per cent $MgCl_2$ [10], calcium chloride ($CaCl_2$) at 5 to 73 per cent concentrations and 212 to 350 F (100 to 177 C) [8-13] and boiling saturated ammonium chloride (NH_4Cl) [8]. We believe that a relationship may exist between the pitting tendency of titanium and its susceptibility to crevice corrosion. If this is true, then other solutions which cause pitting of titanium may also promote crevice attack. Pitting of titanium has been observed in aluminum chloride at elevated temperatures and at concentrations of 25 to 30 per cent [8, 10, 11], as well as boiling 5 and 20 per cent [10] and 86 per cent [8] solutions of zinc chloride ($ZnCl_2$).

Effect of Temperature

No instances of crevice attack of titanium have been reported at ambient temperature. However, at temperatures greater than 200 F (93 C), crevice corrosion can occur, and the frequency of attack increases as the temperature rises. This effect can be shown by the data of Table 1 [7]. Crevices were formed by metal-to-metal bands and metal pins inserted into Teflon.

Attack was observed only once in 126 cases at 212 F (100 C), and then only after 1178 hr. At the higher temperatures, attack was initiated in up to 82 per cent of the specimens. In exposures at 302 F (150 C), attack of the bands often continued after penetration of the 8 mil band into general corrosion outside of the crevice area. At 392 F (200 C), corrosion was even more general.

TABLE 1—Summary of factors affecting crevice attack of titanium in 1 or 2 *N* sodium chloride solutions [7].

Temperature, deg F	pH	Metal-to-Metal Bands		Ti-Pins to Teflon	
		Number Exposed	Per Cent Attacked	Number Exposed	Per Cent Attacked
212 (100 C)	5.5 to 6.5	102	0	24	4
302 (150 C)	5.5 to 6.5	346	32	17	82
392 (200 C)	5.5 to 6.5	98	64	106	79
302 (150 C)	4 to 5	8	100
302 (150 C)	5 to 6	34	32	3	0
302 (150 C)	6 to 7	192	34	22	91
302 (150 C)	7 to 8	126	10	2	50
302 (150 C)	8 to 9	62	5	6	17
302 (150 C)	9 to 10.3	40	0	6	0

Initiation of attack was observed after only 24 hr at 302 F (150 C) in pH 6.5 NaCl solution.

Effect of pH

The crevice corrosion of titanium in hot chloride solutions is affected markedly by pH as well as temperature. The incidence of attack is extremely high in acid and neutral solutions, as shown by the data of Table 1 [7]. Initiation of crevice attack is much less in alkaline solution, in fact, has not been observed at pH 9 to 10.3.

Several commercial applications of titanium tend to confirm this effect of pH [14]. Crevice corrosion of titanium resulted during tests in a salt-refinery evaporator brine at pH 7.5 and 225 F (107 C). No crevice attack was observed, however, in the same plant with an alkaline brine at pH greater than 12 at 208 F (98 C).

In a salt evaporator we have observed, Ti-75A tubes were installed as replacements in a cupro-nickel tubesheet. No observable crevice attack

has occurred in more than two years' service in the saturated brine at pH 10 and 260 F (127 C).

Effect of Crevice Size

A very wide crevice of titanium lowers its susceptibility to attack when compared to a tight crevice. For example, titanium metal bands which had an annulus of about $\frac{1}{32}$ in. show attack on 32 per cent of the exposures at 302 F (150 C), as shown in Table 1 [7]. On the other hand, titanium pins, which were in a tight crevice formed by Teflon, suffered attack in 82 per cent of exposures at 302 F (150 C). It is not believed that the proximity to Teflon caused the high incidence of attack, since autoclave tests excluding Teflon still produce crevice attack of titanium.

Effect of Concentration

The available data on titanium show that pitting attack is more prevalent as the concentration is increased. By relating pitting attack to crevice corrosion, as previously discussed, it seems reasonable to assume that crevice corrosion would be more likely as the chloride concentration of hot solutions is increased. However, within the range of about 6 to 12 per cent NaCl at 212 to 392 F (100 to 200 C), no difference in frequency of titanium-crevice corrosion was observed [7].

Effect of Alloy Composition

Unalloyed titanium and most of the common titanium alloys show similar susceptibility to crevice corrosion in hot chloride solutions. The only alloy to show increased resistance to crevice attack is the alloy containing 0.1 to 0.2 per cent palladium. However, even this alloy suffered some localized attack after long-term exposure to hot chloride solution.

Out of 119 specimens of eight different alloys, an average of 68 per cent exhibited crevice attack in high-temperature neutral-synthetic seawater and NaCl solution [7]. A concentration of 0.5 to 2 *M* and temperature of 302 and 392 F (150 and 200 C) was employed. The corroded alloys were Ti45A, Ti55A, Cast Ti, Ti3.5Al-4.9Cr, Ti4.2Al-4.6Mn, Ti6Al-4V, Ti8Al-2Cb-1Ta, and Ti8Al-8Zr-1Cb. Out of 30 specimens of Ti-0.15Pd exposed, none exhibited any observable attack.

Crevice attack has been observed between a titanium-palladium (Ti-Pd) specimen and Teflon gasket after 82 days' exposure to neutral-deaerated seawater at 265 to 280 F (129 to 138 C) [7]. No attack was indicated after 12 or 32 days, although the unalloyed titanium bolt holding the specimen was pitted after 12 days.

A Ti-0.13Pd alloy was unaffected in a crevice area in boiling 42 per cent MgCl₂ after 72 hr. Similarly, no pitting was observed in boiling 61 per cent CaCl₂ [9] or in 350 F (177 C) 73 per cent CaCl₂ [12,13]. How-

ever, a titanium specimen plated with 3 $\mu\text{in.}$ of platinum was perforated in 350 F (177 C) 73 per cent CaCl_2 after 36 days [13].

Crevice Corrosion of Titanium in Chlorine

Titanium is subject to rapid attack or ignition in dry chlorine, but shows excellent corrosion resistance in moist chlorine at temperatures from 50 to 205 F (10 to 96 C) [9,12,15-17].

Crevice attack of titanium was observed as early as 1950 at a point in a Hooker diaphragm cell where a titanium pipe was inserted through a rubber stopper [15]. The chlorine was reported to be wet and at an elevated temperature, corresponding to saturated gas at 180 to 190 F (82 to 88 C). In a similar case, titanium ductwork handling wet chlorine at 190 F (88 C) revealed crevice corrosion randomly under Teflon-wrapped joints [15]. This attack occurred in as short a time as nine months, resulting in a blue corrosion deposit which turned white on exposure to air. This product is thought to be Ti_2O_3 .

In a chlorine-crevice study [18], deep crevices were shown to be the focal point of attack. It was postulated that slow dehydration below the critical moisture level began. The reaction was then accelerated by the accumulated acidic-hygroscopic corrosion products. Joints sealed by O-rings or chlorine-resistant coatings, such as an anodized film, aluminum paint, coal-tar emulsion, or coal-tar urethane, were more resistant.

The slow dehydration in the crevice area suggested by the above work may be accelerated by a too low moisture level in the bulk media. The required moisture level for complete passivation of titanium in chlorine is actually much higher than previously suggested levels of 0.005 per cent at ambient [18] or 0.6 per cent at 212 F (100 C) [12]. Titanium resistance to chlorine is a function of water content, temperature, flow, and to a lesser extent pressure [16]. In general, conditions of flow required less water for protection of the titanium. With about 0.11 per cent water, no reactions occurred at room temperature, unless the surface was extremely roughened. A minimum amount of water seemed to be required at 125 F (52 C). For complete protection under all conditions studied, 0.4 per cent water is adequate at room temperature, 0.45 at 167 F (75 C), and 257 F (125 C), and about 1.1 per cent at 347 F (175 C). At 383 F (195 C) about 0.9 to 1.5 per cent water is required. Saturation of the gas may not be sufficient, and a film of water on the titanium may be preferred.

Crevice Corrosion in Acids

The presence of crevices will locally accelerate the attack of titanium in certain acid media where it is ordinarily passive. This effect was shown in 1-N sulfuric acid (H_2SO_4), 1.6 and 1.75-N hydrochloric acid (HCl), and 9 per cent oxalic acid, all at 95 F (35 C) and in 50 per cent formic

acid at 212 F (100 C) [19]. Corrosion rates of up to 30 mils per year were measured in crevices in the first three acids and greater than 100 in the latter.

Mechanism

The mechanism of the crevice corrosion of titanium in hot chloride environments is not completely understood at this time. However, it is believed to be associated with microcrevices found on the surface as a result of stress or other factors which rupture the protective oxide films. While initiation of attack is enhanced at crevice areas, it can occur at surface laps, fissures, or inclusions produced during metal fabrication. The availability of oxygen is limited in a deep crevice, and thus the protective oxide film is not reformed. For example, a blue deposit thought to be titanium oxide (Ti_2O_3) was observed after crevice attack by moist chlorine gas.

Hydride formation also appears to be associated with crevice attack. Because of the change in volume by its formation, disruption of the metal surface or the oxide film can occur. This may result in continued attack of titanium far from the crevice which initiated the attack.

Summary

Crevice corrosion of titanium and its alloys has been shown to occur in chloride-salt solutions at elevated temperature. This attack occurs above 200 F (93 C), with increasing frequency from 300 to 400 F (149 to 204 C). Acid and neutral solutions cause the greatest susceptibility, whereas no attack has been observed at pH of 9 or more. Crevice attack occurs with about the same frequency among unalloyed titanium and the common titanium alloys. Only the titanium alloy with about 0.2 per cent palladium provides increased resistance to crevice attack, but it too is attacked after long-term exposure at elevated temperature.

While the mechanism is not completely understood, microcrevices, lack of oxygen, and hydride formation may be involved.

References

- [1] Bomberger, H. B., Cambourelis, P. J., and Hutchinson, G. E., "Corrosion Properties of Titanium in Marine Environments," *Electrochemical Society Journal*, Vol. 101, No. 9, Sept. 1954, pp. 442-447.
- [2] Williams, W. Lee, "The Corrosion and Mechanical Properties of Titanium and Zirconium at Normal Temperatures," U.S. Naval Engineering Experiment Station Report C-3395-B, C-3501-C, NS-013-118, Aug. 1950, p. 42.
- [3] "Report on the Corrosion and Mechanical Properties of Titanium and Zirconium at Normal Temperatures," U.S. Naval Engineering Experiment Station Report C-3395, C-3501-B, NS-013-070, Feb. 1950, p. 39.
- [4] Cotton, J. B. and Downing, B. P., "Corrosion Resistance of Titanium to Sea Water," *Transactions, Institute Marine Engineers*, Vol. 69, Aug. 1957, pp. 311-319.

- [5] Basil, J. L., "Corrosion of Titanium Seal Rings for Salt Water Pumps," U.S. Naval Engineering Experiment Station Report 040039B, Annapolis, Md., March 1954, p. 12.
- [6] Fink, F. W., White, E. L., and Boyd, W. K., "Investigation of Corrosion in Hot Seawater in an Experimental Loop Apparatus," Final Report to Office of Saline Water from Battelle Memorial Institute, Columbus Laboratories, June 1966.
- [7] Bohlmann, E. G. and Posey, F. A., "Aluminum and Titanium Corrosion in Saline Waters at Elevated Temperatures," presented at 1st International Symposium on Waters Desalinization, Oct. 3-9, 1965.
- [8] Shimose, Takaaki and Takamura, Akira, "Corrosion Resistance of Titanium and Titanium-Palladium Alloy in Acid and Chloride Solution," Central Research Laboratory, Kobe Steel, Ltd., Dec. 1965.
- [9] Gegner, P. J. and Wilson, W. L., "Corrosion Resistance of Titanium and Zirconium in Chemical Plant Exposures," *Corrosion*, Vol. 15, July 1959, pp. 341t-350t.
- [10] Golden, Lex B., Lane, I. Roy, Jr., and Acherman, W. L., "Corrosion Resistance of Titanium, Zirconium, and Stainless Steel," *Industrial and Engineering Chemistry*, Vol. 44, No. 8, Aug. 1952.
- [11] Rudinger, Von Klaus, "Titanium as a Material for the Chemical Industry," *Werkstoffe Und Korrosion*, Supplement to Edition No. 7, July 1962.
- [12] Sheppard, R. S. et al, "Performance of Titanium vs Other Materials in Chemical Plant Exposures," *Corrosion*, Vol. 18, June 1962, pp. 211t-218t.
- [13] "Titanium-Palladium Alloy," *Union Carbide Metals Review*, 1960.
- [14] Turnbull, J. M., "Salt Refinery Corrosion Caused by Varying Evaporator Conditions," *Corrosion*, Vol. 16, July 1960, pp. 11-16.
- [15] Gleekman, L. W., "Corrosion Resistant Metals," *Chemical Engineering*, Nov. 11, 1963.
- [16] Millaway, E. E. and Kleinman, M. H., "Water Content of Chlorine for Titanium Passivation," presented at National Association of Corrosion Engineers 22nd National Conference, Miami, Florida, April 18-22, 1966. See *Corrosion*, Vol. 23, No. 4, April 1967, pp. 88-97.
- [17] Cotton, J. B. and Bradley, H., "The Corrosion Resistance of Titanium," *Chemistry and Industry*, May 31, 1958.
- [18] Bomberger, H. B., *Crucible Titanium Review*, Vol. 10, No. 1, Aug. 1962.
- [19] Schlain, David and Kenahan, C. B., "The Role of Crevices in Decreasing the Passivity of Titanium in Certain Solutions," *Corrosion*, Vol. 12, Aug. 1956, pp. 68-72.

Biaxial Properties of Titanium Alloys at Cryogenic Temperatures

REFERENCE: Frederick, S. F. and Corn, D. L., "Biaxial Properties of Titanium Alloys at Cryogenic Temperatures," *Applications Related Phenomena in Titanium Alloys*, ASTM STP 432, American Society for Testing and Materials, 1968, pp. 227-235.

ABSTRACT: The biaxial properties of Ti-6Al-4V and Ti-5Al-2.5Sn were determined at -423 F. Texture strengthening was found to be operative at this temperature, but the magnitude of the increase in strength over uniaxial properties could not be predicted from tension-test techniques for measuring texture strengthening. The strengths of welded joints in Ti-6Al-4V at -423 F were found to be equal to that of the textured parent metal. The dependence of texture strengthening on temperature, strain, and stress state is discussed.

KEY WORDS: titanium alloys, texture, stresses, low temperature

The attractiveness of titanium for aerospace applications becomes considerably enhanced when cryogenic service temperatures are of interest. The low density and high strength of the all-alpha alloys together with adequate toughness, make them highly efficient structural materials. Many of these cryogenic applications involve pressure vessels and, therefore, involve biaxial stress states. Alpha titanium has a hexagonal close-packed crystal structure, and normal mill processing of sheet often produces a strong basal plane texture [1,2].² This type of texture, with the basal planes parallel or nearly parallel to the plane of the sheet, has important consequences in the way the sheet can deform. The three most active slip systems of titanium are shown in Fig. 1. Although there are three major slip planes, each has the same slip direction, and this direction lies in the basal plane. It is apparent then, that if a sheet has a perfect basal plane texture, there is no slip mechanism which results in plastic strain normal to the plane of the sheet (thinning). For a pure, balanced biaxial tension, such as in a spherical pressure vessel, there

¹ Section chief, and research engineer, respectively, Missile and Space Systems Div., Douglas Aircraft Co., Santa Monica, Calif.

² The italic numbers in brackets refer to the list of references appended to this paper.

should be no slip possible on these three planes. Then the maximum stress would be limited by fracture, slip on other planes, or by some other means of deformation such as twinning. For an unbalanced biaxial tensile stress state, slip on the three major planes would be possible, but again, higher stresses than the uniaxial yield would be required.

It has been found that Hill's theory [3] for anisotropic yielding gives

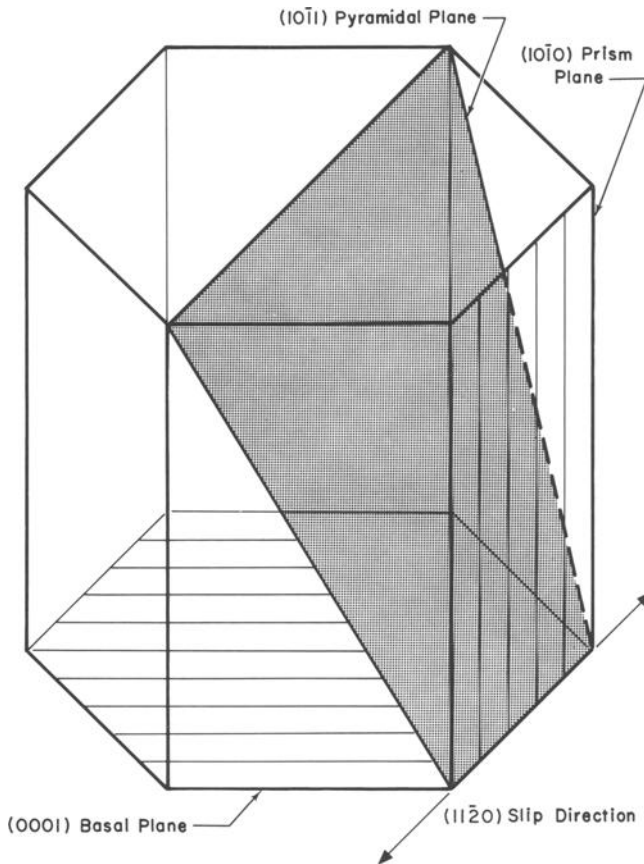


FIG. 1—The major slip systems in alpha titanium.

a good fit to experimental data, at least in the tension-tension quadrant [4]. His parameter R , defined as the ratio of lateral strain to thickness strain in a pure uniaxial stress state, is a convenient measure of the degree of anisotropy. Knowing the value of R , the strength of a material for any biaxial stress can be predicted. Figure 2 gives biaxial data for Ti-5Al-2.5Sn at room temperature showing the fit of the data to the indicated value of R . The difference in R between yield and ultimate indicates an increase of R with strain as also noted by Backofen et al [4].

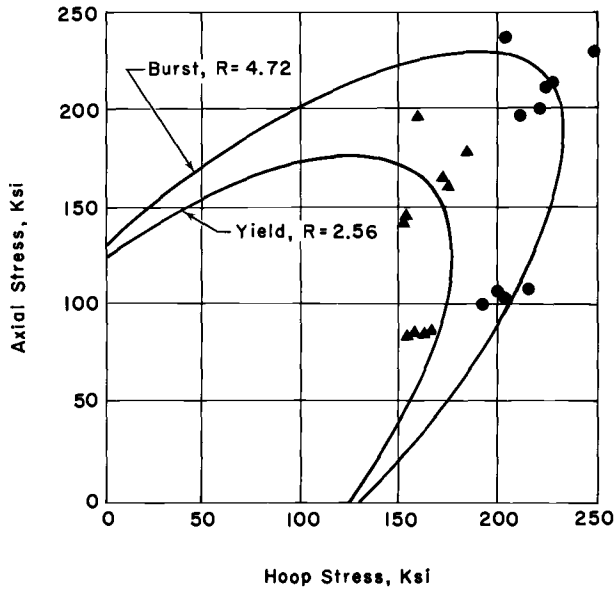


FIG. 2—The biaxial strength of Ti-5Al-2.5Sn at room temperature [6].

TABLE 1—Effect of heat treatment on texture strengthening of Ti-4Al.

Treatment ^a	Phase Field	R
As received.....	...	4.35
1550 F, 1 hr, AC.....	All α	4.98
1800 F, 10 min, AC.....	α + β	3.15
1900 F, 5 min, WQ.....	All β	0.73

^a AC = air cooled; WQ = water quenched.

TABLE 2—Composition of alloys.

Alloy	C	Fe	N	Al	V	Sn	H	O	Mn
Ti-6Al-4V ELI									
0.018 thick.....	0.025	0.10	0.011	5.9	4.0	... ^a	0.003	0.146	... ^a
Ti-5Al-2.5Sn ELI,									
0.020 thick.....	0.025	0.16	0.014	5.2	... ^a	2.5	0.011	0.07	0.002

^a Not analyzed.

There are at least two possible limitations to utilizing texture strengthening in actual structures. First, the desired sheet texture is produced by working and heat treating the alloy at temperatures below the beta transus. If this temperature is exceeded, the resulting transformed alpha has a random texture. Table 1 gives data which illustrate this effect. If welding is used for fabricating a structure, there is of necessity an area which has exceeded the beta transus. The biaxial strength of the weld

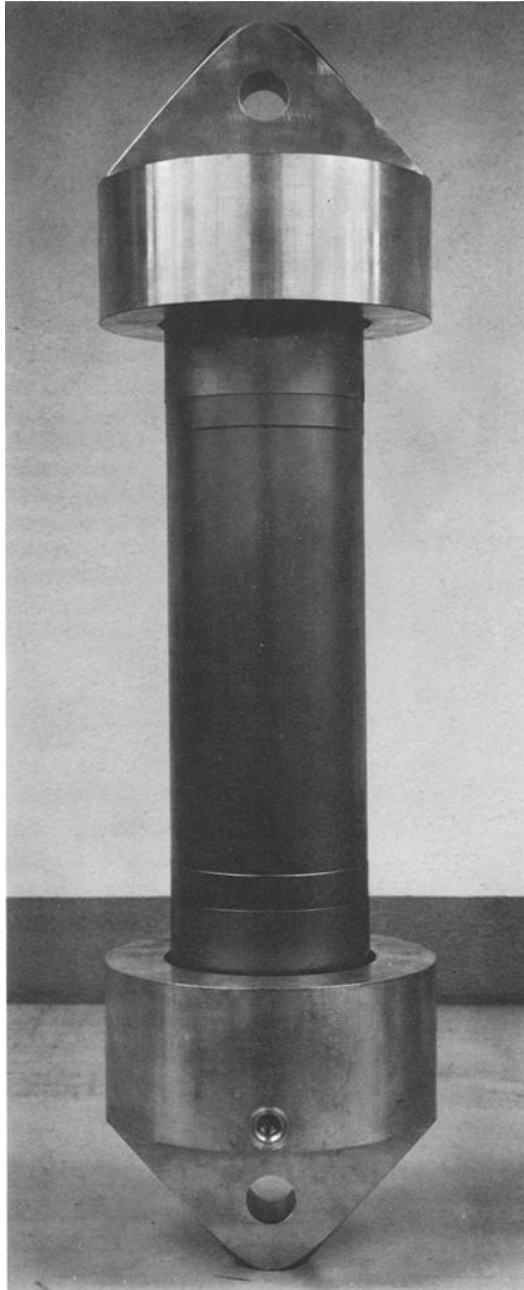


FIG. 3—*The biaxial test specimen.*

would not then be expected to be as high as that of the textured parent metal.

The second possible limitation is the application of texture strengthening to cryogenic applications. It is known that fewer slip systems in titanium are generally operative at low temperatures and that twinning is more prevalent [5]. Twinning itself would provide thinning and in addition, further thinning could occur by slip.

Since a strong interest exists in the use of welded titanium alloys for liquid hydrogen tankage, this study was initiated to evaluate the biaxial properties of titanium alloys at -423 F. Emphasis was on Ti-6Al-4V, but some tests were made with Ti-5Al-2.5Sn.

Procedure

The compositions of the Ti-6Al-4V and Ti-5Al-2.5Sn alloys used for the biaxial tests are given in Table 2.

The specimens were in the form of 4-in.-diameter cylinders with chem-milled "window frames" to isolate the test area. In this way, either parent metal or weld areas can be tested by proper location of the chem-milled area. All welds were by gas-tungsten-arc without filler wire. Complete details on the preparation of this specimen and its suitability for biaxial tests are given in Ref 6. An untested specimen is shown in Fig. 3.

To apply axial loads and contain internal pressure, end caps were added to the cylinders by casting Cerrobend in grooves in the end cap. All testing was done in liquid hydrogen. The calculation of R from the biaxial tests was by the expression

$$\sigma_a^2 - 2 \left(\frac{R}{R+1} \right) \sigma_a \sigma_h + \sigma_h^2 = S^2$$

where:

σ_a = axial stress,

σ_h = hoop stress, and

S = uniaxial strength.

Tension tests were used to measure R for yielding as well as for determining uniaxial strength. In these tests longitudinal and lateral strains were measured by resistance strain gages to obtain Poisson's ratio in the plastic strain region. Then R is calculated by

$$R = \frac{\mu_p}{1 - \mu_p}$$

where μ_p is the plastic Poisson's ratio.

Results and Discussion

The biaxial test results at -423 F are shown in Fig. 4. Each biaxial data point represents a single test. It is apparent that texture strength-

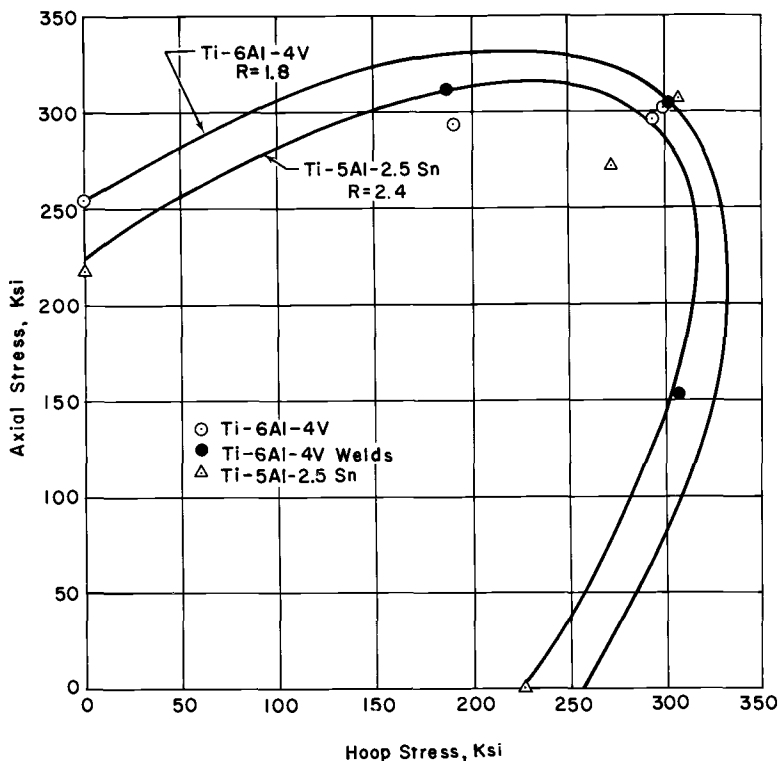


FIG. 4—The biaxial strength of Ti-6Al-4V and Ti-5Al-2.5Sn at -423 F .

TABLE 3—Tension test results.

Alloy	Temperature	Tensile Strength, ksi		R		
		0.2% Yield	Ultimate	Uniaxial Yield	Biaxial ^b Yield	Biaxial ^b Ultimate
Ti-6Al-4V ELI.....	RT ^c	143	147	0.93
	-423 F	240	256	0.64	...	1.8
Ti-5Al-2.5Sn ELI.....	RT	111	117	2.16
	-423 F	214	222	1.12	...	2.0
Ti-5Al-2.5Sn ^a	RT	124	130	2.56	1.7-2.6	4.72

^a Ref 6.

^b From pressure vessel tests.

^c RT = room temperature.

ening is operative at this temperature for both alloys. Of particular interest is that the biaxial strength of the Ti-6Al-4V welds is equal to that of the textured metal. The results of the tension test measurements of texture are presented in Table 3. Data of Babel et al [6] are also presented for comparison.

Several observations can be made from the experimental results. It is

apparent that R for yielding decreased with decreasing temperature. The tensile data provide direct evidence for this. In addition, although not so clearly defined, R for ultimate behaves similarly. This can be seen by comparing the -423 F Ti-5Al-2.5Sn data of this investigation with the room temperature Ti-5Al-2.5Sn data of Babel et al (Table 3). A comparison of the R values for yield obtained at room temperature show

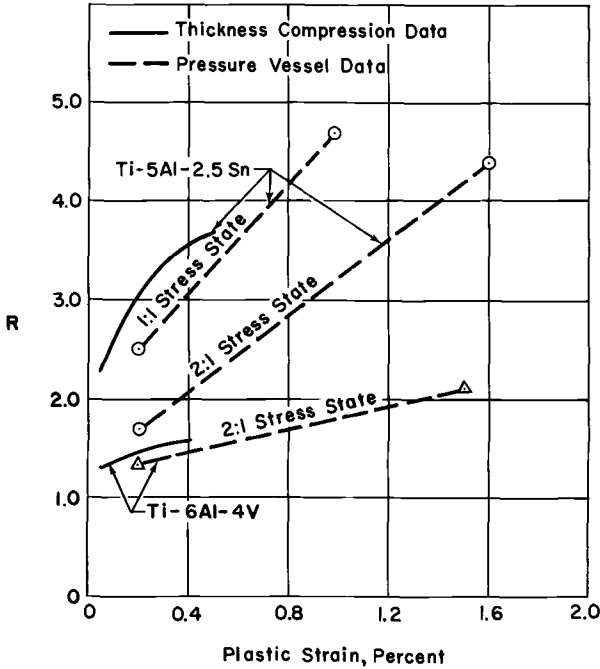


FIG. 5—The variation of R with plastic strain [6,8].

similar texture, while the biaxial burst data give a much lower R value at -423 F (2.0 compared to 4.7). The magnitude of the drop in R at -423 F is somewhat more than would be expected from the data of Sliney et al [7] who investigated the anisotropy of Ti-5Al-2.5Sn as a function of temperature. They found the value of R at ultimate to decrease from 3.1 at room temperature to 2.3 at -157 F and then remain essentially constant down to -320 F. This decrease in R may be related to the increased incidence of twinning noted in titanium alloys as the temperature of deformation is lowered [5], since the basic sheet texture does not change with temperature.

The present data show the same increase of R with strain at -423 F as found by other investigators at room temperature [4,5]. In fact, most of the texture strengthening at -423 F appears to be the result of this increase in R . If so, this would also explain the strength of the welds

in Ti-6Al-4V being as strong as the parent metal, because the parent material and weldments would both be initially isotropic and R for both would increase with plastic strain.

The problem now is to explain the increase of R with plastic strain. The most direct explanation is that during deformation, the basal planes rotate into the plane of the sheet. Then it would be expected that the increase of R with strain would be dependent on the initial texture. Figure 5 presents data from several sources showing that this dependency does exist. Furthermore, it follows the expected behavior of a higher rate of increase of R with a higher initial value of R . This is demonstrated by the fact that the Ti-5Al-2.5Sn alloy, which conventionally exhibits a strong, central, basal plane sheet texture and high R , also exhibits the most pronounced increase in R with respect to strain. Ti-6Al-4V on the other hand usually exhibits a split basal pole figure at 20 to 30 deg from the sheet normal with a low R , and the rate of increase in R with respect to strain is relatively small. It is possible, however, to obtain initial R values in Ti-6Al-4V as high as 10.

It might also be argued that the variation of R with strain depends on temperature and alloy rather than initial texture. This is quite possible since it has been demonstrated here that R decreased with decreasing temperature. Unfortunately, insufficient data exist to clarify these uncertainties. One primary difficulty is that texture strengthening is rather sensitive to small differences in processing history, and any direct comparisons of environmental effects must be made on the same sheet.

There are also indications that the measurement of R may depend on stress state. In particular, R , as measured in a tension test, seldom varies with strain. In a biaxial test, however, R always varies with strain. The latter is a consequence of the lack of appreciable work hardening found in a tension test in contrast to the marked work hardening found in biaxial tests. The biaxial data in Figs. 2 and 4 also show deviations in R with respect to stress state. For a 2:1 stress field, the yield stress of Ti-5Al-2.5Sn at room temperature and the ultimate strength of Ti-6Al-4V at -423 F lies below the locus predicted by the 1:1 stress state data. Using the tension test technique, Larson [9] found large systematic variations in R with respect to sheet orientation for certain alloys. It would appear that predictions and applications of texture strengthening must consider stress state and sheet orientation as well as the value of R measured by some standard test.

Conclusions

Biaxial tests of two titanium alloys at -423 F have shown texture strengthening to be operative. No decrease in strength was found in Ti-6Al-4V when a welded seam was part of the test section.

The degree of texture strengthening, as measured by R , increases with

strain, decreases with decreasing temperature, and depends on stress state.

References

- [1] Holden, F. C. et al, "Flow Properties, Deformation Textures, and Slip Systems of Titanium and Titanium Alloys," TML Report No. 30, Titanium Metallurgical Laboratory, 1956.
- [2] Roberts, W. T., "Preferred Orientation and Anisotropy in Titanium," *Journal of the Less-Common Metals*, Vol. 4, 1962, pp. 345-361.
- [3] Hill, R., "A Theory of Yielding and Plastic Flow of Anisotropic Metals," *Proceedings of the Royal Society*, Vol. 193, Serial A, 1948, p. 281.
- [4] Backofen, W. A., Avery, D. H., and Lee, D., "Deformation Processing of Anisotropic Metals," Final Report of Navy Contract No. NOW 65-0124-d, Massachusetts Institute of Technology, 1965.
- [5] Carmen, C. M., Forney, J. W., and Katlin, J. M., "Plane Strain Fracture Toughness and Mechanical Properties of 5Al-2.5Sn ELI Titanium at Room and Cryogenic Temperatures," NASA CR-54296, U.S. Army Frankford Arsenal, 1966.
- [6] Babel, H. W., Eitman, D. A., and McIver, R. W., "The Biaxial Strengthening of Textured Titanium," *Transactions, American Society of Mechanical Engineers, Journal of Basic Engineering*, to be published.
- [7] Sliney, J. L., Corrigan, D. A., and Schmid, F., "Preliminary Report on the Biaxial Tensile Behavior of Anisotropic Sheet Materials," Report AMRA TR 63-11, U.S. Army Materials Research Agency, 1963.
- [8] Babel, H. W. and Corn, D. L., "A Comparison of Methods for Correlating Texturing with the Biaxial Strengths of Titanium Alloys," *Metals Engineering Quarterly*, American Society for Metals, to be published.
- [9] Larson, F. R., "Anisotropy of Titanium Sheet in Uniaxial Tension," *Transactions, American Society for Metals*, Vol. 57, 1964, pp. 620-631.

Texture Strengthening and Fracture Toughness of Titanium Alloy Sheet at Room and Cryogenic Temperatures

REFERENCE: Sullivan, T. L., "Texture Strengthening and Fracture Toughness of Titanium Alloy Sheet at Room and Cryogenic Temperatures," *Applications Related Phenomena in Titanium Alloys*, ASTM STP 432, American Society for Testing and Materials, 1968, pp. 236–247.

ABSTRACT: Biaxial yield strengths as high as 1.53 times uniaxial yield strength were obtained from burst tests of 6-in.-diameter cylindrical pressure vessels (1 to 2 stress field) fabricated from two textured titanium alloys, Ti-4Al-0.2O and Ti-5Al-2.5Sn ELI. Material nominally 0.020 in. thick was tested at 70, -320, and -423 F. While the Ti-4Al-0.2O alloy generally had superior biaxial smooth properties at the three test temperatures, the Ti-5Al-2.5Sn ELI alloy exhibited less notch sensitivity at -320 and -423 F. It is demonstrated that plastic Poisson's ratio obtained from a uniaxial test could be used to characterize the degree of texture in the two alloys and provide a means for predicting biaxial strengthening.

KEY WORDS: physical properties, fracture toughness, biaxial stress, titanium alloys, plastic Poisson's ratio, cryogenics

Under conditions of biaxial stress a certain type of anisotropy in metallic sheet material can cause strengthening considerably greater than that predicted for the isotropic case [1].² This type of anisotropy, called texturing, is found in some titanium alloy sheet. Uniaxial studies of texturing in titanium alloys have been made by several investigators [2–5]. Sliney et al [6] and Babel and Kam [7] have experimentally investigated the biaxial strengthening of Ti-5Al-2.5Sn at room temperature.

Maximum biaxial strengthening in alpha titanium alloys should occur when the (0001) pole is normal to the sheet plane. Titanium alloyed with 3.8 per cent aluminum (Ti-4Al) is reported to give close to this ideal orientation after rolling [4]. Because of the potential usefulness of this

¹ Aerospace technologist, Materials and Structures Div., Lewis Research Center, National Aeronautics and Space Administration, Cleveland, Ohio.

² The italic numbers in brackets refer to the list of references appended to this paper.

alloy as a cryogenic propellant tank material, a program was conducted to determine the strength and fracture toughness of 0.020-in. thick Ti-4Al-0.2O sheet in uniaxial and 1 to 2 biaxial stress fields at 70, -320, and -423 F. A parallel study was conducted with the extra-low-interstitial (ELI) grade of a less textured titanium alloy, Ti-5Al-2.5Sn. Results for each are compared. In addition the weld strengths of a limited number of uniaxial and biaxial test specimens were determined. The relationship between plastic Poisson's ratio and biaxial strengthening based on Hill's theory [8] is experimentally verified.

Analytical Basis for Texture Strengthening

By applying Hill's theory [8] for the yielding of anisotropic sheet materials Backofen et al [1] indicate that for the case of rotational sym-

TABLE 1—Annealing treatment and composition (per cent by weight) for alloys investigated.

Material	Heat No.	Anneal	C	Fe	N	Al	H	O	Sn	Mn
Ti-4Al-0.2O...	V-3002	1325 F for 4 hr furnace cooled	0.023	0.12	0.014	3.8	0.007 to 0.010	0.21
Ti-5Al-2.5Sn ELI.....	D-3272	1325 F for 4 hr furnace cooled	0.022	0.08	0.014	5.1	0.006 to 0.009	0.08	2.5	<0.006

metry about the thickness direction (isotropy in the plane of the sheet) the yield criterion becomes

$$\frac{\sigma_x}{\sigma_{ys}} = \left[1 + \alpha^2 - \alpha \frac{2R}{R + 1} \right]^{-1/2} \dots \dots \dots (1)$$

where:

- α = ratio of the principal stresses in the plane of the sheet σ_y/σ_x ,
- σ_{ys} = uniaxial yield strength in the plane of the sheet, and
- R = ratio of plastic strain in the width direction of the sheet ϵ_w to plastic strain in the thickness direction of the sheet ϵ_t , these strains being determined from smooth uniaxial tension tests.

It is assumed in Eq 1 that the principal directions of anisotropy correspond with the principal directions of stress. The derivation of this equation is found in Appendix A of Ref 6.

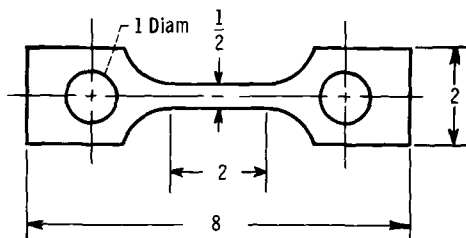
Because of the difficulty in accurately measuring strain in the thickness direction of thin gage materials, it is desirable to base R on a more easily measured quantity such as strain in the length direction ϵ_l . This can be done if constancy of volume is assumed. If yielding has occurred, $\epsilon_w + \epsilon_t = 0$ for small strains. Thus,

$$R = \frac{\epsilon_w}{\epsilon_t} = \frac{\epsilon_w}{-\epsilon_w - \epsilon_t} = \frac{\nu_p}{1 - \nu_p} \dots \dots \dots (2)$$

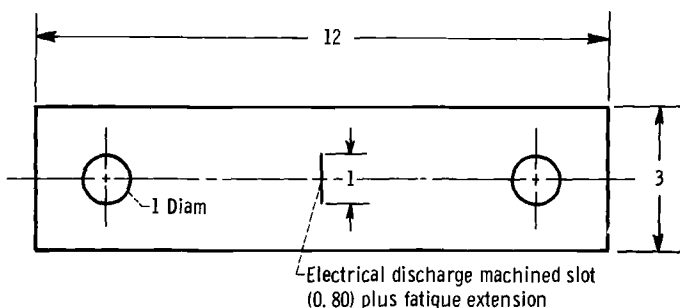
where ν_p is the plastic Poisson's ratio, $-\epsilon_w/\epsilon_t$.

Experimental Apparatus and Procedure

Test specimens were fabricated from sheet nominally 0.020 in. thick produced from a single heat of each alloy. The mill analysis and annealing treatment provided by the supplier are given in Table 1.



(a) Smooth specimen.



(b) Center cracked specimen.

FIG. 1—Sheet tension specimens (all dimensions in inches).

Uniaxial Tests

Conventional smooth properties including 0.2 per cent offset yield strength and plastic Poisson's ratio were obtained using the specimen shown in Fig. 1a. Weld specimens were of this type and had their weld beads normal to the loading axis. Notch strength (based on initial crack length) and fracture toughness (based on critical crack length) were determined using the through-cracked specimen shown in Fig. 1b. Finished uniaxial specimens were stress relieved in the same manner as outlined in the next section for biaxial test specimens.

The NASA continuity gage [9] was used to measure the slow crack

growth which took place prior to catastrophic failure. At -423 F the transition between slow and rapid crack growth was abrupt, and the critical crack length was readily obtainable from the gage output directly. At -320 F, however, the transition was gradual, and a crack velocity of 0.1 in./sec was arbitrarily selected to define the critical crack length. Because the crack velocity selected is relatively slow, the critical crack lengths used to calculate fracture toughness gave conservative results.

Plastic Poisson's ratios were obtained by testing tension specimens upon which were mounted longitudinal and transverse high-elongation copper-nickel foil strain gages. The output of the gages was used to drive an X-Y recorder. The specimen was loaded in tension until yielding had occurred. To restrict the strain ratio to purely plastic (nonrecoverable) strain components, the load was then held constant as the strain continued to increase until the end of the recorder chart travel was reached (about 2 per cent strain). The slope of the curve of ϵ_w versus ϵ_l after yielding occurred was taken as the plastic Poisson's ratio.

Biaxial Tests

Six-inch diameter cylindrical pressure vessels 18 in. long were fabricated using a single longitudinal butt weld. The sheet was oriented so that the rolling direction of the material was normal to the weld. Following fabrication cylinders were stress relieved in vacuum and furnace cooled. The stress relief schedules were 1 hr at 1000 F for the Ti-4Al-0.2O alloy and 2 hr at 1100 F for the Ti-5Al-2.5Sn ELI alloy.

Cracked cylinders were flawed by electrical discharge machining longitudinal slots through the cylinder wall followed by low stress fatiguing to obtain sharp cracks at the slot ends. An internal patch [10] was taped over the crack for pressurizing to failure.

To preclude weld failures in cylinders used to determine parent material biaxial yield and ultimate strengths, it was necessary to reinforce the welds. This was done by bonding internal and external overlays of commercially pure titanium strip to the weld. The strips were 0.004 in. thick and approximately 2 in. wide. End closure was obtained by sealing the cylinder ends in heads filled with a low-melting-point alloy [10]. Strippable-backed nickel-chrome foil strain gages were applied to all uncracked cylinders to provide biaxial stress-strain curves.

The cylinders were pressurized to failure by applying helium pressure to tap water, liquid nitrogen, or liquid hydrogen for tests at 70, -320 , and -423 F, respectively. For the cryogenic tests, the cylinders were placed in a cryostat and both filled and surrounded with the appropriate cryogen. Yield strengths were obtained using the 0.2 per cent offset method. Failure strengths were computed using the burst pressure.

Results and Discussion

Uniaxial Properties

Smooth and notch properties for both alloys are plotted as a function of test temperature in Fig. 2. Specimens were tested with the loading direction both parallel (longitudinal specimen) and normal (transverse

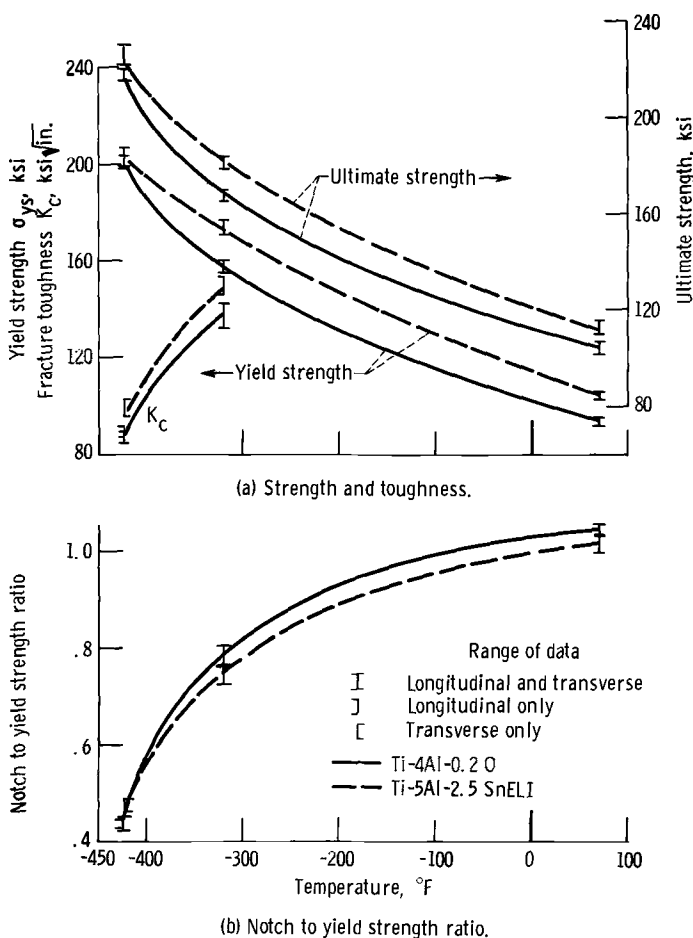


FIG. 2—Uniaxial properties of Ti-4Al-0.2O and Ti-5Al-2.5Sn ELI sheet as a function of test temperature.

specimen) to the rolling direction. At least three specimens were tested for each condition. The Irwin method [11] was used to calculate fracture toughness. In the toughness tests no effort was made to prevent buckling of the crack lips out of the plane of the sheet during testing [11].

For both alloys only slight differences were found between their longitudinal and transverse properties indicating that the materials were es-

entially isotropic in the plane of the sheet. The largest difference occurred with the fracture toughness of the Ti-5Al-2.5Sn ELI alloy at -423 F where the transverse exceeded the longitudinal toughness by about 10 per cent. This alloy also exhibited greater smooth uniaxial strength at the three test temperatures.

A special point should be made regarding the thickness of the materials tested and their notch properties. As would be expected for sheet 0.020 in. thick, all specimen fractures were characterized by full shear fracture surfaces, accompanied by considerable plasticity. A rather com-

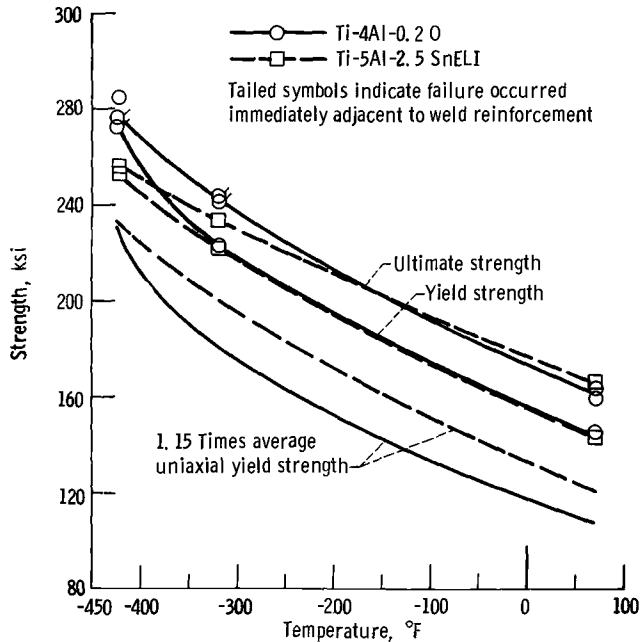


FIG. 3—1:2 biaxial yield and ultimate strength of Ti-4Al-0.2O and Ti-5Al-2.5Sn ELI sheet as a function of test temperature.

plete statement of the effects of sheet thickness on the fracture toughness of Ti-5Al-2.5Sn alloy is reported in Ref 12. It is important to recognize that the present results relate only to 0.020-in.-thick material. While comparison of the two alloys investigated is justified on the basis of identical thicknesses, a comparison with the same or other alloys at thicknesses other than 0.020 in. is to be avoided.

Biaxial Properties

In Fig. 3 the biaxial yield and ultimate strengths are plotted as a function of test temperature for both alloys. To indicate the increase in yield strength predicted for an isotropic material, 1.15 times the average uniaxial yield strength is also included in this figure. At -320 and -423

F the Ti-4Al-0.2O cylinders generally failed immediately adjacent to the weld reinforcement. At -423 F failure occurred before the 0.2 per cent offset strain was reached; in these cases, the stress at burst is plotted in Fig. 3 as the yield strength.

Both alloys developed biaxial yield strengths substantially greater than those predicted for isotropic materials. Strengthening ranged from 1.24 to 1.53 times the uniaxial yield strength. As would be expected, strengthening was greater for the more heavily textured Ti-4Al-0.2O alloy at all

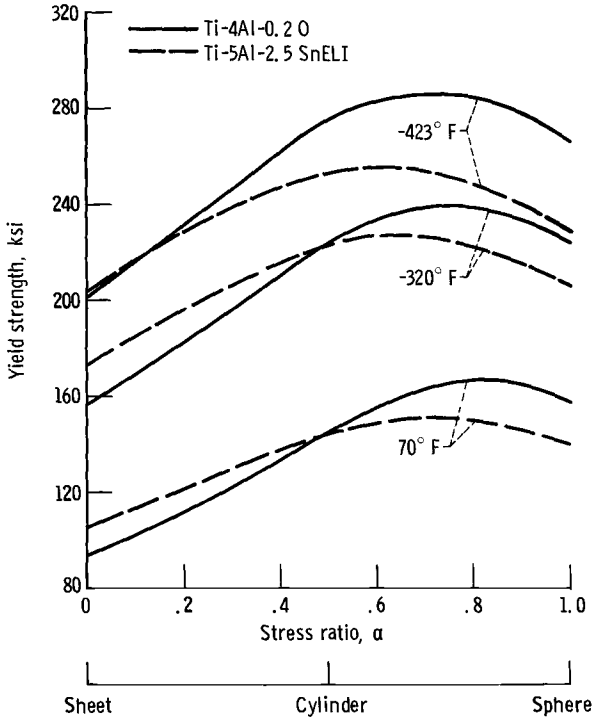


FIG. 4—Projected yield strengths for Ti-4Al-0.2O and Ti-5Al-2.5Sn ELI in a tension-tension biaxial stress field.

temperatures investigated. Consequently, although Ti-4Al-0.2O had lower uniaxial yield strengths than Ti-5Al-2.5Sn ELI at the three test temperatures, the biaxial yield strengths for both alloys at 70 and -320 F were nearly identical. At -423 F the Ti-4Al-0.2O 1 to 2 biaxial yield strength was about 9 per cent greater than that of Ti-5Al-2.5Sn ELI.

Increases in biaxial ultimate strength as high as 55 per cent were obtained. In cases where failure occurred adjacent to the weld reinforcement, it is likely that the stress ratio at the failure location was less than $\frac{1}{2}$, and the values shown in Fig. 3 are probably lower than those which would be obtained in a true 1 to 2 stress field. At 70 and -320 F the

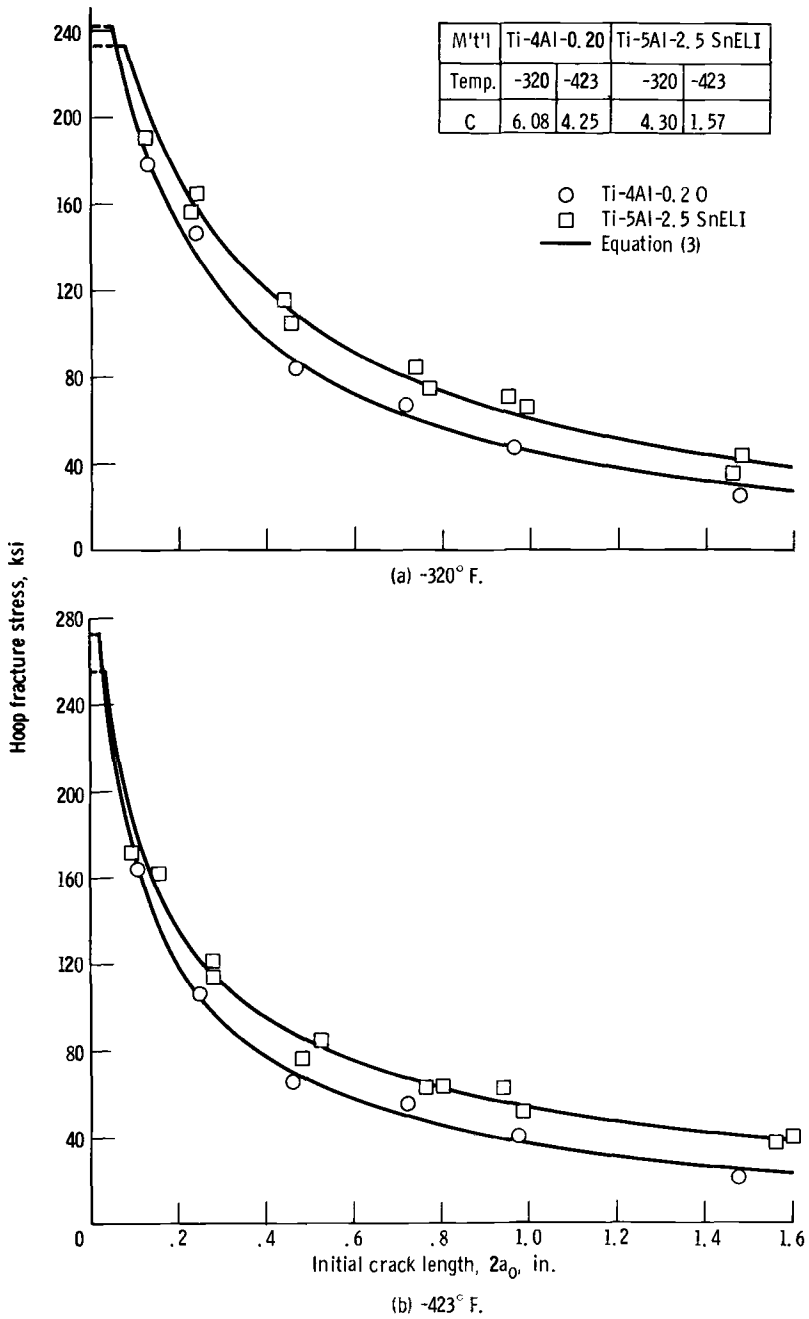


FIG. 5—Fracture strength of cracked titanium cylinders.

percentage increase in failure strength, comparing biaxial to uniaxial results, is about the same as the percentage increase in yield strength for these two stress fields. At -423 F the ultimate strengths were only slightly greater than the yield strengths.

In order to estimate the yield strengths of the two alloys in other stress fields, the experimental results were used to compute values of the strain ratio R in Eq 1. The computed values of R were used in Eq 1 to calculate yield strengths in other biaxial stress fields. These projected yield strengths are shown in Fig. 4. A stress field of particular interest is the 1 to 1 ($\alpha = 1$) which occurs in a pressurized spherical shell. For this case the projected Ti-4Al-0.2O yield strengths exceed those projected for Ti-5Al-2.5 Sn ELI by 13, 9, and 16 per cent at 70, -320 , and -423 F, respectively. It is emphasized that these are projected strengths which have not been experimentally verified.

The results of the through-cracked cylinder tests are shown in Fig. 5. It has been demonstrated in Ref 13 that the biaxial behavior of a material in the presence of a through-crack can be correlated with the uniaxial behavior by

$$\sigma_{hc} = \frac{K_{cn}}{\left(1 + C \frac{a_0}{r}\right) \left(\pi a_0 + \frac{1}{2} \frac{K_{cn}^2}{\sigma_{yb}^2}\right)^{1/2}} \dots \dots \dots (3)$$

where:

- σ_{hc} = critical hoop fracture stress in the cylinder,
- K_{cn} = nominal fracture toughness (based on initial crack length),
- a_0 = initial half crack length,
- σ_{yb} = 1 to 2 biaxial yield strength,
- r = radius of the cylinder, and
- C = dimensionless bulge coefficient.

The term $1 + C (a_0/r)$ takes into account the increase in stress intensity at the crack tips in a pressurized cylinder due to bulging. The values of C used to draw the curves in Fig. 5 were obtained for each material and temperature by averaging the values of C computed using Eq 3 for the individual data points.

For all crack lengths tested, the Ti-4Al-0.2O exhibited greater notch sensitivity than the Ti-5Al-2.5Sn ELI. Because the uniaxial fracture toughness properties of the two alloys were about the same, the relatively large difference in the biaxial results for longer cracks was not expected. A portion of the difference can be attributed to a higher residual stress condition in the Ti-4Al-0.2O due to using a lower temperature and shorter time in the stress relief of these cylinders. By measuring the radius to which the cylinders opened when slit longitudinally, it was calculated that approximately 25 per cent of the residual stress due to forming was still present in the Ti-4Al-0.2O cylinders; this compares to less than 10

per cent in the Ti-5Al-2.5Sn ELI cylinders. However, for small cracks (0.1 in. or less) it is likely that the difference between the notch strengths of the two alloys will be small.

Weld Strength

The weld strengths of the Ti-4Al-0.2O alloy obtained uniaxially and in a 1 to 2 stress field are plotted in Fig. 6 as a function of test temperature. Uniaxially the weld efficiency of the Ti-4Al-0.2O alloy was 100 per cent. Shannon and Brown [12] have shown that weld efficiencies of 100 per cent can be obtained with the Ti-5Al-2.5Sn ELI alloy.

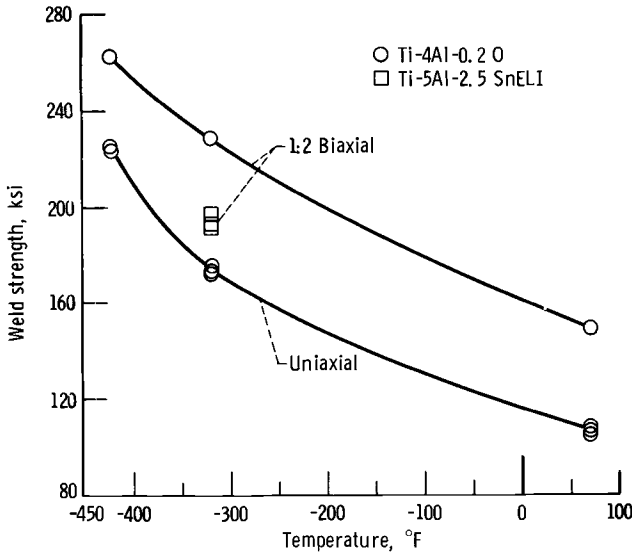


FIG. 6—Uniaxial and 1:2 biaxial weld strength of Ti-4Al-0.2O and Ti-5Al-2.5Sn ELI sheet as a function of test temperature.

Contrary to the uniaxial behavior, the biaxial weld strength was less than the parent material biaxial ultimate strength. In all cases the failure occurred along the fusion line. Biaxial weld data for the Ti-5Al-2.5Sn ELI alloy obtained at -320 F are included in Fig. 6. While the parent material biaxial yield strengths of the two alloys at this temperature were nearly identical, the biaxial weld strength of the Ti-4Al-0.2O alloy was about 17 per cent greater than that of Ti-5Al-2.5Sn ELI.

Correlation of Biaxial Strengthening and Plastic Poisson's Ratio

For a 1 to 2 stress field Eq 1 can be written in terms of plastic Poisson's ratio ν_p as follows:

$$\frac{\sigma_{yb}}{\sigma_{ys}} = \frac{2}{(5 - 4\nu_p)^{1/2}} \dots \dots \dots (4)$$

This relation indicates that it should be possible to characterize the degree of texture strengthening in a sheet material with plastic Poisson's ratio. In order to verify Eq 4, values of ν_p were obtained experimentally. These values are plotted in Fig. 7 versus average σ_{yb}/σ_{ys} obtained from pressure vessel tests.

In general, using ν_p to predict biaxial strengthening resulted in values of σ_{yb}/σ_{ys} close to those obtained experimentally. The greatest difference

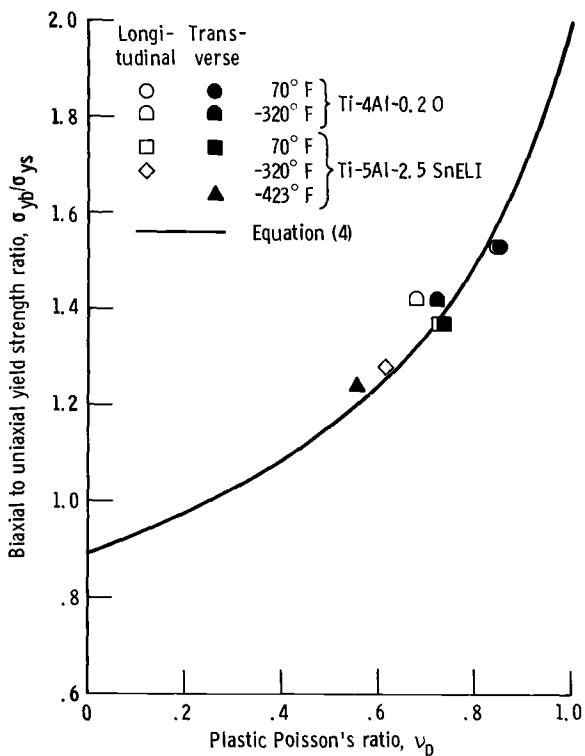


FIG. 7—Correlation of texture strengthening in a 1:2 stress field with plastic Poisson's ratio.

occurred with the Ti-4Al-0.2O alloy at -320 F where the predicted result was 7 per cent less than that obtained experimentally. The relation between ν_p and biaxial strengthening provides a relatively simple and inexpensive means of investigating the variability of the degree of texturing in sheet material.

Summary and Conclusions

Burst tests of cylinders fabricated from two textured titanium alloys, Ti-4Al-0.2O and Ti-5Al-2.5Sn ELI, resulted in yield and ultimate strengths that in some cases were more than 50 per cent greater than

those obtained uniaxially. With both alloys the strengthening effect of texture decreased as temperature decreased. In a 1 to 2 stress field the Ti-4Al-0.2O alloy generally had superior yield, ultimate, and weld strength properties at 70, -320 and -423 F. However, the Ti-5Al-2.5Sn ELI alloy exhibited less notch sensitivity at -320 and -423 F.

Plastic Poisson's ratio obtained from a uniaxial tension test can be used to characterize the degree of texture in sheet material.

References

- [1] Backofen, W. A., Hosford, W. F., Jr., and Burke, J. J., "Texture Hardening," *Transactions*, American Society for Metals, Vol. 55, No. 1, Mar. 1962, pp. 264-267.
- [2] Roberts, W. T., "Preferred Orientation and Anisotropy in Titanium," *Journal Less-Common Metals*, Vol. 4, 1962, pp. 345-361.
- [3] Larson, F. R., "Anisotropy of Titanium Sheet in Uniaxial Tension," *Transactions*, American Society for Metals, Vol. 57, No. 3, Sept. 1964, pp. 620-631.
- [4] Hatch, A. J., "Texture Strengthening of Titanium Alloys," *Transactions*, American Institute Metallurgical Engineers, Vol. 233, No. 1, Jan. 1965, pp. 44-50.
- [5] Larson, F. R., "Textures in Titanium Sheet and Its Effects on Plastic Flow Properties," Technical Report 65-24, DDC No. AD-626410, Army Materials Research Agency, 1965.
- [6] Sliney, J. L., Corrigan, D. A., and Schmid, F., "Preliminary Report on the Biaxial Tensile Behavior of Anisotropic Sheet Materials," Technical Report 63-11, DDC No. AD-421815, Army Materials Research Agency, 1963.
- [7] Babel, H. W. and Kam, C. Y., "Textured Titanium in Design," *Journal of Spacecraft and Rockets*, Vol. 3, No. 12, Dec. 1966, pp. 1779-1782.
- [8] Hill, R., "A Theory of the Yielding and Plastic Flow of Anisotropic Metals," *Proceedings*, Royal Society of London, Vol. 193A, No. 1033, May 27, 1948, pp. 281-297.
- [9] Sullivan, T. L. and Orange, T. W., "Continuity Gage Measurement of Crack Growth on Flat and Curved Surfaces at Cryogenic Temperatures," NASA TN D-3747, National Aeronautics and Space Administration, 1966.
- [10] Calvert, H. F. and Kemp, R. H., "Determination of Pressure Vessel Strengths at -423° F as Influenced by Notches of Various Radii," Paper No. 520B, Society of Automotive Engineers, 1962.
- [11] ASTM Special Committee on Fracture Toughness Testing of High-Strength Metallic Materials, "Fracture Testing of High-Strength Sheet Materials," *Bulletin*, American Society for Testing and Materials, No. 243, Jan. 1960, pp. 29-40.
- [12] Shannon, J. L. and Brown, W. F., "Effects of Several Production and Fabrication Variables on Sharp Notch Properties of 5Al-2.5Sn Titanium Alloy Sheet at Liquid Hydrogen Temperature," *Proceedings*, American Society for Testing and Materials, Vol. 63, 1963, pp. 809-823.
- [13] Anderson, R. B. and Sullivan, T. L., "Fracture Mechanics of Through-Cracked Cylindrical Pressure Vessels," NASA TN D-3252, National Aeronautics and Space Administration, 1966.

Low Cycle Fatigue and Wear

Effects of a 3.5 Per Cent Sodium Chloride Aqueous Saline Environment on the Fatigue Crack Propagation Characteristics of Titanium Alloys

REFERENCE: Crooker, T. W. and Lange, E. A., "Effects of a 3.5 Per Cent Sodium Chloride Aqueous Saline Environment on the Fatigue Crack Propagation Characteristics of Titanium Alloys," *Applications Related Phenomena in Titanium Alloys, ASTM STP 432*, American Society for Testing and Materials, 1968, pp. 251–267.

ABSTRACT: Fatigue crack propagation studies were conducted on Ti-6Al-4V, Ti-7Al-2Cb-1Ta, Ti-6Al-6V-2Sn-1Cu-0.5Fe, Ti-6Al-3V-1Mo, and Ti-7Al-2.5Mo alloys. These materials possess yield strengths in excess of 100 ksi, combined with favorable levels of fracture toughness, and they are currently under evaluation for application in large welded structures. Where an application involves repetitive loading, a knowledge of fatigue crack propagation characteristics is required for failure-safe design against fracture. Fabrication and nondestructive testing procedures cannot guarantee that crack-like defects which can grow to a critical size will not be present in plate-thickness sections containing welded joints. In addition, the role of an aggressive environment, such as salt water, in this failure mechanism is of the utmost importance. This paper reports on fatigue crack propagation data taken in both ambient room air and 3.5 per cent salt water environments. Surface-notched plate bend specimens were cycled in full-reverse (tension-to-compression) sinusoidal loading. The fatigue crack was observed optically, and the crack growth rate is described as an empirical power-law function of the total (elastic plus plastic) strain range. Fatigue crack growth rate relationships are first developed in an air environment and then employed as baselines for establishing the effect of the salt water environment. Comparisons are made among the fatigue crack propagation characteristics of the several titanium alloys described in this paper and among a broad spectrum of high-strength structural alloys, both ferrous and nonferrous, previously studied.

KEY WORDS: titanium alloys, fatigue, crack propagation, aqueous environment

¹ Materials research engineer and head, respectively, Plastic Flow Section, Strength of Metals Branch, Metallurgy Div., Naval Research Laboratory, Washington, D. C. Personal member ASTM.

TABLE 1—Mechanical properties.^a

Alloy	NRL Code	Fracture Path Orientation	0.2% Yield Strength, ksi	Ultimate Tensile Strength, ksi	Reduction of Area, %	Elongation, %	C ₀ at 32 F, ft. lb	DWTT at 30 F, ft. lb	K ₁₀ , ksi√in.	K _{1x} , ksi√in.	K _{1sec} , ksi√in.	Remarks	
Ti-6Al-4V	T5	RW ^b	125	131	44	12	29	2075	...	120	105	"mill annealed"—as-received	
Ti-6Al-4V	T27	RW ^b	116	128	26	12	..	1228	...	88	67	"mill annealed"—as-received	
Ti-7Al-2Cb-1Ta	TA2	RW ^b	107	120	28	13	39	2675	"mill annealed"—as-received	
Ti-7Al-2Cb-1Ta	T78	RW ^b	110 ^d	3281	...	130	88	processing proprietary to TMCA—as-received	
Ti-6Al-6V-2Sn-1Cu-0.5Fe	T-92	A ^c B	122.0 123.8	140.4 140.0	24.4 18.0	10.0 8.9	20 17	681 681	98	111	96	circular rolled plate 50% + reduction below β transus	
Ti-6Al-3V-1Mo	T-93	A ^c B	116.5 109.8	128.4 124.6	27.5 21.5	10.7 8.9	23 25	1173 1540	118	116	110	circular rolled plate 50% + reduction below β transus	
Ti-7Al-2.5Mo	T-94	A ^c B	119.0 120.5	133.1 134.9	24.1 20.2	8.6 8.6	27 30	1540 1662	101	80	circular rolled plate 50% + reduction below β transus

^a Reported in Refs 4 through 8.^b See Ref 3.^c Circular-rolled plate material. Arbitrary orientations designated A and B are chosen at right angles to each other.^d Estimated from producer's data.

For the past several years, high-strength titanium alloys have been the subject of an intensive research program to develop their usefulness for submersible vehicle pressure hulls. Titanium alloys are the most promising weldable structural materials currently available for improving strength-to-density ratios beyond the capabilities of high strength structural steels.

The Metallurgy Division of the Naval Research Laboratory has assumed a position of leadership in this effort through its broad-based titanium research program. The approach to this research effort is grounded on the philosophy that large complex welded structures cannot be fabricated, proof-tested, and subsequently be put into use for service periods spanning decades without encountering sharp flaws in critically stressed locations. Therefore, the failure-safe design of such structures must take into account a high probability of pre-existing flaws whose growth to a critical size under the influence of repeated load and environment must be prevented. In order to provide the necessary knowledge for such design criteria, this research program is investigating high-strength titanium alloys to simultaneously ascertain fracture toughness, weldability, heat treatability, optimization of processing variables, resistance to stress-corrosion-cracking, and resistance to fatigue crack propagation. The fatigue research lays particular emphasis on the role of environment in determining fatigue crack propagation characteristics.

This paper describes the results of the fatigue crack propagation research conducted to date. However, detailed discussion will be limited to the most promising alloys. The problems of stress-corrosion-cracking and corrosion fatigue crack propagation in Ti-7Al-2Cb-1Ta have been the subject of a separate analysis [1]² and will not be discussed in this paper.

Description of Alloys

The alloys studied in this investigation include the following: Ti-6Al-4V, Ti-7Al-2Cb-1Ta, Ti-6Al-6V-2Sn-1Cu-0.5Fe, Ti-6Al-3V-1Mo, and Ti-7Al-2.5Mo. In summary, all of these alloys possess yield strengths in excess of 100 ksi, are weldable, possess favorable levels of fracture toughness, and with the exception of Ti-7Al-2Cb-1Ta, possess favorable stress-corrosion-cracking characteristics in the heat treatment condition studied.

Detailed mechanical properties are listed in Table 1, with references to the source of the data. All mechanical properties reported are from 1-in.-thick plate stock, with one exception. The Ti-7Al-2.5Mo test material was taken from 1.25-in.-thick plate stock. Nominal chemical compositions include a maximum oxygen content of 0.08 per cent by weight.

² The italic numbers in brackets refer to the list of references appended to this paper.

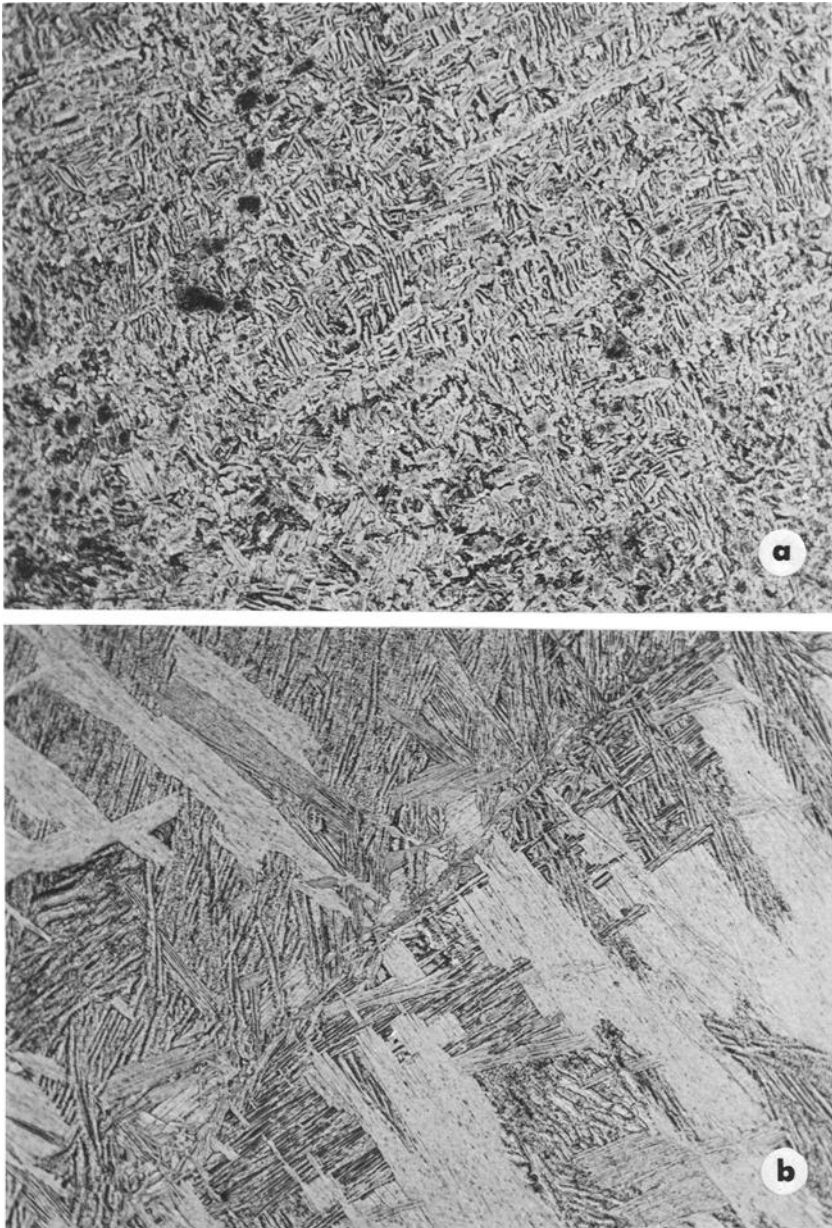


FIG. 1—Typical microstructures observed in (a) *Ti-6Al-4V* (T5), (b) *Ti-6Al-4V* (T27), (c) *Ti-6Al-3V-1Mo* (T93), and (d) *Ti-7Al-2.5Mo* (T94) ($\times 250$).

The investigation described in this paper was conducted in two phases. The initial phase concerned two samples of *Ti-6Al-4V* (NRL code numbers T5 and T27) and one sample of *Ti-7Al-2Cb-1Ta* (code TA2). Work

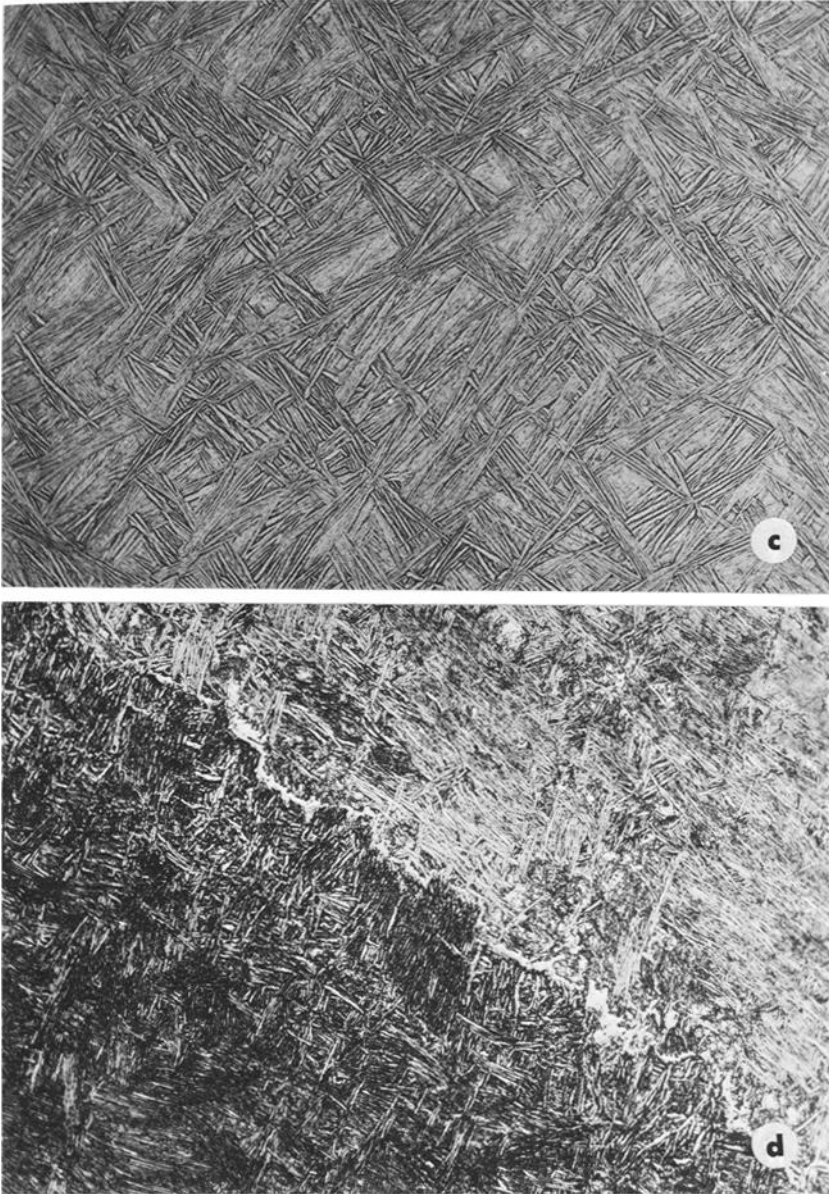


FIG. 1, (c) and (d).

on these alloys was undertaken prior to the discovery of serious stress-corrosion-cracking problems in certain titanium alloys, notably Ti-7Al-2Cb-1Ta and Ti-8Al-1Mo-1V. Consequently, the processing and heat treatment given this initial group of alloys was primarily intended to optimize yield strength and fracture toughness. These alloys were tested in

the as-received mill annealed condition. They had been rolled to 1 in. thickness in the alpha plus beta temperature region, followed by air cooling.

The second phase of this investigation was undertaken after the problem of stress-corrosion-cracking had begun to receive considerable attention. The remaining alloys, Ti-7Al-2Cb-1Ta (T78), Ti-6Al-6V-2Sn-1Cu-0.5Fe (T92), Ti-6Al-3V-1Mo (T-93), and Ti-7Al-2.5Mo (T94), were tested in the as-received condition which now included spray quenching after rolling. The spray quenching has the effect of somewhat reducing fracture toughness but greatly enhancing resistance to stress-corrosion-cracking. This procedure produces the best available trade-off between

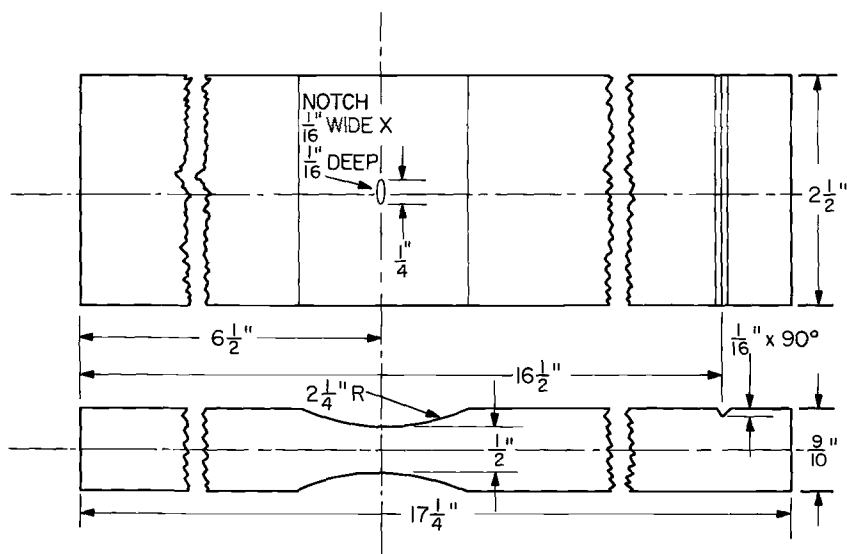


FIG. 2—Dimensions of the plate bend fatigue specimen.

yield strength, fracture toughness, and stress-corrosion-cracking resistance.

A detailed metallurgical description of each alloy is not available because of the large number of commercial and experimental alloys presently being investigated. However, photomicrographs of four alloys, Ti-6Al-4V (T5), Ti-6Al-4V (T27), Ti-6Al-3V-1Mo (T93), and Ti-7Al-2.5Mo (T94) are shown in Fig. 1.

Experimental Approach

Apparatus

The experimental data reported in this paper are based on the optically observed growth of fatigue cracks across the surface of center-notched plate bend specimens. A detailed drawing of the plate bend

specimen is shown in Fig. 2. The specimens are cantilever loaded in full-reverse (tension-to-compression) strain cycling by hydraulically actuated automatic fatigue machines. Figure 3 is a general view of the test setup.

Rapid fatigue crack initiation at relatively low cyclic strain levels is

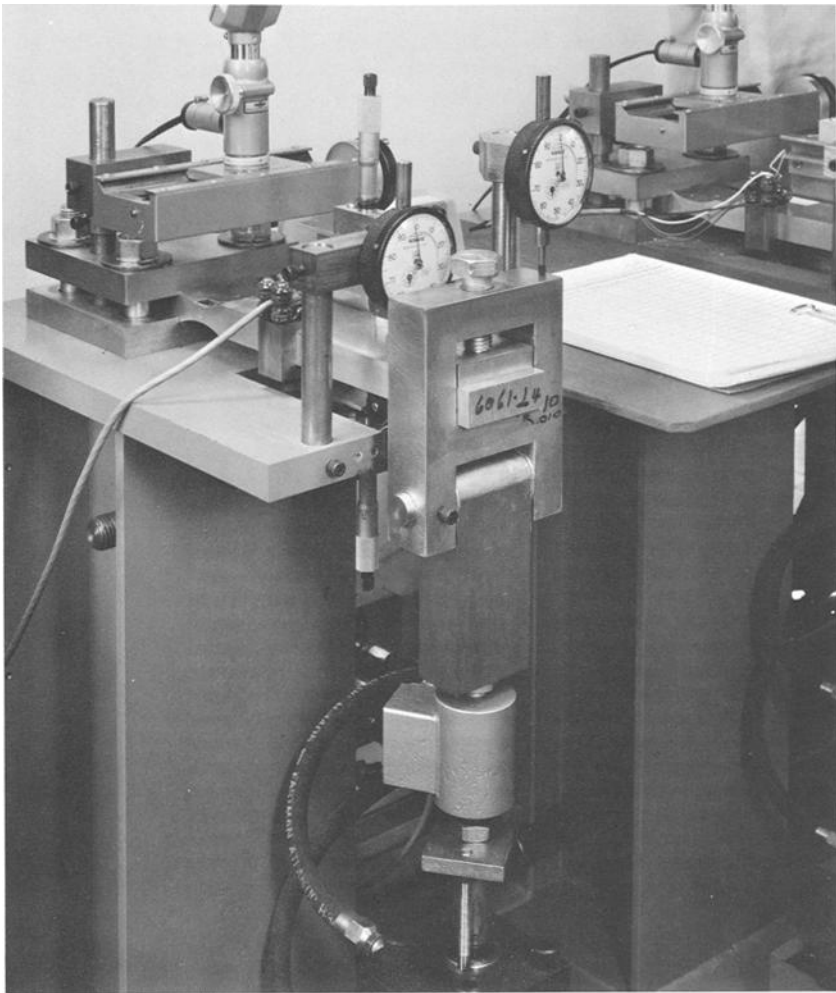


FIG. 3—The plate bend fatigue test setup.

achieved by means of an engraved center surface notch placed at the minimum thickness of the test section. A foil-type resistance strain gage is placed on the test section well ahead of the advancing fatigue crack to monitor nominal surface strains, which are recorded as total (elastic plus plastic) strain range values. These details are shown in Fig. 4.

The progress of the fatigue crack across the test section is observed from directly above through a slide-mounted optical micrometer. Extensions at both ends of the crack are monitored, and the sum is reported. Automatic deflection control of the test is obtained through micrometer adjusted microswitches which contact the specimen arm at the maximum and minimum points in the loading cycle. The automatic op-

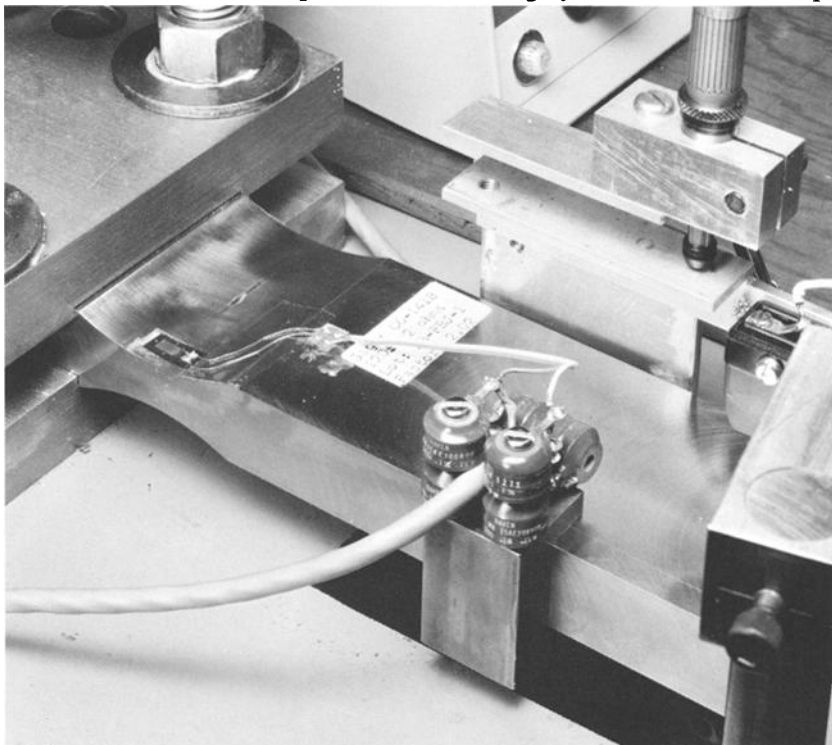


FIG. 4—The plate bend fatigue specimen. Note the machined surface notch to facilitate crack initiation and the foil resistance-type strain gage for measuring the strain range.

eration provides a sinusoidal loading pattern at a cycling rate of approximately 5 cpm.

In the salt water environment tests, a corrosion cell is placed over the portion of the test section containing the fatigue crack. The corrosion cell is made of molded polyurethane which is relatively soft and flexes with the specimen. The 3.5 per cent salt water solution is constantly circulated through the corrosion cell from a reservoir by a small electric pump. The solution undergoes filtering and periodic monitoring of its pH value and salt content. A glass cover at the top of the corrosion cell permits optical observation of the fatigue crack.

Procedure

Based on extensive experience with this test method described in Ref 2, it has been found that in the plate bend specimen constant total strain range cycling results in a constant value of fatigue crack growth rate. For this reason, all tests reported in this paper were conducted under

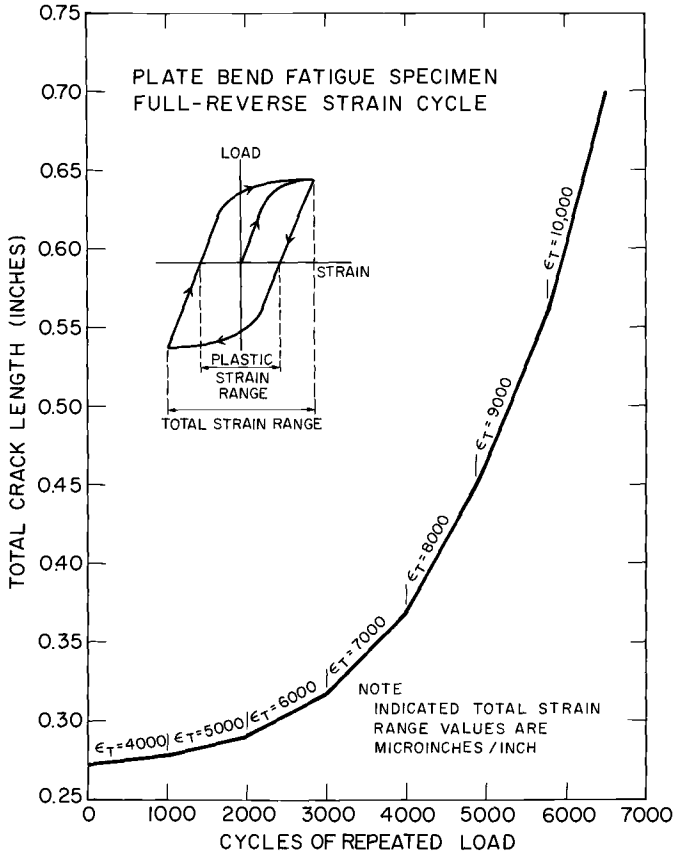


FIG. 5—Illustration showing the experimental procedure of increasing total strain range at given intervals.

constant total strain range loading. Such loading is obtained by gradually reducing the deflection control limits as the fatigue crack increases in size.

The general procedure followed is schematically illustrated in Fig. 5. Cycling is begun at the lowest desired strain range and is continued until a fatigue crack is initiated, propagates away from the mechanical notch, and establishes a constant rate of growth. Then the specimen is loaded

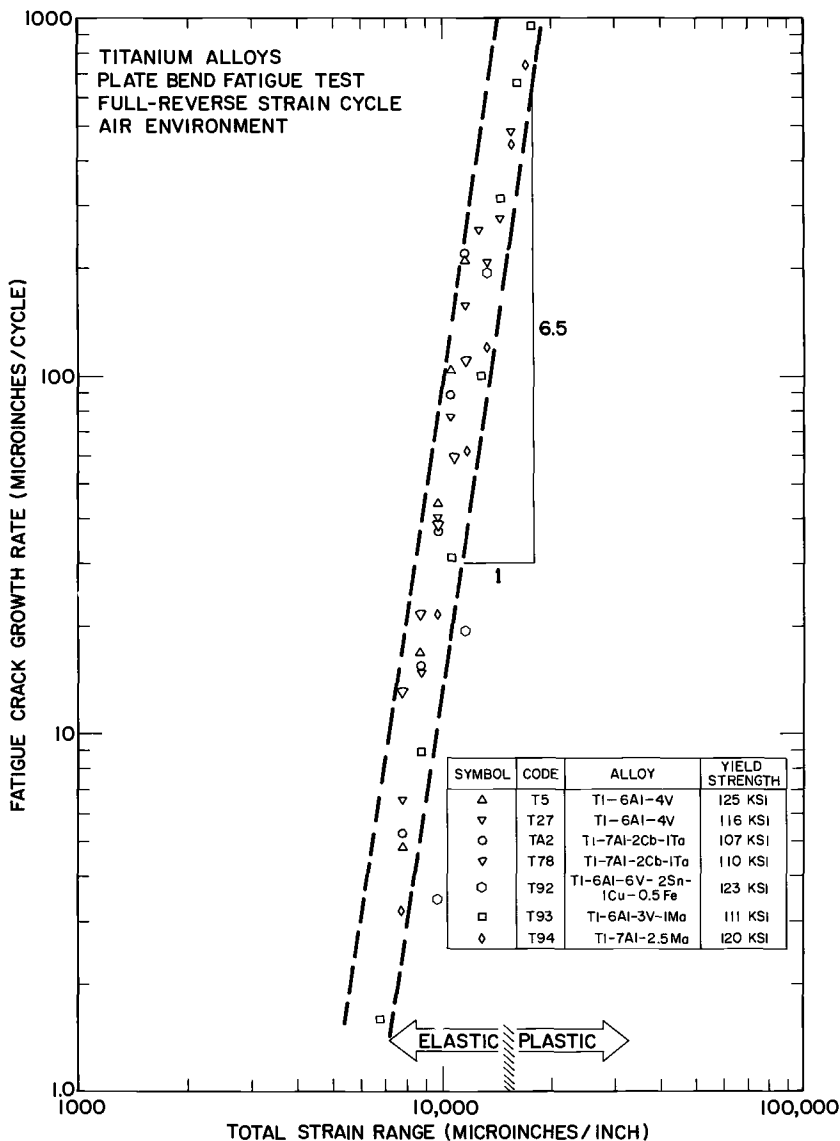


FIG. 6—Log-log plot of fatigue crack growth rate versus total strain range for titanium alloys in an air environment.

to the next higher strain range level desired and cycled until the new, higher rate of growth is established. Using this procedure, one specimen can be used to generate several successive data points. As a general practice, data on a material are first taken in air, and then the test procedures are repeated with fresh specimens under salt water.

Upon completion of fatigue testing, the plate bend specimens are

pulled apart in tension to expose the fatigue surface. Basically, the fatigue crack grows radially from the notch until its downward growth is inhibited by the low-stress region near the neutral bending axis. Beyond this point, the outward growth continues. The shape of the crack front near the test surface remains nearly constant throughout the various stages of growth. This is probably the reason for the singular correlation between the fatigue crack growth rate and total strain range, irrespective of flaw size.

Results and Discussion

Air Environment Data

The air environment fatigue crack propagation data for all titanium alloys studied in this program are shown in Fig. 6. These data are plotted on log-log coordinates in terms of fatigue crack growth rate as a function of total strain range. With the exception of Ti-6Al-6V-2Sn-1Cu-0.5Fe (T92), all of the data are grouped within a single scatter band and will be treated collectively rather than attempting to deal with small individual differences. Seven titanium alloys are included in this plot, and a legend is provided on Fig. 6 for individual identification.

With regard to the fatigue crack propagation characteristics of these alloys, Fig. 6 reveals two points of general discussion. First and most obvious, there are no broad differences in fatigue crack propagation behavior among these alloys. For the most part, these alloys possess similar strength and toughness properties despite their differences in chemical composition. The range of fatigue properties illustrated by the width of the scatter band in Fig. 6 would seem to be in line with variations in other mechanical properties among this group of alloys. Based on the small amount of data available, the behavior of Ti-6Al-6V-2Sn-1Cu-0.5Fe (T92) is considered to be anomalous and bears further investigation. This alloy was highly resistant to the initiation of fatigue cracks, but, once underway, the crack growth rates rapidly increased to similar values measured for the other alloys in the group shown.

Perhaps the most important common characteristic of the data in Fig. 6 is the steepness of the slopes of the individual relationships which fall within the indicated scatter band. The equations between fatigue crack growth rate and total strain range established by this plot have the form:

$$\frac{d(2a)}{dN} \propto (\epsilon_T)^m$$

where:

$d(2a)/dN$ = fatigue crack growth rate,

ϵ_T = total strain range, and

m = power law exponent or slope of the curves.

The slopes of these relationships range from 6:1 to 7:1 for this group of titanium alloys. By way of comparison, 4:1 is the common slope of the fatigue crack propagation relationships for most martensitic structural steels evaluated by this test method.

In order to better illustrate the asymptotic form of these steep power

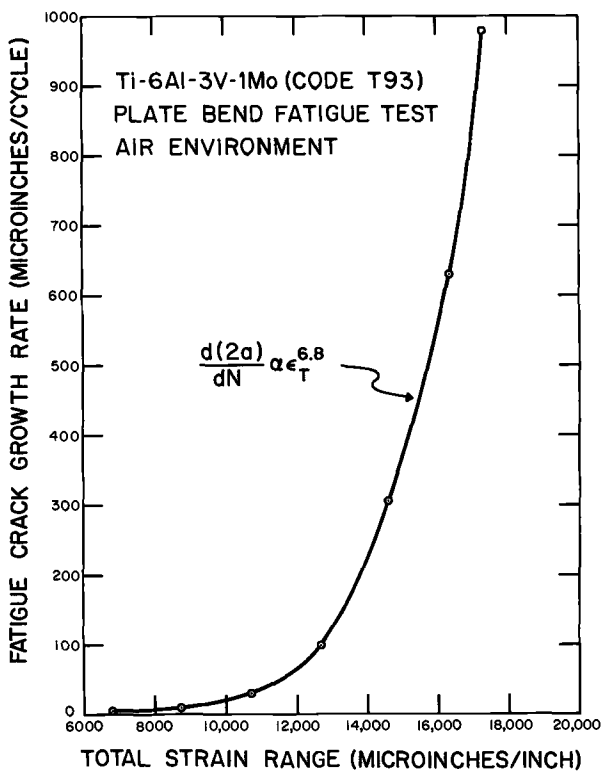


FIG. 7—Linear plot of fatigue crack growth rate versus total strain range for Ti-6Al-3V-1Mo in air environment.

law relationships for fatigue crack propagation in titanium alloys, Fig. 7 shows a linear plot of the data for Ti-6Al-3V-1Mo (T93). This typical plot rises rapidly from almost immeasurably slow rates of crack growth to rates nearly 1000 times greater as the total strain range increases by less than a factor of three. Behavior of this sort suggests that designing titanium structures against failure by subcritical flaw growth in fatigue might best be approached as a “threshold phenomenon.” Below a certain critical level of load intensity, as measured by total strain range or other suitable parameter, subcritical flaw growth by fatigue could be consid-

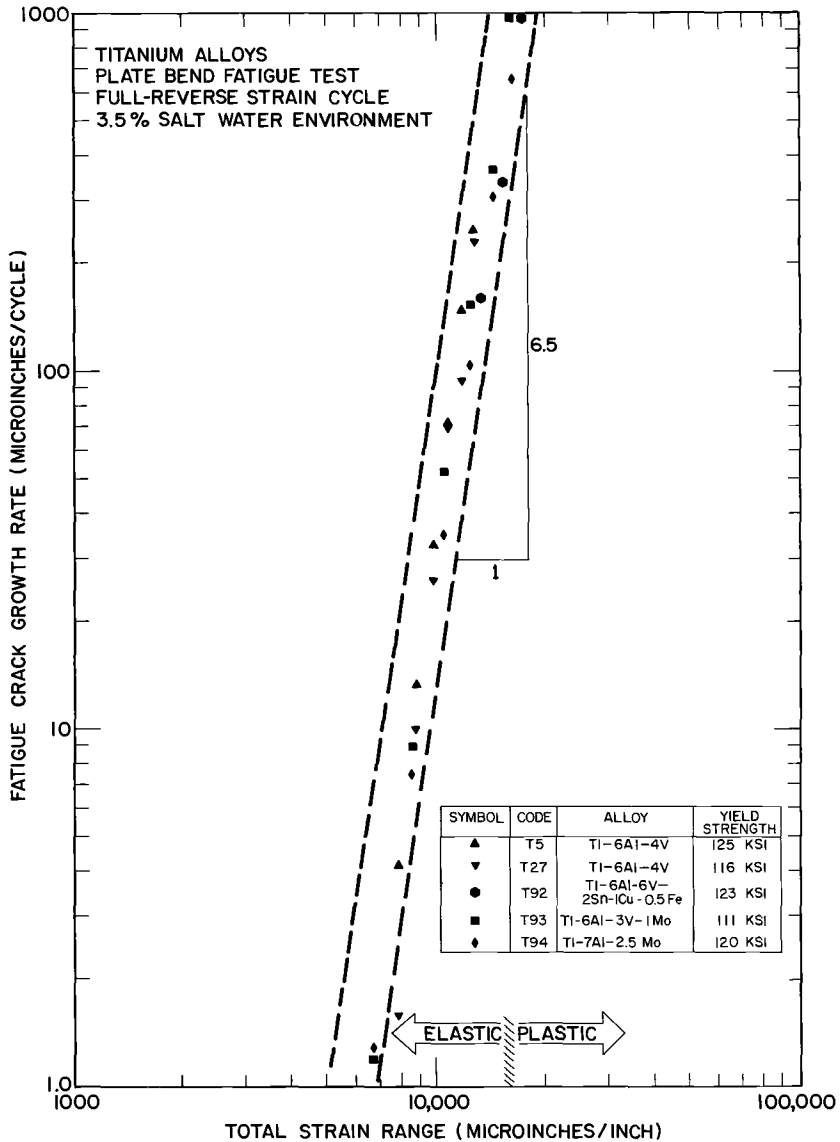


FIG. 8—Log-log plot of fatigue crack growth rate versus total strain range for titanium alloys in a 3.5 per cent salt water environment. The scatterband limits are reproduced from the air environment data plot for reference.

ered harmless; above this critical level of load intensity an increasingly dangerous potential for failure would exist.

Finally, it should be pointed out, in considering the data on Fig. 6, that the total strain range values employed in these tests are well within the nominal working stress levels anticipated for these alloys. The elastic-

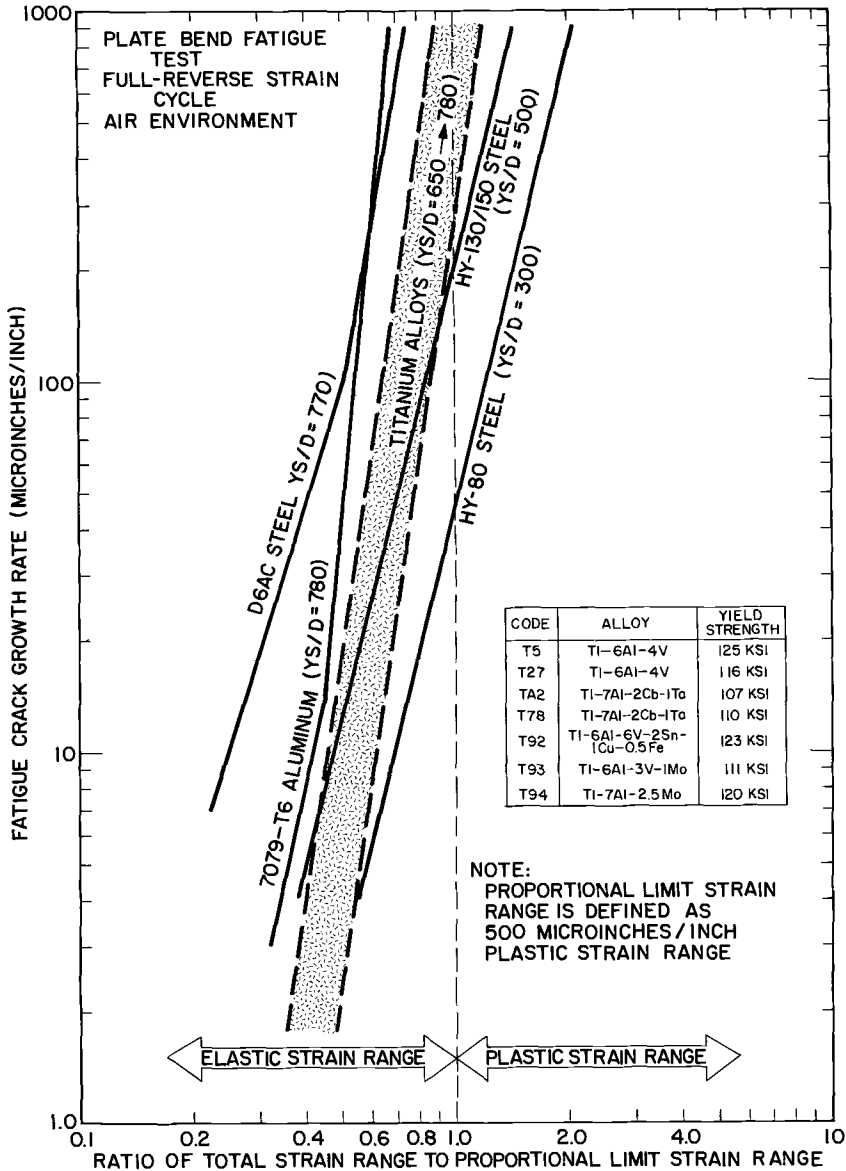


FIG. 9—Log-log plot of fatigue crack growth rate versus the ratio of total strain range to proportional limit strain range for titanium alloys and several conventional structural materials. Yield strength-to-density ratios are indicated for each material.

plastic transition region for these materials in the plate bend specimen configuration is indicated on Fig. 6 for reference. The total strain range values employed are approximately equivalent to cyclic stress amplitudes of 50 to 100 per cent of yield strength for these alloys.

Aqueous Environment Data

The results of the fatigue crack propagation tests conducted in a 3.5 per cent salt water environment are shown on Fig. 8. This is an identical plot to the air environment summary data display, Fig. 6. The scatter band from the air environment data display is reproduced on Fig. 8 for reference purposes. No data from salt water environment tests of Ti-7Al-2Cb-1Ta alloys are included, since the stress-corrosion-cracking phenomenon in these alloys has been documented previously [1].

The salt water environment fatigue data, shown in Fig. 8, lie well within the same scatter band as was drawn for the air environment fatigue data. Whether viewed individually or collectively, there is no evidence of degradation in fatigue crack propagation resistance among these alloys due to the presence of a 3.5 per cent salt water environment. However, a statement of caution is in order. The sinusoidal loading pattern employed in these tests did not include a hold period at peak load. Also, laboratory 3.5 per cent salt water solution has been found to be a less aggressive environment than actual seawater. These two facts should be kept in mind when evaluating the favorable results indicated by the data in Fig. 8.

Comparative Evaluations

A comparative evaluation of the fatigue crack propagation characteristics of these titanium alloys is shown in Fig. 9. This figure is a log-log plot of fatigue crack growth rate versus the ratio of total strain range to proportional limit strain range for each of the materials shown. By converting strain units to this ratio, a normalized basis is established for comparing the fatigue crack propagation behavior of materials possessing widely different elastic moduli and yield strengths. The curves in Fig. 9 are based on the results of plate bend fatigue tests conducted in an air environment.

As in previous plots, the titanium data are treated collectively, and the scatter band limits from Fig. 6 are reproduced for reference purposes. Relationships for four additional structural materials, HY-80, HY-130/150, and D6AC steels, plus 7079-T6 aluminum, are indicated on Fig. 9 as a basis for comparative evaluations. In addition, yield strength-to-density ratios are listed for each material, since this is a critical criterion in aerospace and hydrospace structural applications.

In brief summary, Fig. 9 suggests that this group of titanium alloys possesses inferior fatigue crack propagation resistance when compared to HY-80 or HY-130/150 (5Ni-Cr-Mo-V) steels which have lower yield strength-to-density ratios. This observation is based on the tendency of these titanium alloys to develop much more rapid rates of fatigue crack growth at cyclic strain levels approaching proportional limit strains. However, these titanium alloys are definitely superior in this regard when compared to conventional high-strength steels or aluminum alloys which

possess equivalent yield strength-to-density ratios. The relationships shown for D6AC steel and 7079-T6 aluminum illustrate this point. In addition, all of the materials shown on Fig. 9 for comparative purposes are sensitive to aqueous environments. The presence of an aqueous environment can increase fatigue crack growth rates in HY-80 and HY-130/150 steels by a factor of 5 and by a factor of 10 in D6AC steel and 7079-T6 aluminum, whereas no increases in crack growth rates due to environment were observed in these titanium alloys except for Ti-7Al-2Cb-1Ta. Therefore, from a fatigue crack propagation standpoint, these titanium alloys appear to merit consideration among the promising new materials currently under evaluation for structural applications which require high strength-to-density ratios and resistance to aqueous environmental attack.

Summary and Conclusions

A fatigue crack propagation study was conducted on the following high-strength titanium alloys: Ti-6Al-4V, Ti-7Al-2Cb-1Ta, Ti-6Al-6V-2Sn-1Cu-0.5Fe, Ti-6Al-3V-1Mo, and Ti-7Al-2.5Mo. Plate bend specimens were employed using sinusoidal tension-to-compression strain cycling at a rate of approximately 5 cpm. Data based on optical measurements of fatigue crack growth were taken in both ambient room air and 3.5 per cent salt water environments. The following conclusions were reached from this investigation.

1. In an air environment, all of the titanium alloys tested exhibited similar fatigue crack propagation characteristics, as determined by empirical power law relationships between fatigue crack growth rate and total strain range of the form $[d(2a)/dN] \propto (\epsilon_T)^m$. The average exponent value for these relationships was 6.5, which indicates that fatigue crack propagation in these titanium alloys is highly sensitive to cyclic strain.

2. With the exception of Ti-7Al-2Cb-1Ta, no degradation in fatigue crack propagation resistance was observed with the introduction of the 3.5 per cent salt water environment. This is considered to be a highly favorable resultant but must be tempered by the knowledge that the test conditions, that is, sinusoidal loading pattern and laboratory salt water solution, are not potentially so severe as many actual service situations.

3. The fatigue crack propagation characteristics of these titanium alloys compare favorably with competitive high-strength structural materials. For applications which require high yield strength-to-density ratios and resistance to aqueous environmental attack these titanium alloys merit consideration.

Acknowledgments

The authors acknowledge the efforts of R. E. Morey, S. J. McKaye, and R. J. Hicks, who carried out the experimental work described in this

paper, and the Naval Ship Systems Command and the Deep Submergence Systems Project for a major portion of the support of this research.

References

- [1] Judy, R. W., Jr., et al, "Low-Cycle Fatigue Crack Propagation and Fractographic Investigation of Ti-7Al-2Cb-1Ta and Ti-6Al-4V in Air and in Aqueous Environments," *Transactions, American Society for Metals*, Vol. 59, No. 2, June 1966.
- [2] Crooker, T. W. and Lange, E. A., "Low-Cycle Fatigue Crack Propagation Resistance of Materials for Large Welded Structures," *Fatigue Crack Propagation, ASTM STP 415*, American Society for Testing and Materials, 1967.
- [3] The ASTM Committee on Fracture Testing of High-Strength Metallic Materials, "The Slow Growth and Rapid Propagation of Crack," (Second Report), *Materials Research and Standards*, Vol. 1, No. 5, May 1961.
- [4] Puzak, P. P. et al, "Metallurgical Characteristics of High Strength Structural Materials," (First Quarterly Report), NRL Memorandum Report 1438, Naval Research Laboratory, June 30, 1963.
- [5] Pellini, W. S. et al, "Metallurgical Characteristics of High Strength Structural Materials," (Sixth Quarterly Report), NRL Report 6258, Naval Research Laboratory, Dec. 1964.
- [6] Brown, B. F. et al, "Marine Corrosion Studies," Third Interim Report of Progress, NRL Memorandum Report 1634, Naval Research Laboratory, July 1965.
- [7] Goode, R. J. et al, "Metallurgical Characteristics of High Strength Structural Materials," (Ninth Quarterly Report), NRL Report 6405, Naval Research Laboratory, Nov. 1965.
- [8] Judy, R. W., Jr., and Goode, R. J., "Stress Corrosion Cracking Characteristics of Alloys of Titanium in Salt Water," NRL Report 6564, Naval Research Laboratory, 21 July 1967.

Lubricants and Wear Coatings for Titanium

REFERENCE: Kostman, S. J., "Lubricants and Wear Coatings for Titanium," *Applications Related Phenomena in Titanium Alloys*, ASTM STP 432, American Society for Testing and Materials, 1968, pp. 268–282.

ABSTRACT: Titanium has poor resistance to wear and galling and is among the most difficult of metals to lubricate. This condition is attributable to the nature of the adsorbed gas film on the metal's surface. Emphasis has been placed on modifying the surface to improve wear and lubrication properties. Liquid lubricants were found to have little effectiveness on untreated titanium, but solid lubricants such as molybdenum sulfide (MoS₂) applied to properly roughened surfaces can give useful wear life. Chemical and electrochemical conversion coatings combined with mechanical or chemical roughening provide the optimum pretreatment for bonding solid lubricants to titanium. Surface hardening processes such as nitriding and oxidizing produce wear resistant surfaces which may be lubricated by standard liquid lubricants, even at high loads. Platings of chromium or nickel on titanium are promising from the standpoint of wear resistance, but poor adhesion limits their usefulness. The most practical treatments for improving the wear resistance of titanium involve spraying of metallic or ceramic compounds such as molybdenum, titanium oxide, chromium oxide, and tungsten carbide.

KEY WORDS: titanium, wear, lubricants, anodizing, wear tests, coatings, dry-film lubricants, surface hardening

The poor resistance of titanium to wear and galling has limited its use in some applications where other properties would make it an attractive choice. Furthermore, titanium is among the most difficult of all metals to lubricate, and this is often reflected in the relatively high cost of titanium metal working and fabrication. Considerable effort has, therefore, been expended to devise practical surface treatments, coatings, or lubricants to minimize or eliminate the problem.

Most of the work with titanium has centered around modifying the surface, since it was determined early in the metal's commercial history that standard lubricants would not be effective on bare surfaces. The

¹ Development metallurgist, Technical Service Dept., Titanium Metals Corp. of America, West Caldwell, N. J.

application of a coating or surface treatment effectively eliminates the difficulties of having to lubricate titanium.

The wear evaluation of surface treatments for titanium (or any metal) is not generally simple, however. The problem is mainly involved in the number of variables which need to be controlled, and in the desire to have a test simulate a given set of service conditions. The large variation in test equipment, procedures, and conditions limits the usefulness of the little wear and frictional data available in the literature.

The test program described in this report was designed in part to screen selected coatings, treatments, and lubricants as to effectiveness, applicability, and limitations by the use of a standard testing procedure. The results reported are for the early phases of screening in which a large variety of lubricants and coatings were examined. The discussion will first cover the background of the titanium wear problem with emphasis on surface properties. Then, some of the results of the present program will be presented and discussed in terms of previously published information and potential engineering applications.

General Considerations of Titanium Wear

To understand the wear and frictional behavior of titanium and the performance of lubricants and coatings, it is necessary to first examine the nature of the titanium surface.

The wear and frictional behavior of titanium is presently best explained in terms of a thin, adsorbed film of gases, probably oxygen and possibly nitrogen, on the metal surface. The presence of this film on normally clean titanium has been demonstrated by Farnsworth et al [1]² and Rowe [2], and is now generally accepted [3]. The layer of adsorbed gas prevents metal-to-metal contact at light loads and may explain the low coefficient of friction and relatively low-wear rates observed with unlubricated titanium in sliding contact. In this connection, the dynamic coefficient of friction of clean titanium sliding on titanium, variously reported as between 0.45 and 0.49, is the lowest of any known metal sliding on itself [4]. Furthermore, the wear rate of unlubricated titanium sliding on titanium is correspondingly low, being about one third that found for mild steel on mild steel in a comparable test [5].

The surface film also may be used to explain the poor adhesion of ordinary lubricants to titanium. Apparently, lubricants are unable to combine with the gas layer or to penetrate the layer to form a bond with bare titanium. The ability of the film to reform instantly in air or various aqueous media probably causes the difficulty encountered in electro-

² The italic numbers in brackets refer to the list of references appended to this paper.

plating on titanium. The film acts as a barrier to adhesion of the plated metal.

At high loads, the surface layer is broken up, allowing contact of clean metal surfaces, and subsequent galling and seizing. The particular severity of surface interactions noted with titanium may be attributable

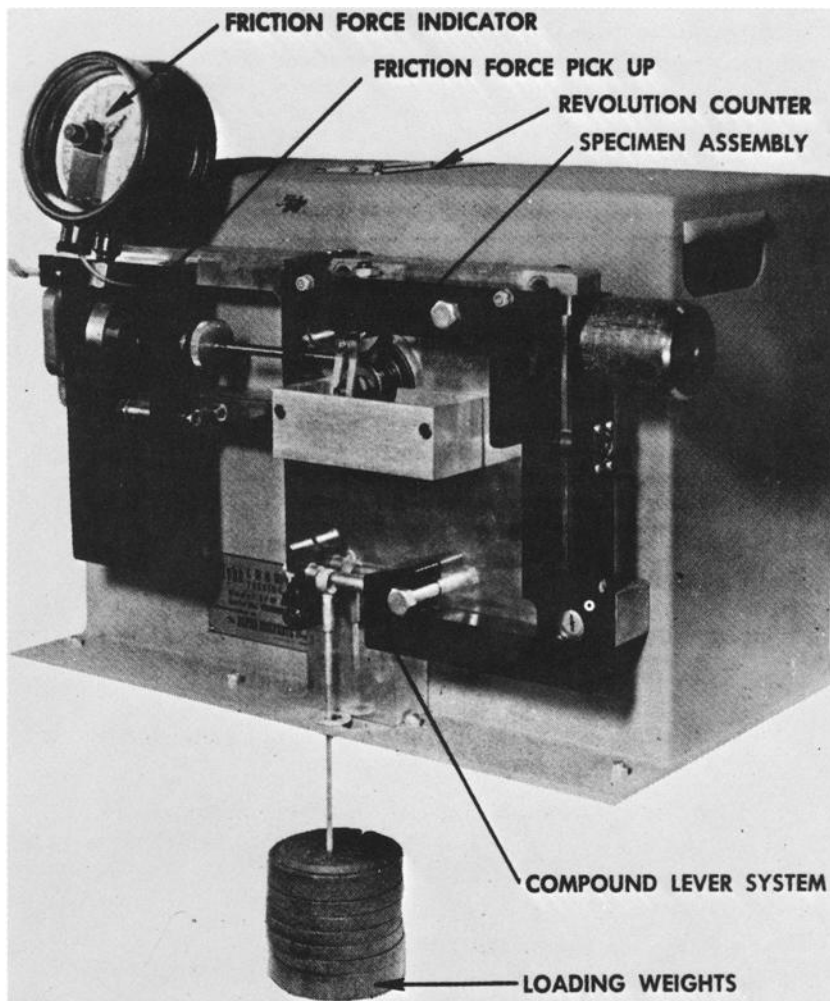


FIG. 1—Alpha LFW-1 lubricant and wear tester.

to an apparently high-surface energy of adhesion for the lubricated metal. Rabinowicz [6] has applied the criterion of the ratio of surface energy to hardness as an indicator of the type of surface interactions to be expected of materials in sliding contact. High ratios, characteristic of soft metals such as antimony and lead are bad, while materials such as ce-

ramics, with low ratios, are good in sliding contacts [6]. Titanium, with only moderate hardness gives a value of the surface energy/hardness ratio of about 20 A, comparable to iron. This, in itself, does not appear extraordinary.

However, the principal effect of a lubricant on a metal is to reduce the surface energy of adhesion and thus prevent severe adhesive interactions

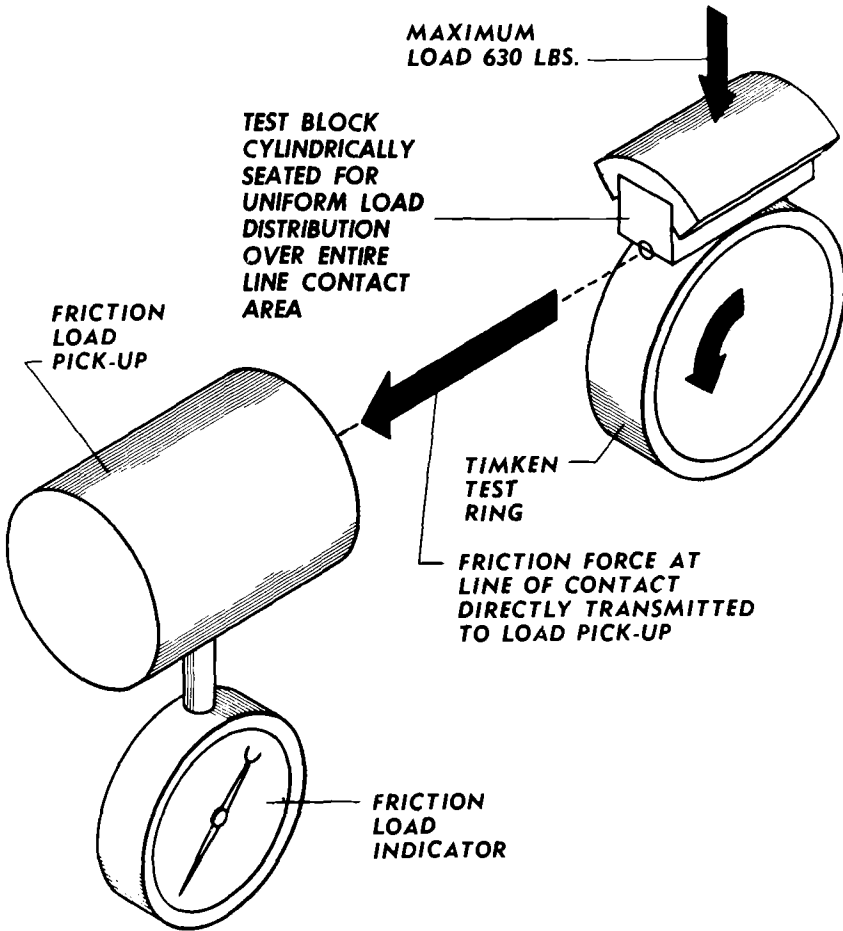


FIG. 2—Wear test specimen configuration.

during sliding contact [7]. In the case of titanium, this reduction in surface energy probably is not achieved because of some yet unknown property of the adsorbed gas film.

Based on these considerations of the titanium surface, it is not surprising that most emphasis has been placed on modifying the surface and then lubricating the new surface with standard lubricants.

Materials and Procedures

Ti-6Al-4V was selected for testing on the basis of ready availability and its wide application. The alloy was used in the annealed condition having a Rockwell-C hardness of 32. While there is undoubtedly some difference to be expected in the performance of various alloy grades, the effect is considered second order in the type of test used. The steel specimens used in several of the tests were heat-treated Starrett-496, hardened to Rockwell C-60. These were obtained from the test machine manufacturer. All test specimens were finish machined 8 to 16 $\mu\text{in. rms}$.

Wear testing was done on an Alpha-Molykote LFW-1 modified test machine. An overall view of this equipment is shown in Fig. 1. The specimen configuration, shown schematically in Fig. 2, is that of the modified "Timken" test, used widely in the United States for evaluating solid film lubricants. The specimen set consists of a cylindrical bearing ring 1.378 in. outside diameter, and a rectangular block 0.250 by 0.400 by 0.620 in. These are arranged to provide a line contact. A normal force is produced on the block by dead weights on the lower end of a compound lever system. The test ring revolves in contact with the block at any speed between 0 and 200 rpm, and the normal load may be applied in 10-lb or 30-lb increments up to a maximum load of 630 lb. During operation the machine provides a continuous read-out of the frictional force between the specimens, a continuous indication of revolutions per minute, sliding velocity, and a count of revolutions. Coefficient of friction is computed from the ratio of the frictional force to normal load.

The range of coating and lubricant types examined in this program, and the lack of prior experience with many of these, indicated that several types of tests would be necessary. Inasmuch as most of the non-metallic surface treatments for titanium, including anodizing and conversion coating, are used in conjunction with solid-film lubricants, the procedure used most frequently in these tests was that generally adopted by the solid-film lubricant industry for use with the Timken configuration. This procedure involves step-wise loading of the specimens to the maximum load at a sliding velocity of 26 ft/min. The stepped loading procedure provides a standardized run-in period before the maximum load is applied. The frictional force is recorded at the instant of each loading. When solid film lubricants are used, the criterion of failure is arbitrarily set at a frictional force of 100 lb. The minimum coefficient of friction at this force is 0.16, which is indicative of lubricant failure. The procedure is presently under study for adoption as a standard by ASTM Technical L-Subcommittee V.

The procedure described previously was also useful for testing certain metallic coatings lubricated by liquids. However, a different procedure was found necessary for evaluating liquid lubricants on uncoated

titanium. The effectiveness of these lubricants is load-limited, and the severe test used with coated specimens caused very rapid surface damage, with little gain in information. Thus, the procedure adopted for liquid lubricants consists of the application of 10 lb of load for 10^4 cycles, at a sliding speed of 26 ft/min. The wear scar is then measured. Coefficient of friction is also recorded at the start, 1000, 5000, and 10,000 cycles. Comparison between lubricants can be made on the basis of frictional properties and wear scar dimensions.

The specific load on a specimen, in pounds per square inch, varies during a test, from a maximum at the start to a minimum at completion. Since wear begins immediately, the line contact broadens to an area contact, and the stress decreases continuously during a test once the maximum load is applied. The minimum contact pressure is calculated at the end of a test from wear scar dimensions.

TABLE 1—Performance of liquid lubricants on untreated Ti-6Al-4V.^a

Lubricant	Coefficient of Friction	Average Wear Rate, in./ft of sliding
SAE-30.....	0.45 to 0.49	4.7×10^{-6}
Cindol 3106 ^b	0.45	3.5×10^{-6}
Halocarbon 11-14 ^c	0.23	1.6×10^{-7}
Organic-Iodide ^d	0.21	2.6×10^{-6}

^a Test conditions: 10-lb load for 140 min at 26 ft/min.

^b Chlorinated oil distributed by E. F. Houghton & Co., Philadelphia, Pa.

^c Chlorofluorocarbon oil, distributed by Halocarbon Products, Inc., Hackensack, N. J.

^d 3 weight per cent iodine in Anisole + SAE-30.

Wear is measured by measuring the wear scar produced in the block. A wear rate is then calculated as wear scar depth in inches per foot of sliding. Results reported are the average of two or more tests.

Results and Discussion

Liquid and Solid Lubricants

Rabinowicz [8] concluded, after extensive wear testing, that the usual liquid lubricants are ineffective on bare titanium. Of all the lubricants he evaluated, only the halogenated hydrocarbons produced any beneficial effect, reducing the coefficient of friction to about 0.2 to 0.3 from the unlubricated value of 0.49. Lubricants containing halogens, especially straight chain hydrocarbons with fluorine, can apparently react with the adsorbed gas film or penetrate the film and adhere to bare titanium [3]. Owens and Roberts [9] reported that titanium could be effectively lubricated by a charge transfer complex of iodine in an aromatic hydrocarbon.

Three halogenated lubricants were evaluated in the present program. The results are summarized in Table 1. The friction values are in good agreement with previous work. From a wear standpoint, Halocarbon 11-14 is superior to the other halogenated oils. In each case, however, the wear surfaces were significantly scored. It is not likely that any of these lubricants would be useful on bare titanium in practical engineering applications, because of the high friction and consequent surface damage. However, they may find application in some machining operations such as drilling and tapping.

Solid lubricants applied to bare titanium surfaces improve wear and frictional properties significantly. This is particularly true when the lubricants are bonded to the surface with plastic resins or other binders. The wear test results of Table 2 illustrate this effect as well as the effect of surface roughening prior to lubricant application. The advantage of obtaining a suitable surface for bonding dry-film lubricants is clearly

TABLE 2—Performance of solid lubricants on bare Ti-6Al-4V and steel.^a

Lubricant	Specimen Finish, μ in. rms	Wear Life, min	Wear Rate, in./ft of sliding	Minimum Contact Pressure, psi
Bonded MoS ₂	8-16	4 ^b	1.5×10^{-6}	40 000
Bonded MoS ₂	30-40 (Vapor Blasted)	2 920	2.3×10^{-8}	25 000
Bonded MoS ₂ on 4620 steel	8-16	4 200	1.3×10^{-8}	25 000

^a Test conditions: 630-lb load; sliding speed 26 ft/min (72 rpm).

^b Test failed during stepped loading at 210-lb load.

evidenced by the effect of vapor blasting. Significantly, obtaining the same measured surface finish by glass bead peening was not nearly so effective, with tests on this finish failing quite rapidly. While the peening hardens the surface, the distribution and size of asperities are evidently not suitable for bonding.

The coefficient of friction in these tests is typically between 0.05 and 0.09, characteristic of molybdenum sulfide (MoS₂). Wear life obtained with vapor blasted titanium and resin-bonded MoS₂ is comparable to that of untreated hardened steel under similar conditions. The rate of wear measured is basically that of the bonded film. Film performance, however, is a function of substrate condition and properties and, to this extent, is a measure of pretreatment effectiveness.

Bonded solid lubricants should find use in areas where liquid lubrication is not feasible, and where a finite but predictable wear life can be tolerated.

Chemical Conversion Coatings

Several chemical or electrochemical surface treatments have been used

successfully to improve the wear resistance of titanium [10]. These coatings have been especially useful in metal working. Generally, aqueous inorganic solutions containing alkali metal salts, especially phosphates, and fluorides and hydrofluoric acid (HF) will form useful coatings by simple immersion. Anodizing has been accomplished in a great many

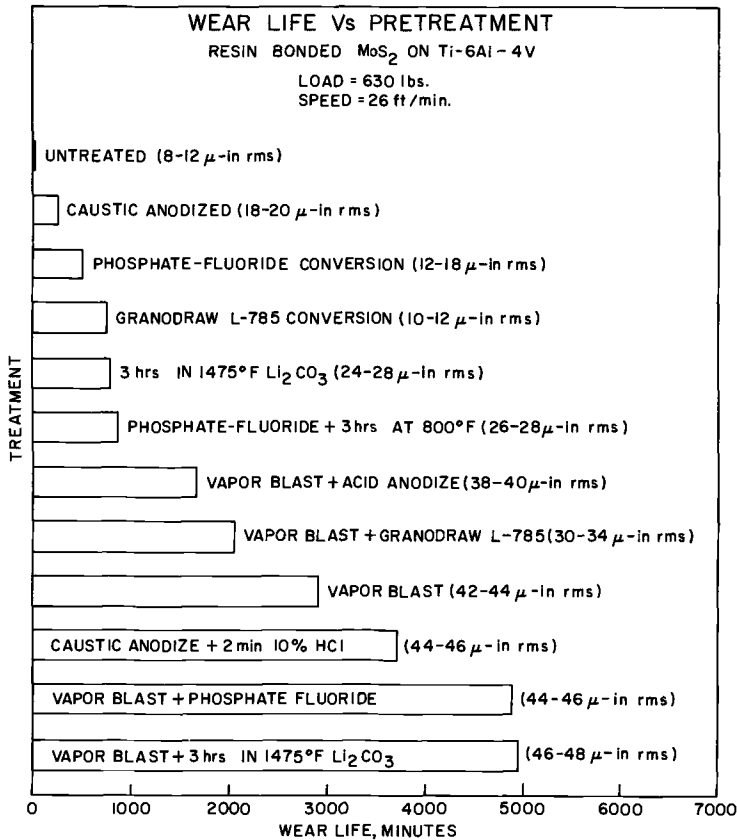


FIG. 3—The effect of surface pretreatment on the wear life of bonded molybdenum sulfide films on Ti-6Al-4V.

solutions, but those containing sodium hydroxide (NaOH) as the major ingredient have reportedly produced the best coatings [11].

Conversion coatings, in which a chemical compound is formed on the titanium surface, may improve wear properties by two mechanisms. First, the compound formed is often harder than the substrate titanium. Second, the coated surface will have better lubricant retention properties due to its roughening effect. Because the coating thickness will typically be between 0.0001 and 0.001 in., it is likely that the primary effect is improved lubricant retention. These coatings are likely to be most useful in combination with liquid or solid lubrication.

The wear test results obtained for several coatings previously reported to be effective with titanium are shown graphically in Fig. 3. The data reveals several interesting trends. Significantly, the performances of both the chemical and electrochemical surface treatments are poorer than for bare, vapor-blasted titanium in a comparable test. This is undoubtedly due to differences in surface roughness and subsequent adhesion of the lubricant film. Comparison with the data from Table 2 indicates the advantage to be obtained from vapor blasting, and supports the thesis that there is little benefit gained from the small hardness increase of the as-coated surface alone. This is further supported by the results for the lithium carbonate (Li_2CO_3) oxidizing treatment.

When the vapor blast treatment and conversion coating are used in combination, however, there is a wear life improvement of about 60 per cent. For the caustic anodic hardcoat (Watervliet Arsenal Process), the effect of chemical roughening by immersion in hydrochloric acid (HCl) is to increase wear life by more than a factor of 10. The improvement is related to the change in as-coated surface finish from about 16 to 32 $\mu\text{in. rms}$. These results are expected based on the specifications generally applied to steel parts which are to be dry film lubricated. Most often a mechanical and chemical pretreatment are specified.

Conversion and anodic coatings do not appear to be effective with liquid lubricants at loads as low as 10 lb. In several tests using mineral oils on coated specimens, failure was rapid at a load of 10 lb, with galling immediately evident. However, data reported by Battelle Memorial Institute shows a clear advantage for conversion coated titanium over bare titanium when the lubricants are liquids or greases [11]. The type of test used was less severe than the rotary wear test of this study. Widespread use of conversion coatings in titanium metal-working is indicative of their effectiveness.

One of the important aspects of any surface coating is the effect it may have on mechanical properties. For conversion coatings and anodized coatings on titanium this effect is likely to be small. This is due both to the shallowness of the coatings and to the reasonably good elastic and plastic properties they exhibit. The Watervliet Arsenal anodized hardcoat is the only chemical process for which extensive mechanical property data are available [11]. Fatigue and tension test results indicate no effect due to the coating. In fact, some improvement in fatigue life is reported, based on results of smooth rotating beam tests.

The potential advantages of anodic or conversion coatings for engineering applications are predicated on their use in combination with dry film lubricants. The coatings can be applied to hard-to-reach recesses, deep bores, and threads without difficulty. Furthermore, in some processes vapor blasting may not be practical, and these aqueous coating methods are then the only solution to improved dry-film lubricant bond-

ing. Obviously the use of a bonded solid lubricant implies a finite limit on wear life, and this must be taken into consideration by the designer.

Interstitial Surface Hardening

Titanium may be hardened by the addition of the interstitial elements oxygen, nitrogen, carbon, boron, and hydrogen. Hardening occurs by solid solution strengthening in a diffusion zone near the metal surface and by compound formation at the surface. The compounds of titanium with the interstitial elements are generally quite hard and afford the possibility of producing wear resistant, adherent, hard-facing on the metal. Brittleness of the coating and impairment of mechanical properties are the major disadvantages of these treatments. However, most of the treatments also require long times at elevated temperatures with subsequent distortion to parts and damage to other metallurgical characteristics. Hydrogen has not been used for hardening because of its deleterious effect on metallurgical properties. Little work has been reported on the use of boron, although Minkevich and Shul'ga [12] have experimented with molten borate salt baths. They report the formation of brittle but wear resistant coatings.

Nitriding of titanium has received wide attention. The preferred technique utilizes ultrapure nitrogen gas and temperatures of 1600 to 1800 F [13]. Times of about 16 hr are required to produce useful cases. Exposure to these temperatures for the necessary length of time has several significant disadvantages. Grain growth and distortion of machined parts becomes a serious problem under these conditions. Mitchell and Brotherton [14] have also pointed out that purity control of the gas is critical for reproducibility. While the wear life of nitrided parts under light loads has been shown to be about equal to carburized mild steel, the use of nitriding must be approached with the processing difficulties in mind.

Oxidation of titanium is inherently more attractive than nitriding. This is due to the higher rate of diffusion of oxygen in titanium and the corresponding reduction in time-temperature to produce a given case thickness. Air or oxygen oxidation of titanium usually produces a flaky scale which can embrittle the metal surface and impair wear properties. Oxidation in reduced pressure oxygen can eliminate this problem but does not appear to be commercially practicable. Mitchell and Brotherton have studied the use of molten salt baths to produce wear resistant oxide coatings on titanium [14]. In particular, treatments in salt baths containing alkali metal carbonates were found to be most promising. Heating titanium in mixtures of lithium carbonate (Li_2CO_3) and potassium carbonate (K_2CO_3) at temperatures from 1200 to 1470 F for from 2 to 4 hr gave the best results.

The work of Mitchell and Brotherton prompted the present examination of these molten salt treatments for wear resistance. Specimens were

treated in pure Li_2CO_3 at temperatures from 1400 to 1475 F and times of 1 to 4 hr.

The first wear tests, run with bonded dry-film lubricants were disappointing. As shown in Fig. 3 wear lives comparable only to chemical conversion coatings were obtained. It was believed that the smooth, lustrous, black coating was not providing a good adhesion surface for the lubricant. Vapor blasting prior to the oxidation treatment improved lubricant adhesion and consequent wear life by about a factor of 5, tending to verify this. Failure in these tests was confined to the block as opposed to ring and block failures with conversion coated specimens. However, wear performance was still not sufficient to warrant the relatively drastic oxidation treatment.

Additional tests were performed using oxidized specimens lubricated by SAE-30. In the case where both ring and block were oxidized titanium, the block wore rapidly causing early failure. The rings in this case were completely free of any scars or evidence of wear. The tests using a hardened steel block (R_c60) running against an oxidized titanium ring typically produced no failure after more than 300 hr. For comparison, bare titanium rings run against hardened steel in SAE-30 fail in approximately 5 min. It is more significant that in tests with oxidized titanium blocks run against hardened steel rings wear lives of 300 hr were obtained.

There is no doubt that the oxidation treatment has serious shortcomings. Some preliminary test results indicate a 40 to 50 per cent decrease in smooth, rotating beam fatigue life. At present, the use of material in the annealed condition is dictated by the temperature and time of treatment. Removal of adhering salts after treatment may pose some processing difficulties. Nevertheless, in those applications in which fatigue may not be critical, it appears that molten salt oxidation can provide an excellent means for improving wear resistance, especially at high loads.

Plated Coatings

Conventional electroplating has had little success on titanium. Substantial effort has been expended to develop processes for plating both chromium and nickel, but no reliable techniques have been found [13]. The problem is evidently involved in removing the stable oxide film on the surface to obtain plating adhesion. Various post-plating treatments have been tried, usually involving a diffusion anneal to promote adherence. Any improvements are gained at the price of a deleterious effect on mechanical properties. Diffused electroless nickel plate appears at present to offer the greatest reliability at the lowest mechanical property penalty.

There are little data available, specifically, on the wear of plated titanium. Some limited test data for chromium and silver electroplates,

and electroless nickel, gathered as a part of this screening program are given in Table 3. Specimens were plated 0.0015 to 0.002 in. by techniques generally recommended in the literature. Use of plated titanium rings and blocks and the standard high-load test procedure resulted in very rapid failure. Typically, the failure mode involved stripping of the plate from the base metal rather than excessive wear. When the loads were reduced in later tests and bare steel blocks substituted for titanium, longer lives were obtained. Wear resistance was judged to be good. However, the failures were the result of chipping, spalling, and peeling of the plating even in these cases. In the case of electroplated silver, the entire plating was stripped, intact, from the specimens.

While the wear resistance of chromium and nickel plates should be excellent, it is evident that poor adherence of as-plated metals is still a problem to be overcome before plating can be used as a practical means of coating titanium. The principal stumbling block to acceptance of

TABLE 3—Wear test results for plated Ti-6Al-4V.^a

Plating	Time to Failure, min	Load at Failure, lb	Minimum Contact Pressure, psi
Chromium.....	3	210	2 400
Chromium.....	173	210	2 200
Chromium against R _c 60 steel block.....	15	630	20 000
Electroless Ni.....	5	390	...
Electroless Ni.....	187	210	6 800
Silver.....	4	100	3 600
Silver against R _c 60 steel block.....	19	300	...

^a Test conditions: 26 ft/min sliding speed; lubricant SAE-30.

plated and diffused coatings, which show adherence, is the loss of mechanical properties which must be expected. Work is now in progress to improve metallic platings by two alternate routes. The first is an attempt to improve the adherence of as-plated coatings, using novel pretreatment techniques. The second is to avoid the deterioration of mechanical properties obtained with diffused coatings by the use of interlayer metals which might prevent formation of harmful intermetallic compounds.

Sprayed Metallic and Ceramic Coatings

A variety of metal and ceramic hard coatings can be flame or plasma sprayed on titanium by several commercial processes. The work of Mitchell and Brotherton [14] and others indicate that adherent sprayed deposits can be obtained on titanium using the techniques developed for steel. Typically, surfaces require some form of mechanical roughening or "keying" to obtain good adherence. Among the advantages of sprayed coatings is the range of metals and ceramics which can be used, the low temperatures generated in the part during coating and the ease of build-

ing up thick adherent deposits. The main problem associated with the use of sprayed coatings involves their inherent brittleness. It is also likely, based on limited data in the literature [13], that fatigue and other mechanical properties will be detrimentally affected by many of the sprayed coatings. Nevertheless, sprayed coatings have probably seen the widest commercial application of any titanium surface treatment.

A variety of sprayed metals and ceramics were tested in this program. The wear properties measured are those of the coating material, and the high load test is a means of measuring adherence to the titanium substrate. The results of wear tests are shown in Table 4. All of the tests were run in SAE-30 oil, on coatings of about 0.004 in. thickness. The tests were characterized by higher friction coefficients than noted with other types of coatings, perhaps due to the general difficulty of lubricating ceramics. Typical friction coefficients were about 0.15.

TABLE 4—Wear test results for flame and plasma spray coated Ti-6Al-4V.^a

Coating ^b	Time to Failure, min	Load at Failure, lb	Minimum Contact Pressure, psi
Nickel aluminide against R _c 60 steel block . . .	166	630	4 000
Molybdenum against R _c 60 steel block	11 700 ^c	630	10 000
Tungsten carbide against R _c 60 steel block . . .	1 000+ ^c	630	16 000
Titanium dioxide against R _c 60 steel block . . .	1 400+ ^c	630	24 000
Chromium oxide against hardened steel block.	2 300+ ^c	630	12 500

^a Test conditions: speed 26 ft/min; lubricant SAE-30.

^b All coatings were applied by Metco, Inc., Westbury, L. I.

^c No failure in coated part.

In those tests in which both the block and ring were coated titanium, failure generally occurred by a wearing through of the block coating. The rings, in this case, were always intact and unscarred. The fact that the block coatings were worn through rather than chipped or spalled indicated that adhesion was good. When hardened steel blocks were used against coated rings, failure was always manifested as excessive wear in the blocks with virtually no damage to the titanium ring. A flame sprayed molybdenum ring was only lightly worn after more than 180 hr of sliding at 26 ft/min, and 630-lb load. The porosity of sprayed coatings appears to play a beneficial part in the retention of lubricant.

With the exception of nickel aluminide, all of the coatings tested showed excellent wear resistance. The ceramic coatings were more prone to spalling and chipping than the metallics and appeared to be less impact resistant. However, all the materials showed good adherence to titanium, and coatings of this type should find wide application. Selection of a specific coating material can only be made when consideration is given to requirements of the application. Such parameters as tempera-

ture of operation, corrosiveness of environment, stress levels, and type of mating surface must be taken into consideration.

Conclusions

1. Liquid lubricants do not appear to be effective on bare titanium surfaces. Halogenated hydrocarbons reduce friction by about 50 per cent but do not protect titanium against excessive wear at light loads.

2. Titanium may be effectively lubricated by bonded solid films containing MoS_2 and graphite applied to prepared surfaces. Chemical conversion coatings enhance the adhesion of bonded solid lubricants, but a simple vapor blasting is more effective. A surface roughness of 36 to 44 $\mu\text{in. rms}$ is suitable for bonding dry-film lubricants to titanium.

3. A combination of chemical or electrochemical conversion coating, and mechanical or chemical surface roughening, offers the optimum surface treatment for solid lubricants on titanium. Coatings of this type are capable of limited-life, high load, application with little expected detrimental effect on mechanical properties.

4. Oxidation in molten lithium carbonate produces a thin wear resisting surface on titanium. Coatings produced in this fashion afford long wear life with liquid lubricants at high loads rubbing against steel. Fatigue properties have been shown to be reduced approximately 50 per cent by oxidation, however.

5. The poor adherence of electroplated metals to titanium severely limits their usefulness in wear applications. Diffusion treatments are likely to improve adhesion but be detrimental to mechanical properties.

6. Flame sprayed coatings of molybdenum on titanium give excellent wear life when rubbed against hardened steel. Sprayed ceramic coatings such as tungsten carbide (WC), titanium oxide (TiO_2) and chromium oxide (Cr_2O_3) are also very effective for wear protection of titanium but tend to chip and spall. Hard metal and ceramic coatings result in high wear on the steel test blocks and are known to have deleterious effects on mechanical properties.

References

- [1] Farnsworth, H. E., Schlier, R. E., and George, R. T., "Corrosion and Passivity Studies of Titanium," Brown University, Providence, R. I., Contract DA-19-020-ORD-1816, July 1, 1952, Sept. 30, 1955.
- [2] Rowe, G. W., "Vapor Lubrication of Titanium and Zirconium," *British Journal of Applied Physics*, Vol. 7, No. 4, 1956.
- [3] Miller, P. D. and Holladay, J. W., "Friction and Wear Properties of Titanium," *Wear*, Vol. 2, Nov. 1958.
- [4] Rabinowicz, E., "Frictional Properties of Titanium and Its Alloys," *Metal Progress*, Vol. 65, No. 2, 1954, p. 107.
- [5] Rabinowicz, E., "The Frictional Properties of Titanium," Progress Report, Mass. Inst. of Technology to Navy Bureau of Aeronautics, Contract No. NO as 51-1185c, Oct. 1, 1952.

- [6] Rabinowicz, E., "Surface Energy Approach to Friction and Wear," *Product Engineering*, Vol. 20, March 1965, pp. 95-97.
- [7] Rabinowicz, E., *Friction and Wear of Materials*, Wiley, New York, 1965.
- [8] Rabinowicz, E., "Lubricants for Titanium," *Metal Progress*, Vol. 67, No. 5, May 1955.
- [9] Owens, R. S. and Roberts, R. W., *Nature*, Oct. 26, 1963 correspondence, p. 200.
- [10] White, E. L., Miller, P. D., and Peoples, R. S., "Antigalling Coatings and Lubricants for Titanium," TML Report No. 34, Feb. 1956.
- [11] Wood, R. A., "Surface Treatment of Titanium," DMIC Technical Note, March 15, 1965.
- [12] Minkevich, A. N. and Shul'ga, Y. N., "Surface Hardening of Titanium in Fused Borax," (abridged translation), *Metal Industry*, Vol. 93, 1958, pp. 67-69.
- [13] Mallett, M. W., "Surface Treatments for Titanium Alloys," NASA Technical Memorandum, NASATM-X-53429, Oct. 1965.
- [14] Mitchell, E. and Brotherton, P. J., "Surface Treatments for Improving the Wear-Resistance and Friction Properties of Titanium and Its Alloys," *Journal of the Institute of Metals*, Vol. 93, 1965, pp. 381-386.

Surface Treatment of Ti-6Al-4V for Impact-Fatigue and Wear Resistance

REFERENCE: Weltzin, R. D. and Koves, G., "Surface Treatment of Ti-6Al-4V for Impact-Fatigue and Wear Resistance," *Applications Related Phenomena in Titanium Alloys, ASTM STP 432*, American Society for Testing and Materials, 1968, pp. 283–298.

ABSTRACT: Tests have shown that the Ti-6Al-4V alloy performs best under impact-fatigue loading conditions. This type of test best simulated actual loading conditions in many components in electro-mechanical devices. While the desired impact-fatigue performance is obtained with Ti-6Al-4V, the tendency of the alloy to gall and seize in wear indicated the desirability of some means of surface treatment for improved wear resistance. The combination of improved or unimpaired fatigue performance, along with improved wear, are not necessarily complementary results of surface treatment. Three basic types of surface treatments were investigated: (1) nonmetallic compound or gaseous diffusion coatings, (2) intermetallic-compound coatings, and (3) diffused metal coatings. After eliminating a number of surface treatments on the basis of hardness testing and microstructural examination, the following were selected for impact-fatigue and wear testing: (1) nitriding, (2) heat treatable titanium-chromium alloy layer, (3) heat treatable titanium-chromium alloy layer plus nitriding, and (4) oxygen-saturated alpha-titanium layer. The impact-fatigue testing showed that it is possible to obtain a surface treatment which results in improved fatigue life of Ti-6Al-4V. The results of all impact-fatigue testing will be presented, along with a discussion of subsequent wear testing of each surface treatment.

KEY WORDS: titanium alloys, fatigue, wear, surface treatment

Titanium and its alloys have outstanding properties which are utilized primarily in aerospace and defense applications. Perhaps the most important of these properties is the very high strength to density ratio obtainable with heat treatable alloys. The high strength, combined with relatively low density, makes titanium alloys attractive for a number of industrial applications.

Electro-mechanical data processing machines such as document handling and other input/output units contain numerous critical compo-

¹ Senior associate engineer, IBM Systems Development Div., Rochester, Minn.

² Manager, Materials Laboratory, IBM Systems Development Div., Rochester, Minn.

nents which are rapidly rotating, oscillating, or undergoing continuous rapid successions of stop and go motion. Many of these components are highly stressed and carry a complex impact-fatigue wear load. The continuous quest for higher machine speeds requires strong and lightweight components.

Titanium alloys certainly offer such combinations, and a study by Weltzin and Koves³ resulted in the selection of the Ti-6Al-4V alloy for optimum impact-fatigue properties. While in many applications this is the only important criterion, in some other cases a wear resistant surface is also required. The objective of this investigation was to develop

TABLE 1—Typical properties of hard surface layers on Ti-6Al-4V alloy.

Treatment	Peak Hardness, Knoop units	Depth of Layer from Surface				Hardness of Base Metal of Core, Knoop units
		at 550 Knoop		at 500 Knoop		
		in.	mm	in.	mm	
Oxidizing.....	950	0.0020	0.0508	0.0040	0.1016	450
Nitriding.....	1650	0.0015	0.0381	0.0040	0.1016	450
Chromium diffusion..	660	0.0040	0.1016	0.0060	0.1525	450
Chromium diffusion + nitriding.....	1600	0.0060	0.1525	0.0120	0.3050	450

NOTE: ALL DIMENSIONS IN INCHES

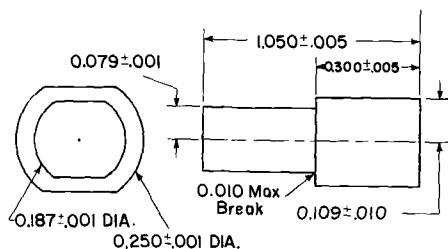


FIG. 1—Impact-fatigue specimen. The change of cross section introduces a stress raiser which localizes failure at that point.

some methods of achieving surface wear resistance and to arrive at favorable combinations of high impact-fatigue strength and wear resistance.

The Development of Treatments for Surface Wear Resistance

After a survey of available surface treatments for titanium alloys, a joint project was set up with Battelle Memorial Institute in Columbus, Ohio, to explore further possibilities. At Battelle the work was carried out under the direction of Russell Ogden. The desired wear resistant surface layer was to be both hard and stable.

³ Weltzin, R. D. and Koves, G., "Impact-Fatigue Testing of Titanium Alloys," Presented at 1967 American Institute of Mining, Metallurgical, and Petroleum Engineers, Annual Meeting, Feb. 23, 1967.

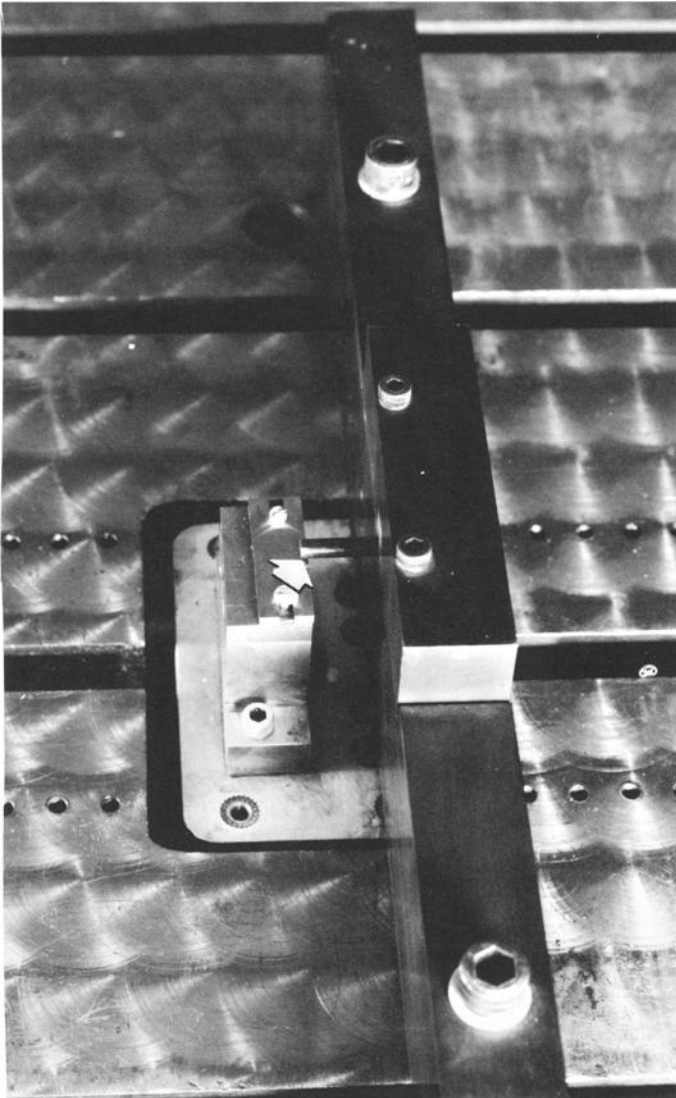


FIG. 2—Impact-fatigue testing apparatus ($\times\frac{1}{2}$). The arrow points to the area of contact between the stud and the striker. The same arrangement was used in conjunction with a calibrated microscope to measure impact wear.

In the first phase of the development project, five different treatments were tried. Three of them—oxidizing, boriding, and nitriding—created a very hard but thin surface compound layer, while two other treatments resulted in the diffusion of chromium and copper respectively to provide a not-so-hard but deeper and more stable surface layer. Two of these treatments were quickly abandoned—boriding, due to its extreme

brittleness, and the copper diffusion because it did not result in any significant increase of hardness. In the second phase of the project the remaining treatments were further refined, and the two treatments with the most promising properties were thoroughly tested for impact-fatigue and wear resistance. These treatments were: (1) a diffused chromium treatment, and (2) a combination of diffused chromium and a surface nitriding treatment.

The diffused chromium treatment produced a layer approximately

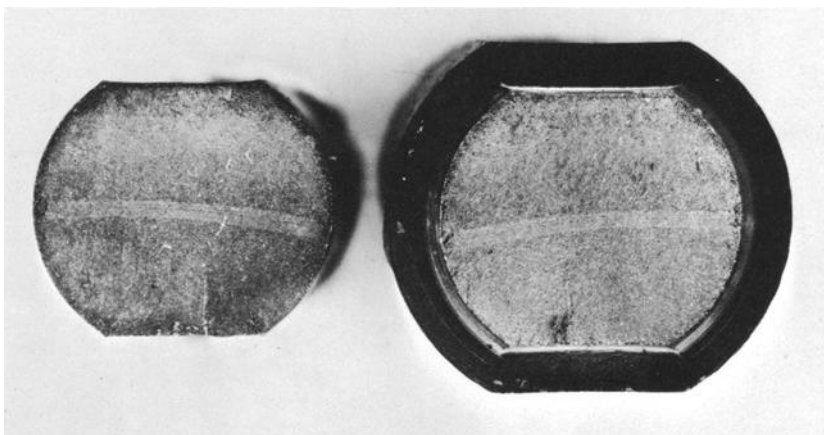


FIG. 3—Optical-fractograph of fatigue failed impact specimen. On the left is the tenon portion, on the right head portion of the specimen.

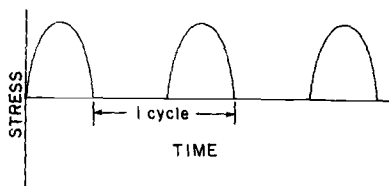


FIG. 4—Stress pattern applied on specimen during testing.

0.005 in. (0.127 mm) thick with a peak hardness about 150 to 200 Knoop units above that of the fully heat treated base alloy. The combination chromium diffusion nitriding treatment produced, in addition, a thin but very hard (approximately 1000 Knoop units) compound layer on the surface. For comparison, more conventional oxide and nitride surface layers were also tested. Table 1 summarizes typical properties of all surface layers.

Impact-Fatigue Testing

The impact-fatigue testing was performed on an experimental arrange-

ment originally devised by Koves⁴ and later used by Weltzin and Koves.³ The basic tool of this apparatus was a Wiedemann-Baldwin SF-01-U⁵ universal fatigue testing machine. For this machine, a fixture was designed such that a dynamic, cyclic impact load could be applied to the test specimen. Figure 1 is a drawing of the test specimen used in this testing. The holding fixture for the stud and the striking head through which the impact load is applied are shown mounted on the fatigue machine in Fig. 2. In these experiments the specimen was held by the head and struck on the tenon. Failure, thereby, occurred at the deliberately introduced notch due to the change of cross section of the stud. The impact-fatigue experiments consisted of dynamically applying a load of predetermined magnitude to the stud and recording the results as stress applied versus the number of cycles to failure. The fatigue strength was determined for 10^7 cycles, at which point testing was halted. A photograph of a typical impact-fatigue failed specimen is shown in Fig. 3.

The loading pattern in this impact-fatigue testing is illustrated in Fig. 4. There is no preload present on the specimen, and the loading is unidirectional, with load applied during one half of a complete cycle.

The calculation of the stress applied to the cylindrical stud during one loading cycle is derived in the Appendix. The equation resulting from this calculation is

$$S = 1180 F$$

where F = applied impact load imposed on the fatigue specimen.

To correctly interpret the data resulting from these impact-fatigue tests, the load must be accurately determined. The impact load applied by the fatigue machine used in these experiments resulted from the motion of an eccentric rotating weight. The load applied by this rotating weight is calibrated for fatigue testing where the oscillating platform is connected to the seismically isolated table by the fatigue specimen. To do this, we determined the displacement of the stud associated with a given eccentric weight setting. We then measured the static load needed to achieve the same displacement. This calibration resulted in a determination that the actual applied load on the stud was approximately three times greater than that indicated by the eccentric weight.

The calculation of applied stress was based on the assumption that no areas of localized high stresses are present. In this testing, a stress concentrator was deliberately introduced (that is, 0.010-in. or 0.254-mm max break). The localization of high stresses can be expressed by a theoretical stress concentration factor, K_t . The value of K_t for a given

⁴ Koves, G., "The Applicability of AISI C-1213 Free Machining Steel to Complex Fatigue-Shock-Wear Load," *Transactions, American Institute of Mining, Metallurgical, and Petroleum Engineers*, Vol. 230, Feb. 1964, p. 58.

⁵ Trademark of Wiedemann Div., Warner and Swasey Co., King of Prussia, Pa.

loading condition and notch geometry is easily determined using the data given in the book of stress concentration design factors by Peterson⁶.

The effect of a notch on the fatigue strength of a component varies considerably with notch geometry and material. The effect of a notch is usually less than one might expect from the value of K_t . A scale of notch sensitivity, which is related to the degree to which the theoretical effect is obtained, may be defined as

$$q = \frac{K_f - 1}{K_t - 1}$$

where:

q = notch sensitivity factor,

K_f = fatigue notch factor = fatigue strength of unnotched specimen / fatigue strength of notched specimen, and

K_t = theoretical stress concentration factor.

Using the data available in Peterson, the effect of the deliberately introduced stress raiser, for Ti-6Al-4V with no surface treatment and in the solution treated and aged condition, is expressed by

$$K_t = 2.06$$

$$q = 0.35$$

A compilation of K_t and q for all the surface treatment conditions studied is given in Table 2.

TABLE 2—Effect of the stress concentrator on the notch sensitivity of surface treated Ti-6Al-4V titanium alloys.^{a, b}

Surface Treatment	Fatigue Strength		K_f	q	Relative Notch Sensitivity
	psi	kgf/mm ²			
Untreated	73 000	51.0	1.37	0.35	moderate
Sandblasted	94 000	66.0	1.06	0.056	low
Nitrided	45 000	31.5	2.22	1	fully notched specimen
Oxidized	35 000	24.5	2.86	1	fully notched specimen
Diffused chrome + nitrided	40 000	28.0	2.50	1	fully notched specimen
Diffused chrome + pickle	94 000	66.0	1.06	0.095	low
Diffused chrome (no pickle)	57 000	40.0	1.75	0.71	high

^a $K_t = 2.06$.

^b Unnotched bending fatigue strength = 100,000 psi (70.0 kgf/mm²).

Wear Testing

Two types of wear tests were used to determine the effectiveness of the surface treatment procedures in improving wear resistance. The first

⁶ Peterson, R. E., *Stress Concentration Design Factors*, Wiley, New York, 1965.

provided a measure of resistance to sliding abrasive wear, the second to wear due to repeated impact.

The sliding or abrasive wear was performed using the apparatus shown in Fig. 5. This test consisted of abrading a case-hardened steel disk (solid arrow) against the treated titanium specimen (hollow arrow) at a fixed speed of 3400 rpm. The load applied at the end of the lever arm was adjusted so that Hertz Contact stresses of 20,000 and 10,000 psi (14.0 and 7.0 kgf/mm²), respectively, were obtained. The rate of wear was

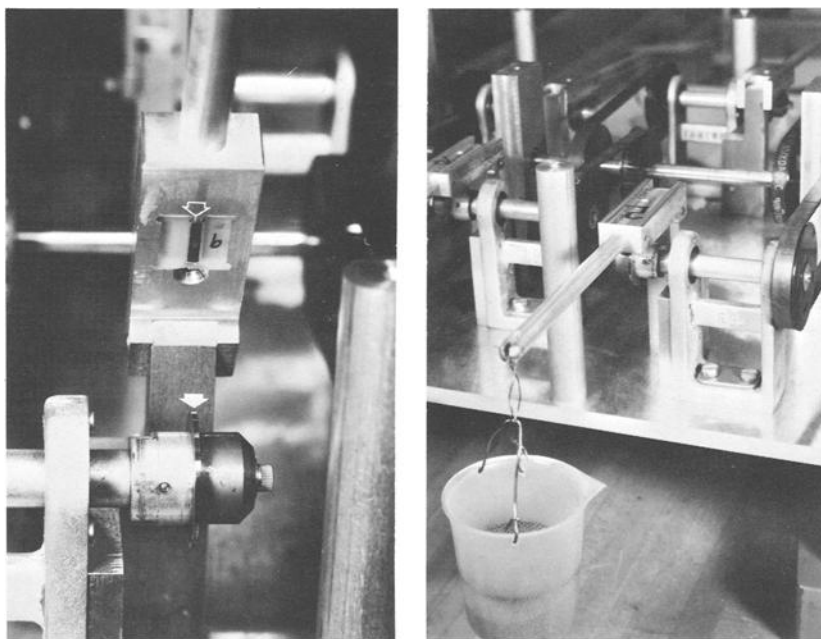


FIG. 5—Sliding abrasive wear testing apparatus. The photo on the right shows an overall view of the tester. The left photo shows in detail the case-hardened disk (white arrow) and the tested specimen (hollow arrow). The contact stress between specimen and disk is determined by the amount of weight at the end of the lever arm.

determined by the total weight loss of the specimen measured at intervals of 2 min. No discernible loss of weight of the case-hardened disks was obtained.

Resistance of the various treatments to wear due to impact loading was determined by the impact-fatigue apparatus shown in Fig. 1 and discussed previously. This test involved impact-fatigue loading a heat-treated stud at a stress (20,000 psi or 14.0 kgf/mm²) such that fatigue failure would be avoided up to 10^7 cycles. At intervals of a given number of loading cycles, we determined the wear on the tenon of the stud impacted by the striking head of the oscillating platen, using a calibrated

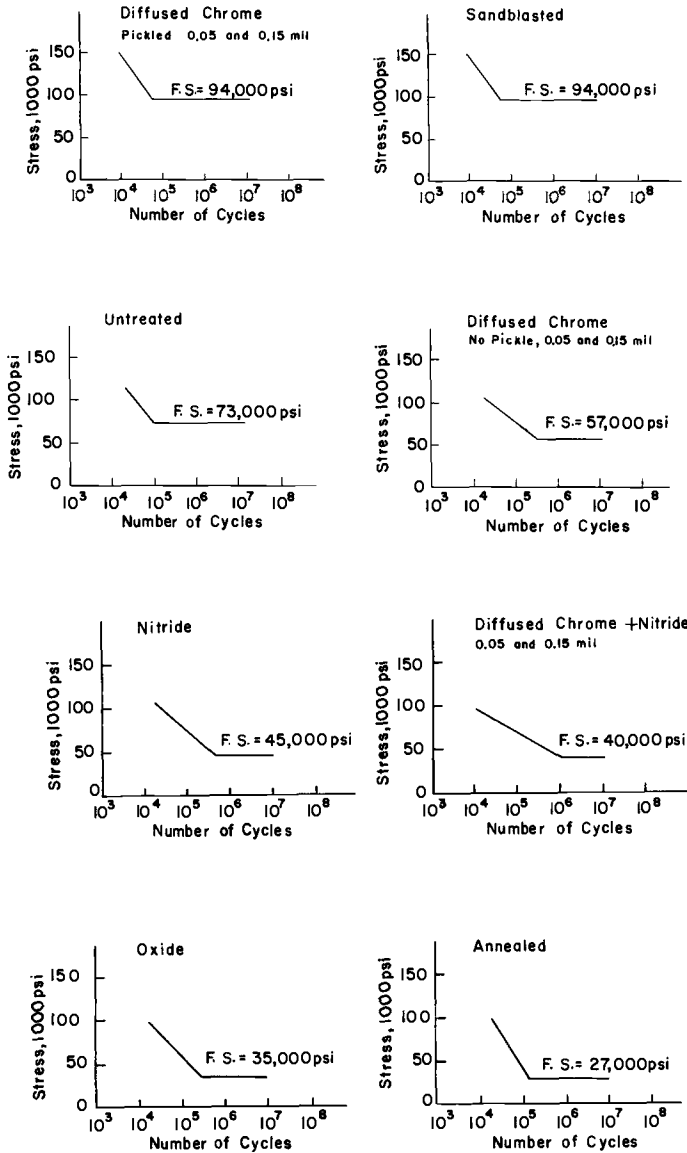


FIG. 6—Fatigue curves for surface treatments of Ti-6Al-4V.

measuring stage. We plotted as total wear versus the number of loading cycles for constant impact stress.

Impact-Fatigue Testing Results

The impact-fatigue testing data were recorded as applied impact stress versus the number of cycles of failure, that is, in the standard *S-N* curve form. The fatigue curves are given in Fig. 6. The impact-fatigue strength

at 10^7 cycles for Ti-6Al-4V in the solution treated and aged condition, with no surface treatment, was 73,000 psi (51 kgf/mm²). The impact-fatigue strength was increased by the diffused chrome plus pickle surface treatment procedure, and by abrasive blasting of the surface. Each procedure resulted in a fatigue strength of 94,000 psi (66 kgf/mm²). This was an increase of almost 30 per cent and restored the fatigue

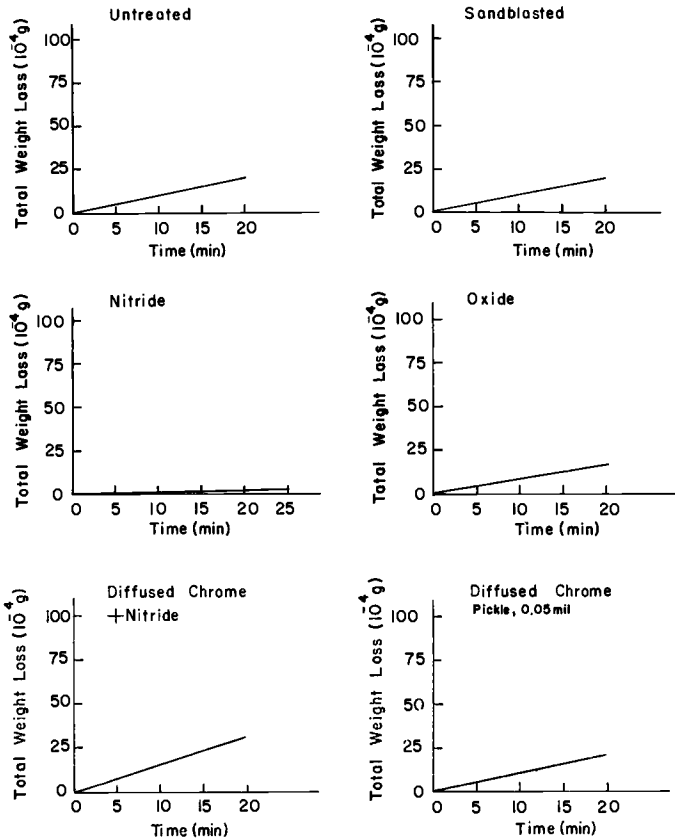


FIG. 7—Abrasive wear of surface treated Ti-6Al-4V. Hertz contact stress = 10,000 psi.

strength to approximately the value for the unnotched condition obtained by other investigators. All other surface treatment procedures resulted in a marked reduction of the fatigue strength. The fatigue strength ranged from 57,000 psi (40 kgf/mm²) for the diffused chrome (no pickle) surface treatment, to 35,000 psi (24.5 kgf/mm²) for the oxidized surface. A fatigue curve was also generated for Ti-6Al-4V in the annealed condition, in order to determine if the lower strength might result in a tougher, more impact-fatigue resistant material. The fatigue strength obtained for

this modification was 27,000 psi (19 kgf/mm²), only one third that of the Ti-6Al-4V in the solution treated and aged (STA) condition.

An interesting result of the impact fatigue testing is the beneficial effect of a pickling treatment on the diffused chrome treated material prior to aging at 1000 F (538 C). When identical treatment procedures were used to prepare different chrome surface treated specimens, except for pickling one batch of specimens prior to aging, the pickled specimens gave an increase of the fatigue strength to 94,000 psi (66 kgf/mm²),

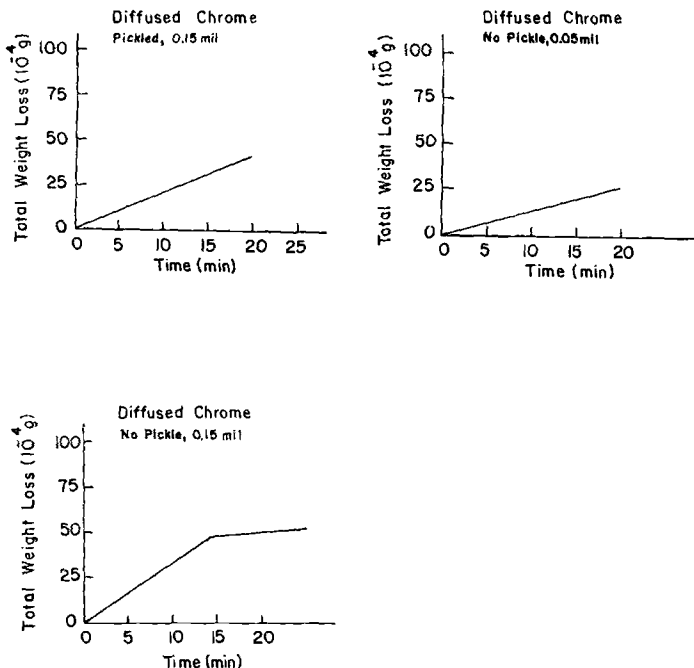


FIG. 7 (Cont.)

while the specimens not pickled exhibited a fatigue strength reduction to 57,000 psi (40 kgf/mm²).

Wear Resistance Testing Results

The wear resistance of the surface treatments of Ti-6Al-4V was studied with two types of wear tests. The first determined the surface treatment resistance to sliding abrasive wear; the second provided a measure of the surface resistance to impact wear. Figures 7 and 8 and Table 3 present the results of the sliding abrasive wear study; Fig. 9 and Table 4 the results of the impact-wear investigation.

The sliding abrasive wear tests described earlier were performed at Hertz Contact stresses (HCS) of 10,000 psi (7.0 kgf/mm²) (Fig. 7) and

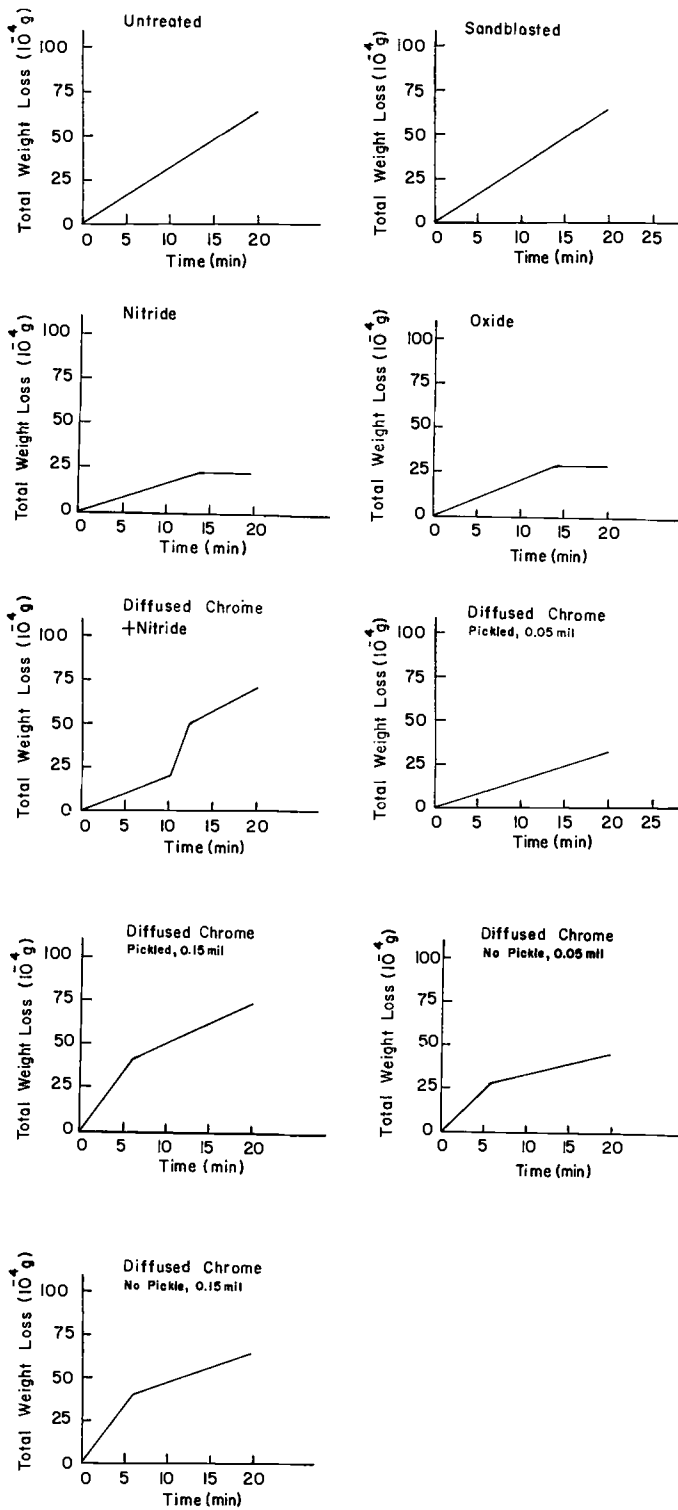


FIG. 8—Abrasive wear of surface treated Ti-6Al-4V Hertz contact stress = 20,000 psi.

20,000 psi (14.0 kgf/mm²) (Fig. 8). The nitride and oxide surface treatments, which resulted in the greatest reduction of the impact fatigue strength, provided improved resistance to sliding wear. The duplex diffused chrome + nitride treatment provided improved wear resistance for a short time (HCS = 20,000 psi) (14.0 kgf/mm²) and then degraded to a greater sliding wear rate. The diffused chrome surface treatment procedures resulted in degraded sliding wear resistance, with one exception. The diffused chrome treatment obtained by diffusing 0.05-mil (0.00127 mm) chrome plate into Ti-6Al-4V, solution treated, pickling, and finally aging, provided improved sliding wear resistance. This treatment also produced improved fatigue life and excellent surface appearance. As a general conclusion, the harder, more notch-sensitive surface treat-

TABLE 3—Total wear under sliding abrasive wear conditions for various surface treatments of Ti-6Al-4V STA.

Surface Treatment Condition	Total Wear, g, after 20 min, HCS = 10,000 psi or 7.0 kgf/mm ²	Total Wear, g, after 20 min, HCS = 20,000 psi or 14.0 kgf/mm ²	Fatigue Strength	
			psi	kgf/mm ²
Nitride.....	0	0.23×10^{-4}	45 000	31.5
Oxide.....	0.17×10^{-4}	0.30	35 000	24.5
Sandblasted.....	0.20	0.64	94 000	66.0
No treatment.....	0.20	0.64	73 000	51.0
Diffused chrome + nitride.....	0.32	0.70	40 000	28.0
Diffused chrome (0.05 ml or 0.00127 mm) pickle.....	0.22	0.32	94 000	66.0
Diffused chrome (0.15 ml or 0.00371 mm) pickle.....	0.42	0.74	94 000	66.0
Diffused chrome (0.05 ml or 0.00127 mm) no pickle.....	0.27	0.45	57 000	40.0
Diffused chrome (0.15 ml or 0.00371 mm) no pickle.....	0.52	0.64	57 000	40.0

ment provides improved resistance to sliding wear, but at the same time results in decreased impact-fatigue life. Table 3 lists the relative wear rates for the various surface treatments under abrasive sliding wear conditions.

The impact wear test data are given in Fig. 9, with a compilation of total wear at 10^6 cycles in Table 4. In this type of wear condition improvement was obtained with three surface conditions, notably the abrasive blasted which also improved fatigue strength. In general, the harder surface treatments (that is, oxide and nitride) had a very high impact wear rate compared to untreated Ti-6Al-4V STA.

The combined results of the wear tests on the surface treated Ti-6Al-4V shows that the surface treatment best for resistance to sliding wear is also the worst for resistance to impact wear. The impact-fatigue testing did not detect any difference resulting from the thickness of the

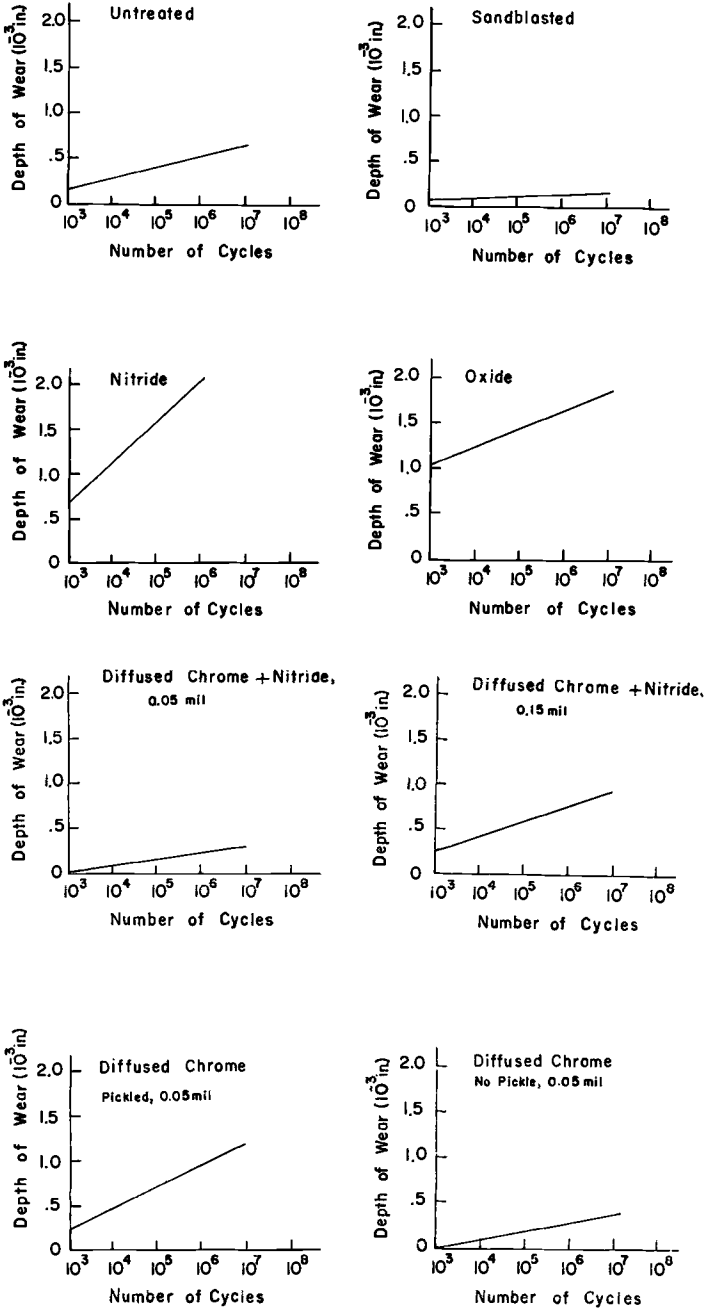


FIG. 9—Impact wear on surface treated Ti-6Al-4V.

TABLE 4—Total wear after 10^6 impact cycles at an operating stress of 20,000 psi (14 kgf/mm²).

Surface Treatment Condition	Impact Wear		Fatigue Strength	
	in.	mm	psi	kgf/mm ²
Sandblasted	0.170×10^{-3}	0.0043	94 000	66.0
Diffused chrome + nitride (0.05-mil or 0.00127 mm chrome)	0.220	0.0056	40 000	28.0
Diffused chrome (0.05-mil or 0.0127 mm chrome)	0.300	0.0076	57 000	40.0
None	0.520	0.0153	73 000	51.0
Diffused chrome + nitride (0.15-mil or 0.00371 mm chrome)	0.780	0.0229	40 000	28.0
Diffused chrome + pickle (0.05-mil or 0.00127 mm chrome)	0.950	0.0249	94 000	66.0
Oxide	1.68	0.0426	35 000	24.5
Nitride	2.08	0.0528	45 000	31.5

TABLE 5—Relative performance of surface treatment as determined by impact-fatigue, sliding abrasive wear, and impact wear tests.

Surface Treatment	Impact-Fatigue	Abrasive Wear (HCS = 20,000 psi or 14 kgf/mm ²)	Impact Wear
No treatment	good	poor	fair
Abrasive blasted	excellent	poor	good
Nitride	poor	good	poor
Oxide	poor	good	poor
Diffused chrome + nitride (0.05-mil or 0.00127 mm chrome)	poor	poor	good
Diffused chrome + nitride (0.15-mil or 0.00371 mm chrome)	poor	poor	poor
Diffused chrome-pickle (0.05 ml or 0.00127 mm)	excellent	good	poor
Diffused chrome-pickle (0.15 ml or 0.00371 mm)	excellent	poor	...
Diffused chrome (0.05 ml or 0.00127 mm)	fair	fair	good
Diffused chrome (0.15 ml or 0.00371 mm)	fair	poor	...

chromium plate diffused into the titanium. An effect of the original depth of chrome plate is seen for both the diffused chrome and diffused chrome plus nitride in wear testing. The effect of the depth of original chrome plate and the pickling treatment was variable, resulting in either an increased or decreased wear resistance, depending on the treatment procedure and type of wear test. A performance rating scale of the various surface treatments has been established in Table 5.

Conclusion

The results of the various tests indicate that for a complex impact-fatigue-wear load, simultaneous optimization of all characteristics in the

Ti-6Al-4V alloy cannot be achieved. Nevertheless, several combinations of improved properties are available, depending on the basic condition of the alloy and the surface treatment used. The design engineer must evaluate the service requirements of a given component and decide on the most important functional property. He then can select a treatment which will provide maximum performance for that characteristic and maintain fair-to-good properties in the other needed areas. Optimum combinations for many applications can be obtained using this procedure.

APPENDIX

Calculation of Applied Impact Stress

Calculation of the stress applied to the cylindrical stud during one loading cycle was determined as follows: As the plate on the oscillating platform (see Fig. 2) hits the specimen with a force F , the force creates a bending moment.

$$M = Fl \dots \dots \dots (1)$$

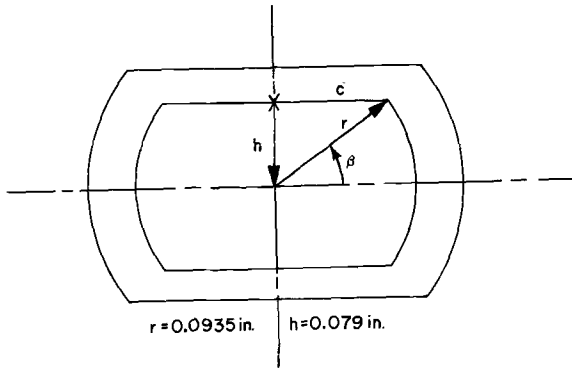


FIG. 10—Relationships used in calculating maximum stress applied to specimens in impact-fatigue testing.

where l = bending lever arm.

This causes a maximum stress in the outer fibers of the specimen.

$$S_{\max} = \frac{Mh}{I} \dots \dots \dots (2)$$

where:

I = moment of inertia, and

h = one-half distance between parallel flats of specimen tenon.

Dimensional quantities used in calculating the stress in the specimen are indicated in Fig. 10.

The moment of inertia for a specimen of this configuration is

$$I = \frac{r^4}{2} \beta \frac{ch}{2} (2c^2 - r^2) \dots \dots \dots (3)$$

As $r^2 = c^2 = h^2$ and $\sin \beta = h/r$. Then the relation for I may be simplified to

$$I = \frac{r^4 \beta}{2} - \frac{h}{2} (r^2 - 2h^2)(r^2 - h^2)^{1/2} \dots \dots \dots (4)$$

and for the specimen used.

$$h = 0.079 \text{ in. and } r = 0.0935 \text{ in.} \quad h = 2.0 \text{ mm and } r = 2.38 \text{ mm}$$

Therefore,

$$I = 0.458 \times 10^{-4} \text{ in.}^4 \quad I = 16 \text{ mm}^4 \dots \dots \dots (5)$$

Substituting Eq 5 into Eq 2,

$$S = \frac{Flh}{0.458 \times 10^{-4}} = \frac{F(0.069) 0.079}{0.458 \times 10^{-4}}$$

$$S = 1180F, \text{ psi} \quad S = 2.19F \text{ kgf/mm}^2 \dots \dots \dots (6)$$

where F is the applied impact load imposed on the fatigue specimen.

THIS PUBLICATION is one of many issued by the American Society for Testing and Materials in connection with its work of promoting knowledge of the properties of materials and developing standard specifications and tests for materials. Much of the data result from the voluntary contributions of many of the country's leading technical authorities from industry, scientific agencies, and government.

Over the years the Society has published many technical symposiums, reports, and special books. These may consist of a series of technical papers, reports by the ASTM technical committees, or compilations of data developed in special Society groups with many organizations cooperating. A list of ASTM publications and information on the work of the Society will be furnished on request.